THE OXIDATION, DESEGREGATION, AND PLASTICITY OF Si-Al-O-N CERAMICS

by

COLIN RAYMOND PICKERING

A thesis submitted for the degree of PhD to

The University of Warwick

Department of Physics

February 1984

CONTENTS

PAGE

PAGE

FIGURES

PAGE

TABLES

ACKNOWLEDGEMENTS

This work has been completed with the substantial and varied support and assistance of many friends and colleagues. Space precludes full acknowledgement. I hope those not mentioned below will recognise in this statement an expression of my gratitude.

I am grateful to the Department of Physics at the University of Warwick for the provision of laboratory facilities and technical support. In particular, the work of Gerry Smith (Electron Microscopy Unit), Roy McLeod (Photography) and Bill Jones, Dan Lee and Pat Beecraft (technical workshops) and their colleagues is much appreciated.

This work has been carried out under the supervision of Dr. Mike Lewis to whom I am grateful for advice, direction and assistance in interpretation throughout the whole scope of the work.

For assistance, discussions of the work and creation of a healthy working atmosphere in the laboratory I am grateful to my research colleagues, B. S. B. Karunaratne, John Meredith, Steve Winder and Gary Heath. Gary's assistance in the preparation of some of the figures presented is particularly noted. Discussions and the assistance of Russell Ball, Roger Bayliss and Nick Butler is also appreciated.

I am also grateful to a number of correspondents who have generously discussed my work in relation to their own and have provided details of their published and unpublished work. I am grateful to Dr. George Rowlands of the Warwick Physics Department for the solution of the diffusion equation presented in the Appendix.

I acknowledge with thanks the financial assistance of UKAEA (Harwell) and the SERC. I am grateful to my employers, Ceramic Developments (Midlands) Ltd., who have provided time for the completion of this work and photocopying facilities.

Finally, I dedicate this work to my parents whose own efforts over many years have made possible my own contribution.

DECLARATION

This thesis describes my own work except where specifically acknowledged in the text.

Summary

The high oxidation resistance of ceramics based on silicon nitride has contributed to their potential for use in high-temperature structural engineering applications. The oxidation behaviour and its effect on mechanical properties of a range of hot-pressed ceramic alloys of composition $Si_{6-z}\ Al_z\ O_z\ N_{8-z}$ ($1 \leq z \leq 4$) has been investigated at temperatures between 1200° and 1400°C.

The mechanism of oxidation has been identified by determination of the kinetics of oxidation and the nature of the oxide scales using X-ray diffractometry, and scanning and transmission electron microscopy. The rate-controlling process in the oxidation of these ceramics is that of the inward diffusion of oxygen to the ceramic/oxide interface where the oxidation reaction takes place. In the early stages of oxidation the composition of the oxide scale and the rate of oxidation is modified by the diffusion of grain-boundary segregated additive and impurity ions such as Mg and Ca into the scale.

The redistribution of these elements on oxidation creates a ceramic of more stabilised structure and of higher oxidation resistance. By heat-treatment of large blocks of ceramic the mechanism of this redistribution has been identified as that of diffusion into the oxide scale with negligible dissolution into the β′ crystal phase of the ceramic. The out-diffusion of elements is accompanied by the removal of grain boundary phases by the local growth of the β′ phase.

Local enhancement of the rate of oxidation by the out-diffusion of the elements Mg and Ca towards the scale gives rise to a low creep rupture stress for the ceramic via the formation of intergranular cracks which grow at sub-critical stresses. This has been determined by tensile creep rupture tests which have been performed on two ceramics of composition Si_5AlON_7 at temperatures between 1275° and 1325°C.

CHAPTER ONE

THE DEVELOPMENT OF SI-AL-O-N CERAMICS

The primary motivation behind the development of silicon nitride-based materials has been the recognition of their potential for use as components in high-temperature structural applications, most notably in heat engines. This chapter surveys the advantages and limitations of the use of ceramic materials as structural engineering components prior to a discussion of the development of silicon nitride and related ceramics. Their fabrication routes, properties and applications will be discussed and the objectives of the current research defined.

1.1. Ceramic technology in high-temperature engineering

The upper working temperature limit of metallic alloys is imposed by the deterioration in their physical properties, especially their creep and oxidation resistance. For use at higher working temperatures ceramic materials have been considered to show greater potential than the further development of metallic alloys.

A primary motivation for the development of materials which would be capable of withstanding substantially increased operating temperatures was the requirement to increase the working temperature of gas turbine engines in order to maximise efficiency [Godfrey 1968] and minimise exhaust gas pollution levels [Proust 1980]. The gas turbine engines currently in use, for example, are limited to an upper component working temperature of $\sim$ 1050°C [Moulson 1979], which is imposed by the creep life of the components, particularly the rotor blades [Godfrey 1968]. In addition, the use of refractory metallic alloys at these temperatures

requires the application of an oxidation-resistant coating to the components [Godfrey 1968] and the use of sophisticated cooling systems [Proust 1980]. The development of an inherently oxidation-resistant refractory material capable of withstanding the extreme working environment of gas turbine engines would eliminate the requirement for such protective measures.

Ceramic/metal composite materials in which ceramic particles are surrounded by a metal matrix were first developed in the 1950's as a preliminary approach to the development of new materials but were found to be unsuitable for use as structural engineering components since they were found to combine the worst characteristics of the metal and ceramic phases [Parr 1960, Godfrey 1968]. Current development centres on wholly ceramic materials for "substitution" of the metallic components currently in use. Ceramic materials were felt to offer substantial advantages over metallic alloys but their general properties also impose limitations on their use as structural components.

Advantages and limitations of ceramic components

In turbine applications the use of ceramic components is expected to raise the component working temperature of engines to ~ 1370°C, resulting in increases in efficiency of up to 20% [Proust 1980] and fuel savings as high as 50% [Moulson 1979]. In addition, considerable savings should eventually be made on the cost of materials since the constituents of ceramic materials are naturally abundant. Freedom from strategic considerations is also provided by this natural abundance. Metallic alloys, for example, are dependent on the supply of strategically sensitive materials such as Ni and Cr [Proust 1980]. The reduced density of ceramic materials over metals should enable engine

weight reductions of up to 50% to be made [Proust 1980] increasing their speed of response [Hartley 1982] and their attractiveness for such weight-sensitive applications as aeronautics. The chemically inert nature of ceramics is likely to give rise to better corrosion resistance and obviate the requirement for protective coatings for exposed components. Increased corrosion resistance should also enable the use of lower grade fuels of a wider variety, resulting in a further reduction in fuel costs [Proust 1980]. Finally, the high abrasion resistance of ceramics will give rise to an increased resistance to dust erosion.

Substantial modifications to engineering designs have to be made, however, if ceramic components are to be substituted for metallic components. The direct substitution of ceramic for metal components is seldom possible because of the very limited ductility of ceramics which makes them susceptable to stress concentrations as a precursor to mechanical failure [Godfrey 1968]. This low ductility and the low tensile strength typical of ceramic materials combine to demand substantial design modifications [Parr 1960, Godfrey 1968, Proust 1980]. Care must be taken to avoid material flaws and sharp edges and the loading of ceramic components in tension [Parr 1960]. The thermal expansion mismatch between ceramic-ceramic and ceramic-metal materials at joints must be properly taken into consideration. The misfitting of ceramic turbine shrouds in a metallic housing, for example, has been found to be a major cause of the failure of the ceramic component [Messier et al 1981]. Surface flaws which may be introduced on machining the ceramic to its final form must also be minimised. The ceramic shrouds were also found to fail at these flaws [Messier et al 1981]. Final machining of ceramic components can seldom be avoided due to the requirement for fine tolerances in engine applications

[Parr 1960] and the inevitable shrinkage on fabrication of ceramic materials. Despite these limitations on the use of ceramic materials as structural components the potential benefits of their use have provided the motivation for their substantial development over the last three decades.

1.2. Properties and applications of silicon nitride and related ceramics

The properties required of a material for use as a high temperature structural material include a high modulus of rupture, a high resistance to creep, high oxidation and corrosion resistance, low thermal expansion coefficient and high dimensional stability, and high resistance to thermal shock. An early investigation listed a large number of ceramics which were considered for use as engineering materials [Godfrey 1968]. At that time a number of materials showed potential for use in demanding high-temperature working environments. This potential was determined by reference to such properties as modulus of rupture, thermal stability, oxidation resistance, and resistance to thermal shock, and the temperature-dependence of these properties. Of over 250 materials studied hot-pressed silicon nitride, silicon carbide, alumina, and aluminium nitride showed the best combination of properties. In particular, the "instantaneous" thermal shock resistance of hot-pressed silicon nitride was found to be the highest of the materials studied.

Widespread attention has been given to the development of silicon nitride and silicon carbide materials. The commercial development of silicon nitride ceramics is currently hindered by a sufficiently inexpensive and reliable fabrication route [Katz 1983]. The ease of

fabrication of α-SiC ceramic, on the other hand, has led to its widespread acceptance as a competing material and transformation-toughened zirconia is being considered for use in diesel engines in addition to its deployment as drawing and extrusion dies [Katz 1983].

Silicon nitride ceramics can be obtained by a wide variety of fabrication routes (section 1.3.2) and have a wide variation in chemistry and microstructure. Hot-pressed materials of near-theoretical density possess the best properties which include high strength, high wear resistance, excellent resistance to thermal shock, good high temperature hardness, high oxidation resistance, and low coefficient of friction. This combination of properties has led to research aimed at realising the potential of materials based on silicon nitride in a wide variety of applications.

Their exploitation in the metals processing industry has been supported by studies which have shown that they are not wetted by a variety of common metals and steels [Parr 1960, Fisher 1977, Phelps and Weyland 1983, Mehan et al 1983], including Si, Al, Fe, Cu and Ni at temperatures < 1000°C, and that their thermal shock resistance enables them to withstand large-scale molten steel splash tests [Jack 1976]. The compatability of silicon nitrides with metals at higher temperatures has also commanded widespread attention in view of their potential use in combination with metallic alloys as structural materials. Some corrosion of silicon nitride was noted when in contact with alkali metals at elevated temperatures, and Ti and Mo were also found to react with the ceramic [Fisher 1977]. Silicon nitride was found to corrode when in contact with some Ni, Fe, and Cu compounds [Bennett and Houlton 1979], and corrode very seriously with Fe if Mg was present in the ceramic [Lange 1978a].

The resistance of silicon nitrides to molten salt and V compound corrosion has also been investigated and found to be significant at temperatures >1000°C [Tressler et al 1976].

Components made of silicon nitride materials have, however, been satisfactorily tested in prototype engines. Turbine shrouds have been tested for 4h at an inlet temperature of 925°C with localised temperatures of 1100°C for short periods. These components also withstood thermal shock cycling for over 500 cycles [Messier et al 1981]. A ceramic radial turbine has been tested at an operating temperature of 1400°C resulting in a fuel economy of 30% and reduced pollution levels. A silicon nitride rotor has been tested satisfactorily at a burner flame temperature of 1650°C, the blade temperature being 1315°C and rim temperature 1100°C for 4h [McLean 1982]. The engine speed was 50,000 rpm in this test.

Components made of silicon nitride ceramics have also been tested in more traditional engines. A 50 c.c. two-stroke engine was tested with silicon nitride cylinder, cylinder head, piston, connecting rods and crankshaft. An air-cooled 2.7ℓ diesel engine was operated using silicon nitride cylinders, pistons, gudgeon pins, tapets, pushrod tips, rocker pads, head plates, and turbocharger rotor. It has been estimated that high volume production of these ceramic parts will be available by 1985 with production of an all-ceramic engine by 1990 [Hartley 1982].

The commercial exploitation of silicon nitride ceramics has already begun with the development of cutting tool materials. Their high abrasion resistance and low creep rate have enabled their use without coolants at higher speeds and greater depths of cut on some common metal alloys [North and Baker 1983]. Their electrical and thermal properties are currently under investigation in order to

evaluate their potential for such purposes as radomes [Moulson 1979, Lowell 1983, Katz 1983] and electrical [Parr 1960] and thermal insulators.

1.3. Structure and fabrication

1.3.1. The synthesis and crystal chemistry of silicon nitride (Si_3N_4)

Silicon nitride (Si_3N_4) does not occur naturally. It is artifically synthesised by a variety of routes of which the nitridation of silicon in N_2, NH_3 or $N_2 + H_2$ atmospheres [Glasson and Jayaweera 1968], chemical vapor deposition [Prochazka and Greskovich 1978, Niihara and Hirai 1976], and silica reduction [Komeya and Inoue 1975] are the most common. Silicon nitridation produces a fine high-purity powder product which is the most desirable form for most subsequent fabrication routes [Katz 1983], CVD produces a high purity, dense ceramic but current rates of deposition are very low, and silica-reduction results in a product containing undesirable SiC and Si_2N_2O impurity phases.

Crystalline Si_3N_4 exists in two distinct structural forms, designated α and β. Of these, β Si_3N_4 is believed to be of the stoichiometric composition whereas some authors believe α-Si_3N_4 to be an "oxynitride" of approximate composition $Si_{11.5}O_{0.5}N_{15}$ [Jack, 1976]. On densification of powders the α form usually converts to β. Since the transformation $\beta \rightarrow \alpha$ has never been observed it is thought that β-Si_3N_4 is the thermodynamically more stable phase.

The structural unit of Si_3N_4 is illustrated in figure 1.1. It consists of tetrahedrally-bonded Si with each N atom bonded to three Si atoms. Si_3N_4 may therefore be visualised as consisting of groups of SiN_4 tetrahedra joined together at their corners [Jack 1976]. The crystal structure may be considered to consist of

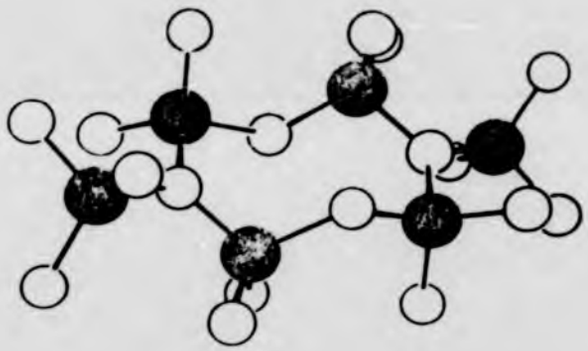

Figure 1.1: The structural unit of Si_3N_4 [Jack 1976].

puckered eight-membered rings stacked vertically along the c-direction of an hexagonally symmetric unit cell.

The structure of β-Si_3N_4 is similar to that of phenacite (Be_2SiO_4) in which the O is replaced by N and the Be by Si atoms respectively. The "stacking sequence" of layers in the c-direction is ABABAB..... α-Si_3N_4 has a similar structure to that of the β phase except that every third and fourth layer in the vertical stacking sequence is effectively rotated around the c-axis by 180° to give a stacking sequence ABCD ABCD... The unit cell size of α is therefore twice that of β.

1.3.2. The densification of Si_3N_4 powders

The fabrication of silicon nitride as a dense ceramic can be achieved by a variety of processes, each of which combines relative ease of densification with correspondingly poorer properties respectively in the final ceramic. As expected, fully dense ceramics possess the greatest mechanical strength but ease of fabrication or dimensional precision may be overriding commercial considerations.

Silicon nitride can be densified by pressureless sintering at temperatures in the range 1250 - 1750°C although full density cannot be achieved without the use of a sintering aid [Yeh and Sikora 1979]. Commonly used sintering aids are MgO or Y_2O_3 which promote densification by forming a low-melting point liquid with impurity SiO_2 and so enhance the liquid-assisted solution precipitation densification process. Full densification can be achieved by pressureless sintering with Y_2O_3 [Smith 1977] but care must be taken to avoid the formation of certain Y_2O_3 phases in the ceramic since their physical expansion on oxidation at 800-1000°C can lead to material degradation. [Clarke et. al. 1982]. Full densification cannot be achieved by pressureless sintering using an MgO additive due to the countervailing processes of liquid phase sintering (pore removal) and bulk

decomposition (pore growth). Under optimum conditions a maximum density of ∿ 90% of theoretical may be obtained [Terwilliger and Lange 1975]. Suppression of bulk decomposition can be achieved by sintering under a high N_2 gas pressure leading to ceramics with a room temperature strength approaching that of hot-pressed material. The room-temperature bend strength of sintered ceramics is reported to be as high as 600 MN m^{-2} [Giachello et. al. 1980], compared with that of 900 MN m^{-2} for hot-pressed materials. Although a relatively simple fabrication route, sintering is necessarily accompanied by substantial dimensional shrinkage.

An interesting sintering process which has been found to be accompanied by negligible dimensional change is that of "reaction-bonding" in which a green compact of Si is nitrided. Silicon powder compacted at ∿ 200 MN m^{-2} is presintered at ∿ 1200°C in an inert atmosphere prior to a nitriding heat treatment at 1250-1450°C under 1 atm N_2 pressure, resulting in a ceramic of 70-80% density [Moulson 1979, Yeh and sikora 1979]. Due to its porosity the strength of this ceramic is rather poor but the ease with which the prenitrided compact may be machined prior to the shrinkless nitriding process has made this material commercially attractive. Production units of this material may be made by any of the usual ceramic processes including slip casting, extrusion, injection moulding, die pressing and flame spraying.

Fully dense ceramics of the highest strength have been produced by hot pressing fine Si_3N_4 powders under pressures of 25-40 MN m^{-2} at temperatures of 1650-1800°C for 1-4 h [Yeh and Sikora 1979]. Full density cannot be achieved without the use of a sintering aid, commonly MgO, Y_2O_3 or CeO_2 added in quantities of 1-5 wt %. More effective consolidation can be achieved by isostatic pressing [Yeh and Sikora 1979, Yamada et al 1981b]. Pressures of 100-400 MN m^{-2} are used in this technique. Densification aids are still required in order to achieve full density.

1.4. Ceramic alloying: Si-Al-O-N ceramics

1.4.1. The system Si-Al-O-N

The high temperature mechanical strength of hot-pressed silicon nitride is dominated by the softening of an intergranular glassy phase which is the residue of the liquid phase solution-precipitation densification process. The softening of this phase at high temperatures gives rise to dramatic decreases in the mechanical strength [Evans and Sharp 1971] (figure 1.2). Several approaches to overcoming this limitation are open to materials engineers. One is to increase the refractoriness of the residual phase by careful choice of additive chemistry or post-fabrication crystallisation. Another is phase minimisation by careful control of additive and impurity contents of the batch composition. A further approach has been to minimise the second phase content by the incorporation of excess glass forming ions, notably impurity O, into the major crystalline phase via the concept of ceramic alloying. This has been achieved by the development of ceramic alloys consisting of phases in the system Si-Al-O-N.

A convenient representation of this system has been formulated by assuming that each constituent element takes only its accepted valency, namely Si^{4+}, Al^{3+}, O^{2-} and N^{3-}, and treating the elements as being ionically bonded, that is, treating the system as being composed of ionic salts [Jack 1976]. The system can then be represented as a square in which any point represents the sum of twelve positive and twelve negative valencies. The corners of the square represent the compounds Si_3N_4, Si_3O_6, Al_4O_6 and Al_4N_4. The system and the subsolidus phase fields which have been identified is presented in figure 1.3.

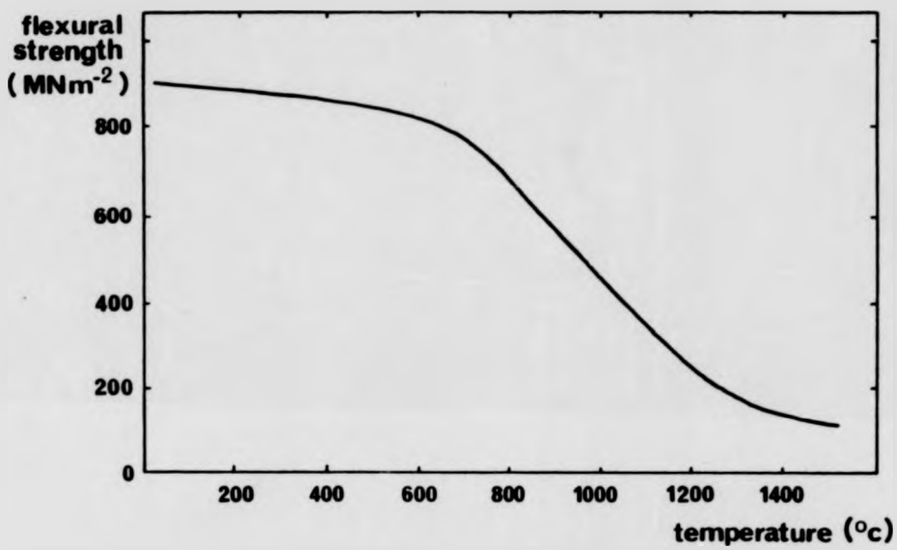

Figure 1.2: Temperature-dependence of the strength of Si_3N_4 hot-pressed with MgO [Evans and Sharp 1971]

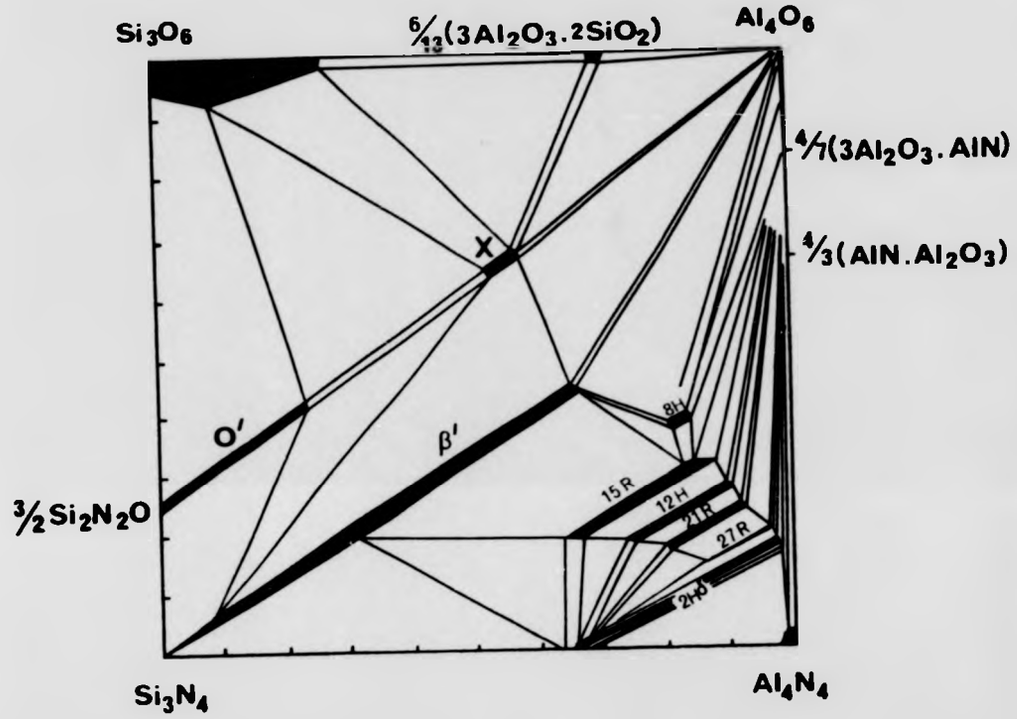

Figure 1.3: Sub-solidus phases in the system Si-Al-O-N [Jack 1976]

A very large quantity of O may be accommodated in β Si_3N_4 by its substituting for N. In order to maintain charge neutrality, Al simultaneously replaces Si. In this way β Si_3N_4 extends as a continuous phase along the line represented by the formula $Si_{6-z}Al_zO_zN_{8-z}$. The "substitution level", z, of Al for Si (or O for N) varies between 0 and ∿ 4.2 along a single phase field known as β′, with a neglible extent with respect to excess solution away from the metal/non metal atomic ratio of 3/4 (figure 1.3).

1.4.2. Fabrication and properties of β′ Si-Al-O-N ceramics

Si-Al-O-N ceramics are usually fabricated from appropriate quantities of Si_3N_4, Al_2O_3, and AlN. Additions of SiO_2 have been observed to give rise to accelerated densification. The fabrication of dense β′ Si-Al-O-N ceramics has been achieved by the processes of sintering and hot pressing which are used to fabricate β-Si_3N_4 compositions.

β′ ceramics can be pressureless sintered to high density without the use of a sintering aid but densification of an overall composition corresponding to β′ occurs very slowly under these conditions. An oxygen rich composition is required if a high-density ceramic is to be produced within a reasonable timescale [Mitomo et al 1979, Rahaman et al 1981, Benn and Riley 1980]. Additions of sintering aids such as MgO or Y_2O_3 allow densification of compositions corresponding to β′ to be achieved more quickly. However, large quantities of MgO gives rise to a ceramic containing large quantities of intergranular glassy phase [Lewis et al 1980]. The large quantities of second, intergranular phase of a Y_2O_3 sintered ceramic gave rise to a very poor high-temperature (> 1300°C) oxidation resistance despite good mechanical properties conferred by crystallisation of the intergranular phase [Lewis and Barnard 1980]. Improvements in density and

a reduction in the quantity of Y_2O_3 sintering additive have been achieved. A high oxidation resistance was reported for a material containing 1.1 wt% Y_2O_3 which had been sintered at 1760°C for 4hr under a gas pressure (N_2) of 34.5 kNm^{-2} [Arias 1979].

A much higher oxidation resistance was reported for fully dense hot-pressed β′ Si-Al-O-N fabricated under a pressure of 15 MN m^{-2} at 1800°C for 1 hr. This material required the addition of sintering aid (1% MgO) to facilitate full densification under these conditions [Lewis et al 1977]. Materials of compositions corresponding to β′ Si_5AlON_7 were reported to contain minimal quantities of intergranular phase with respect to O or N-rich compositions of the same substitution level. This material formed the basis of an investigation into the high-temperature mechanical behaviour of hot-pressed β′ Si-Al O-N ceramics which demonstrated the dominance of the nature and quantity of intergranular phase in determining the mechanism of mechanical deformation [Karunaratne 1980]. Ceramics of very low intergranular phase content exhibited "superplastic" creep behaviour. Outer tensile strains of up to 4% were observed under four-point bend loading conditions. In addition, the modification of the intergranular phase by oxidative heat-treatments of the ceramic formed the basis of improved creep resistance and, in a ceramic of high intergranular phase content, a change to a greater creep and creep-rupture resistance. A preliminary investigation of the oxidation behaviour of this material demonstrated that long-range diffusional processes involving the formation of a diffusion couple between the oxide scale and the grain boundary phase was in large measure responsible for this behaviour [Lewis and Barnard 1980].

1.5. Objectives of the current research

The work reported here was undertaken to fulfil three main objectives:

(1) The mechanism of oxidation of β′ Si-Al-O-N ceramics was to be defined. Although the oxidation of β Si_3N_4 has been widely discussed in the literature (Chapter 2), few studies of the oxidation of β′ ceramics have been published. This work describes the oxidation behaviour of hot-pressed β′ ceramics of widely differing substitution and additive element levels. This behaviour allows a general definition to be made of the mechanism of oxidation of these materials.

(2) The mechanism by which oxidation leads to improved mechanical properties of these materials was to be defined. Oxidation-induced microstructural changes were to be observed together with an analysis of the results of oxidation experiments.

(3) The effect of oxidation on the creep behaviour of β′ ceramics was to be observed. In particular it was hoped to be able to demonstrate the "superplastic" behaviour of oxidised ceramics under conditions of uniform (tensile) stress.

CHAPTER TWO

MICROSTRUCTURE, OXIDATION AND DEFORMATION OF HOT-PRESSED Si_3N_4 and SI-Al-O-N CERAMICS: A REVIEW

Part One: Densification and microstructure

The microstructural features which determine the high-temperature oxidation and mechanical behaviour of hot-pressed Si_3N_4 and Si-Al-O-N ceramics are characteristic of the mechanism of densification. Of particular importance are intergranular phases. In this section the mechanism of densification and the microstructure of the hot-pressed ceramics will be reviewed with particular reference to these phases.

1.1. The densification mechanism

Hot pressing of constituent batch powders is typically carried out at temperatures in the range 1700-1800°C under pressures of 30-60 MNm^{-2} [Jack 1976]. The mechanism of densification has been independently identified from studies of the densification and phase transformation kinetics [Bowen et al 1978] and examination of the microstructures of partially hot-pressed ceramics [Drew and Lewis 1974, Lewis et al 1977]. These studies have shown that the densification mechanism of both β Si_3N_4 and β′ Si-Al-O-N ceramics is that of liquid phase sintering in which initial powder rearrangement is followed by powder dissolution and precipitation of the β or β′ crystal phases respectively. In β Si_3N_4 initial liquid formation is believed to be facilitated by the presence of large quantities of SiO_2 derived from impurity SiO_2 which had existed on the large surface area of the Si_3N_4 batch powder. The later stages of hot-pressing densification are

believed by some authors to be assisted by diffusional (Coble) creep [Rahaman et al 1980, Kuwabara et al 1980].

Densification of β Si_3N_4 cannot proceed below ∿ 1750°C without the use of a hot-pressing aid such as MgO or Y_2O_3 which enhances the densification kinetics by lowering the eutectic temperature of the liquid sintering phase and reducing its viscosity at the sintering temperature. These aids are typically added as fine powders in quantities of 1-7 wt%. The amount of sintering aid in the ceramic has a pronounced effect on the oxidation and mechanical properties of the material since the residue of the liquid sintering phase after full precipitation of the β or β′ crystal phase forms an intergranular glassy phase on cooling. This phase, whose quantity increases with increasing quantities of sintering aid [Drew and Lewis 1974], is described more fully in section 1.3 below.

1.2. Microstructure

The microstructures of hot-pressed β Si_3N_4 and β′ Si-Al-O-N are very similar, consisting of β or β′ grains surrounded by a small quantity of grain boundary second phase. Figure 2.1 illustrates a typical microstructure as observed via bright field diffraction contrast in the transmission electron microscope. In addition to the β′ and intergranular phases there exists a dispersion of heavily electron-absorbing particles associated with Fe impurity, usually situated at grain boundaries.

The major crystalline phase in hot-pressed Si_3N_4 has been identified by X-ray or electron diffraction to be β Si_3N_4 [Drew and Lewis 1974, Evans and Sharp 1971, Krivanek et al 1979, Kossowsky 1973]. The only other phase to be detected by these methods was α-Si_3N_4 which was reported to vary in quantity from ∿ 1% [Kossowsky 1973]

believed by some authors to be assisted by diffusional (Coble) creep [Rahaman et al 1980, Kuwabara et al 1980].

Densification of β Si_3N_4 cannot proceed below ∿ 1750°C without the use of a hot-pressing aid such as MgO or Y_2O_3 which enhances the densification kinetics by lowering the eutectic temperature of the liquid sintering phase and reducing its viscosity at the sintering temperature. These aids are typically added as fine powders in quantities of 1-7 wt%. The amount of sintering aid in the ceramic has a pronounced effect on the oxidation and mechanical properties of the material since the residue of the liquid sintering phase after full precipitation of the β or β′ crystal phase forms an intergranular glassy phase on cooling. This phase, whose quantity increases with increasing quantities of sintering aid [Drew and Lewis 1974], is described more fully in section 1.3 below.

1.2. Microstructure

The microstructures of hot-pressed β Si_3N_4 and β′ Si-Al-O-N are very similar, consisting of β or β′ grains surrounded by a small quantity of grain boundary second phase. Figure 2.1 illustrates a typical microstructure as observed via bright field diffraction contrast in the transmission electron microscope. In addition to the β′ and intergranular phases there exists a dispersion of heavily electron-absorbing particles associated with Fe impurity, usually situated at grain boundaries.

The major crystalline phase in hot-pressed Si_3N_4 has been identified by X-ray or electron diffraction to be β Si_3N_4 [Drew and Lewis 1974, Evans and Sharp 1971, Krivanek et al 1979, Kossowsky 1973]. The only other phase to be detected by these methods was α-Si_3N_4 which was reported to vary in quantity from ∿ 1% [Kossowsky 1973]

Figure 2.1: Typical microstructure of hot-pressed β Si_3N_4 or β′ Si-Al-O-N (β′ $Si_4Al_2O_2N_6$ hot-pressed with MgO)

Figure 2.1: Typical microstructure of hot-pressed β Si_3N_4 or β′ Si-Al-O-N (β′ $Si_4Al_2O_2N_6$ hot-pressed with MgO)

Figure 2.1: Typical microstructure of hot-pressed β Si_3N_4 or β' Si-Al-O-N (β' $Si_4Al_2O_2N_6$ hot-pressed with MgO)

to ∿ 20% [Evans and Sharp 1971]. The large differences in these observations may be accounted for by the different batch sources and pressing procedures employed.

Most β grains were reported to be approximately equiaxed with grain diameters in the range 0.1 - 3 μm. Occasional large grains with diameters up to 8 μm were also reported. Up to 20% of the volume was reported to be composed of acicular grains [Kossowsky 1973] with aspect ratios varying between 1 and 10 [Nuttall and Thompson 1974]. The grains were of random orientation but displayed a pronounced hexagonality similar to that illustrated in figure 2.1 due to the preferential growth of $[10\bar{1}0]$ facet planes during the liquid-assisted densification process. The grain boundary phase was observed to exist as a glass, primarily next to these prism plane facets [Drew and Lewis 1974]. In the absence of the glassy phase, and in materials which contained smaller quantities of the sintering additive, the grain shape was observed to be more irregular and the amorphous phase was only observed at multiple grain junctions.

The highly electron-absorbing particles were typically of ∿ 0.1 μm diameter and were estimated to comprise up to 5 vol% of the material[Nuttall and Thompson 1974]. The quantity and type of these impurity particles were dependent on the source of the batch materials and the milling procedures employed. They have been variously identified as WC clusters introduced during the ball-milling process, Fe-W clusters, free Si, and Cr-,Fe-, and Ni-rich particles. The larger of these particles have been observed to affect the low temperature strength of the ceramic, acting as Griffith-type flaws, but they have not been observed to have a direct effect on the high temperature properties.

Few studies have been reported on the detailed microstructure of β′ Si-Al-O-N. A study of a series of ceramics of substitution level $z \sim 1$ hot-pressed with 1% MgO showed that the microstructure was essentially the same as that of β Si_3N_4 with faceted, equiaxed β′ grains with a glassy intergranular phase. The quantity of this intergranular phase was observed to be minimised for a composition corresponding to the "balanced" (β′) formula Si_5AlON_7 [Lewis et al 1977].

1.3. Solid solubility in β′ Si-Al-O-N and the intergranular phase

The intergranular phase consists of the residue of the liquid sintering medium after precipitation of the β or β′ crystal phases. It exists because of the very low solubility limit for excess ions or impurity ions in the β and β′ crystal phases.

Early work suggested that up to ∼ 20% Mg may be accommodated in β′ Si-Al-O-N crystals by interstitial and substitutional means, the level of solubility being dependent on the availability of vacant metal ion sites [Hendry et al 1975]. Neutron diffraction studies of a ceramic hot-pressed from Si_3N_4-Al_2O_3 mixtures showed that up to 5% of the sites may be vacant at room temperature. However, Si_3N_4-Al_2O_3 mixtures do not form single phase ceramics (see figure 1.1) and it was not known how the presence of second phases affected the interpretation of the results [Gillot et al 1981].

Microscopical and analytical studies have shown, however, that the solubility of such elements as Mg in β′ Si-Al-O-N is very low. Lewis et al [1980] showed that the quantity of intergranular glassy phase in β′ Si_5AlON_7 ceramics increased with increasing quantities of MgO from 1-6%. They concluded that Mg was soluble in β′ only in small quantities. Attempts to grow Mg-substituted "β′-" Si-Al-O-N s with a range of compositions in the 3M/4X plane of the

Mg-Si-Al-O-N system only succeeded in producing crystal phases with compositions near the line $Mg_x Al_{4-x} Si_2O_{4+x} N_{4-x}$, indicating that Mg is not soluble in β′ [Wild et al 1981]. A study of a range of single-phase hot-pressed β′ ceramics of substitution levels $0.8 \leq z \leq 4.0$ led to the conclusion that the maximum solubility of Mg in β′ is $\leq$ 1.5% [Gauckler et al 1978].

The very high creep resistance of a β′ Si_5AlON_7 ceramic hot-pressed with MgO and the non-faceting nature of its grain structure was attributed to a minimisation of the quantity of intergranular phase due to the accommodation of excess impurity ions, notably Mg and O, in the β′ phase [Karunaratne and Lewis 1980a]. Lattice imaging in the transmission electron microscope supported this suggestion since no second phase was observed down to a spatial resolution ∿ 7 Å. However, an Auger Electron Spectrographic examination of the intergranular high-temperature fracture surface of a ceramic of similar composition showed it to be rich in O, Al, Mg and Ca in comparison to the sub-surface material [Lewis et al 1977]. An estimate of the composition of this segregate was 0.08 CaO. 0.22 Al_2O_3. 0.42 MgO. $2SiO_2$. A depth profile of the concentration of these elements was obtained by the removal of the surface layers by bombardment with Ar ions. The results were complicated by the poor spatial resolution of the Auger apparatus and the presence of an initial contamination layer but were consistent with the presence of a grain boundary segregate of width ∿ 10 Å. A limited degree of structural and chemical inhomogeneity is therefore believed to exist at boundaries in ceramics in which no grain boundary phase can be resolved in the transmission electron microscope.

A grain boundary layer of such limited thickness cannot be satisfactorily labelled as a distinct phase but local structural and chemical inhomogeneity is likely to give rise to enhanced local atomic mobility in addition to facilitating grain boundary sliding. The rate of atomic grain boundary migration is important in determining the resistance of the material to diffusion-accommodated creep and has been found to be directly related to the rate of oxidation of hot-pressed β′ Si-Al-O-N ceramics (see Part Two and Chapter 4). For maximisation of creep and oxidation resistance it is therefore desirable to reduce the quantity of the intergranular phase as far as possible.

Part Two: Oxidation

In this section the oxidation of hot-pressed β Si_3N_4 and β′ Si-Al-O-N ceramics will be reviewed after a discussion of the principles of oxidation.

2.1. The oxidation of metals

2.1.1. Initial reaction

In the presence of oxygen metals readily corrode at their exposed surfaces according to a reaction of the type

$$xM + \frac{y}{2} O_2 \rightarrow M_xO_y$$

where M represents a metal atom and x and y are constants whose values depend on the valency of M. The formation of a monolayer of O on the surface of the metal usually occurs very rapidly due to the high electron affinity of O and the ready availability of electrons from the conduction band of the metal. Many models have been proposed to describe this initial reaction. These models have been comprehensively and critically reviewed by Lawless [1973].

The initial rapid oxidation of the metal surface occurs by the process of chemisorption in which a partially ionic M-O bond is formed by the transfer of electrons via reactions of the form

$$O_2 + e^- \rightarrow O_2^-$$

$$O_2 + 2e^- \rightarrow O_2^{2-}$$

$$O_2 + 4e^- \rightarrow 2O^{2-}$$

$$O_2 + 2e^- \rightarrow 2O^-$$

where e^- represents an electron derived from the conduction band of the metal.

Chemisorption is followed by local atomic rearrangement and surface reconstruction in which oxygen atoms are incorporated into the metal. The reconstructed "oxide" layer may take an irregular form. At low temperatures and oxygen pressures, for example, the oxides of the metals Al and Si form as an amorphous layer. Reconstruction of a regular layer may require a critical surface concentration of O to be reached or may require relatively high O pressures. Further growth of the oxide may occur by chemisorption since electrons are readily available from the metal and are believed to be capable of tunnelling through oxides of thickness up to $\sim$ 50 Å.

Isolated pockets of reconstructed oxide have been observed to grow to form thin films of oxide up to $\sim$ 100 Å thick by a process similar to that of the nucleation and growth of a crystal phase from a melt. Lateral growth of these oxide nuclei precedes outward growth and the formation of a thick, coherent oxide layer. Further

growth of the oxide phase requires the diffusion of the reacting species across this scale.

2.1.2. Thick-film oxidation

The rate of growth of oxide scales in which further incorporation of oxygen by chemisorption is not possible is dependent on the slowest mechanism involved in the total oxidation reaction. This may be the incorporation of O in the scale, electron or atom migration of reacting species across the scale, or the reaction of metal and oxygen to form the oxide. Many models have been proposed to describe the rate of oxidation with regard to the rate-controlling process for scales of thickness, 50-1000 Å. These models have described the rate of reaction in terms of linear, parabolic, cubic, quartic, logarithmic, or inverse logarithmic time-dependences. Furthermore, different models and assumptions may give rise to the same time-dependence. For example, oxidation can be described by a logarithmic rate law if any of the following processes are assumed to be rate-controlling: quantum mechanical electron tunnelling, cationic diffusion in a large space field, O incorporation into the metal, or deactivation of the oxide surface for chemisorption as the oxide scale thickness increases.

All of these models for oxidation have been derived under the assumption of low to intermediate temperatures and low O pressures. At elevated temperatures and pressures oxide layers grow to > 0.1 μm thickness very rapidly and the assumptions underlying the above models are not believed to be relevant to further growth of the oxide scale.

Under these new conditions the rate at which oxidation proceeds has generally been observed to be dependent linearly or parabolically on the duration of oxidation according to equations of the form:-

$$w = k_l t + c$$
$$w^2 = k_p t + c \qquad \} \ 2.1$$

where w represents the extent of oxidation at time t, k is a rate constant, and c is a constant which takes account of the initial reaction.

If diffusion of one or both of the reacting species (M or O) across the oxide scale to the reaction zone is assumed to be the rate-controlling process in the oxidation reaction, the time-dependence of the oxidation is observed to be parabolic. This conclusion was first derived theoretically by Wagner [1933].

A linear time-dependence is usually attributed to rate-control by phase-boundary reactions. In this case the necessarily rapid diffusion of the reacting species may be facilitated by a porous oxide caused by mechanical failure, vacancy condensation or scale evaporation.

2.1.3. Temperature-dependence of the rate of oxidation

The activation energy, Q, of oxidation may be measured by reference to the temperature-dependence of the rate constant of oxidation, k (equation 2.1). The temperature-dependence is usually of the form

$$k(T) = k_o \exp(-Q/RT) \qquad 2.2$$

where k_o is a constant and R is the gas constant. This form of temperature-dependence arises due to the temperature-dependence of the rate-controlling mechanism in the oxidation process. In the case of diffusion-controlled reactions this may be the transition probability of atomic jumping or the number of lattice defects facilitating diffusion, both of which have exponential temperature dependencies.

By experimentally determining the activation energy of oxidation, the species whose diffusion rate-controls the oxidation process can often be determined by reference to independent, controlled experiments.

2.2. The oxidation of β Si_3N_4 and β' Si-Al-O-N Ceramics

2.2.1. "Passivity" in oxidation

The thermal oxidation of silicon nitride may take place with concurrent weight gain or weight loss depending on the temperature and oxygen potential during oxidation. "Active" oxidation is characterised by specimen weight loss due to the development of a gaseous oxide species according to reactions of the type

$$Si_3N_4\ (s) + 3\ SiO_2\ (s) \rightarrow 6\ SiO\ (g) + 2N_2\ (g)$$

and

$$2Si_3N_4\ (s) + 2O_2\ (g) \rightarrow 6\ SiO\ (g) + 4N_2\ (g)$$

[Signhal 1976a]. "Passive" oxidation results in the formation of a solid oxide product at higher oxygen potentials according to reactions of the type

$$Si_3N_4 + 3O_2 \rightarrow 3\ SiO_2 + 2N_2 \qquad 2.3$$

The transition pressure between the two regimes can be calculated for a given temperature of oxidation by using a thermodynamic argument developed by Wagner [1958]. The transition pressure for the oxidation of silicon nitride as a function of oxidising temperature as calculated using the Wagner model by Singhal [1976b] is presented in figure 2.2.

Experimentally, the transition pressure for Si_3N_4 hot-pressed with MgO has been observed to occur at oxygen partial pressures of $< 10^{-7.3}$ atm for oxidation at 1400°C [Tripp and Graham 1976] and at $\sim 10^{-5.3}$ atm for oxidation at $\sim$ 1100°C [Sheehan 1982]. These pressures are near

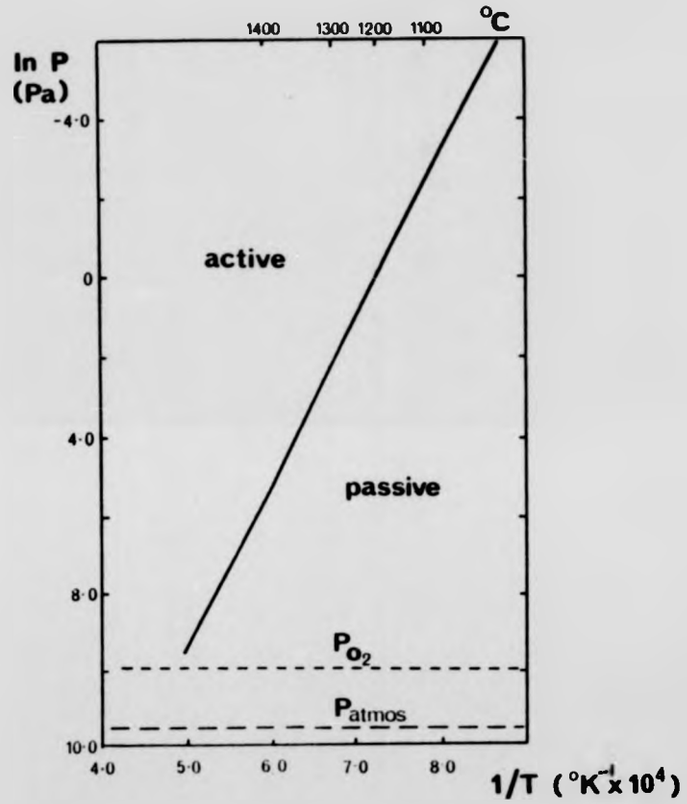

Figure 2.2: Calculated 0_2 partial pressures for the transition from active to passive oxidation of Si_3N_4 [Singhal 1976b].

to or rather below those predicted by Singhal and are considerably lower than the partial pressure of O_2 in the atmosphere [Zucrow 1976]. The oxidation of Si_3N_4 at or about atmospheric pressure in the temperature range 700° - 1400°C has therefore been observed to occur in a passive manner with the formation of a thick oxide scale. The transition pressure for the oxidation of β′ Si-Al-O-N is not known but may be expected to be similar to that of β Si_3N_4 at least at low substitution levels.

At the high oxygen potentials which prevail under normal oxidation conditions the oxidation of β′ Si-Al-O-N ceramics has been observed to occur with the development of a thick oxide layer according to a reaction of the type

$$Si_{6-z}Al_zO_zN_{8-z} + (6 - \tfrac{3z}{4})\,O_2 \rightarrow (6 - z)SiO_2 + \tfrac{z}{2}\,Al_2O_3 + \tfrac{8-z}{2}\,N_2 \qquad 2.4$$

[Desmaison et al 1983]. Under normal atmospheric conditions thick oxide films $\geq$ 500 Å are formed rapidly at elevated temperatures and the oxidation behaviour is therefore described by the "thick-film" conditions of section 2.1.3. Reaction (2.3) has been observed to occur at temperatures as low as 700°C in hot-pressed Si_3N_4 [Kiehle et al 1975], although, in general, the rate of oxidation of β Si_3N_4 and β′ Si-Al-O-N ceramics is reported to be very low at temperatures < 900°C.

Despite the partial release of N as N_2 molecules to the atmosphere the formation of an oxide layer involves an increase in specimen weight over that of the unreacted material. This change in weight allows the rate of oxidation of β Si_3N_4 and β′ Si-Al-O-N ceramics to be monitored by the change in weight of the specimens on oxidation. This has usually been achieved by the use of the technique of continuous

thermogravimetry in which the weight of the specimen is continuously monitored during oxidation. The alternative method of weighing specimens before and after oxidation is costly in terms of material used. It is also usually desirable to ensure continuous oxidation at temperature since spalling of the oxide scales of Si_3N_4 and Si-Al-O-N ceramics has been observed on thermal cycling into and out of the oxidation regime [Dutta 1982]. In addition, changes in the structure of the scale induced by specimen cooling and reheating, such as cracking due to thermal expansion mismatch between the scale and the ceramic or cooling-induced scale phase changes, may lead to changes in the rate of oxidation on continuation. Consolidation of the porous scale of a hot-pressed Si_3N_4 ceramic, for example, has been shown to cause a marked increased in the oxidation resistance of the material [Quackenbush and Smith 1980].

2.2.2. The oxidation of porous ceramics

Ceramics such as reaction-bonded Si_3N_4 in which there is a residual interconnected porosity display anomalous oxidation behaviour. The extent of oxidation does not increase continuously as the temperature of oxidation is increased. Rather, the behaviour illustrated in figure 2.3 is typical of the oxidation of these materials.

Low-temperature oxidation proceeds by the continuous internal oxidation of the material by atmospheric penetration into the internal cavities in addition to the oxidation of the external surface [Evans and Davidge 1970]. The oxidation rates at low temperatures and in the initial stages of high temperature oxidation follow parabolic rate laws [Warburton et al 1978, Mayer and Riley 1978], and parabolic rate constants, kp (equation 2.1) can be determined for the reaction. Figure 2.4 summarises the parabolic rate constants determined for the oxidation of a variety of Si_3N_4 ceramics. The low-temperature rate of

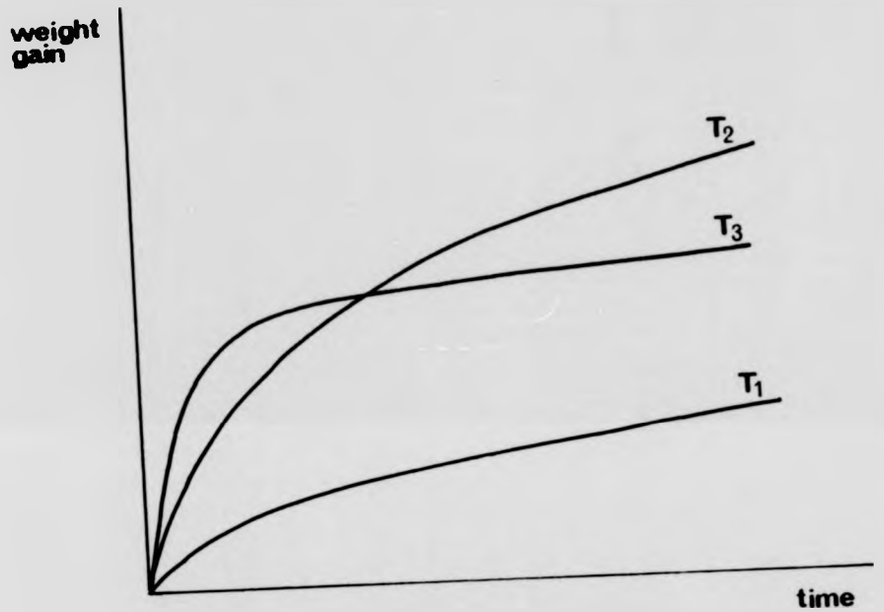

Figure 2.3: Oxidation kinetics of reaction-bonded Si_3N_4 ($T_3 > T_2 > T_1$)

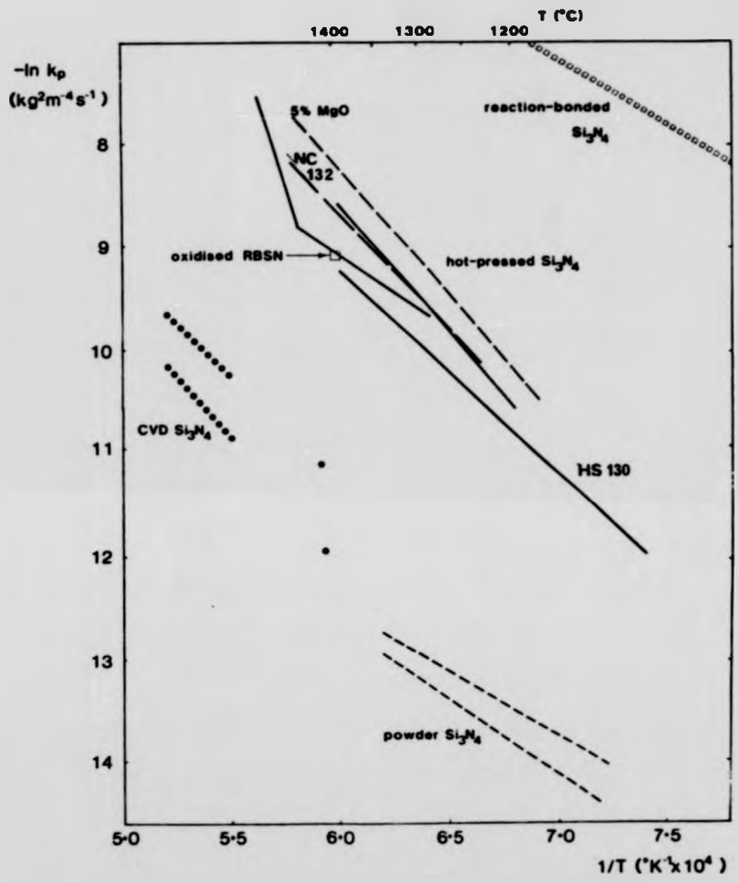

Figure 2.4: Parabolic rate constants of oxidation of Si_3N_4 ceramics [Horton 1969, Singhal 1976a, Singhal 1976c, Tripp and Graham 1976, Schlicting and Gauckler 1977, Cubicciotti and Lau 1978, Mayer and Riley 1978, Barlier and Torre 1979, Hirai et al 1980, Quackenbush and Smith 1980].

oxidation of reaction-bonded ceramics is very much greater than that of more dense ceramics such as the hot-pressed form. This is due to the very much greater reaction surface area presented by the internal surfaces of the interconnected porosity. The surface area of reaction-bonded material has been estimated to be as high as 12,000 m^2kg^{-1} [Mayer and Riley 1978], some 10^5 times greater than the external surface of the material. In consequence the reaction rate constants are very much greater than the nominally-pure dense materials such as powdered Si_3N_4 or CVD Si_3N_4 (figure 2.4). Oxidation occurs throughout the pore network and up to 70% of the material may be converted to the oxide if oxidation is allowed to continue for long periods at sufficiently low temperatures [Warburton et al 1978].

The non-parabolic high-temperature oxidation behaviour does not imply a breakdown in the diffusional-control of the oxidation process. The dramatic improvement in the material's oxidation resistance at the "knee" of the high temperature oxidation curve (figure 2.3) is due to the closure of surface porosity due to the development of a coherent oxide layer at the external surface of the material. The formation of this layer inhibits further rapid diffusion of oxygen to the internal surfaces [Evans and Davidge 1970].

The oxidation behaviour becomes parabolic again once a coherent surface layer has formed [Davidge et al 1972]. The reaction surface area has fallen several orders of magnitude at this stage. The rate of oxidation falls to a similar value to that observed for fully dense ceramics (figure 2.4) [Barlier and Torre 1979].

2.2.3. The oxidation of dense ceramics

Dense silicon nitride materials ($\geq$ 95% of theoretical density) oxidise primarily at their external surface. Oxidation kinetics are commonly, but not exclusively, reported to be of the form:-

$$w^2 + \Delta w = k_p t + c$$

[Horton 1969]. The second term in this equation is usually observed to be negligibly small within several minutes on oxidation at temperatures > 1000°C. Materials displaying this parabolic behaviour include hot-pressed β Si_3N_4 and β′ Si-Al-O-N, powdered Si_3N_4 and CVD Si_3N_4. The rate of oxidation and the activation energy for oxidation vary widely depending on the composition of the material, especially with regard to the type and quantity of its hot-pressing aids and accidental impurity elements. The rates of oxidation have been summarised in terms of the parabolic rate constants, kp, in figures 2.4, 2.5 and 2.6, and the reported activation energies are tabulated in Table 2.1. Also noted in Table 2.1 is the time-dependence of the rate of oxidation summarised in terms of an oxidation exponent, n, from the equation $w^n = kt$ where w represents the extent of oxidation at time t and k is a rate constant.

(a) β Si_3N_4

The oxidation of nominally pure, dense β Si_3N_4 has been observed to be diffusion-controlled by one of the species engaging in reaction 2.2. The various possible diffusing species are illustrated in figure 2.7. Diffusional rate control has been inferred from the parabolic form of the rate of oxidation of powdered Si_3N_4 [Horton 1969] and CVD Si_3N_4 [Hirai et al 1980]. The rate of reaction has been found to be markedly dependent on the nature of the oxide layer. It was found that a change in the nature of the oxide layer from an amorphous to a partially crystalline form resulted in a change in the apparent activation energy for oxidation [Horton 1969]. Diffusion-controlled oxidation of these nominally-pure ceramics has only been observed as long as the oxide scale was compact and pore-free. A

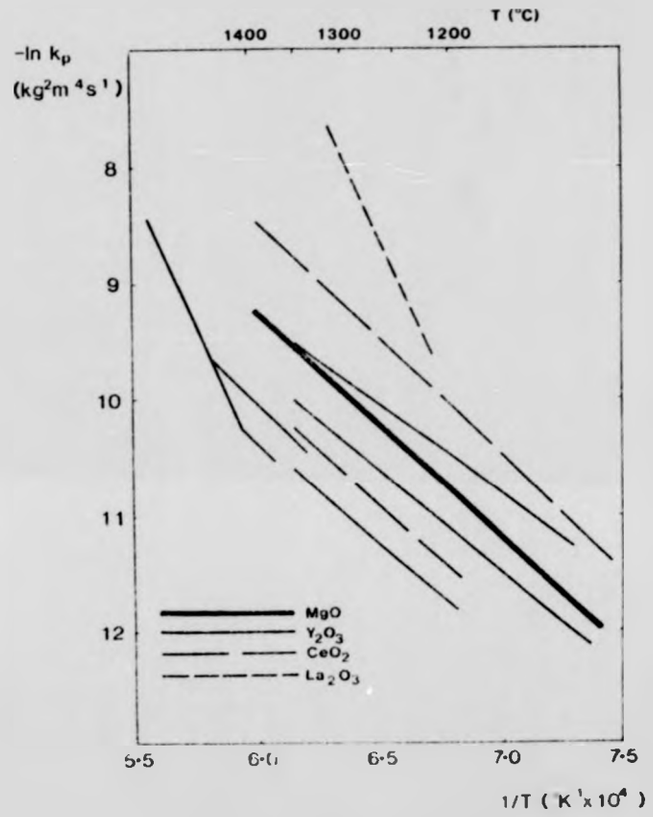

Figure 2.5: Parabolic rate constants of oxidation of hot-pressed β Si_3N_4 ceramics. [Singhal 1976a, Schlicting and Gauckler 1977, Cubiciotti and Lau 1979, Quackenbush and Smith 1980, Babini et al 1981].

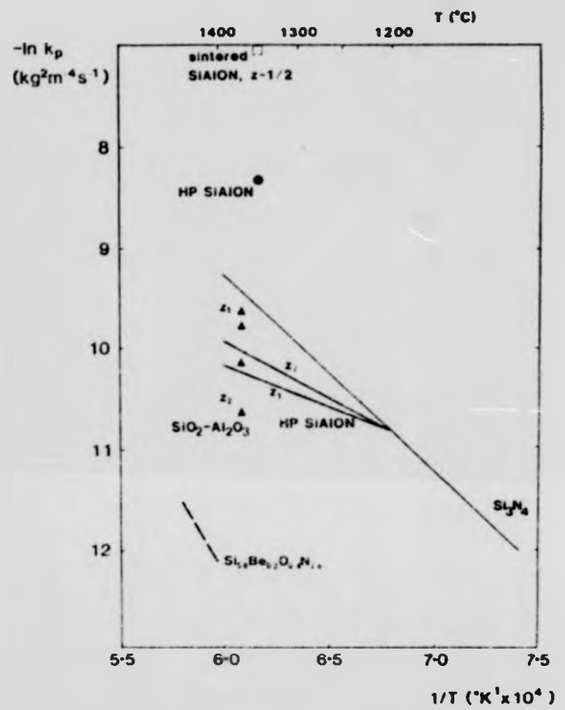

Figure 2.6: Parabolic rate constants of oxidation of Si-Al-O-N ceramics (substitution level, $Z_2 > Z_1$).
[Singhal 1976a, Schlicting and Gauckler 1977, Singhal and Lange 1977, Lewis and Barnard 1980, Palm and Greskovich 1980].

Table 2.1.

Characteristics of oxidation of β Si_3N_4 and β′ Si-Al-O-N ceramics

Material	Additive	Temperature (°C)	Atmosphere	Pressure (atm)	Oxidation exponent, n	Activation energy, Q (kJ mol^{-1})	Reference
HS 130	MgO	1300 - 1350	dry O_2	0.2	2	293	Tripp & Graham 1976
HS 130	MgO	1000 - 1400	dry O_2	1	2	375	Singhal 1976a
		1200 - 1400	wet O_2	1	2	488	
NC 132	MgO	1405	air	1	2→8	-	Palm & Greskovich 1980
NC 132	MgO	1250 - 1450	dry O_2	0.16	2	440	Cubicciotti and Lau 1978
HPSN	MgO	1000 - 1200	air	1	2	469	Schlicting & Gauckler 1977

Table 2.1. (Cont.)

Material	Additive	Temperature	Atmosphere	Pressure	Oxidation exponent	Activation energy	Reference
NC X34	Y_2O_3	1370 - 1520	dry O_2	0.20	2	980 (high T) 450 (low T)	Cubicciotti and Lau 1979
HPSN	Y_2O_3	900 - 1350	air	1	2, $T>T_c$ 1, $T<T_c$	327	Quackenbush and Smith 1980
HPSN	Y_2O_3 + MgO	920 - 1385	air	1	2	120 (low T) 580 960 (high T)	Babini et al 1983
HPSN	CeO_2	700 - 1400	dry air	1	2	385	Babini et al 1981
HPSN	CeO_2	900 - 1350	air	1	2, $T>T_c$ 1, $T<T_c$	327	Quackenbush and Smith 1980
HPSN	La_2O_3	1000 - 1400	air	1	2	883	Schlicting and Gauckler 1977

Table 2.1. (Cont.)

Material	Additive	Temperature	Atmosphere	Pressure	Oxidation exponent	Activation energy	Reference
Si_3N_4 powder	-	1065 - 1340	dry air	1	2	255	Horton 1969
			dry 0_2	1	2	285	
CVD Si_3N_4	-	1550 - 1650	dry 0_2	1	2	390 (C) 460 (A)	Hirai et al 1980
CVD Si_3N_4	-	1100 - 1300	-	-	1	∿140	Billy 1983
β´Si-Al-0-N	-	1450 - 1619	-	-	1	-	Desmaison & Riley 1981
β´Si-Al-0-N	-	1200 - 1400	air	1	2	102 - 147	Schlicting & Gauckler 1977
β´Si-Al-0-N	-	1000 - 1400	-	-	-	147	Billy 1983

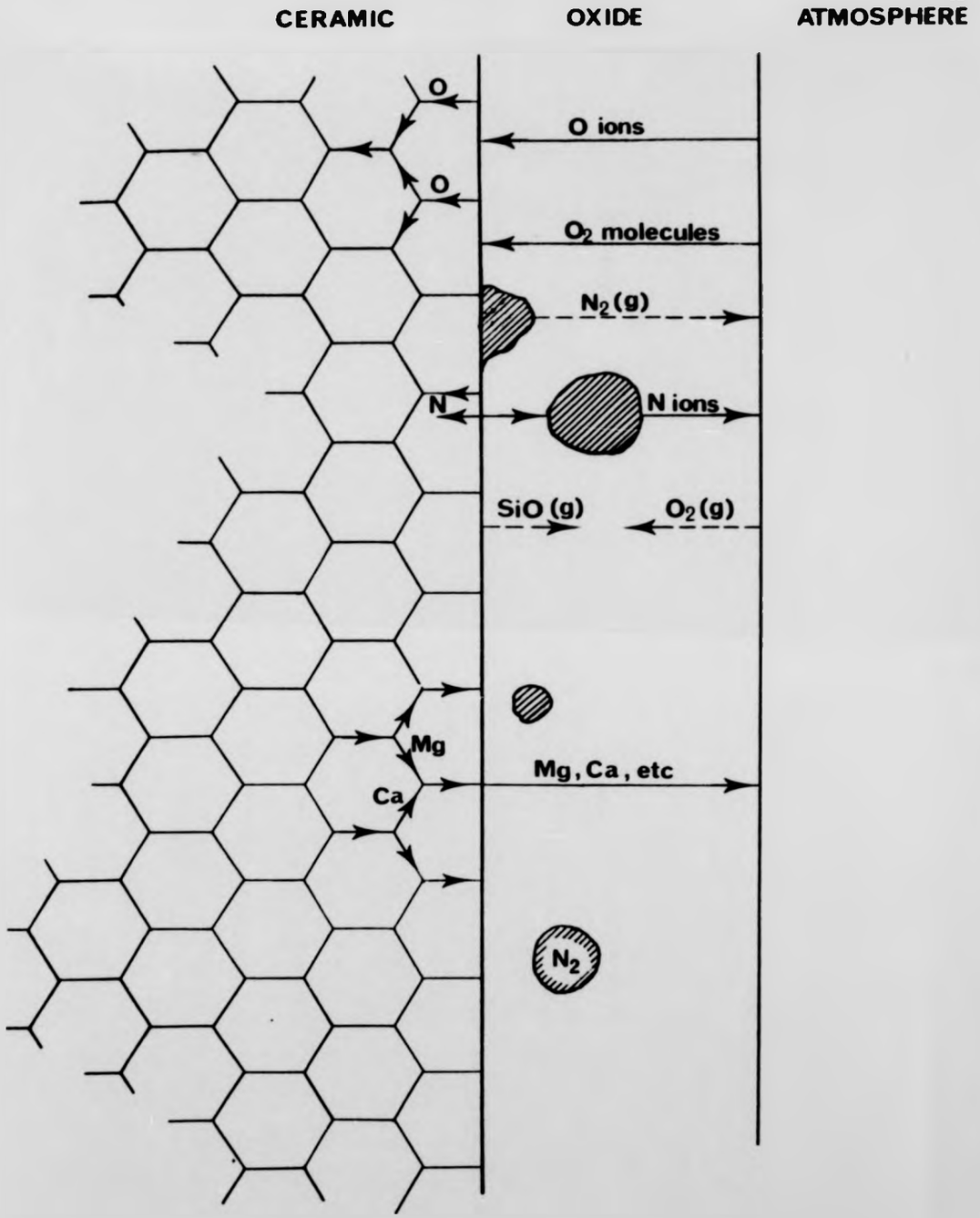

Figure 2.7: Diffusing species accompanying oxidation of β Si_3N_4

porous oxide layer resulted in linear oxidation kinetics [Hirai et al 1980]. These observations both support the contention that oxygen diffusion through the oxide scale is the rate-controlling step in the oxidation of nominally pure, dense silicon nitride, despite the wide differences in the activation energies of oxidation which have been reported (Table 2.1).

The oxidation kinetics of fully-dense, additive-containing, hot-pressed β Si_3N_4 have also usually been observed to be parabolic in nature (Table 2.1), indicating diffusional rate-control. As was the case for the nominally pure materials the rate of oxidation has been observed to be dependent on the structural nature of the oxide scale. A change in the apparent activation energy for oxidation of a MgO hot-pressed ceramic (figure 2.4), for example, was attributed to the melting of crystalline oxide phases, giving rise to an increased coefficient of diffusion for the rate-controlling species [Tripp and Graham 1976]. A similar change in the rate of oxidation of a Y_2O_3 hot-pressed ceramic (figure 2.5) was attributed to increased mechanical disruption of the oxide at higher temperatures [Cubicciotti and Lau 1979]. It is therefore believed that the oxidation of additive-containing hot-pressed β Si_3N_4 is rate-controlled by the diffusion of an atomic species through the oxide.

The structure of the oxide scale is itself heavily dependent on its constituent chemical species. On oxidation the grain-boundary segregated additive and impurity cations have been observed to collect in very large quantities in the oxide layer [Billy 1983, Singhal 1976a, Cubicciotti et al 1977, 1978, 1979, Kiehle et al 1975, Tripp and Graham 1976, Schlicting and Gauckler1977, Wu et al 1981, Clarke and Lange 1980, Lange 1978b, Williams and Tennery 1979, Das et al 1982, Babini et al 1981, 1983]. For example, the oxide scale formed on a

magnesia hot-pressed β Si_3N_4 was reported to be composed of up to 26% Mg [Tripp and Graham 1976]. This diffusion is due to the formation of a diffusion couple between the initially pure SiO_2 oxide scale and the impurity-containing grain boundary phase. Rapid atomic transport is facilitated by the structural irregularity of the additive and impurity element-containing grain boundary regions. The presence of large quantities of such elements as Mg, Ca, Fe, Na and Fe is believed to be the cause of the partial crystallisation of a liquid oxide scale to cristobalite at temperatures as low as 750°C [Kiehle et al 1975]. Their presence also leads to the formation of higher silicate phases. In MgO hot-pressed β Si_3N_4 enstatite ($MgSiO_3$) is the phase most commonly observed in addition to crystalline silica [Kiehle et al 1975, Singhal 1976a, Cubicciotti & Lau 1978, Clarke & Lange 1980]. Higher silicates such as forsterite (Mg_2SiO_4) have been less commonly observed [Clarke and Lange 1980, Kiehle et al 1975], and akermanite (Ca_2MgSiO_3) and diopside ($Mg\ Ca\ (SiO_2)_3$) have only been reported for a material containing a relatively high level of Ca impurity [Kiehle et al 1975]. The rate of oxidation is therefore dependent on the nature and amount of the hot-pressing aid employed, the rate of oxygen transport across the oxide scale being dependent on its viscosity and extent of crystallisation.

Increased quantities of such viscosity-reducing ions as Mg or Ca in the partially-amorphous SiO_2 oxide layer gives rise to a much higher oxidation rate for the additive-containing materials than was observed for the nominally pure materials (figure 2.4). Although this may suggest that the oxidation is rate-controlled by the diffusion of an atomic species through the oxide layer an alternative mechanism may be that of the dissolution of the β phase in the glassy oxide. It is known that the rate of dissolution of Si_3N_4 in a slag glass

increases with increasing quantities of MgO in the glass [Dancy and Jansen 1976]. The dependence of the rate of oxidation on the quantity of various sintering aids in the as-pressed material is summarised in figure 2.8. The rate of oxidation has been observed to increase continuously with increasing quantities of MgO [Wu et al 1981] as expected from increasing solubility of Si_3N_4 in the oxide or decreasing viscosity of the oxide scale. The oxidation resistance of Y_2O_3-sintered β Si_3N_4 is dependent on which phases form on oxidation and on the melting point of the grain-boundary crystalline yttria oxynitride phases whose composition reflects the quantity of hot-pressing aid present in the material [Babini et al 1983]. There is no change in varying the amount of CeO_2 in the ceramic due to there being no change in the nature of the oxide [Babini et al 1981]. This is probably also the case for the ZrO_2-fluxed ceramic.

(b) Activation energies of oxidation

The reported activation energies for oxidation of dense β Si_3N_4 vary widely (Table 2.1). Some activation energies for diffusion of oxygen and metallic cations in silicate materials are listed in tables 2.2 and 2.3. These activation energies, determined from independent experiments, also vary widely according to the diffusing species, host material and method of measurement. Some authors have attributed the high activation energies of oxidation to rate control by metallic ion diffusion through the oxide scale [Singhal 1976a] and others low activation energies to rate control by oxygen diffusion through the oxide [Billy 1983]. In view of the complexity of the oxide, the variously high and low activation energies reported for the oxidation of nominally-pure CVD Si_3N_4 (see table 2.1), and the wide variation in the reported values of the diffusion coefficients

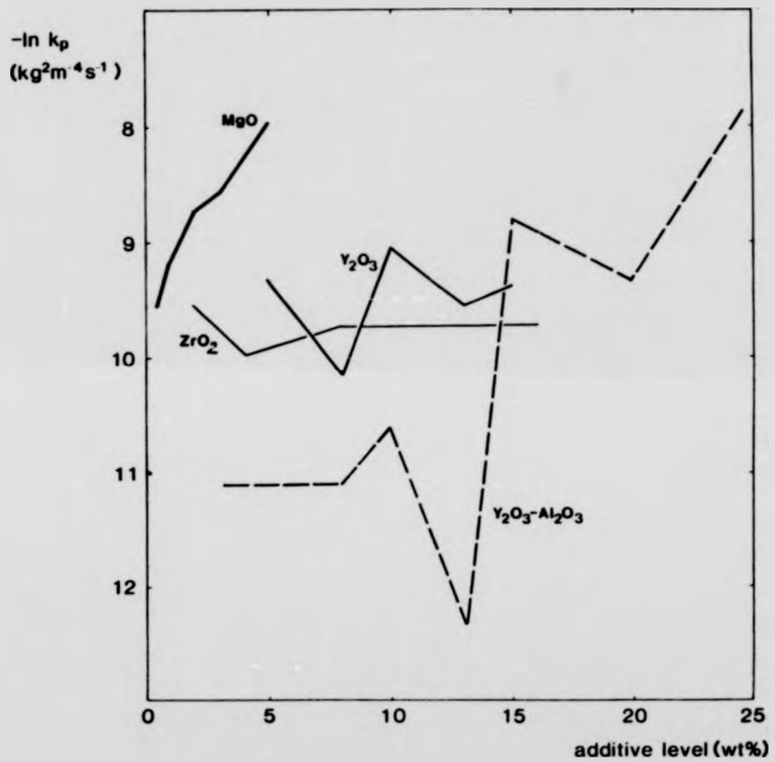

Figure 2.8: Rate constants of oxidation of Si_3N_4 hot-pressed with additive oxides. [Quackenbush and Smith 1980, Wu et al 1981].

Table 2.2

Activation energies of diffusion of O in silicates at ~ 1350°C

	Material	Activation energy, Q ($kJ\ mol^{-1}$)	Notes	Reference
Melts	SiO_2	~ 100		Schaeffer 1980
		121	Extrapolated from 1250°C	Williams 1965
		298	Extrapolated from 1225°C	Sucov 1963
	0.10 Al_2O_3.0.90 SiO_2	250		Ueda & Oishi 1970
Polycrystals	MgO	252		
		233	well-sintered	Freer 1980
		426	loosely-sintered	
	Mg Al_2O_4	384		Freer 1980
Single Crystals	Mg_2SiO_4	377		Hallwig et al 1981
	Mg Al_2O_4	440		Ando & Oishi 1974
		415		Reddy & Cooper 1981

Table 2.3

Activation energies of diffusion of cations in silicates at ~ 1350°C

	Diffusant	Host	Activation energy, Q ($kJ\ mol^{-1}$)	Notes	Reference
Melts	M cation	$CaO.SiO_2$	142	from electrical conductivity	Bockris et al 1948
		0.55 CaO.0.45 SiO_2	147	from electrical conductivity	Bockris et al 1948
	Ca	$CaO-Al_2O_3-SiO_2$	249		Terai & Hayami 1975
		$CaO-Al_2O_3-SiO_2$	296		Oishi et al 1982
		0.40 CaO.0.20 Al_2O_3 0.40 SiO_2	306		Towers et al 1953
Polycrystals					
	Ca	SiO_2	460		Brown and Mackenzie 1982
	Mg	MgO	331	extrapolated from 1400°C	Lindner and Parfitt 1957
	Mg	MgO	230	from electrical conductivity	Mackenzie and Ryan 1981
	Mg	$MgAl_2O_4$	175	from electrical conductivity	Mackenzie and Ryan 1981
	Ca	Ca_2SiO_4	272		Freer 1981
	Ca	$Ca_3Si_2O_7$	242		Freer 1981
	Ca	SiO_2	284		Freer 1980
	Mg	Mg_2SiO_4	373		Freer 1981
	Mg	Mg_2SiO_4	173		Freer 1981
	M vacancies	$MgAl_2O_4$	208	from electrical conductivity	Weeks and Sander 1980

for ions in silicates it is not believed that determination of the activation energy for oxidation of silicon nitride ceramics allows unambiguous determination of the rate-controlling mechanism of oxidation.

(c) Short-term subscale diffusional control

It has been suggested that the oxidation of magnesia hot-pressed Si_3N_4 (NC 132) is rate-controlled by a mechanism other than that of diffusion through the oxide scale of one of the species engaged in the oxidation reaction (equation 2.2) [Cubicciotti and Lau 1979]. The rate of oxidation of this material after removal of the scale which had formed on oxidation at 1370°C for 24 h was similar to that which had been observed immediately prior to its removal (figure 2.9 (a)). It was claimed that under these circumstances diffusion of an oxidising species through the oxide could not have been rate-controlling. The oxide was therefore said to be "non-protective". Similar, partly-protective, behaviour was observed for the oxidation of a ceramic hot pressed with Y_2O_3 (figure 2.9 (b)) [Cubicciotti and Lau 1979].

The rate-controlling process in the parabolic oxidation of the magnesia-containing material was attributed to the outward diffusion of magnesia from the bulk of the ceramic into the oxide, in which the β Si_3N_4 dissolved according to the reaction

$$^1/3\ Si_3N_4 + Mg^{2+} + 3O^{2-} \rightarrow MgSiO_3 + {}^4/3\ N^{3-}$$

accompanied by the reaction

$$^3/2\ O_2 + {}^4/3\ N^{3-} \rightarrow 3O^{2-} + {}^4/3\ N_2.$$

These reactions and the accompanying atomic diffusion are summarised in figure 2.10.

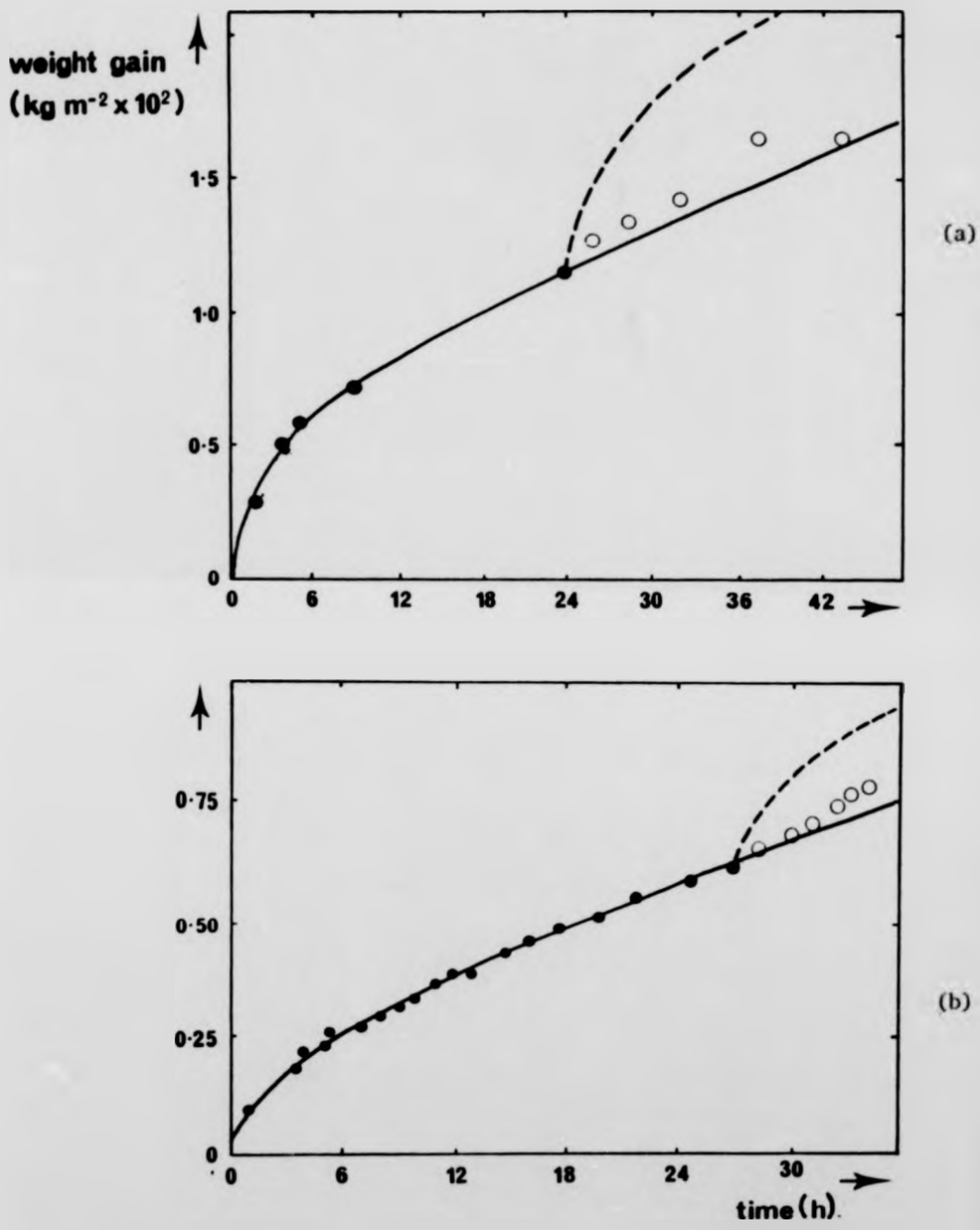

Figure 2.9: Kinetics of oxidation of β Si_3N_4 hot-pressed with (a) MgO (b) Y_2O_3 [Cubicciotti and Lau, 1978, 1979].

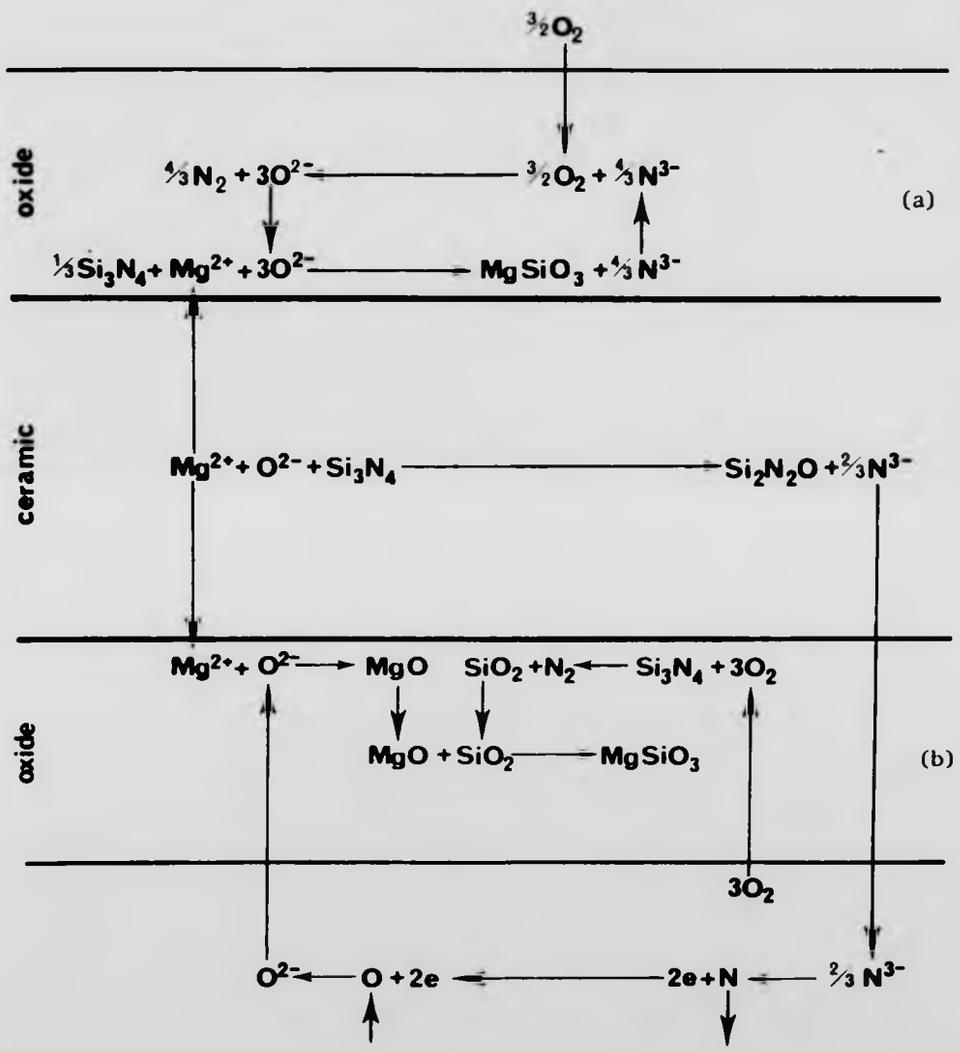

Figure 2.10: Diffusion and reaction processes in the oxidation of Si_3N_4 hot-pressed with MgO. (a) Cubiciotti and Lau 1978 (b) Clarke and Lange 1980.

The rate controlling effect of magnesia was attributed to the dependence of the rate of solubility of Si_3N_4 in the MgO-fluxed scale on the quantity of MgO in the oxide. Enhanced solubility of Si_3N_4 in regions of high scale metallic ion content is supported by the observations that increased oxidation occurs at sites of grain boundary /surface intersections in MgO hot-pressed ceramics [Schlicting and Gauckler 1977] and at regions of high CaO content in CeO_2 hot-pressed material [Babini et al 1981].

A similar, but more sophisticated, model for oxidation rate-control by subscale diffusion has been presented in which it was suggested that the out-diffusion of Mg is accompanied by the out-diffusion of N with internal oxidation to Si_2N_2O according to the reactions

$$Mg^{2+} + O^{2-} \rightarrow Si_3N_4 \rightarrow Si_2N_2O + {}^{2}/_{3}\, N^{3-}$$

$$Mg^{2+} + O^{2-} \rightarrow MgO$$

$$MgO + SiO_2 \rightarrow MgSiO_3.$$

(The internal oxidation of Mg hot-pressed ceramics to form Si_2N_2O has been confirmed by independent experiments [McDonough et al 1981]). These reactions and the accompaying diffusion processes are also illustrated schematically in figure 2.10. It was proposed that the oxidation rate was enhanced over that of unfluxed ceramics due to Mg providing an additional diffusive flux [Clarke and Lange 1980].

However, the experiments giving rise to these conclusions were conducted within a period of continuous oxidation of $\leq$ 40 h. The rate of oxidation of NC 132 material has been found to become apparently more protective than parabolic on oxidation at 1405°C for periods in excess of $\sim$ 30 h [Palm and Greskovich 1980] (figure 2.11). Long term oxidation (> 300 h) of an MgO hot-pressed material

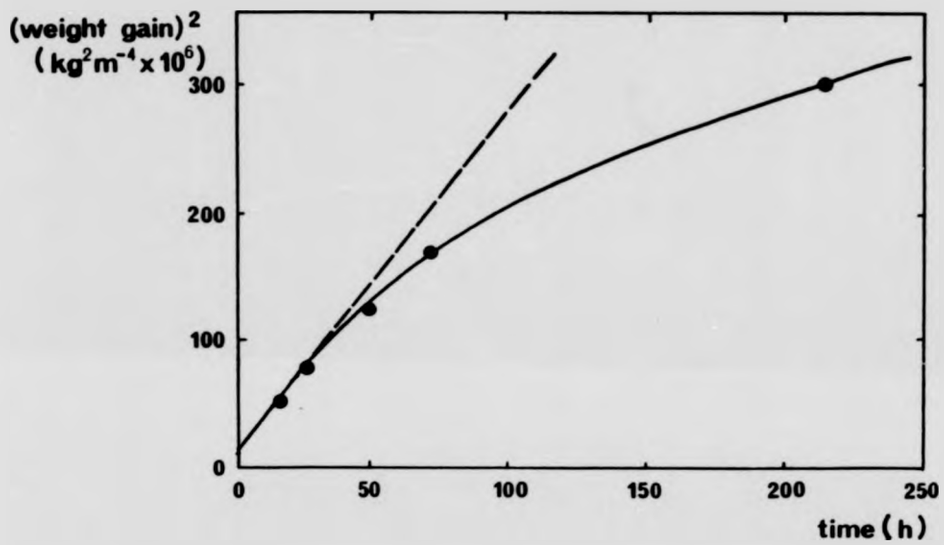

Figure 2.11: Non-parabolic long-term kinetics of oxidation of Si_3N_4 hot-pressed with MgO [Palm and Greskovich 1980].

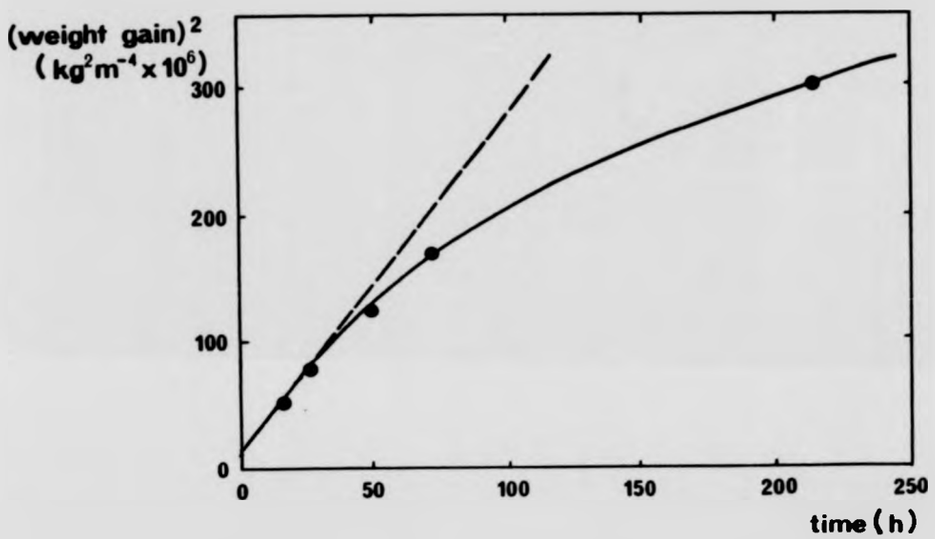

Figure 2.11: Non-parabolic long-term kinetics of oxidation of Si_3N_4 hot-pressed with MgO [Palm and Greskovich 1980].

at 1375°C also gave rise to increased protectivity [Lange 1978b]. In view of these observations and those made in this study it is believed that the apparently "non-protective" nature of the oxidation of Mg-containing β Si_3N_4 is a short term phenomenon related directly to compositional modifications of the oxide caused by the out-diffusion of additive and impurity elements from the grain boundaries of the ceramic (see Chapter 4).

(d) β′ Si-Al-O-N

The rates of oxidation of fully dense single-phase β′ Si-Al-O-N ceramics and of multiphase β′ ceramics produced by hot-pressing mixtures of Al_2O_3 and SiO_2 are summarised in terms of their parabolic rate constants, kp, in figure 2.6. The oxidation rate of material hot pressed from a mixture of Al_2O_3 and Si_3N_4 which contained large quantities of X-phase was slightly lower than that of MgO hot-pressed silicon nitride (figure 2.6) [Singhal and Lange 1977]. The oxidation resistance of this material increased with increasing Al_2O_3/SiO_2 ratio. In contrast, the oxidation resistance of a series of compositions corresponding to β′ Si-Al-O-N decreased as the substitution level increased [Schlicting and Gauckler 1977] (fig. 2.6), but was also lower than that observed for HPSN. The oxidation rate of another β′ Si-Al-O-N hot-pressed with magnesia was markedly higher than that of the magnesia hot-pressed Si_3N_4 (figure 2.6) [Lewis and Barnard 1980]. Furthermore, the oxidation rate of powdered β′ Si-Al-O-N of substitution level $z \sim 3$ was found to be higher than that of silicon nitride powder of β/α ratio ∿ 4.9 [Brossard et al 1979].

The oxidation kinetics of all these materials was of parabolic form. The low-resistance magnesia hot-pressed ceramic

was found to display the "non-protective" behaviour described above for magnesia hot-pressed Si_3N_4. However, an observed activation energy of $\sim$ 100-150 kJ mol^{-1} for the oxidation of β' Si-Al-O-N was believed to indicate that the diffusion of oxygen through the oxide was the rate controlling process [Billy 1983]. Unlike the case of the oxidation of the dense silicon nitride ceramics a change in the oxide of β' Si-Al-O-N material from glassy to partially crystalline was reported not to affect the activation energy of oxidation [Billy 1983].

Linear, or paralinear, oxidation kinetics have been reported for the oxidation of β' Si-Al-O-N ceramics of substitution level $z = 0.75$ which were hot-pressed without the use of a densification aid [Desmaison and Riley 1981, Desmaison et al 1983]. The rate-controlling step was assumed to be the inward diffusion of oxygen through the oxide to the ceramic/oxide scale where the oxidation reaction took place. The paralinear kinetics were believed to be due to local variations in the ease with which oxygen could diffuse to the reaction zone due to such features as local porosity, N_2 gaseous bubbles and fissures in the oxide. The paths available to oxygen according to this model are illustrated schematically in figure 2.12. Enhanced oxidation rates are to be expected if easy access to the reaction zone is available for the reacting species.

2.3. The present work

The present work was undertaken in part in order to compare the oxidation kinetics of hot-pressed β' Si-Al-O-N ceramics and to define the mechanism of their oxidation. In particular:

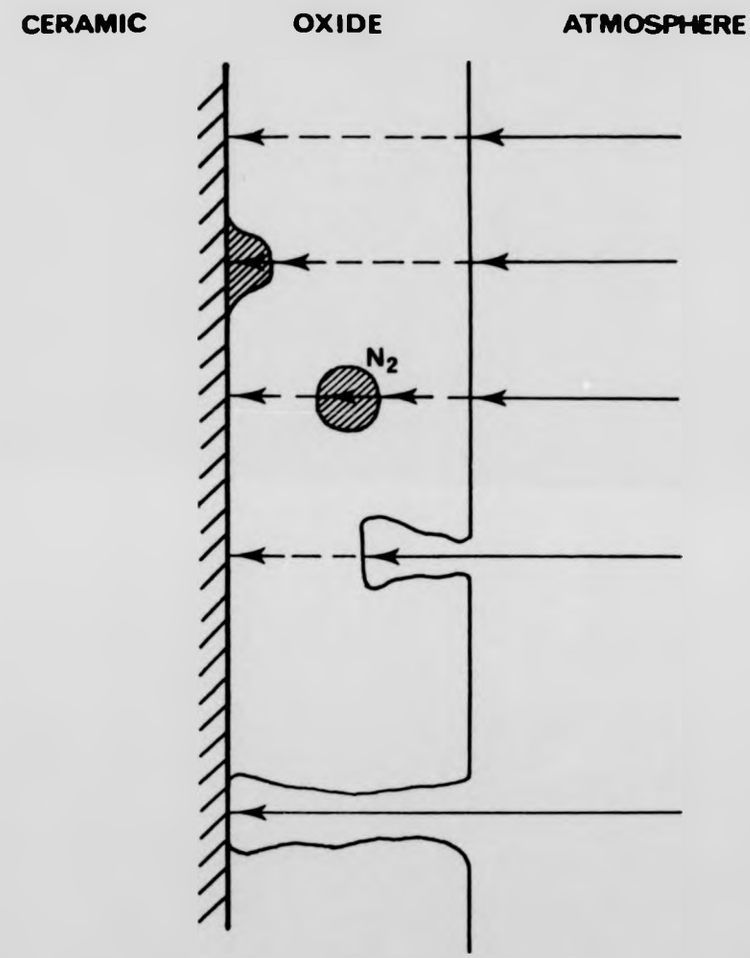

Figure 2.12: Oxygen diffusion paths in the oxidation of silicon nitride ceramics [Desmaison et al 1983].

(1) the relative oxidation resistance of β′ Si-Al-O-N ceramics was to be defined with respect to the substitution level of the β′ phase and their additive chemistry.

(2) the importance of short-term processes such as the subscale diffusional control observed in the oxidation of hot-pressed β Si_3N_4 in the oxidation of β′ Si-Al-O-N s was to be determined. The mechanism of operation of these processes was to be defined.

(3) the relative importance of the mechanisms by which modifications to the grain boundary regions takes place on oxidation was to be defined. These mechanisms determine the time-dependence of the oxidation of the ceramics [Lewis and Barnard 1980]. They are also particularly relevant to the time-dependence of the mechanical deformation of low substitution level β′ Si-Al-O-N ceramics [Karunaratne 1980].

Part Three: Mechanical properties

An understanding of their high-temperature deformation and fracture mechanisms has been of primary importance in the development of silicon nitride and related ceramics in view of the demanding physical environment of their intended use. This section surveys the creep and fracture behaviour of ceramics and outlines appropriate mechanical deformation techniques before reviewing the creep behaviour of hot-pressed silicon nitride and Si-Al-O-N ceramics.

3.1. Fracture and creep of ceramics

Ceramic materials are characterised by their lack of ductility due to the limited number of slip systems available for dislocation glide. The fracture of ceramics therefore usually occurs in a brittle

manner from macroscopic flaws such as pores, inclusions or machining-related defects. These flaws enhance the local stress to a value which is determined by the size, shape and orientation of the flaw and the elastic modulus and thermodynamic surface energy of the material. For example, an edge crack of length a in a semi-infinite material stressed in uniform tension (figure 2.13a) enhances the applied stress, σ_o, to a value σ given by

$$\sigma = \sigma_o \, 2\sqrt{\frac{a}{\rho}}$$

where ρ is the radius at the crack tip [Davidge and Evans 1970]. Failure occurs when σ reaches the value of the fracture stress, σ_f.

Alternatively, the failure criterion may be expressed as the point when the strain energy released on opening of the crack exceeds the energy required to form the new surfaces which are generated [Griffith 1920]. For a flaw of general shape and orientation, the failure stress is

$$\sigma_f = \frac{1}{Y}\sqrt{\frac{2E\gamma}{a}}$$

where Y is a geometrical factor. For a general level of stress applied to a flaw of size a a"stress intensity factor", K, may be defined as

$$K = \sqrt{2E\gamma} = Y\sigma\sqrt{a}.$$

Catastrophic (brittle) failure of the material takes place when the value of K reaches a critical value K_c at the worst stress-intensifying flaw.

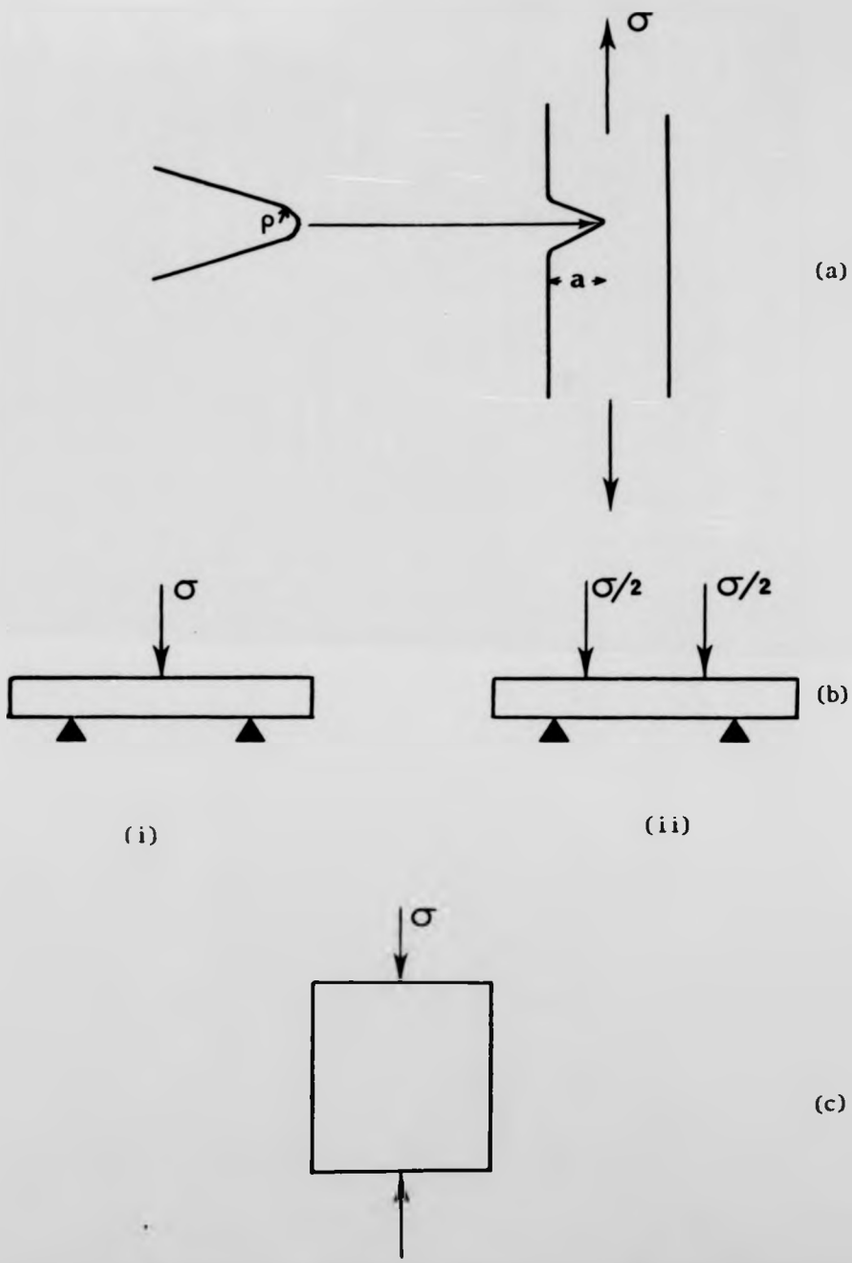

Figure 2.13: Experimental loading conditions in mechanical testing of ceramics (a) uniaxial tension (b) (i) 3-point (ii) 4-point bending (c) uniaxial compression.

At elevated temperatures ceramics may creep under static or cyclic stresses. Any of the three commonly-observed stages of creep may be absent depending on the nature of the material and the experimental conditions of temperature and stress.

The creep mechanism is usually deduced from the behaviour of the ceramic under steady-state (secondary) creep conditions. The general expression which describes steady state creep in ceramics is

$$\dot{\varepsilon} = \frac{ADGb}{kT} \left(\frac{b}{d}\right)^m \left(\frac{\sigma}{G}\right)^n$$

where $D = D_o \exp(-Q/RT)$ is the diffusion coefficient of rate-controlling migrating species with activation energy Q, $\dot{\varepsilon}$ is the strain rate generated by the static load σ, $\underline{b}$ is the Burgers vector of moving dislocations, G is the shear modulus, d is the grain diameter, and n, m and A are constants.

The micromechanism of creep in ceramics is usually determined from an experimental evaluation of the parameters n, m and Q via experiments in which the strain rate is monitored under conditions of the independent, controlled changing of grain size, applied stress, and temperature respectively.

Lattice mechanisms of creep, in which deformation is accommodated within the crystalline phase, usually by dislocation motion, are characterised by a grain-size exponent m=0 and a stress exponent $3 < n < 5$ [Cannon and Langdon 1983]. In materials in which dislocation activity is limited the stress exponent is observed to be in the range $1 < n < 3$.

The creep rupture of ceramics occurs by "subcritical" or "slow" crack growth (SCG). Nucleated microcracks grow by thermally activated

processes or unaccommodated grain boundary sliding until they reach the critical size at which catastrophic failure occurs.

3.2. Mechanical testing of ceramics

The application of a uniform stress distribution is desirable if the inherent mechanical properties of a material are to be determined. A convenient method of achieving this is to test specimens under uniaxial tensile stresses (figure 2.13(a)). Proper uniaxial tensile testing of ceramics is difficult to achieve because of (1) the very high temperatures at which specimen deformation is required to take place, and (2) their inherent lack of ductility and difficulty of machining. First, the gripping of the specimen at high temperatures (up to $\sim$ 1450°C) requires the use of cooled high-temperature metallic alloys or the use of ceramic materials. Both are expensive and difficult to prepare in an adequate form which will allow the specimen alignment necessary to minimise undesirable bending and twisting moments. Secondly, because of the lack of total stress relaxation by plastic deformation ceramic specimens must be carefully machined to minimise the effects of such features as surface flaws or sharp edges. Such machining is both costly and time-consuming, especially if high surface polishes are to be attained.

In view of these difficulties ceramics have often been deformed using the 3- or 4-point bending configuration illustrated in figure 2.13(b). Specimens are usually prepared in the form of a rectangular-sectioned bars or plates which can easily be polished to a high surface finish and hence a carefully-controlled surface flaw population. This method overcomes the difficulties encountered in uniaxial tensile testing. However, deformation in bending results in inhomogeneous

stress distribution and may accentuate the effect of machining-related surface flaws [Roebuck 1979, Davidge and Evans 1970]. Although these effects have been felt to better simulate non-uniform service conditions [Davidge and Evans 1970], premature specimen failure due to brittle fracture or SCG from flaws may complicate a proper evaluation of the mechanisms of deformation. In addition, the proper calculation of the applied stress and the strain deformation depends on the mechanical properties of the material being identical under tensile and compressive stress conditions. This is only the case for mechanisms which give rise to stress exponents, n=1. Finally, the maximum tensile strain which is attainable is limited by the geometry of the test configuration to the order of a few per cent. Ceramics, however, commonly fail below this limit.

A third common method of creep deformation of ceramics is that of uniaxial compression in which a cylindrical or short bar specimen is deformed under an axial load (figure 2.13(c)). This technique possesses the advantages of a uniform application of load and, due to the high compressive strength of ceramics, the ability to sample the creep behaviour under a wide range of stresses. However, accurate measurement of the very low creep strains generated under compressive conditions presents difficulties, and care must be exercised in the interpretation of results. The tensile stresses generated under compressive conditions are only $\sim$ 1/10 those generated under uniaxial tension. In ceramics whose behaviour is dominated by tensile stresses compression is not a suitable deformation mode for the determination of creep mechanisms.

3.3. Creep deformation of hot-pressed β Si_3N_4 and β'Si-Al-O-N

3.3.1. Creep behaviour

The creep behaviour of Si_3N_4 hot-pressed with MgO has been widely studied using the techniques of uniaxial tension [Kossowsky et al 1975, Lange et al 1979, Arons and Tien 1980, Seltzer 1977], bending [Ashcroft 1975, Din and Nicholson 1975], and uniaxial compression [Dixon-Stubbs and Wilshire 1979, Lange and Davis 1982, Birch and Wilshire 1978, Lange et al 1980, Sanders 1978, Seltzer 1977], at temperatures in the range 1150-1475°C. Three-stage creep behaviour has often been observed, particularly in ceramics which contained a relatively high quantity of intergranular second phase [Kossowsky et al 1975, Lange et al 1980]. With low second phase levels and high stresses only primary and secondary creep were observed.

Long periods of transient (primary) creep in excess of 40 h have been observed prior to the onset of steady-state (secondary) creep [Din and Nicholson 1975]. In one study steady-state creep was not observed before specimen failure within periods as long as 400 h or strain levels as high as 2.25% [Arons and Tien 1980, Lange et al 1980], although the rate of change of creep strain was observed to be very low. This behaviour was attributed to viscoelasticy. A model was proposed in which creep was rate-controlled by the sliding of grains due to the low viscosity of the intergranular glassy phase. Viscoelasticity was attributed to a strain hardening effect in which grain rotation continuously reduced the ease of grain boundary sliding [Arons and Tien 1980]. This model was supported by microscopical evidence which showed the existence of "strain whorls" within β grains surrounding regions of grain impingement [Lange et al 1980]. By considering conditions

of constant "creep structure" stress exponents were calculated to lie within the range $1.3 < n < 5.5$ and activation energies in the range $290 < Q < 850$ kJ mol^{-1} . These values are similar to those obtained by other authors who had determined their values from a consideration of apparently steady-state behaviour. These values are listed in table 2.4.

In general, stress exponents lay within the range 1.7 to 3, indicating a creep mechanism involving dislocation motion. However, dislocation activity in β Si_3N_4 was expected to be very low at temperatures < 1700°C [Dixon-Stubbs and Wilshire 1979]. Microscopical studies confirmed that dislocation activity was very low in material which had been deformed in bend [Henshall et al 1975], nor was any extra dislocation activity observed in specimens tested in tension [Kossowsky et al 1975] or compression [Lange et al 1980], except for one report of dislocations in the compressive side of a bend specimen which had been tested at 1400°C [Tighe 1978]. Dislocation plasticity was more usually found to be limited to the highly stressed region around microcrack tips [Coppola et al 1972, Tighe 1978] and near voids which formed in bend tests [Din and Nicholson 1975]. A calculation made of the contribution of the dislocation activity to the cyclic fatigue of hot-pressed β Si_2N_4 showed it to be very low, $< 10^{-5}$ [Kossowsky 1973].

Studies of the microstructures of the deformed creep specimens revealed the presence of grain boundary voids, usually at multiple grain junctions, which were not present in the as-received material. These voids were associated with the separation of grains caused by the mechanical failure of the intergranular phase [Kossowsky et al 1975, Din and Nicholson 1975, Lange et al 1980]. The fracture surfaces of materials crept to failure was observed to be intergranular

Table 2.4

Characteristics of creep of β Si_3N_4 hot-pressed with MgO

Material	Deformation mode	Atmosphere	Stress exponent, n	Activation energy, Q ($kJ\ mol^{-1}$)	Strain at failure (%)	Reference
HS110, HS130	Tension	air	∿ 2	535	∿ 1	Kossowsky et al 1975
		He	∿ 3			
Annealed NC 132	Tension	air	1.7 - 4.1	400 - 850	∿ 2	Arons and Tien 1980
HS 130	Compression	air, Ar	2	703	-	Seltzer 1977
NC 132			1.9			
HPSN	Compression	air	2.1 - 2.4	650	> 2	Birch and Wilshire 1978

Table 2.4 (Cont.)

Material	Deformation mode	Atmosphere	Stress exponent, n	Activation energy, Q	Strain at failure	Reference
HPSN + Y_2O_3	Compression	air	2.1 - 2.3	650	-	Dixon-Stubbs and Wilshire 1979
HPSN	Compression	air	2	660	-	Lange and Davis 1982
Annealed HPSN	Compression	air	1	1080	-	Lange and Davis 1982
HPSN	Bend	-	2.7	-	∿ 1	Ashcroft 1975
HS 130	Bend	air	1.7	586	3	Din and Nicholson 1975

[Kossowsky et al 1975, Ashcroft 1975].

Creep occurs by grain boundary sliding, facilitated by a viscous intergranular phase, and accomodated by the formation of intergranular cavities. Under these conditions the creep stress exponent is > 1. An early model which accounted for the non-linearity of the stress-dependence of strain rate in cavitational creep was proposed by Morrell and Ashby [1973] to explain the creep behaviour of a glass ceramic which consisted of rigid grains in a continuous viscous matrix. In this model the application of a stress, σ, caused the formation of $x(\sigma)$ number of voids the area around which was thus stress-relieved. The stress sustained by the rest of the ceramic was therefore increased by a factor $x_o/(x_o - yx(\sigma))$ where x_o is the number of potential cavity nuclei and y the number of glassy areas in the stress-relieved region. The stress exponent under these conditions is given by

$$n = \left.\frac{\partial \ln \dot{\varepsilon}}{\partial \ln \sigma}\right|_T = 1 + \frac{\sigma y}{x_o - y x_o} \left.\frac{\partial x(\sigma)}{\partial \sigma}\right|_T$$

The theoretical conditions for the nucleation and growth of intergranular cavities has been widely discussed in the literature. Conditions for the suppression of cavity nucleation have been defined with the attendant suggestion that "superplastic" behaviour may result [Evans et al 1980]. Although the low rate of atomic diffusion in ceramic materials limits the prospect of commercially useful superplasticity, the suppression of cavitation does provide the basis for the development of ceramics highly resistant to cavity-induced creep rupture (section 3.3.4.).

3.3.2. The rate-controlling mechanism

As in the case of their oxidation it is not believed that the activation energy of creep allows a precise definition of the mechanism of deformation. Three mechanisms have been proposed to account for the observed activation energy of $\sim$ 600 kJ mol^{-1} (table 2.4).

First, the activation energy was compared with that of viscous flow in silicate melts in support of a mechanism of grain flow over a glassy intergranular phase [Dixon-Stubbs and Wilshire 1979, Lange and Davis 1982, Kossowsky et al 1975]. The activation energy of viscous flow of hot-pressed β Si_3N_4 was determined to be $\sim$ 690 kJ mol^{-1} from measurements of internal friction [Tsai and Raj 1980, Mosher et al 1976]. Secondly, rate-control by solution-precipitation of β via the intergranular phase has been proposed [Raj and Morgan 1981]. The activation energy for creep was compared with that of densification and the heat of sublimation of β Si_3N_4. Thirdly, rate-control via a mechanism of cavity nucleation and growth has been suggested. The activation energy was compared with that of stress rupture and crack growth [Birch and Wilshire 1978].

Differences in creep rates under tensile and compressive stress conditions have been held to support the view that cavity nucleation and growth contribute to creep. The tensile stress necessary to generate a given strain rate is 7-10 times less than the compressive stress [Talty and Dirks 1978, Kossowsky et al 1975], since the tensile stresses generated under compression are $\sim$ $^1/_{10}$ of the applied stress [Birch et al 1976]. Rate control by grain boundary sliding would be expected to give rise to identical creep rates under tensile and compressive creep conditions.

3.3.3. Influence of intergranular phase composition

The creep and fracture of β Si_3N_4 hot-pressed with MgO is dependent on the viscosity or quantity of the intergranular phase. Decreased quantities of the glass modifying elements MgO and Ca or a minimal quantity of intergranular phase cause an increased resistance to fatigue and creep [Kossowsky 1973, Kossowsky et al 1975, Ashcroft 1975, Birch and Wilshire 1978, Lange et al 1978b, 1979, 1980, Dixon-Stubbs and Wilshire 1979].

Additions of CaO had a particularly deleterious effect on the high-temperature mechanical properties. The addition of 0-2% CaO to a ceramic hot-pressed with 5% MgO caused a continuous decrease in creep resistance as the CaO content was increased. Additions of FeO, Al_2O_3 and Mn_3O_4 were found to have a similar effect. The composition of the grain boundary phase was estimated from the batch compositions and the observed strength reductions were correlated with reductions in its liquidus temperature [Richerson 1973]. The deliberate reduction in the quantity of the intergranular phase or increase in its viscosity was therefore expected to give rise to materials with a greatly increased resistance to high-temperature creep and fracture. Such changes may be achieved by (1) careful control of the hot-pressing additive quantity and type or (2) post-fabrication heat-treatments.

3.3.4. Creep mechanisms in improved β Si_3N_4 and β′ Si-Al-O-N ceramics - interrelation with oxidation

By reducing the quantity of intergranular phase in hot-pressed β′ Si-Al-O-N hot-pressed with ∿ 1% MgO ceramic by careful control of its batch composition a ceramic was produced which, in addition to a very high resistance to creep deformation, undergoes deformation

by a non-cavitating, diffusional mechanism [Karunaratne and Lewis 1980b]. Compressive and bend creep tests showed that the steady-state creep stress exponent was $n \sim 1$ with a creep activation energy of $\sim$ 830 kJ mol^{-1}.

The diffusional mechanism of creep was observed after a long period ($\sim$ 250 h) of transient creep. Extensive heat-treatment of this material in air produced an improvement in its creep resistance and removal of the period of transient creep. The behaviour of this ceramic was contrasted with that of a ceramic whose batch composition and fabrication were the same except that $\sim$ 1% Mn_3O_4 was used as a hot-pressing aid. This ceramic underwent creep deformation accompanied by cavitation with a creep stress exponent of $n \sim 1.7$ in the as-received condition. However, after an extensive heat-treatment in air it exhibited non-cavitational, diffusion-controlled creep (n=1) and a creep resistance similar to that of the MgO hot-pressed material.

The transient behaviour of the MgO-containing material and the increased creep resistances on oxidation of both materials was attributed to oxidation-induced modification of the grain boundary phase. In particular, glassy multiple-grain junction phases in the Mn_3O_4-containing ceramic which had acted as nuclei for cavitation in the as-received material were removed on oxidation and the composition of the intergranular regions in both ceramics was believed to be modified via the collection of viscosity-reducing ions such as Mg, Mn and Ca in the oxide layer. This was believed to give rise to increased intergranular cohesion.

The heat-treatment of a cavitating β Si_3N_4 ceramic hot-pressed with MgO also produced increased resistance to creep and a change to a purely diffusional (n=1) mechanism of creep. It was proposed that prolonged oxidation gave rise to a decrease in the quantity

or viscosity of the intergranular phase [Lange and Davis 1982].

The suppression of cavitation in these ceramics gave rise to the "superplastic" deformation behaviour expected in the absence of slow crack growth. The non-cavitating β′ Si-Al-O-N ceramic was deformed without fracture in bend tests to the remarkably high total strain of ∿ 4% [Karunaratne 1980].

3.4. The present work

The mechanism of oxidation-induced modifications to the intergranular phase in β′ Si-Al-O-N ceramics was to be identified in the present work. The creep behaviour of the ceramics was to be observed under conditions of uniaxial tension. This would avoid any irregularities in creep behaviour due to the application of non-uniform stresses and would allow the attainment of high (superplastic) strains to failure. These tests were to be carried out in air at similar temperatures to those of the oxidation experiments in order to observe the effect of oxidation on the creep behaviour.

CHAPTER THREE

EXPERIMENTAL TECHNIQUES AND THE FABRICATION AND CHARACTERISATION OF MATERIALS

In this chapter the experimental techniques used in the characterisation and testing of the ceramics investigated in this study will be described. Their composition and fabrication will be described and their microstructural characteristics defined.

Part One: Fabrication and experimental techniques

1.1. Composition and fabrication

The β′ Si-Al-O-N ceramics were of a wide range of chemical composition with respect to both the substitution level of the β′ crystalline phase and the quantity of hot-pressing additive. They were hot-pressed from powder compositions which were chosen to produce ceramics whose main crystalline phase would be β′ $Si_{6-z}Al_zO_zN_{8-z}$ and which would contain minimal quantities of second phases. The batch compositions of the ceramics are presented in table 3.1. The ceramics have been designated A, B, C or D according to their substitution level and composition, and 1, 2, or 3 according to the type or quantity of their hot-pressing additive. The average Si-Al-O-N compositions of the ceramics as predicted from these batch compositions are presented in figure 3.1, superimposed on the sub-solidus "phase diagram" of the system. In view of excess impurity silica on

Ceramic	Composition (wt %)							Substitution level		
	Si_3N_4	AlN	SiO_2	Al_2O_3	MgO	Mn_2O_3	ZrO_2	(1)	(2)	(3)
A1	78.4	13.1	5.6	1.9	1.0	-	-	1	1.00	0.98 ± 0.07
A2	77.6	12.9	5.6	1.9	0.4	1.5	0.2	1	1.00	0.88 ± 1.4
B1	53.2	29.3	17.5	-	-	-	-	2	2.00	2.00 ± 0.16
B2	52.4	28.9	17.2	-	1.5	-	-	2	2.00	1.88 ± 0.16
C1	64.6	17.9	8.8	8.7	-	-	-	2	1.71	1.95 ± 0.12
C2	63.0	17.5	8.6	8.5	2.4	-	-	2	1.71	1.86 ± 0.17
D1	2.0	53.5	44.5	-	-	-	-	4	3.75	3.38 ± 0.13
D2	17.0	40.0	20.5	22.5	-	-	-	4	4.01	4.11 ± 0.05
D3	16.8	36.6	23.3	22.3	1.0	-	-	4	3.84	3.88 ± 0.20

Table 3.1: Batch composition of ceramics

Substitution level: (1) nominal

(2) estimated from batch composition

(3) TEM EDAX analysis (Chapter 3, part 2)

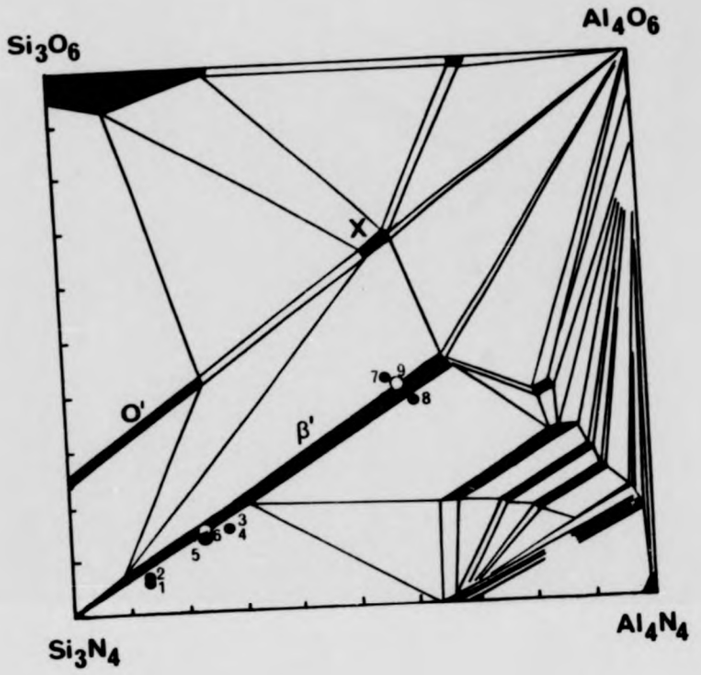

Figure 3.1: Average batch compositions of ceramics used in this study

Designation	Material
1	A1
2	A2
3	B1
4	B2
5	C1
6	C2
7	D1
8	D2
9	D3

the Si_3N_4 batch powder the actual compositions are expected to be shifted slightly towards the Si_3O_6 corner of the diagram.

The substitution level of the ceramics varied across the entire extent of the β′ phase, from ∿ 1 to ∿ 4. By assuming that all the constituents Si, Al, O and N from the batch materials form the β′ phase it is possible to estimate the substitution level of the ceramics from the batch compositions. These calculated values are listed in table 3.1.

Some of the ceramics of high substitution level were prepared without the use of a hot-pressing aid. Otherwise, up to 2.6% MgO was added to the batch materials. Ceramics of substitution level z ∿ 1 could not be densified without the use of a sintering aid. Fully-dense ceramics of this substitution level were therefore prepared by adding ∿ 1% MgO or Mn_2O_3 to their batch compositions.

The ceramics were prepared at the Lucas Group Research Laboratories. Mixtures of the batch powders were colloid milled in isopropyl alcohol in order to reduce particle sizes to < 5 μm and to thoroughly mix the constitutents. After drying, the powders were hot-pressed between graphite dies under a pressure of ∿ 15.4 MN m^{-2} for a period of ∿ 1h at a temperature of ∿ 1800°C to form slabs of ceramic of between 10 and 25 mm thickness.

1.2. Specimen preparation and oxidation

The ceramics were cut to convenient sizes for oxidation using diamond-edged annular cutting wheels. The oxidation samples were cut to dimensions ∿ 10 x 3 x 0.7 mm. Particular attention was paid to the oxidation behaviour of one of the 10 x 3 mm faces. The samples were mounted in 'Lakeside' thermosetting resin on a glass

plate and these primary oxidation surfaces were polished using water-lubricated SiC paper of 240 grit grade. This grade was chosen in order to produce a highly polished surface finish within short polishing periods. An optically polished surface was achieved by this method on the ceramics of low substitution level, z=1, A1 and A2. The surfaces of the ceramics of higher substitution level were less highly polished, but were of a reproducible standard. The mounting resin was removed by washing the specimens in hot acetone. Cleaning of the samples was completed by successive rinses in methanol and diethyl ether.

For oxidation the samples were mounted on pieces of Pt foil which were washed in HF between oxidation runs to remove traces of oxide from samples of differing composition. The Pt was folded to ensure minimal contact with the sample and maximise the free flow of air around it. The polished primary oxidation surface was uppermost. Samples were oxidised in an open-eneded Al_2O_3 tube furnace heated by SiC resistance elements and temperature controlled by a "Eurotherm" stepless controller. The samples were positioned in the centre of the furnace whose internal temperature had previously been calibrated using a Pt/Pt -13% Rh thermocouple, such that samples were oxidised within ± 5°C of a mean temperature, the highest temperature being that recorded in this work. Samples were rapidly inserted into and removed from the furnace ($\leq$ 5s) and were not force-cooled.

1.3. Tensile creep deformation

Tensile creep specimens were prepared from slices of ceramics A1 and A2 of dimensions 50 x 15 x 3 mm, the long dimension being perpendicular to the hot-pressing direction. The sides of the slices

were ground parallel to a good surface finish using a diamond-coated wheel on a Jones-Shipman surface grinding machine. A gauge length of $\sim$ 9 mm^2 cross-section and 30 mm length was produced using a profiled wheel coated with 320 grit diamond. This grade of diamond was chosen as a compromise between the requirements of a good surface finish and an acceptable wheel life. The profiled wheel produced gauge length corner radii of $\sim$ 2.5 mm. A creep specimen is illustrated in figure 3.2a.

Examination of the specimens in the scanning electron microscope showed that the flaws associated with the profiling process were generally not severe. Pits of diameter $\sim$ 100 μm were located on the profiled surface but the machining flaws perpendicular to the loading direction were of very limited depth, generally less than a few microns (figure 3.3.). A better finish could be produced with a different wheel, but the square gauge length corners produced by this wheel led to premature specimen failure due to stress concentration at the corners. Bearing holes of diameter 5mm were drilled with centres 5 mm from the gauge length using a diamond-edged core drill. The material around the edges of the bearing holes was severely flawed due to chipping away of material on drilling (figure 3.2a). Only one specimen, however, failed at this bearing.

The creep specimens were tested in a creep rig designed and built in the laboratory. The specimen was linked to two "Refel" SiC loading rods, each of cross-section 80 mm^2, using SiC bearing pins which had been machined to ensure a close fit in the specimen bearing holes. The SiC rods were similarly connected to Al_2O_3 rods of cross-sectional area 650 mm^2. The connection between the SiC and Al_2O_3 rods was sometimes achieved using SiC connections pieces. These loading arrangements are

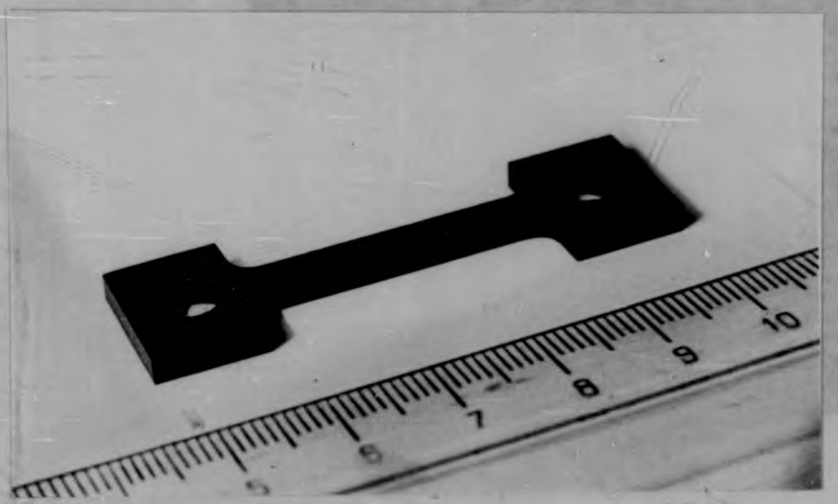

(a)

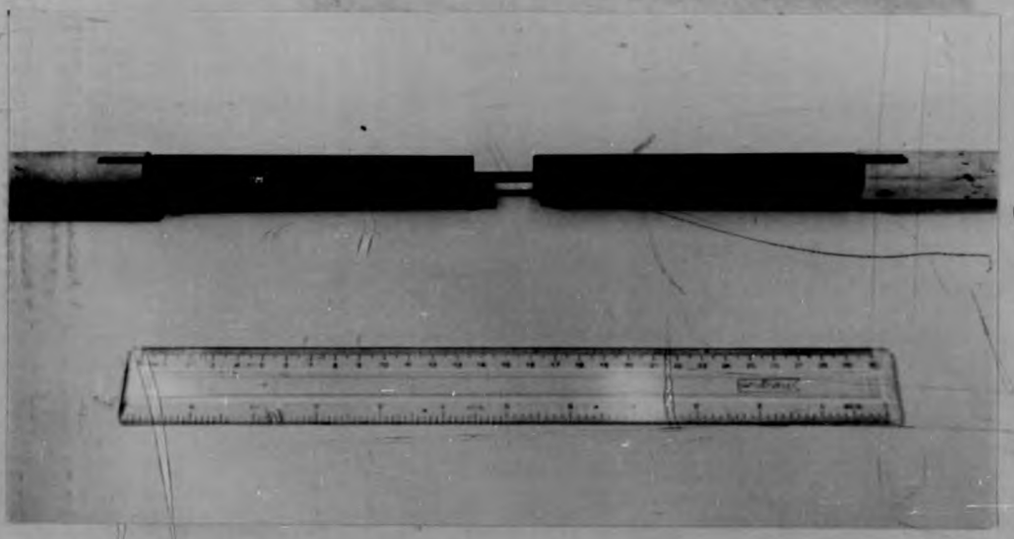

(b)

Figure 3.2: (a) Creep specimen

(b) Loading column

(a)

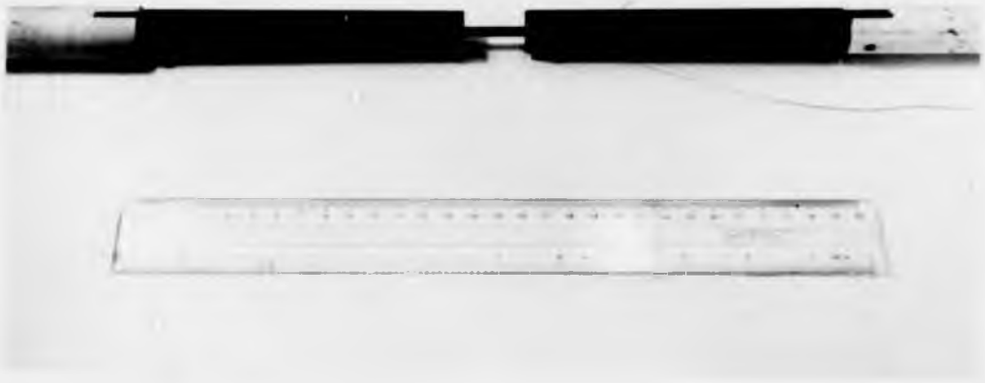

(b)

Figure 3.2: (a) Creep specimen

(b) Loading column

(a)

(b)

Figure 3.2: (a) Creep specimen

(b) Loading column

(a)

100 µm

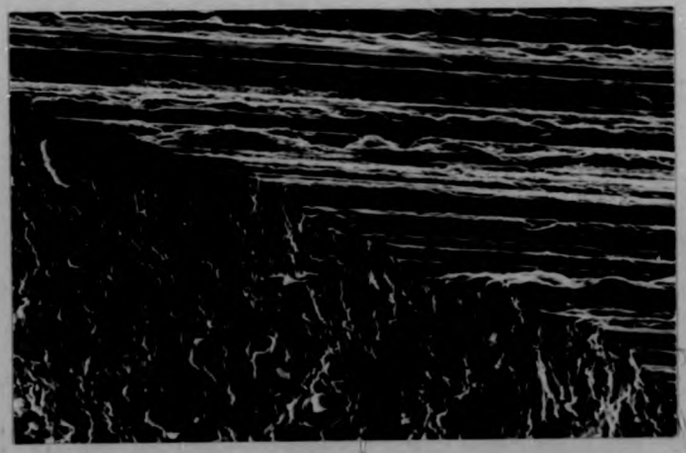

(b)

10µm

Figure 3.3: Machining flaws in profiled surface of tensile creep specimens.

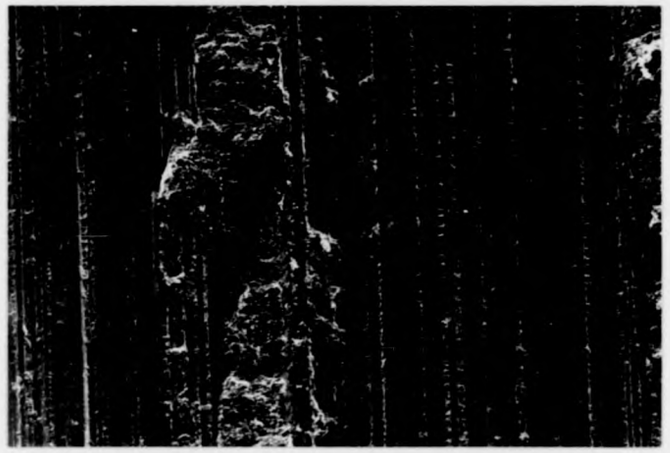

(a)

100 µm

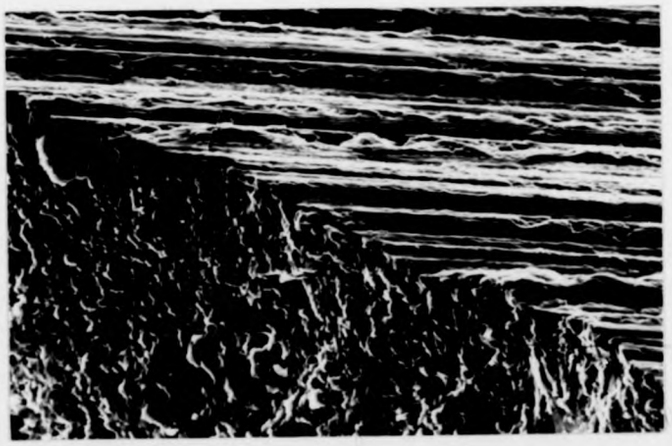

(b)

10 µm

Figure 3.3: Machining flaws in profiled surface of tensile creep specimens.

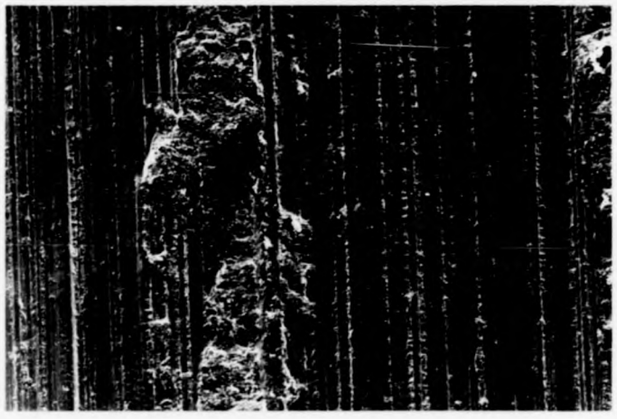

(a)

100 μm

(b)

10 μm

Figure 3.3: Machining flaws in profiled surface of tensile creep specimens.

illustrated in figures 3.2(b) and 3.4. SiC is the preferred material over Al_2O_3 in the hot zone of the furnace due to its lower reactivity with Si_3N_4 and its better high-temperature creep resistance. One Al_2O_3 rod was rigidly secured perpendicular to the base of the creep rig by means of a steel bearing pin. The other Al_2O_3 loading rod was secured with a steel bearing pin to a steel rod which formed part of a lever arm loading system which gave a loading ratio of 10=1. Care was taken to ensure that the loading column remained as tightly linked as possible during initial loading.

The entire loading column was encased in an Al_2O_3 tube furnace which was heated by SiC resistance elements and temperature-controlled by a "Eurotherm" stepless controller. The temperature profile was determined prior to commissioning using a Pt/Pt 13% Rh thermocouple. The temperature variation over the gauge length of the specimen varied by no more than ± 5°C from a mean temperature, the highest temperature being that recorded in this work. Creep strain was measured using a d.c. inductive LVDC. (Electro-Mechanisms model D402-01) which was attached between the outer Al_2O_3 furnace tube and the upper Al_2O_3 loading rod in order to minimise extraneous deflections caused by differential thermal expansion of the apparatus. The strain was continuously monitored using a JJ Instruments chart recorder. The LVDC/chart recorder arrangement was calibrated at room temperature prior to commissioning using controlled deflections generated by a surface micrometer. The creep rig and LVDT arrangement is illustrated in figure 3.5.

1.4. Phase identification by X-ray diffraction

The analysis of phases present after oxidation was attempted by use of the technique of Debye-Scherrer X-ray diffractometry.

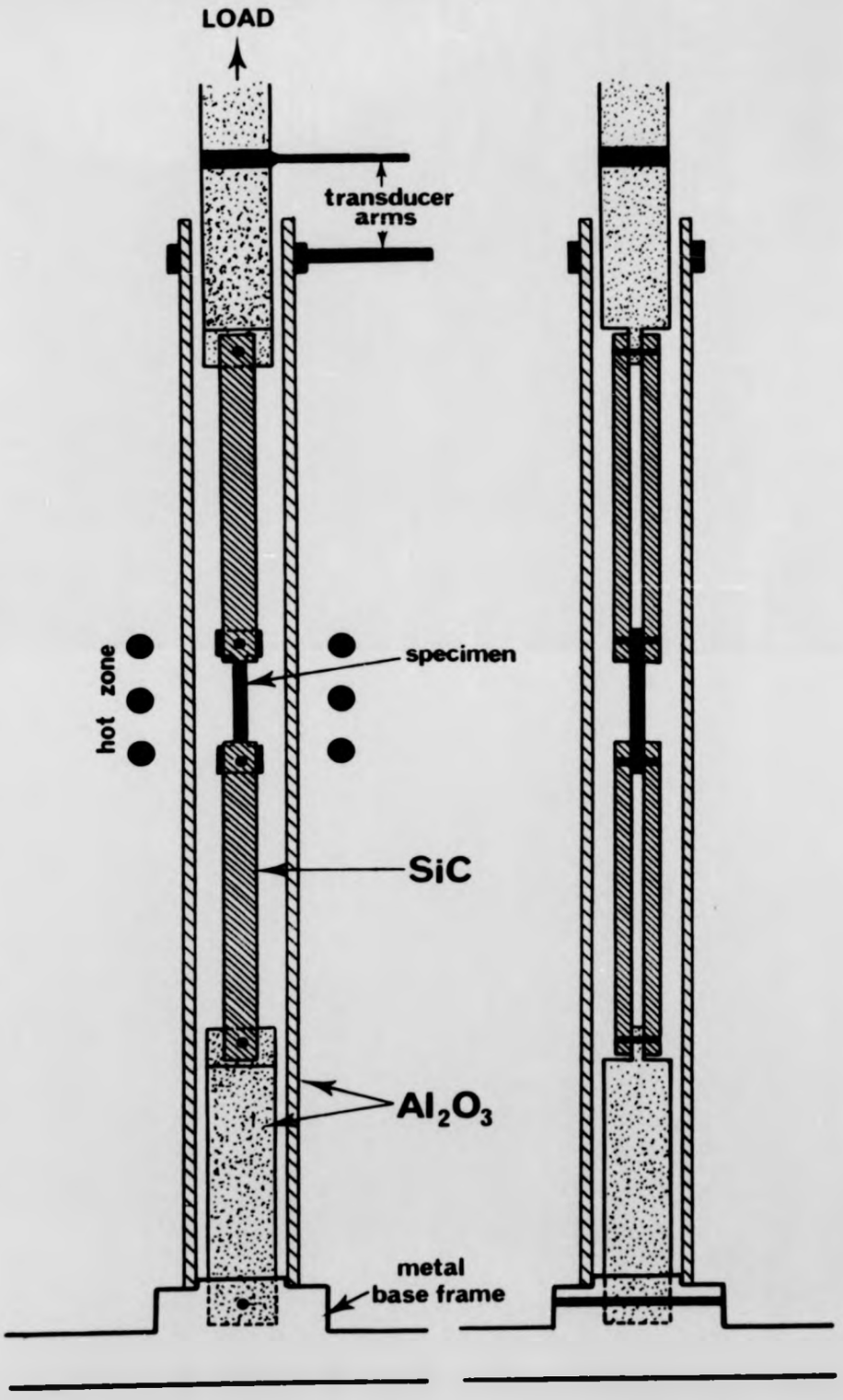

Figure 3.4: Schematic representation of creep rig loading column.

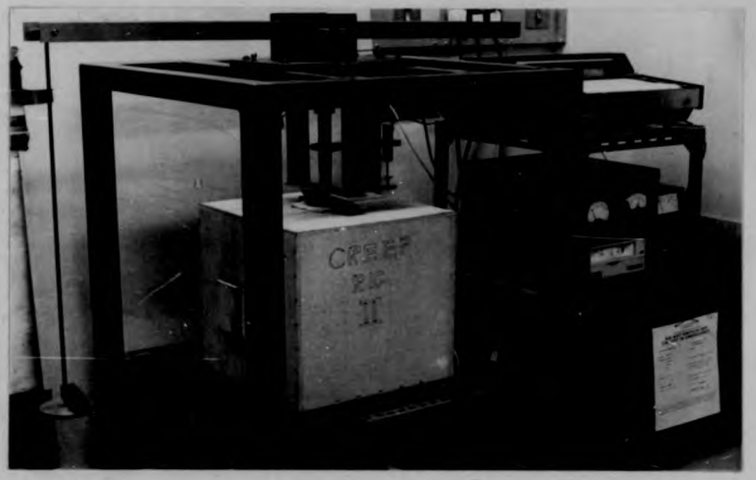

(a)

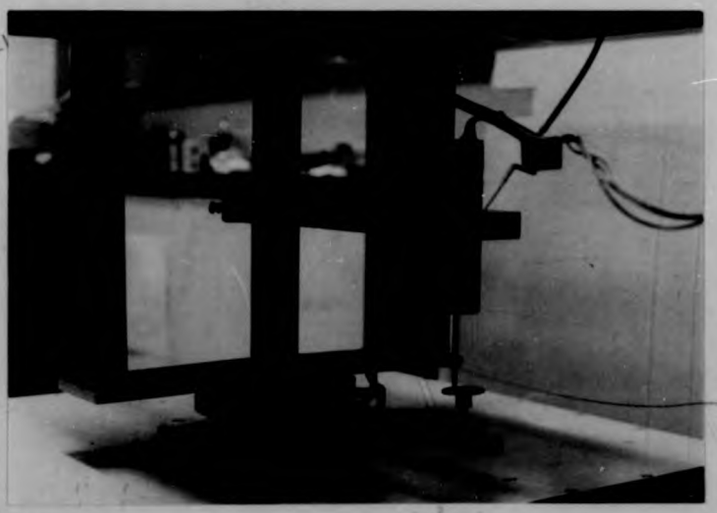

(b)

Figure 3.5: (a) Tensile creep rig

(b) LVDT arrangement

(a)

(b)

Figure 3.5: (a) Tensile creep rig

(b) LVDT arrangement

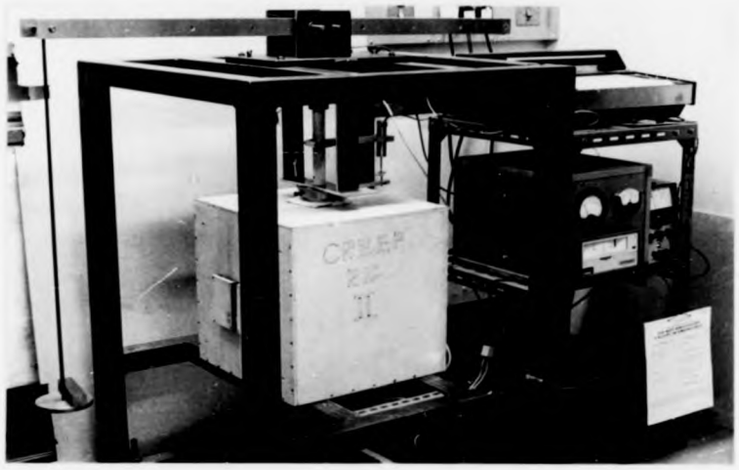

(a)

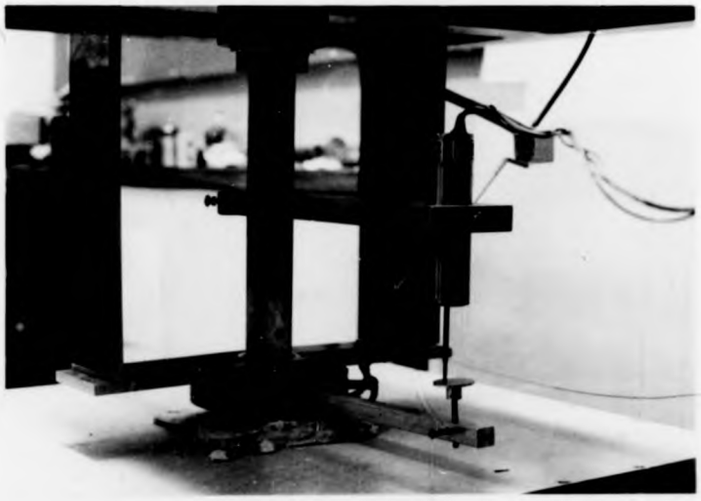

(b)

Figure 3.5: (a) Tensile creep rig

(b) LVDT arrangement

Samples of as-pressed or oxidised ceramic were positioned centrally in a Debye-Scherrer camera (Phillips model PW 1009/80). Cu Kα X-rays were directed obliquely at a low angle to the sample surface and the diffraction pattern was recorded on photographic film. Quantitative analysis of the phases present was not possible due to the difficulty of positioning the sample centrally in the X-ray camera. However, the technique was useful in confirming the amorphous nature of the oxide scale which formed on some of the ceramics.

1.5. Electron microscopy and microanalysis

1.5.1. Scanning electron microscopy

The extent of oxidation has been determined by measuring the thickness of the oxide layer formed at the primary oxidation surface of the ceramic. This thickness has been measured directly from secondary-electron images of fracture surfaces of the oxidised specimens in a Cambridge "Stereoscan" microscope.

Approximately planar cross-sections of oxidised material were prepared by manual fracture across the narrower dimension of the oxidised sample, care being taken not to damage the oxide layer at the position of the fracture. The samples were mounted onto a graphite disc using a mixture of "Durafix" polymeric cement and colloidal graphite. The graphite disc prevented the fluorescence of x-rays from the underlying metallic specimen plate during in-situ microanalysis of the specimen. The colloidal graphite was necessary to facilitate charge removal from the specimen to earth. For the same purpose the upper surface of the sample was coated with a thin layer of carbon produced by vacuum evaporation after mounting. This layer was deposited whilst rapidly rocking and rotating the sample in order to deposit an even layer over the

topographically rough fracture surface. Oxidised samples were similarly mounted and coated for examination of the outer surface of the oxide scale.

Microanalysis

Semiquantitative microanalysis of the compositions of the SEM specimens was carried out by the energy-dispersive analysis of characteristic X-rays (EDAX) generated by the interaction of the electron beam and the specimen. For this purpose the electron beam was usually focussed onto the region of interest although linescans or small two-dimensional scans were also used.

The spectrometer system employed had a very high detection efficiency over a wide range of x-ray energies (figure 3.6) and elements of atomic number > 10 were readily detected and identified by reference to the energies of their $K_{\alpha,\beta}$ X-rays. The detection efficiency and accuracy of the EDAX technique is further affected by the solid angle of X-ray collection and the physical processes of X-ray emission. To minimise errors in comparing the analyses of different specimens care was taken to maintain the same specimen position with respect to the X-ray collector during the microanalysis of different areas.

In order to facilitate rapid microanalysis ($\sim$ 2-3 min) the beam energy used to excite the X-rays was fixed at the relatively high value of 30 keV. Analysis was allowed to continue until the peak number of counts of the K_{α} X-rays of the most common element reached 10,000. The presence of minor elements could then be detected within the resolution determined by the locally random energy distribution of the background Bremsstrahlung radiation. Minimum resolution was $\sim$ 1% of the concentration of the most common element.

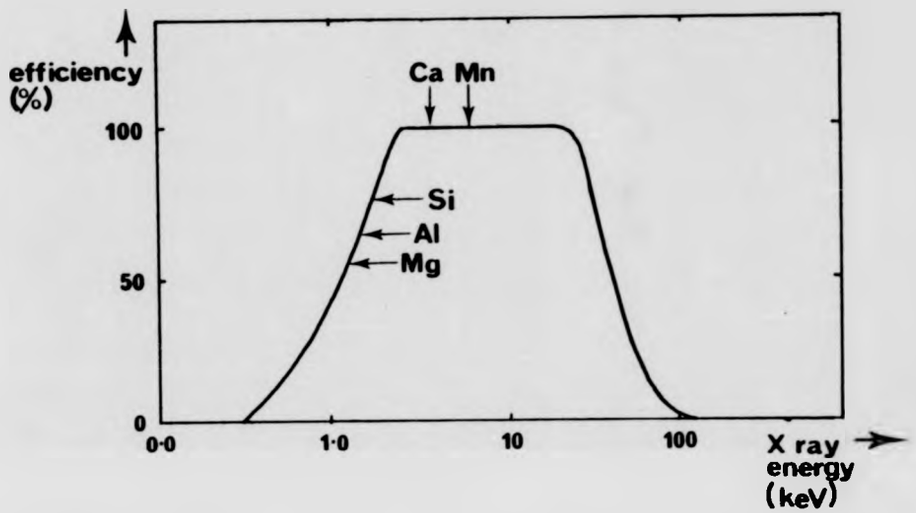

Figure 3.6: LDAX spectrometer detector efficiency [Russ 1972]

In determining the concentration of a given element the number of counts under the Gaussian distribution of energies for a given characteristic energy was recorded rather than the peak number of counts. In this way counts due to the X-ray energies which had been dispersed due to the statistics of charge production in the X-ray detector were included in the analysis. The local concentrations of the elements were calculated by referring the number of counts of the characteristic X-ray energy to that of the most common element, usually Si. Due to the uncertainty of the volume of material excited by the electron beam and the complexity and variation of the composition of the atomic systems that were analysed no correction was made for the detection efficiency or the internal absorption and fluorescence of x-rays within the excited material. The local concentrations quoted in this work are therefore only semi-quantitative.

Spatial definition

The local concentration of an element determined by the use of a spot probe represents an average of the concentration of the element throughout the volume of material excited by the probe. An upper estimate of the lateral width of this area may be gained by the detection of elements in the oxide scale which exist in too small an average concentration to be detected in the β'' ceramic. In figure 3.7, for example, the cross-sectional radius of the volume excited by the electron probe in position Y cannot be greater than X/2. The concentration of element M at position Y is then an averaged concentration over the transverse distance X.

The choice of an electron beam spot probe in the determination of element concentration may be criticised as being too selective with regard to local variations in the scale composition. In this work the use of the spot probe in preference to linescans of the electron beam parallel to the oxidation front was dictated by the rough topography of the fracture surfaces and, in some specimens, by local

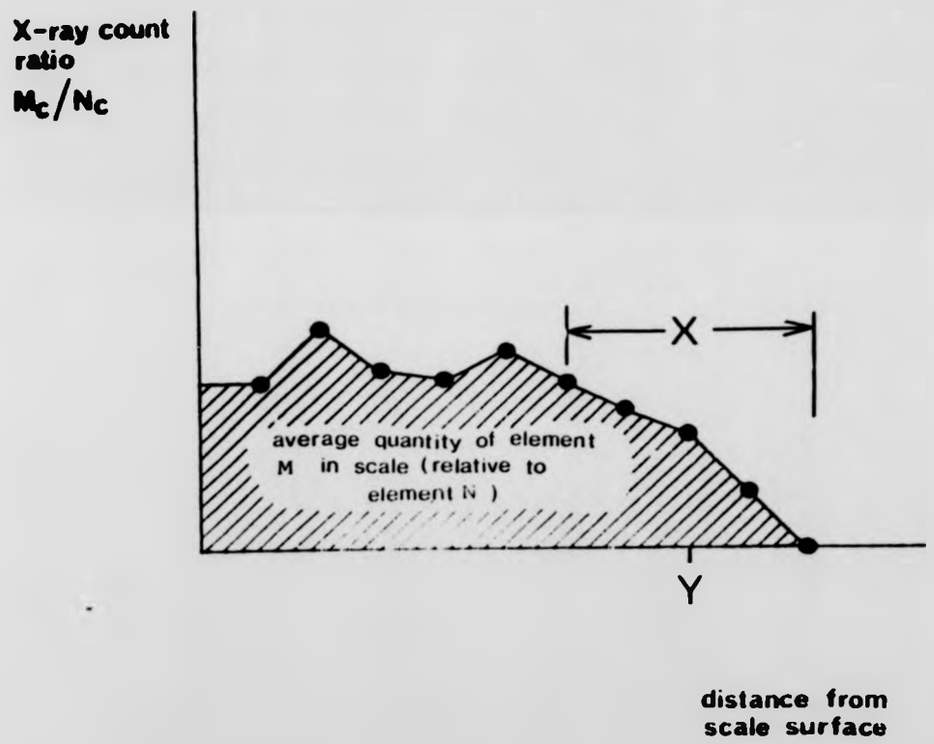

Figure 3.7: Method of determination of average element quantity in oxide scale.

variations in the thickness of the scale.

In figure 3.8 the relative concentrations of elements determined using linescans of width ∿ 40 μm is compared with those determined using point probes separated by 20 μm. In view of the similarity of the concentrations of the elements determined by the two methods of X-ray generation it is believed that the use of point probes is justified.

Local variations in element concentration

Very high concentrations of minor scale constituents were occasionally observed (spotprobe, figure 3.8). These were associated with high detected quantities of Fe and the other minor scale constituents. These high concentrations may have been due to the shielding of the X-ray detector by locally uneven specimen topography. Under these conditions relatively more X-rays generated by scattered electrons penetrating the structural members of the microscope enter the detector. These X-rays also fluoresce the lighter elements in the surface of the specimen. Alternatively, these high element concentrations may have been due to their release into the scale when the oxidation front encroached upon Fe-silicide particles in the ceramic (Chapter 3) which do not dissolve on oxidation (Chapter 5, section 1.2.2), due either to their presence in the silicide or due to inhibition of local grain boundary diffusion by the particle.

Despite these limitations imposed by the physical processes of X-ray emission and spatial resolution it is believed that this method of the determination of local element concentration allows comparison to be made of the concentrations of the same element in different regions of the same specimen, or of the same element in different specimens of the same ceramic, given that care has been taken to ensure the same physical configuration of the specimen with respect to the X-ray detector in all cases.

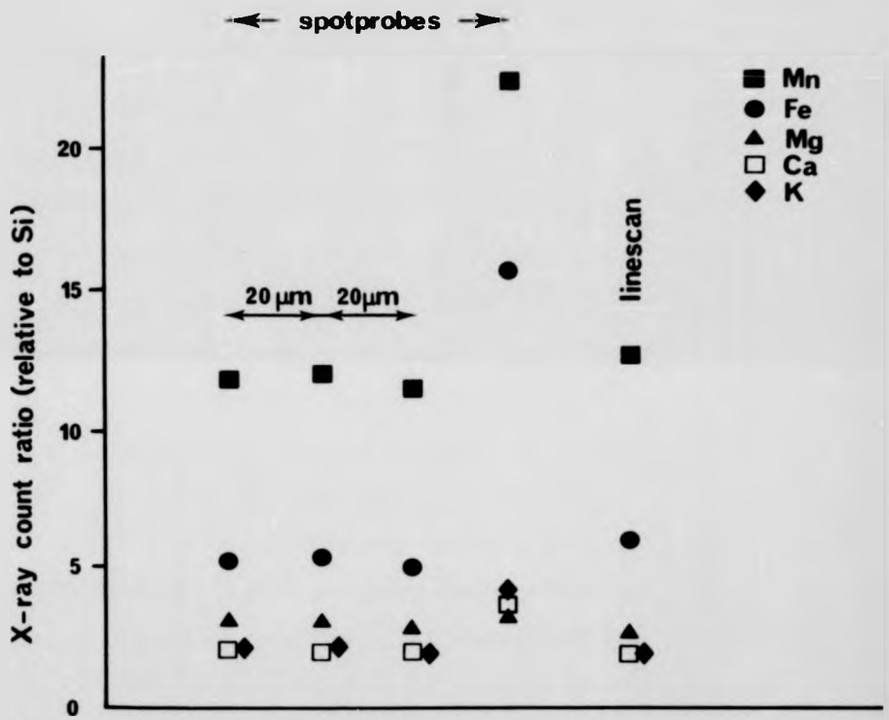

Figure 3.8: Concentration of elements in an oxide scale determined by linescan and point electron beam probes (ceramic A2 oxidised at 1350°C for 42 h).

Quantitative comparisons of the concentrations of different elements at the same position cannot be made due to the differing probability factors for X-ray generation and detection. Neither can comparisons be made of the concentrations of the same elements in scales of different ceramics due to the different concentration of the most common element.

Average element quantities in the oxide scales

Estimates of the average quantity of an element M in structurally homogeneous (amorphous) oxide scales, relative to the most common element, N, have been made by the following method. Analyses of the scale composition were made at a series of positions across the thickness of the scale using focussed-beam probes. For each position the number of X-ray counts for the element M, Mc, was referred to that of the element giving the highest count rate, Nc (N usually = Si). The quantity Mc/Nc was summed across the thickness of the scale as illustrated in figure 3.7 to give the average element quantity.

Determination of the average relative element quantities in this manner is believed to allow a direct comparison to be made of quantities of the same element in different regions of the same specimen or in the oxide scales of different samples of the same ceramic. Comparisons between the quantities of different elements in the same ceramic or the same elements in different ceramics cannot be made for the reasons outlined above for the determination of local element concentrations.

1.5.2. Transmission electron microscopy

The microstructures and compositions of "as-pressed" and oxidised ceramics and particles of their oxide scales have been examined by direct imaging and microanalysis in a JEOL 100C transmission electron microscope.

Electron-transparent sections of "as-pressed" and oxidised ceramics were prepared by the following procedure. Thin slices of material were attached to a glass slide with "Lakeside" thermosetting resin and ground to a thickness of $\sim$ 50 μm using water-lubricated SiC paper. The most

extensive electron transparent regions were achieved if these thin slices were surface-polished on both sides to 1 μm grade diamond at this stage. The thermosetting resin was removed by wiping the speciment on filter paper soaked in acetone on an electrical hot plate. The slices were then mounted on a 3 mm diameter brass ring suitable for insertion into the goniometer stage of the electron microscope using "Araldite" epoxy resin. Final thinning was achieved by bombbardment with 5 kV Ar ions directed at ∿ 20° to the slice. In order to minimise charging effects in the electron microscope the slices were coated with a thin layer of vacuum-evaporated amorphous carbon.

It was not believed to be possible to prepare bulk specimens of the oxide scale of the ceramics for transmission electron microscope due to its limited thickness (≤ 30 μm) and poor mechanical strength. (Non-glassy oxides could easily be removed from the underlying ceramic by scraping with an unoxidised piece of ceramic). In order to examine the microstructure and composition of the scale small particle samples were prepared by the following method. The oxidation product was removed from the ceramic using an unoxidised piece of ceramic. The scale was manually ground to a fine powder using an agate pestle and mortar, prior to suspension in acetone. This suspension was deposited on a thin amorphous carbon film supported on a copper grid. The particles of scale ranged in size up to ∿ 2μm width and some of these were amenable to diffraction contrast imaging and EDAX microanalysis.

Microanalysis

Selected-area microanalysis was carried out with the same EDAX spectrometer that was employed with the scanning electron microscope. Probe diameters down to 0.1 μm were used. The volume of material excited by the electron beam in the transmission electron microscope is very small due to the very narrow width of the specimen. In the case of electron transparent specimens the level of absorption and fluorescence of characteristic X-rays within the specimen can

be considered to be negligible [Russ 1972]. A good estimate of the specimen composition can then be derived from the recorded X-ray intensities of the elements by application of a correction factor which accounts for the ionisation, emission, and detection probabilities of the elements.

If it is assumed that the ratio of the intensity of the characteristic X-rays to Bremstraahlung is proportional to concentration, the ratio of concentration of two elements is

$$\frac{C_1}{C_2} = k_{12} \frac{I_1}{I_2}$$

where I_1 and I_2 are the recorded X-ray intensities of the elements 1 and 2 respectively, and k_{12} is a constant. For more than one element,

$$C_1 : C_2 : C_3 : \ldots = \frac{I_1}{P_1} : \frac{I_2}{P_2} : \frac{I_3}{P_3} : \ldots$$

where P_i is the relative intensity of X-rays from each element in a given concentration in the excited volume. The factors P are the product of four probabilities Q_i, W_i, R and T_i where Q_i is the probability that an electron will ionise an atom of element i, W_i is the probability of X-ray emission from an ionised atom, R is the probability that the X-ray is of the energy being measured, and T_i is the probability of X-ray detection. The values of P have been calculated from theoretical formulations of the factors Q, W, R and T. The values for the elements of interest in this work are listed in table 3.2. From experimental tests on standard specimens these factors were claimed to be accurate to within 10% of the true relative concentration of elements [Russ 1972]. The factors listed

Element	Correction factor
Mg	0.45
Al	0.57
Si	0.66
K	0.92
Ca	0.93
Mn	1.00
Fe	0.99

Table 3.2: Calculated correction factors for TEM EDAX quantitative microanalysis [Russ 1972].

in table 3.2 were used in the correction of the recorded intensities of X-rays determined in TEM microanalysis. The count rate was very much lower than that recorded in the scanning electron microscope due to the much smaller excitation volume. The peak count rate of the most common element was therefore allowed to reach a value of 5000 or 1000 during microanalysis depending on the count rate obtained or the resolution required.

Part Two: Ceramic microstructures

2.1. Ceramics of low substitution level, $z \sim 1$ (ceramics A1 and A2)

The microstructures of ceramics A1 and A2 have been well characterised by Karunaratne in his study of their high-temperature mechanical deformation [Karunaratne 1980]. Both ceramics consisted of approximately equiaxed β'' grains with an average grain size of ~ 1 μm. Microanalysis of the grains using a spot probe confirmed their composition to correspond to substitution levels of 0.98 ± 0.07 and 0.88 ± 1.4. in ceramics A1 and A2 respectively. The grain size

distribution was narrow. The grains were non-faceting but were of hexagonal morphology (figure 3.9).

No intergranular phase was detected at bi-grain junctions in either ceramic by conventional diffraction contrast in the transmission electron microscope or by the use of the high-resolution "lattice-imaging" technique. The extent of the intergranular segregate was therefore $\leq$ 6.6 Å. Some multiple grain junctions of ceramic A2 contained Si-rich glassy pockets of up to 500 Å across (Figure 3.10). This "triple junction" phase was absent in ceramic A1.

Both ceramics contained fine dispersions of Fe-rich silicide particles similar to those found in hot-pressed β Si_3N_4. In ceramic A2 these particles contained a high quantity of Mn.

2.2. Ceramics of intermediate substitution level, z ∿ 2 (ceramics B1, B2, C1 and C2)

The microstructure of the ceramics of substitution level z ∿ 2 were similar to those of ceramics A1 and A2. They consisted of β′ grains of between ∿ 0.1 and 2 μm diameter of equiaxed hexagonal morphology.

2.2.1. Ceramics B1 and B2

The microstructure of ceramic B1, hot-pressed without the use of a sintering aid, is illustrated in figure 3.11. It consisted of approximately equiaxed hexagonal grains of diameter up to ∿ 1 μm. The compositions of these grains analysed by EDAX microanalysis indicated that the ceramic substitution level was 2.02 ± 0.16, consistent with the value of 2.00 calculated from the hot-pressing batch composition (table 3.1). The grain boundaries were curved and multiple grain junctions were sharp. No intergranular phase

Figure 3.9: Microstructure of ceramic A1

Figure 3.9: Microstructure of ceramic A1

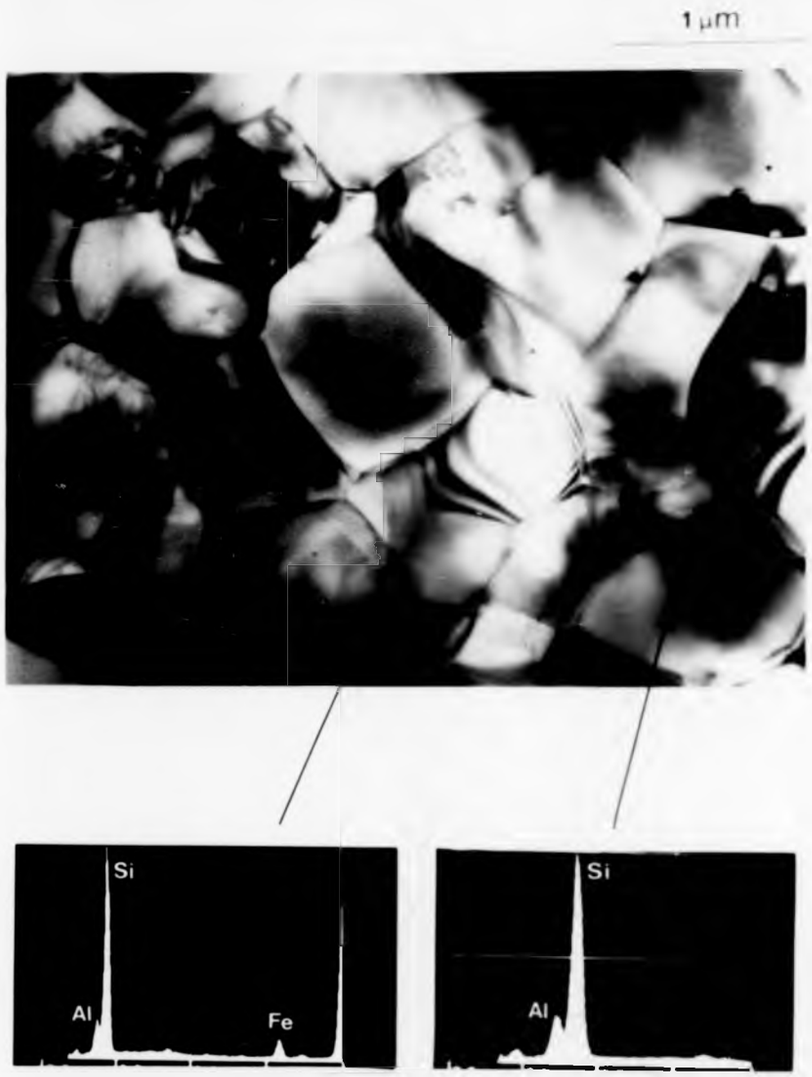

Figure 3.9: Microstructure of ceramic Al

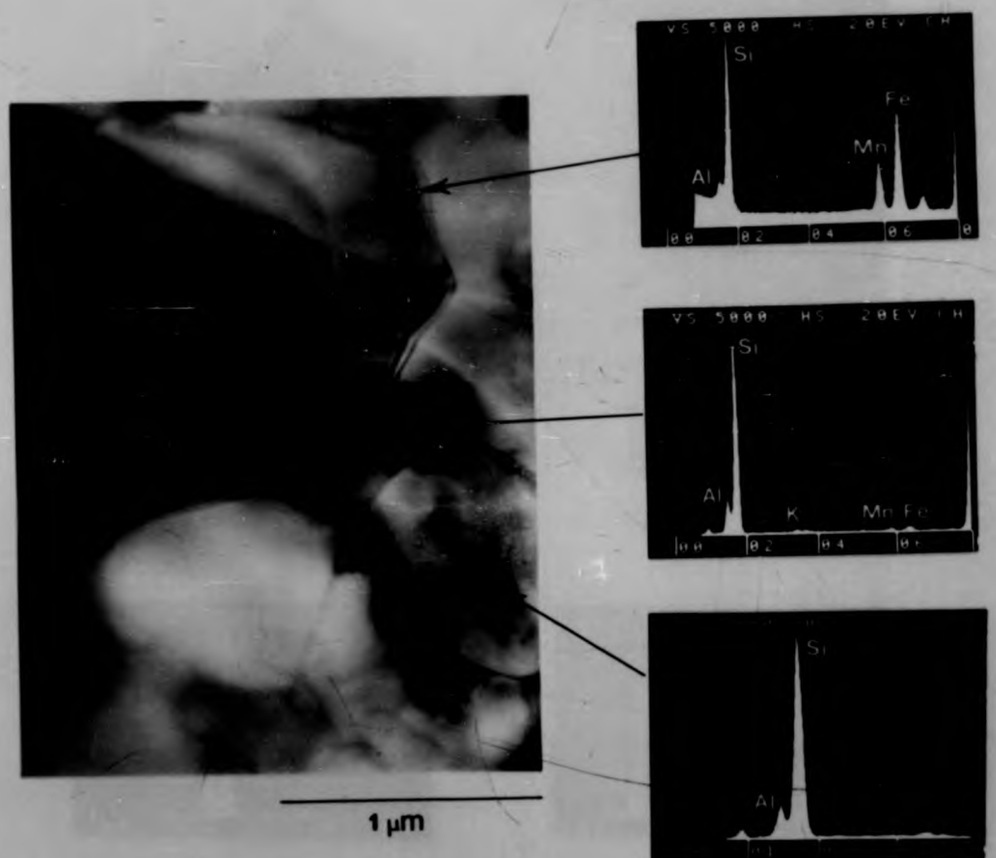

Figure 3.10: Multiple-junction intergranular phase in ceramic A2.

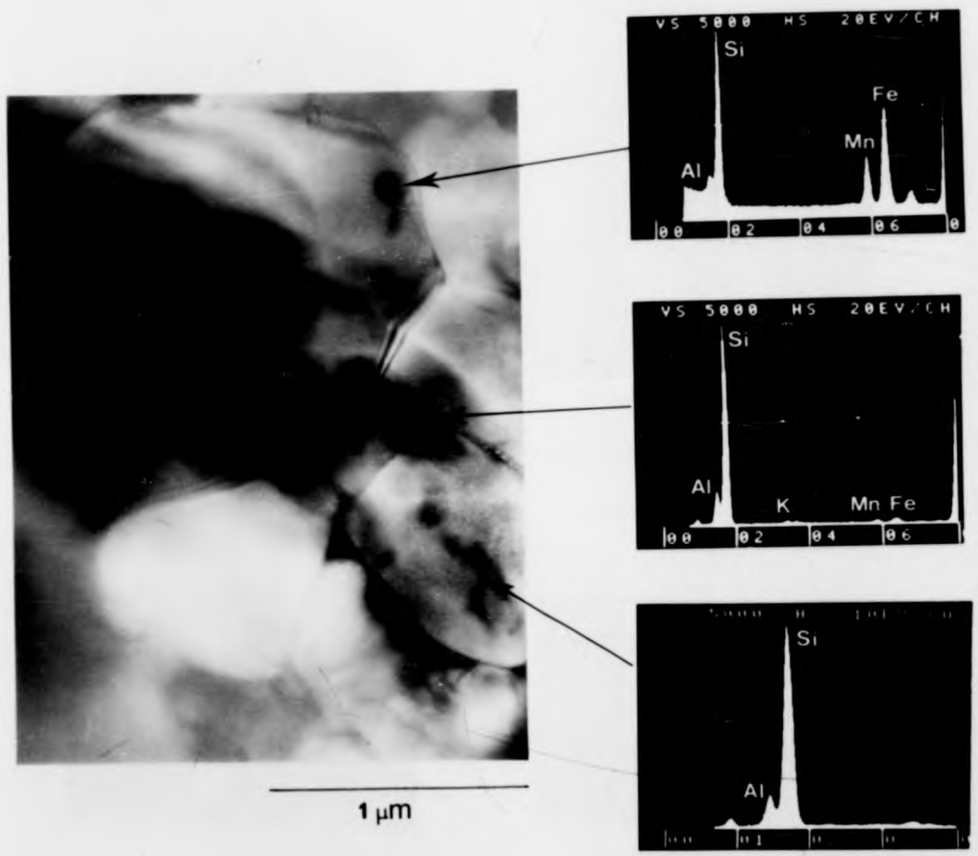

Figure 3.10: Multiple-junction intergranular phase in ceramic A2.

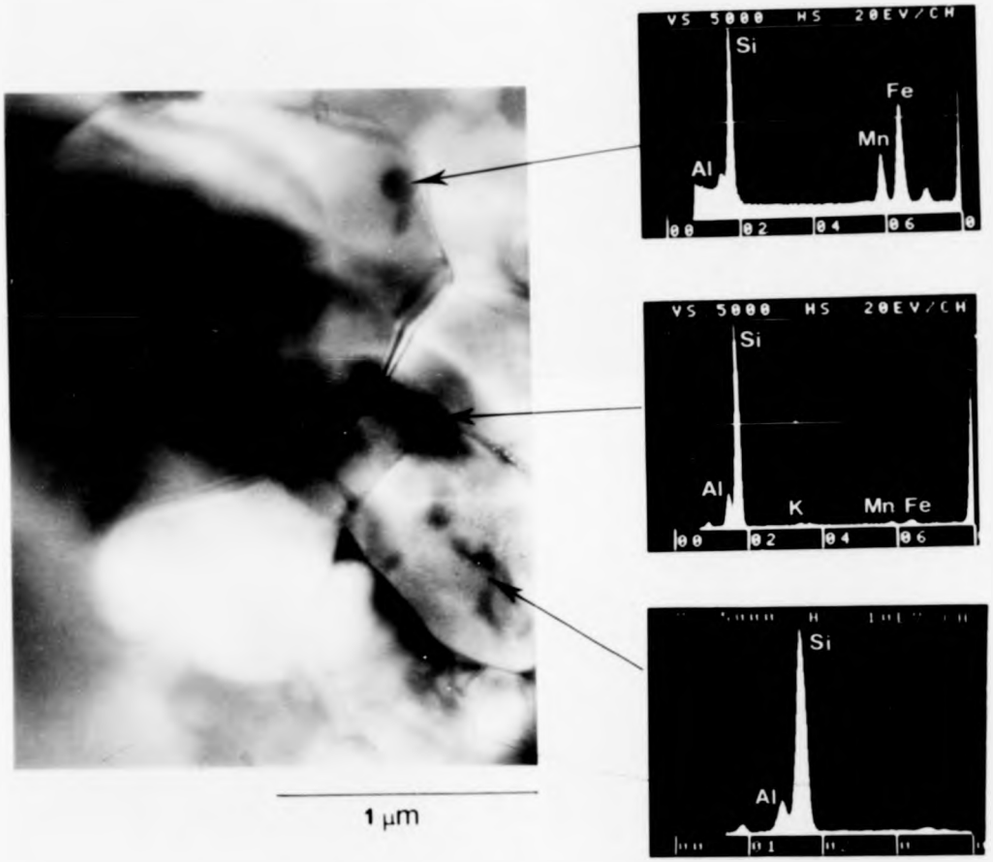

Figure 5.10: Multiple-junction intergranular phase in ceramic A2.

Figure 3.11: Microstructure of ceramic B1.

Figure 3.11: Microstructure of ceramic B1.

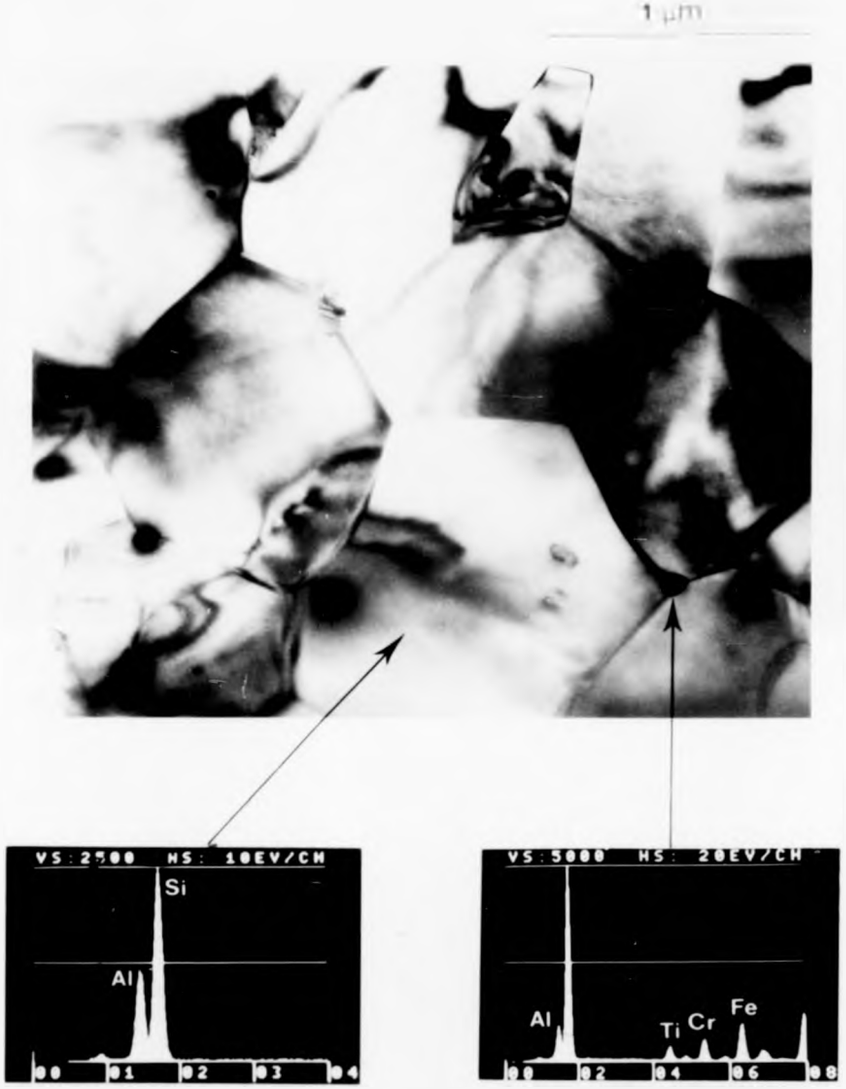

Figure 3.11: Microstructure of ceramic 51.

could be resolved by bright field diffraction contrast. Small, $\leq$ 0.1 μm Fe-rich particles were homogeneously distributed throughout the microstructure, usually situated at grain junctions.

The microstructure of ceramic B2, whose batch composition differed from that of ceramic B1 by the addition of 1.5% MgO, is illustrated in figure 3.12. The microstructure was similar to that of ceramic B1. The major crystalline phase was β′. Although another crystalline phase was indicated by X-ray diffractometry this phase was not identified in the transmission electron microscope. The crystal morphology was usually equiaxed and hexagonal. The grain size was similar to that of ceramic B1. Edax microanalysis of the grains showed their composition to be 1.88 ± 0.16, consistent with the value of 2.00 predicted from the hot-pressing batch composition. The grain boundaries were curved and the multiple grain junctions were sharply resolved. No intergranular phases were imaged. However, concentrations of up to ∿ 1% Mg was detected in the microanalysis of the β′ grains. Fe-rich impurity-containing particles existed as an inhomogeneous distribution.

2.2.2. Ceramics C1 and C2

The microstructure of ceramic C1 differed slightly from those of ceramics A and B. The batch composition of this ceramic had contained a relatively large quantity of Si_3N_4 and less of AlN and SiO_2 (table 3.1). The β′ crystal phase was equiaxed and hexagonal, but was of smaller grain size. This may have been due to a greater number of nucleation sites associated with Si_3N_4, available for β′ during the densification of the ceramic. The composition of the β′ grains was 1.95 ± 0.12, slightly higher than that predicted from the hot-pressing batch composition. This high value may have been due to the formation of Si-rich intergranular phases. Occasional

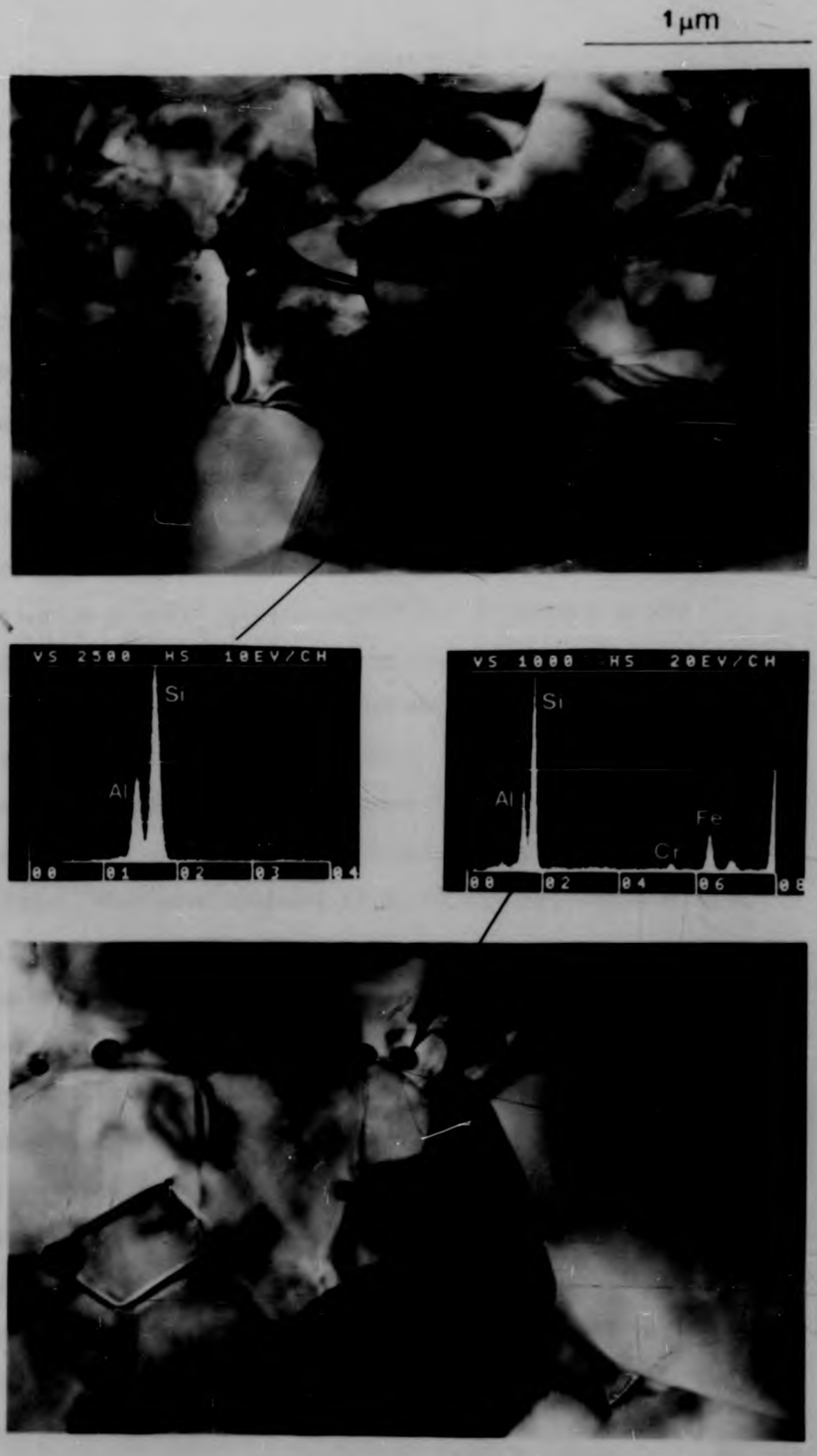

Figure 3.12: Microstructure of ceramic B2.

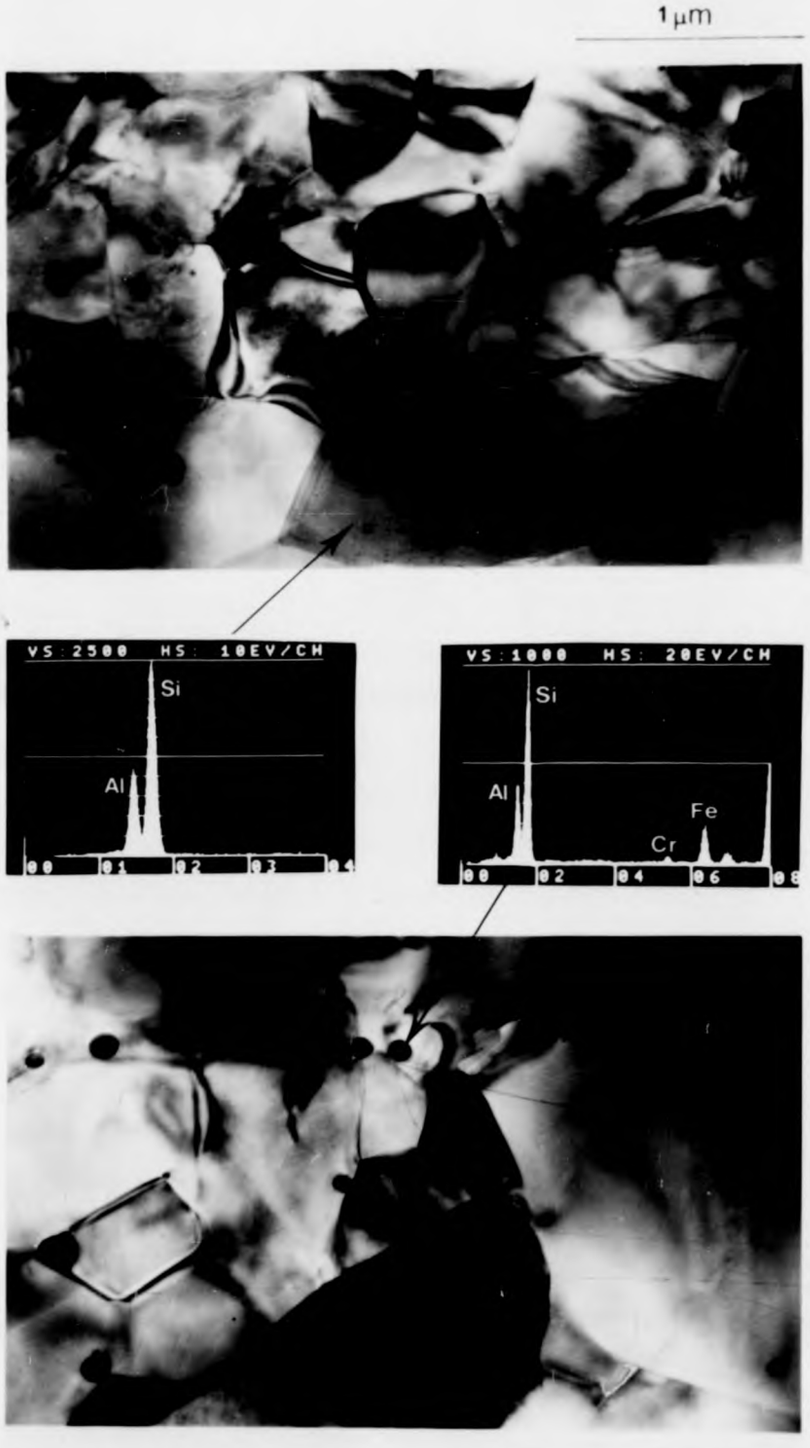

Figure 3.12: Microstructure of ceramic B2.

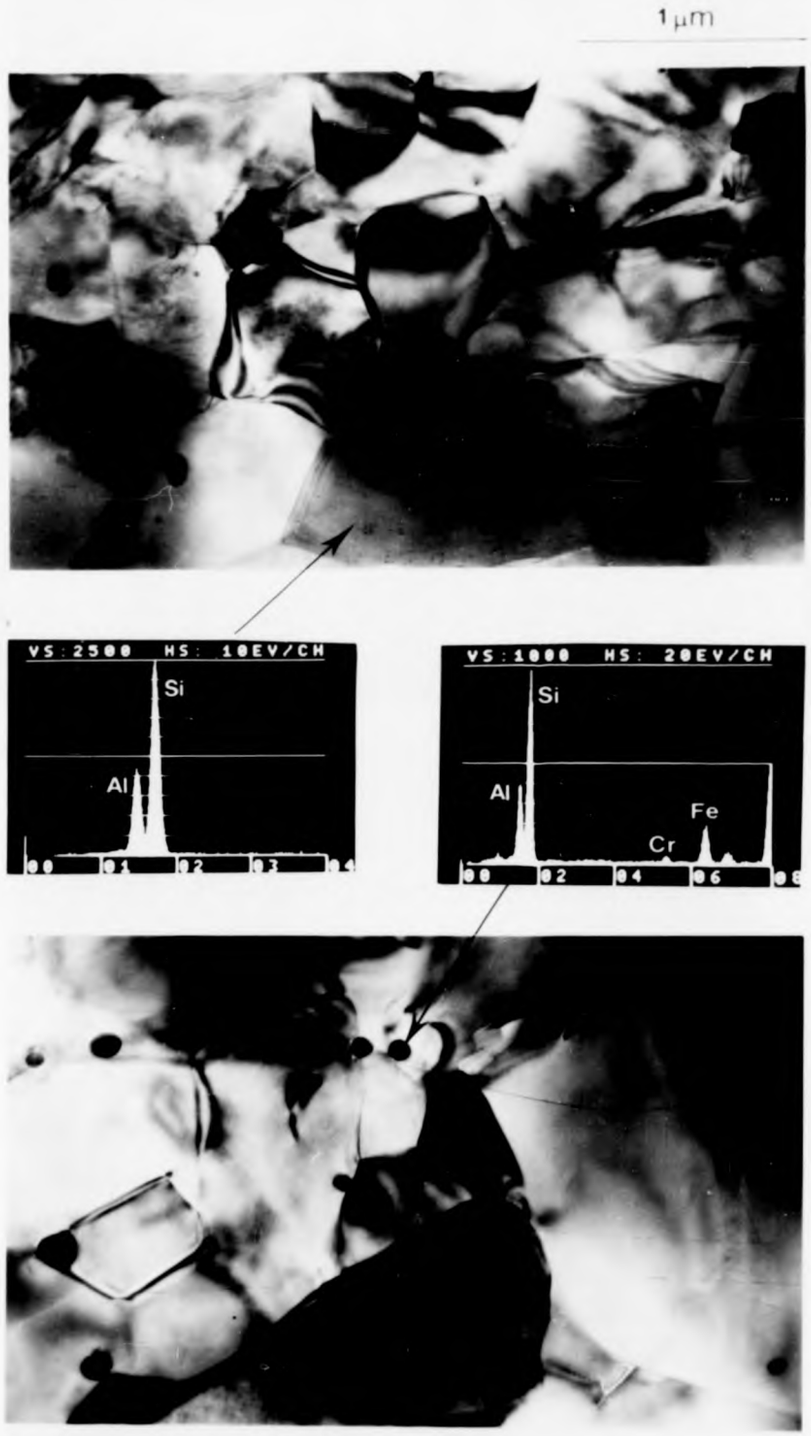

Figure 3.12: Microstructure of ceramic B2.

crystalline pockets of intergranular phase were resolved (figure 3.13). Fe-rich impurity particles were again present as an inhomogeneous distribution.

The microstructure of ceramic C2 is illustrated in figure 3.14. This ceramic was fabricated from the same batch composition as ceramic C1 but with the addition of 2.4% MgO. The grain morphology was equiaxed and hexagonal. The substitution level of the grains was 1.86 ± 0.17, consistent with that calculated from the hot-pressing batch composition.

The microstructure of ceramic C2 differed from that of the other ceramics of substitution level $z \sim 2$ in respect of its containing a large quantity of intergranular second phase. Many grains were of rounded morphology and sharp junctions. No intergranular phase could be imaged locally. However, large quantities of intergranular phase were imaged next to prism plane facets of β' grains. These areas were up to $\sim$ 0.3 μm across and were non-crystalline. They were composed of up to $\sim$ 8% Mg, compared to a maximum concentration of 2% in the β' grains.

The presence of large quantities of intergranular hot-pressing residue in ceramic C2 is due to the oxygen-richness of its composition relative to the β' phase line. Independent studies have shown that β' ceramics which are O-rich relative to the β' phase line contain second phases other than β' [Lewis et al 1977, Greil and Weiss 1982]. This extra phase was not present in the MgO-containing ceramic B2 due to its relative N-richness (figure 3.1). Although it has been suggested that N-rich β' ceramics do not fully densify [Kuwabara et al 1980], all the ceramics of this study were observed to be locally dense.

Figure 3.13: Microstructure of ceramic C1.

Figure 3.13: Microstructure of ceramic C1.

Figure 3.13: Microstructure of ceramic C1.

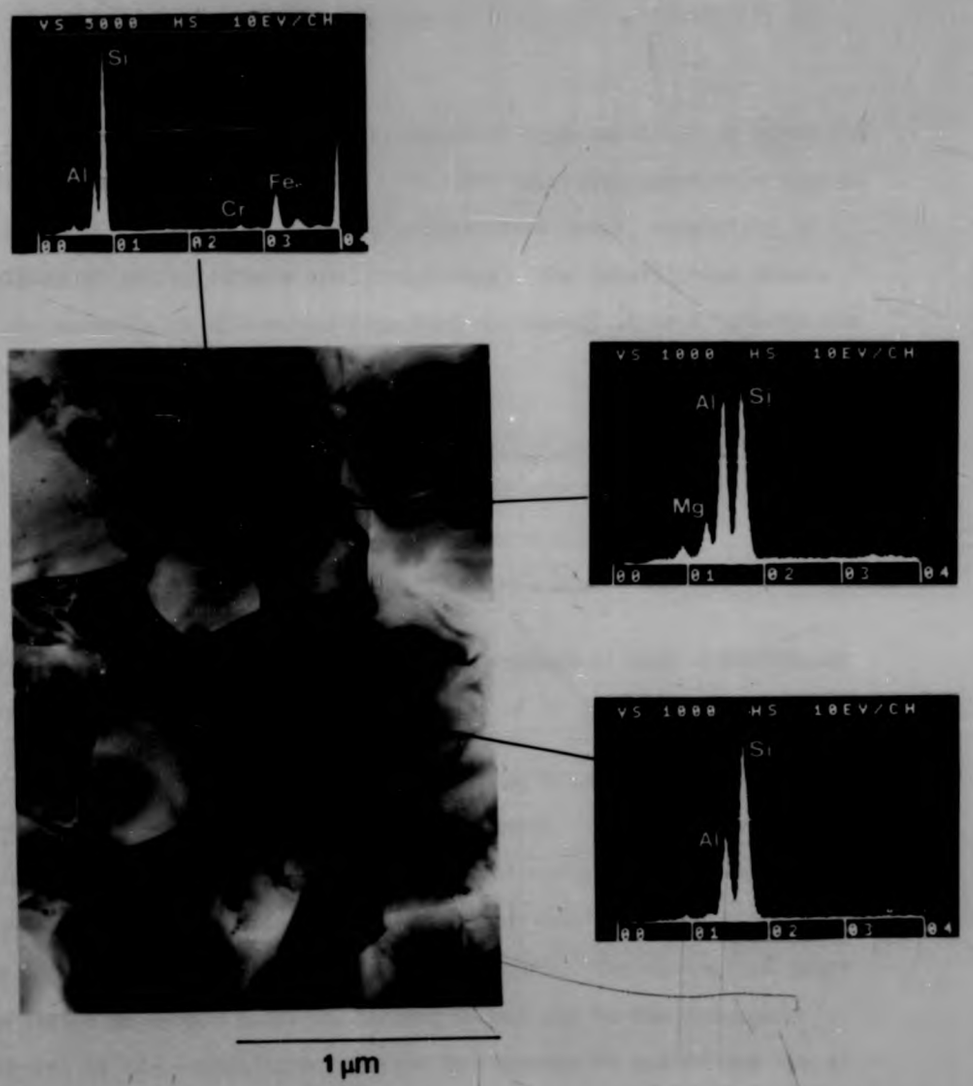

Figure 3.14: Microstructure of ceramic C2.

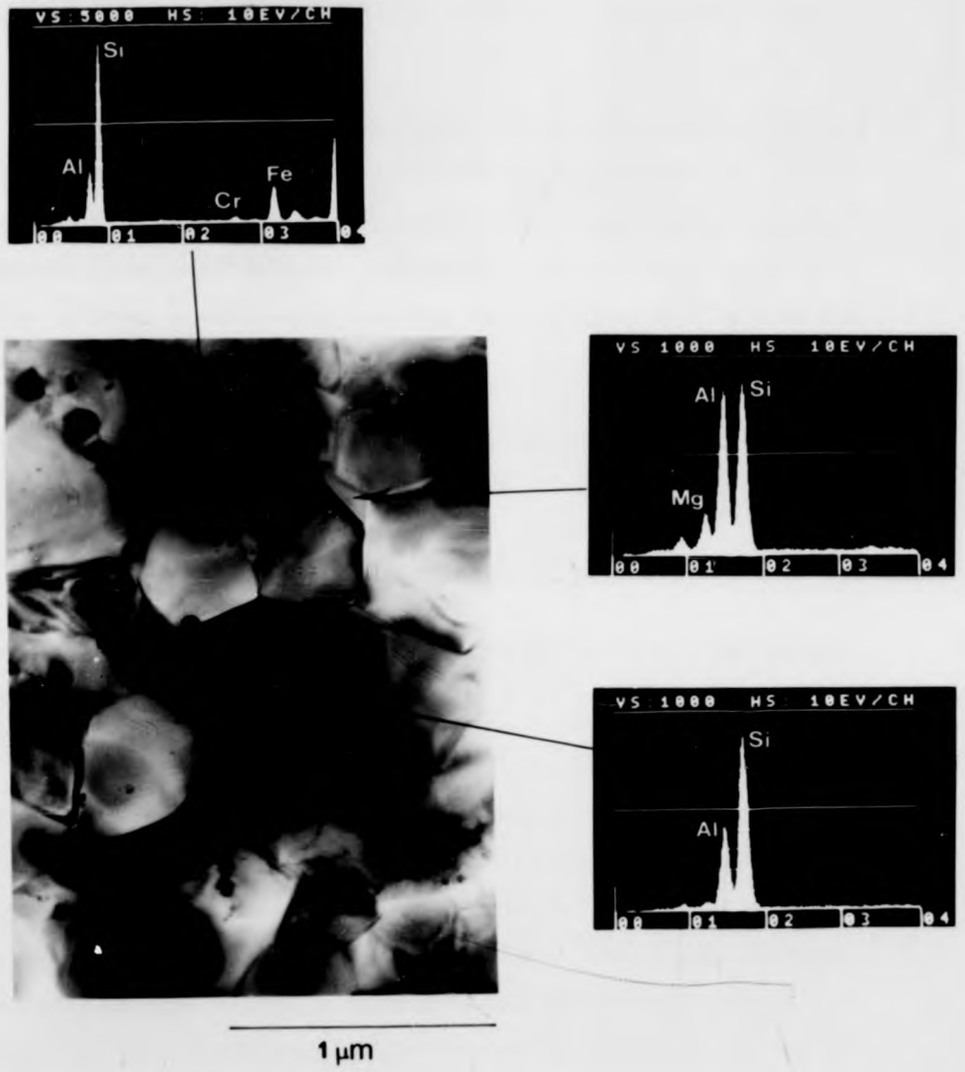

Figure 3.14: Microstructure of ceramic C2.

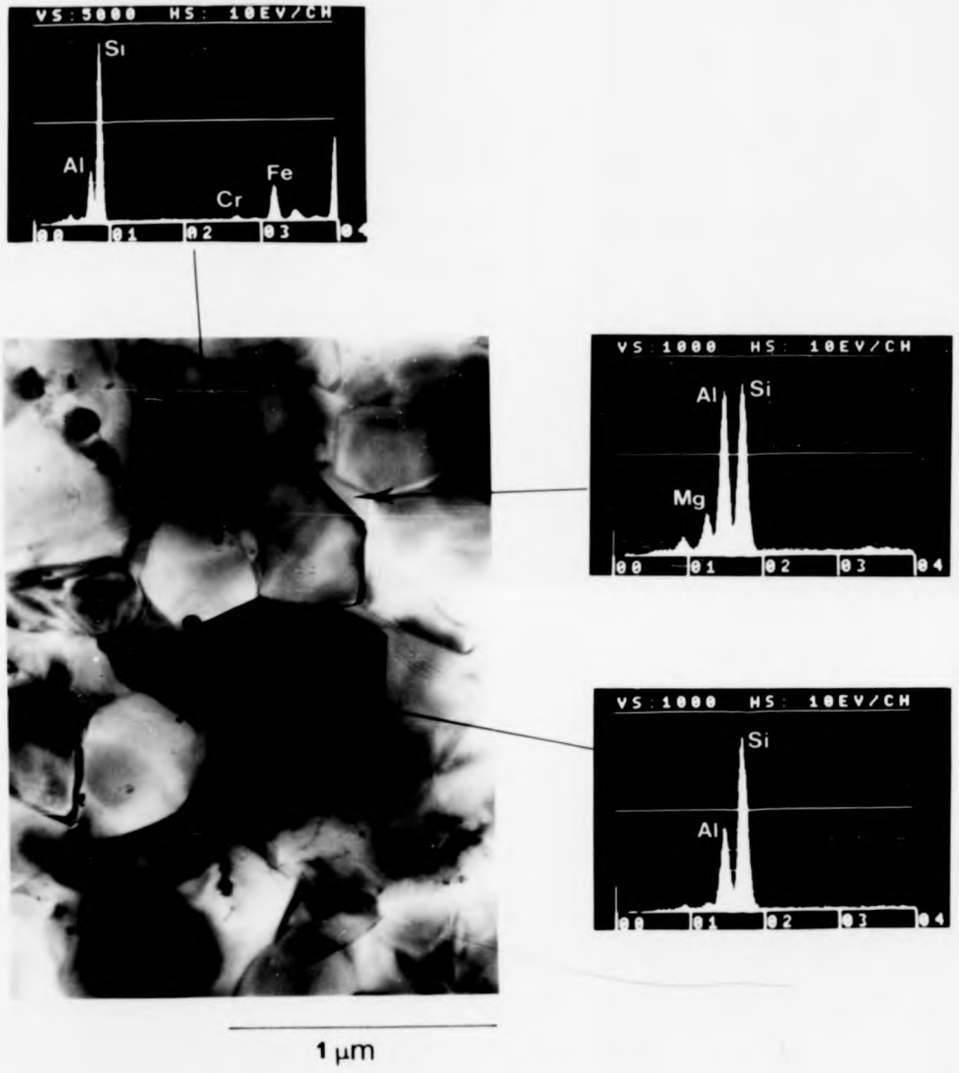

Figure 3.14: Microstructure of ceramic C2.

2.3. Ceramics of high substitution level, $z \sim 4$ (ceramics D1, D2 and D3)

The microstructures of the ceramics of high substitution level are illustrated in figures 3.15 and 3.16. The microstructures were similar to those of the ceramics of lower substitution level, consisting of equiaxed β' grains of hexagonal morphology. The substitution levels of the ceramics as determined from EDAX microanalysis of β' grains are listed in table 3.3.

Ceramic	Substitution Level
D1	3.38 ± 0.13
D2	4.11 ± 0.05
D3	3.88 ± 0.20

Table 3.3: Substitution level, z, of the ceramics of high substitution level as determined by EDAX microanalysis of β' grains in the TEM.

No intergranular phase was imaged using bright field diffraction contrast at bi-grain junctions in the ceramics. Grain boundaries were usually sharply resolved. The silica-rich intergranular phase was confined to widely-dispersed pockets at multiple grain junctions in the ceramics D1 and D3 (figures 3.15 and 3.16). The absence of large quantities of such a phase in ceramic D2 was due to the nitrogen-richness of its composition relative to ceramics D1 and D3 and the β' phase line (figure 3.1).

All three ceramics contained the Fe and impurity-rich particles observed in all the ceramics.

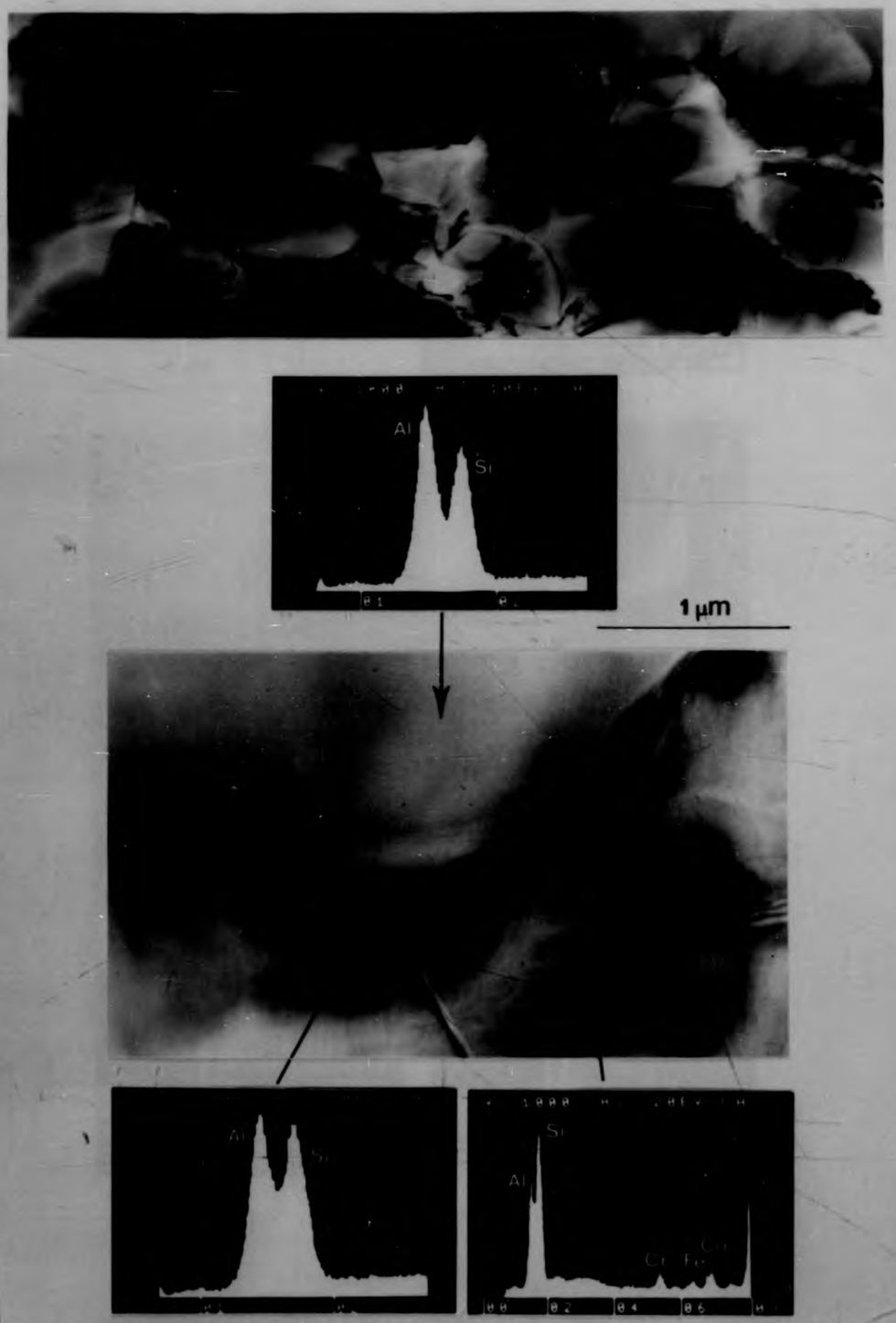

Figure 3.15: Microstructure of ceramic D1.

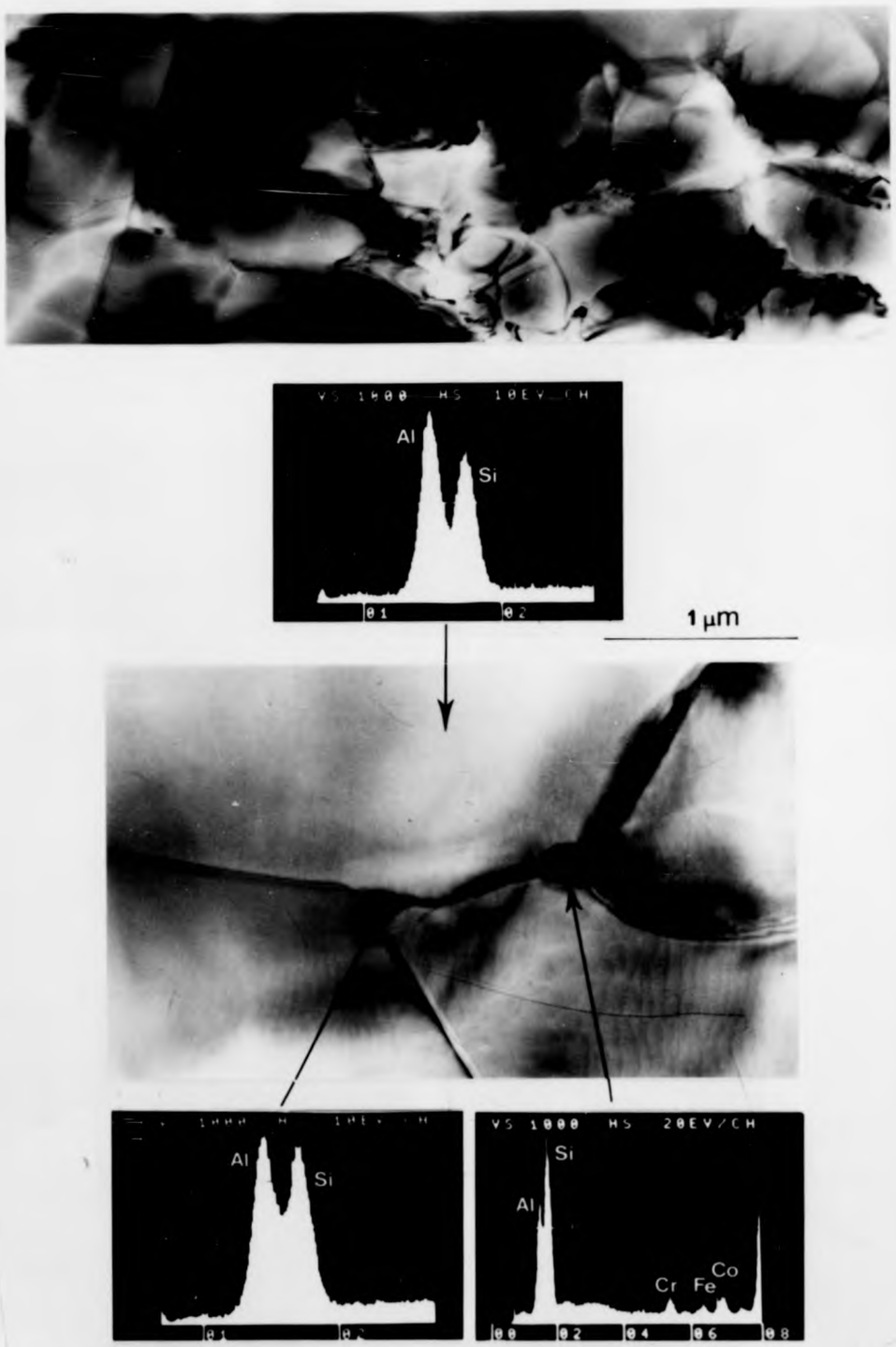

Figure 3.15: Microstructure of ceramic D1.

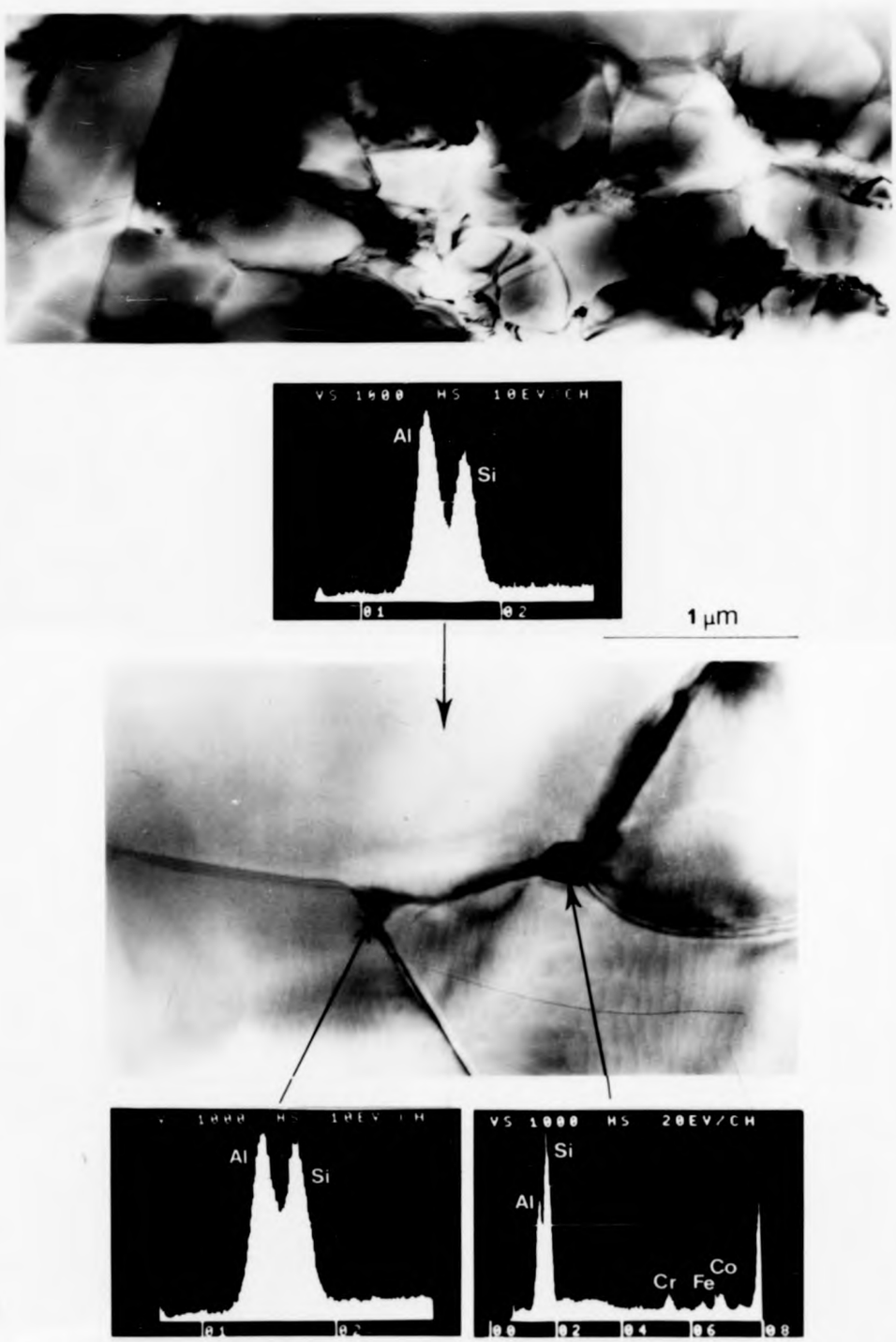

Figure 3.15: Microstructure of ceramic D1.

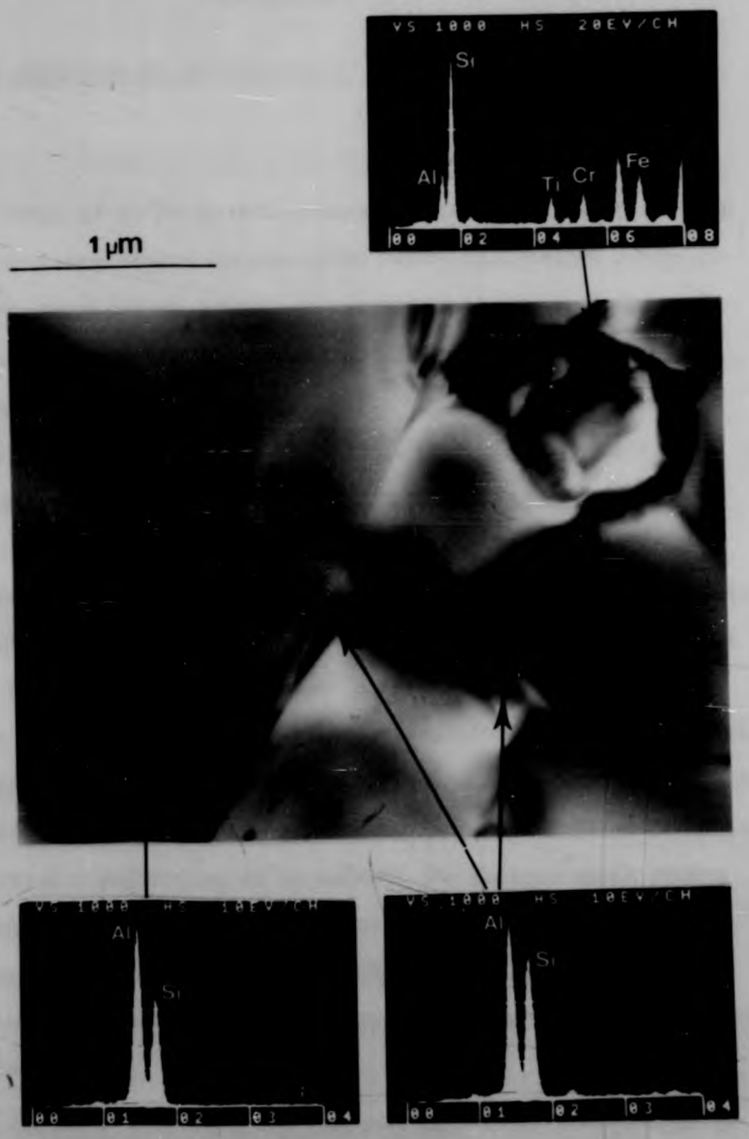

Figure 3.16: Microstructure of ceramic D3

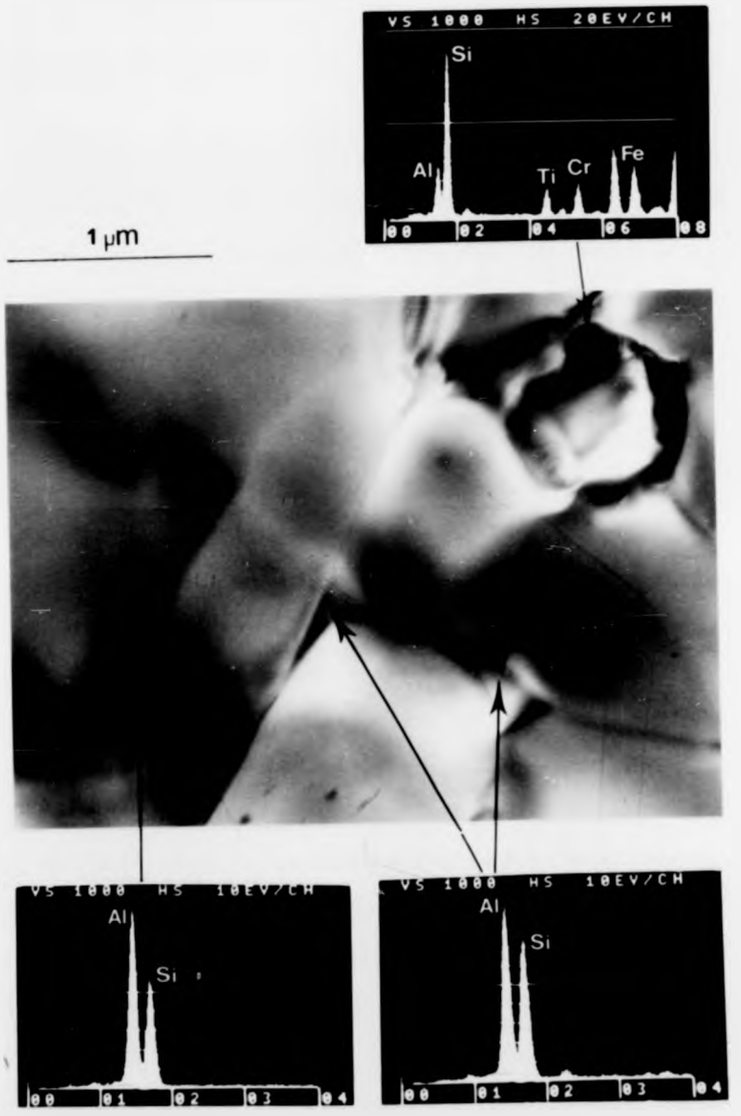

Figure 3.16: Microstructure of ceramic D3

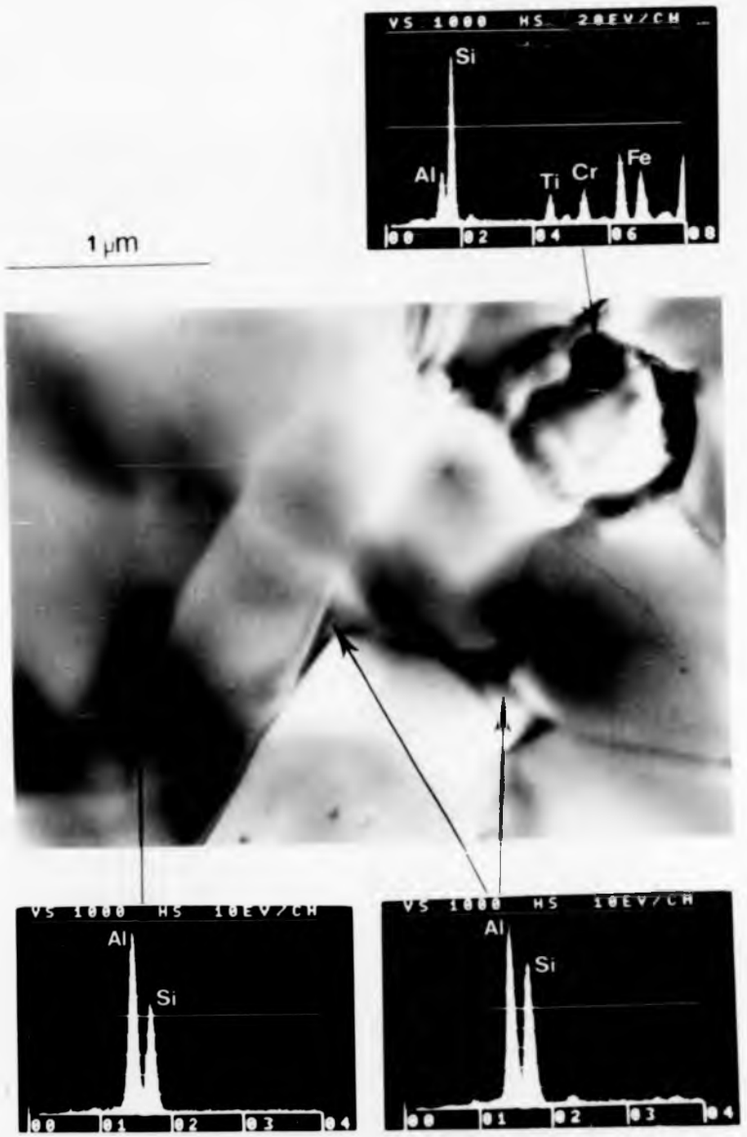

Figure 3.16: Microstructure of ceramic D5

CHAPTER FOUR

THE OXIDATION OF HOT-PRESSED β′ Si-Al-O-N CERAMICS

The range of β′ Si-Al-O-N ceramics chosen for study have been oxidised at temperatures between 1200-1400°C for periods of up to 400h. A temperature of 1350°C was chosen as the most suitable for comparison of the oxidation behaviour of the ceramics since this temperature is close to the anticipated upper working temperature of ceramic engine components. In addition this temperature range was chosen so that the results of the oxidation experiments could be related to the investigation of the mechanical deformation behaviour of ceramics A1 and A2 which had been carried out previsouly [Karunaratne 1980] and which has been further defined in this work (Chapter 5). At these temperatures a thick, coherent oxide layer formed on the surface of all the materials. Characterisation of the structural and compositional natures of these layers and analysis of the kinetics of oxidation of "as-pressed" and heat-treated ceramics has permitted a definition to be made of the factors which govern the oxidation process. From these observations a model for the mechanism of oxidation of β′ Si-Al-O-N ceramics has been defined. This is presented in this chapter after a description of the experimental observations.

4.1. Oxide scale structure and composition

4.1.1. The oxide scales of ceramics of low substitution level, $z \sim 1$ (ceramics A1 and A2)

The oxide scales of ceramics A1 and A2 were completely amorphous.

X-ray diffraction traces of the surface of the oxide layers which formed on oxidation at 1350°C indicated that no crystalline phases formed which were not present prior to oxidation (figures 4.1 and 4.2). Visual examination showed the surfaces of the scales to be smooth, dark and highly reflective. No crystalline fragments other than β´ Si-Al-O-N were found in the dispersed scales in the transmission electron microscope (figures 4.1 and 4.2). No scale crystallinity could be resolved in the outer surfaces of the scales which were structureless and uncracked, or in fracture surfaces observed in the scanning electron microscope.

Large spherical pores were observed in the scales. These pores often extended across the entire width of the scale (Figures 4.1 and 4.2). The spherical shape of the pores confirmed that the scale is liquid at the oxidation temperature. The pores are composed of N_2 gas which formed on oxidation according to reactions of the type

$$4\ Si_5AlON_7 + 21\ O_2 \rightarrow 20\ SiO_2 + 2Al_2O_3 + 14\ N_2 \qquad (4.1)$$

The N_2 generated by this reaction precipitates as a gas because the solubility of N in $MgO\text{-}SiO_2\text{-}Al_2O_3$ glass is low, < 10% [Loehman 1980], and the diffusion rate of N is low compared with that of the other constituents of the scale because of its relatively large atomic size [Billy 1983]. The formation of other gaseous species such as Si(g), SiO(g) and SiO_2(g) is not expected because the partial pressure of these gases at the ceramic/oxide interface in β Si_3N_4 has been calculated to be low, $\leq 10^{-2}$ atm [Singhal 1976a]. The location of the pores close to the oxidation front indicates that the oxidation reaction (equation 4.1) takes place at this position.

Figure 4.1: Oxide scale of ceramic A1

(a) TEM

(b) SEM

(c) surface X-ray diffractometry

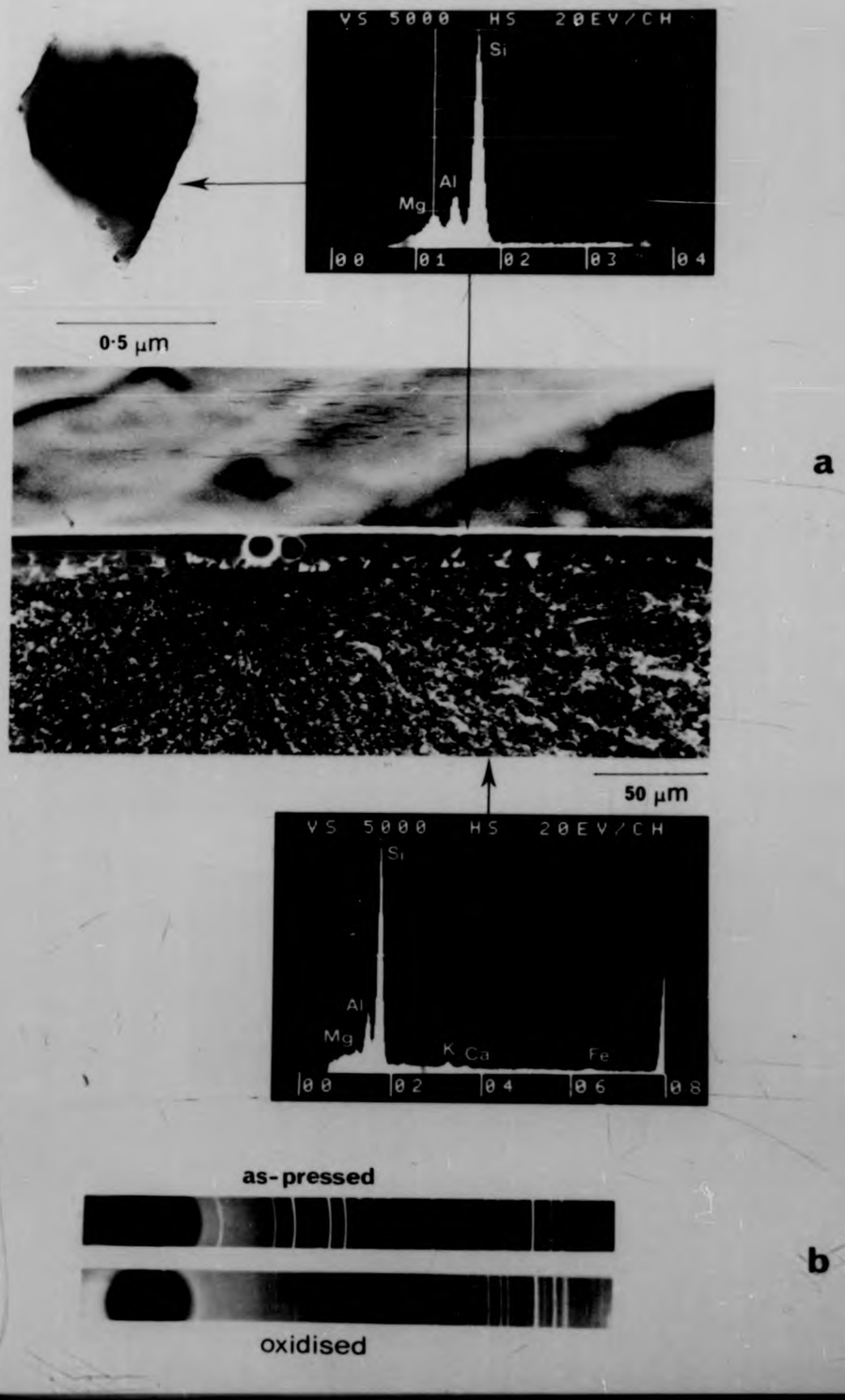

Figure 4.1: Oxide scale of ceramic Al

(a) TEM

(b) SEM

(c) surface X-ray diffractometry

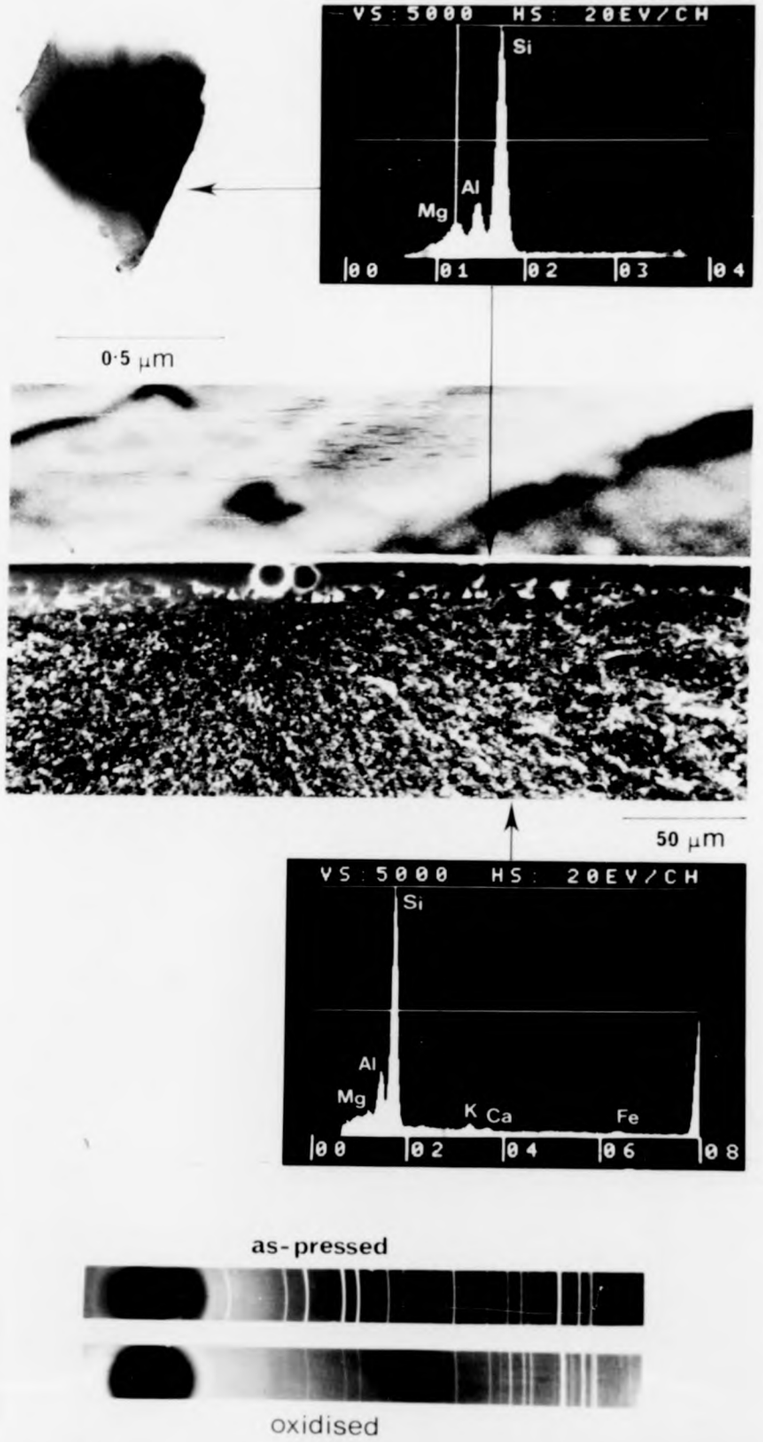

Figure 4.1: Oxide scale of ceramic Al

(a) TEM

(b) SEM

(c) surface X-ray diffractometry

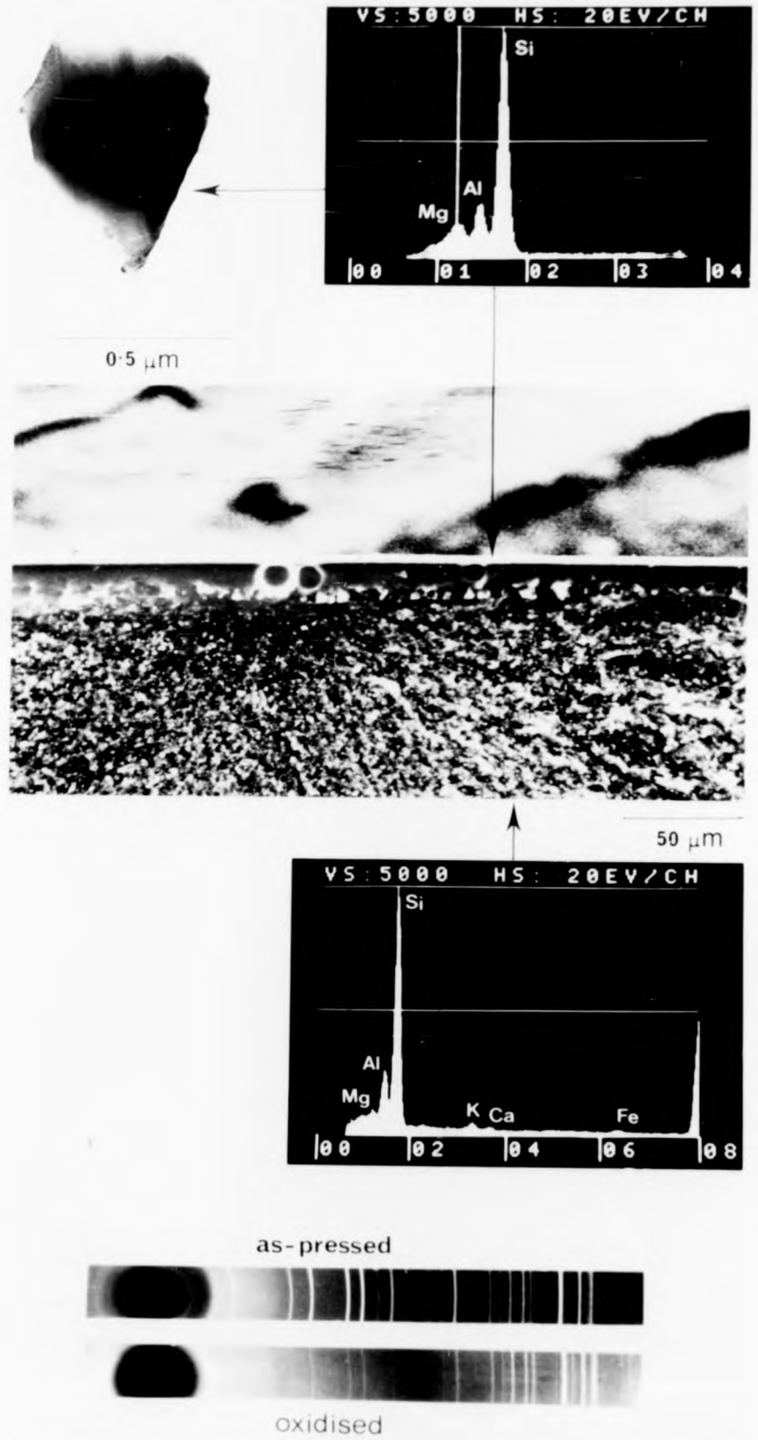

Figure 4.2: Oxide scale of ceramic A2

(a) TEM

(b) SEM

(c) surface X-ray diffractometry

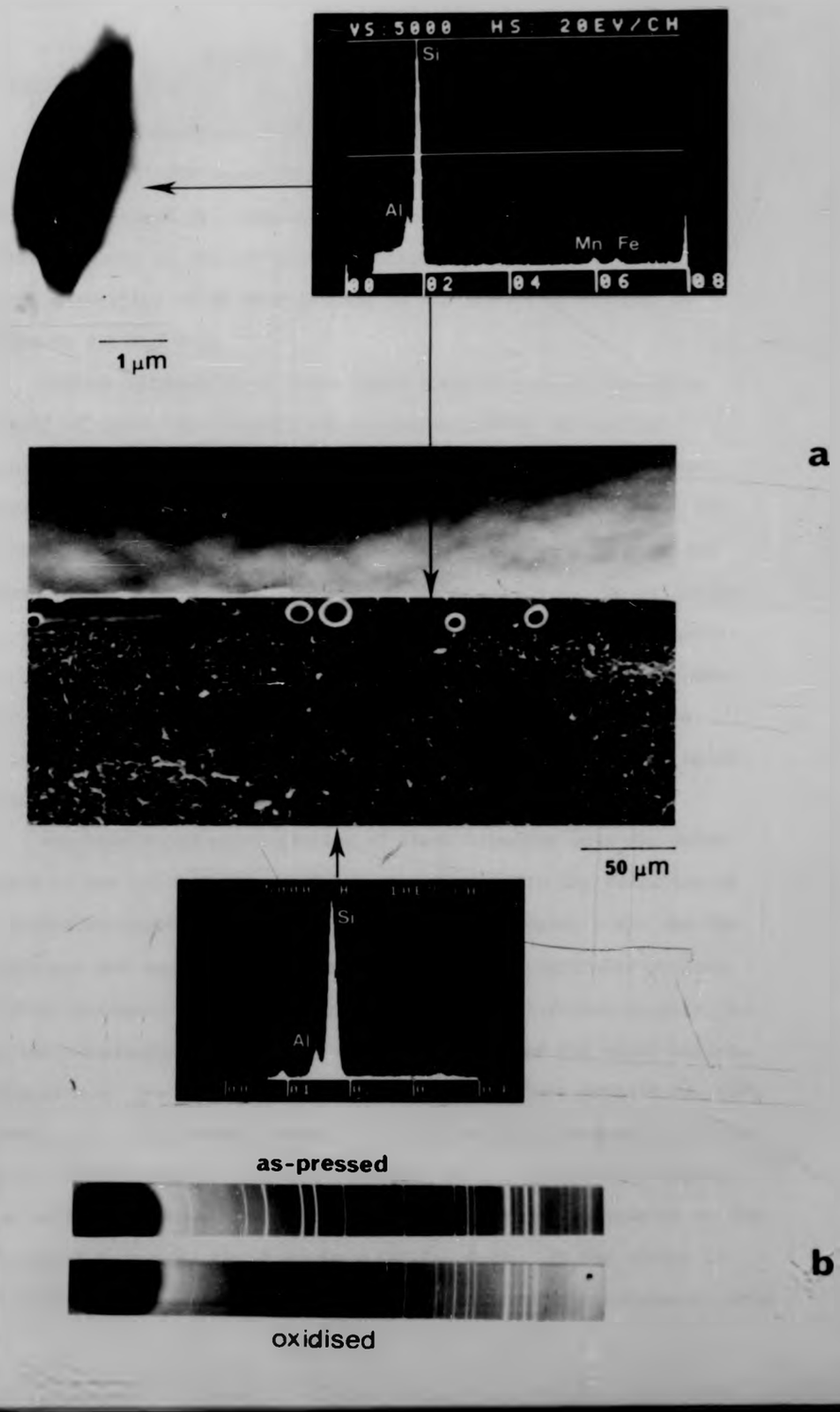

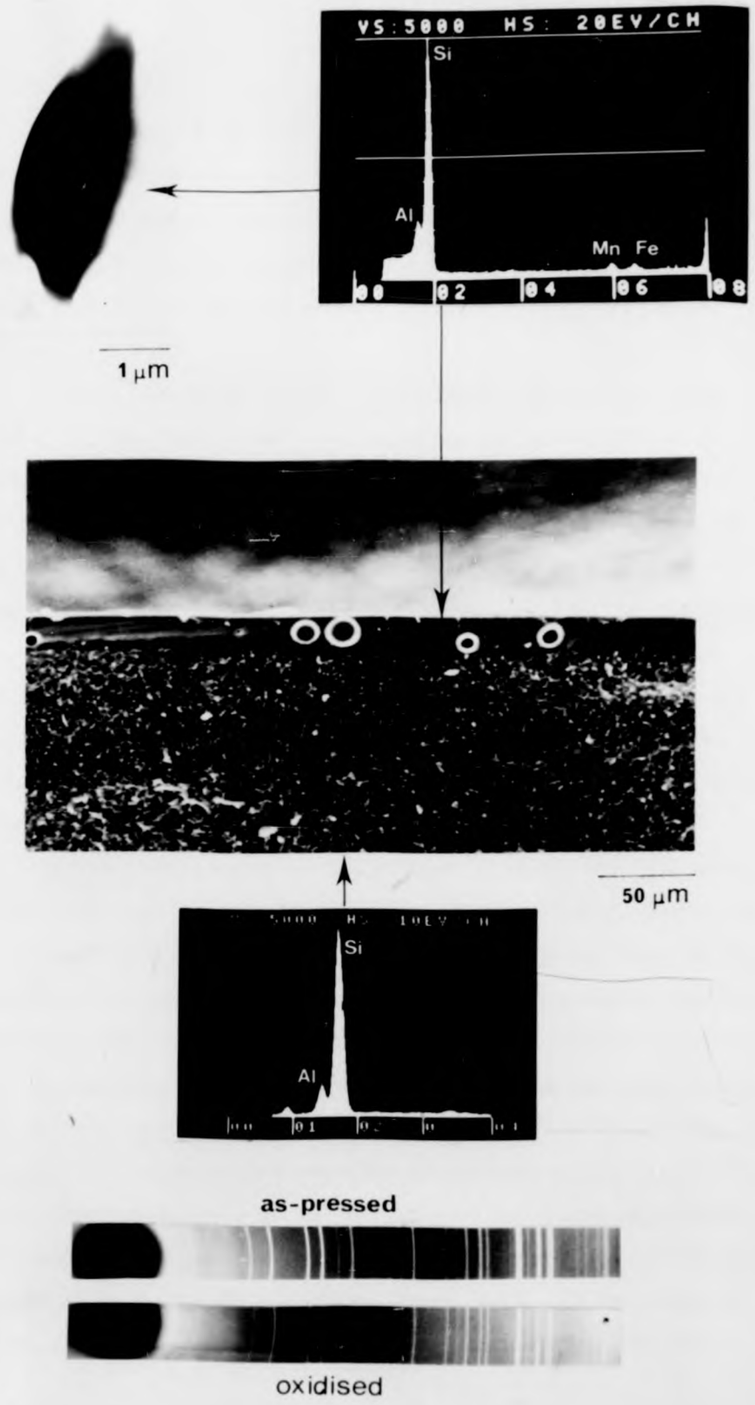

Figure 4.2: Oxide scale of ceramic A2

(a) TEM

(b) SEM

(c) surface X-ray diffractometry

Figure 1.2: Oxide scale of ceramic 'A'

(a) TEM

(b) SEM

(c) surface X-ray diffractometry

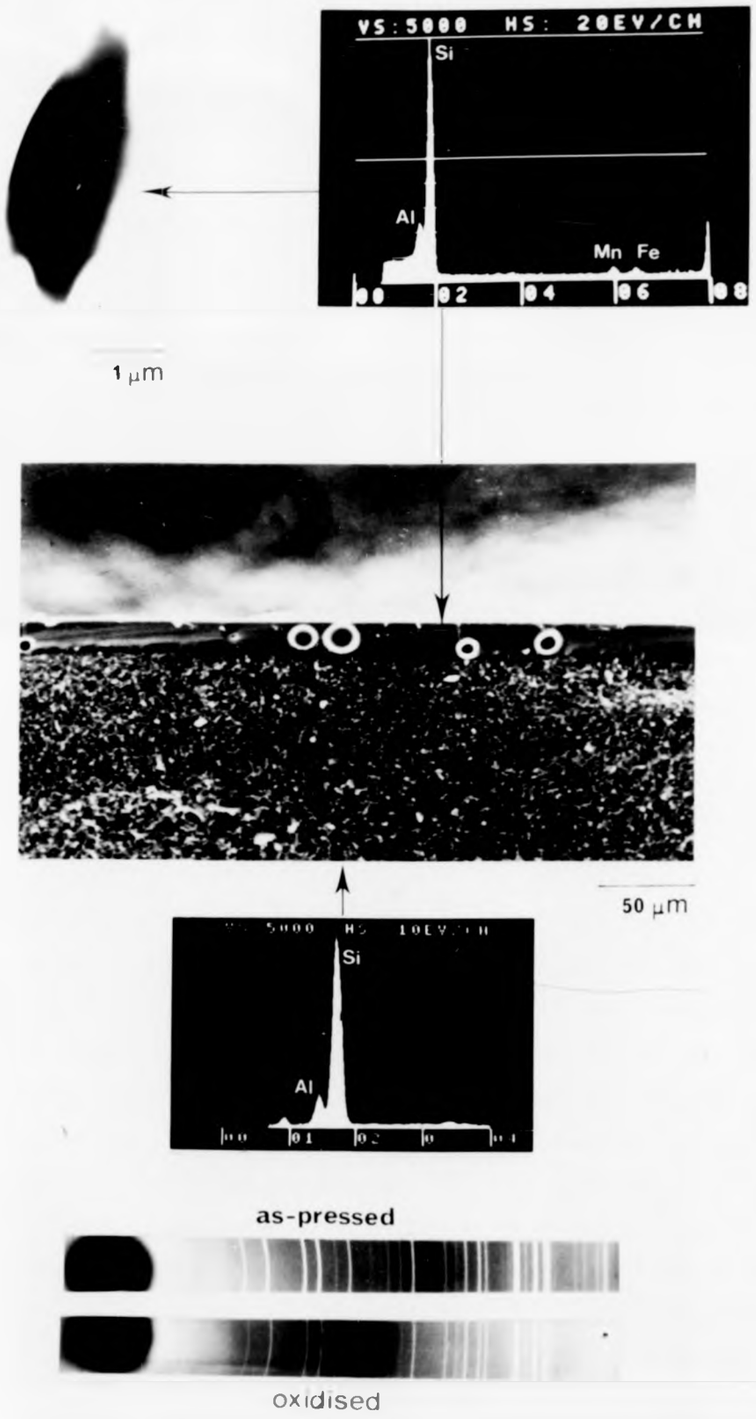

Scale composition

EDAX microanalysis of the oxide scales of ceramics A1 and A2 in both SEM and TEM revealed them to be very rich in the elements Na, Mg, K, Ca and Fe, compared with the low average quantities of these elements in the hot-pressing batch compositions ($\leq$ 1%). Large quantities of Mn were present in the scales of ceramic A2 (figures 4.1 and 4.2).

Average quantities of these minor constituents in the oxide scales of these two ceramics can be determined by the method described in Chapter 3 (section 3.1.5(a)) because of their homogeneous structure. These are presented in figures 4.3 and 4.4 for ceramics oxidised at 1350°C. The scatter in the data is high and does not admit of a fully unambiguous interpretation. On oxidation at this temperature the average concentration of the minor constitents in the oxide scales of each of these ceramics rapidly becomes very high relative to that of these elements in the bulk of the ceramic ($\leq$ 1%). This concentration changes little on further oxidation over about 20 hours duration, up to at least 300 hours.

The very rapid out-diffusion of these elements into the oxide scale in the initial stages of oxidation is due to the formation of a diffusion couple between the alumino-silicate oxide scale and the additive- and impurity-rich alumino-silicate intergranular regions. Further evidence for the rapidity of their out-diffusion is provided by their concentration profile across the width of the oxide scales. In scales of specimens oxidised for relatively short periods Mg, for example, is concentrated towards the outer scale of ceramic A1 (Fig. 4.5). The consequent very low viscosity of the scales of ceramics oxidised for up to 8 h at 1350°C gave rise to their distortion by the escape of N_2 gas to the atmosphere (figure 4.6). In the scales of ceramics oxidised for longer periods the minor scale constituents were

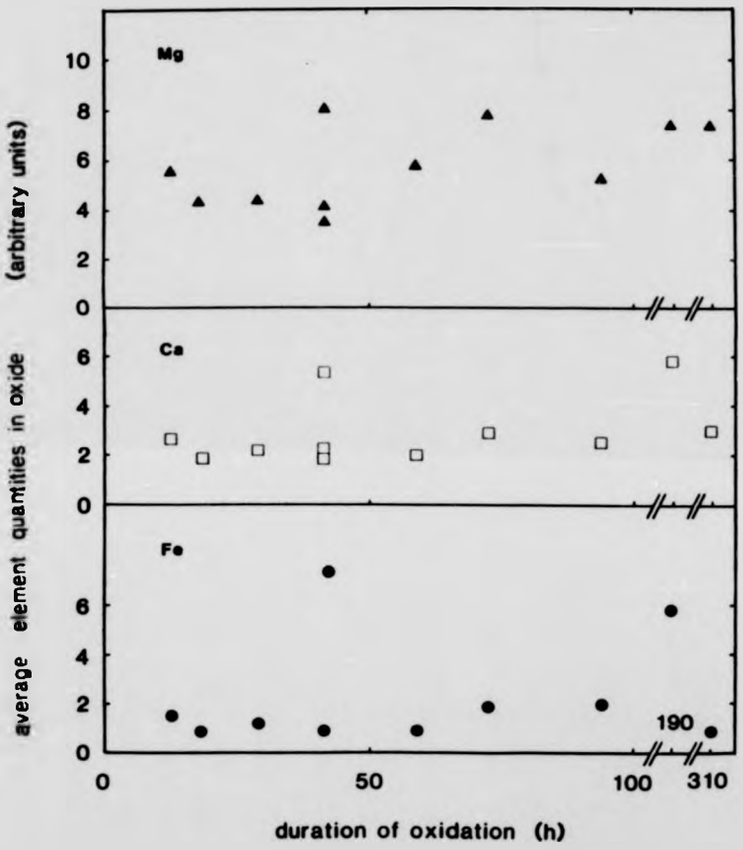

Figure 4.3: Average quantities of elements in the oxide scales of ceramic A1 oxidised at 1350°C.

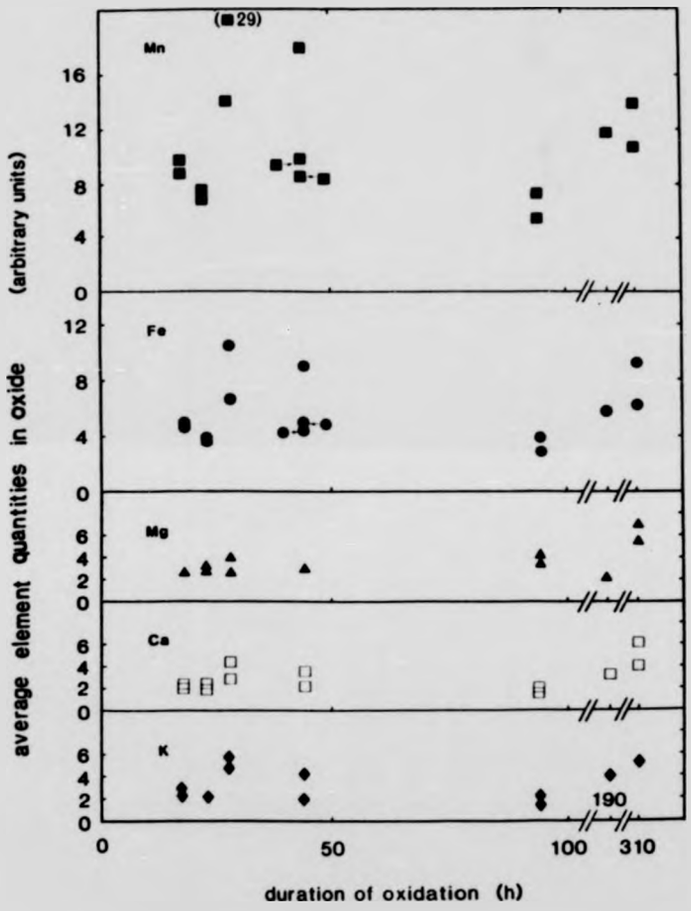

Figure 4.4 Average quantities of elements in the oxide scales of ceramic A2 oxidised at 1350°C.

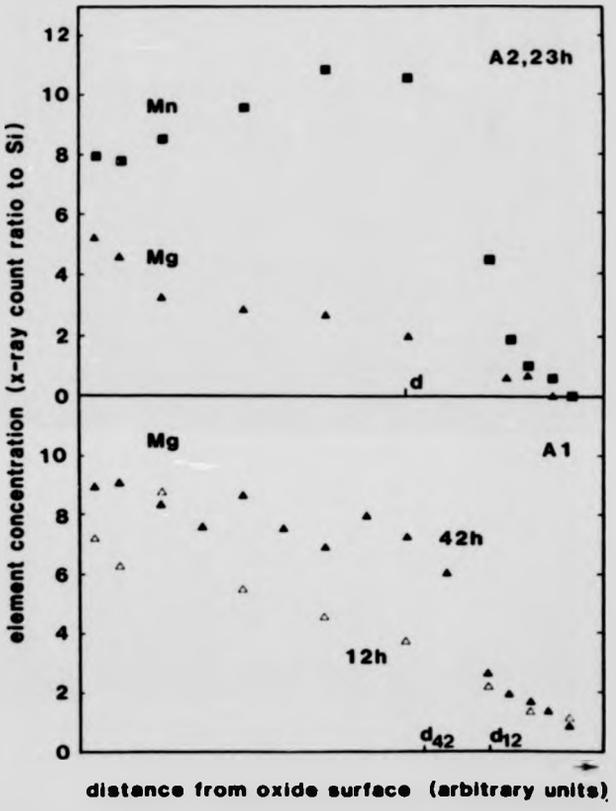

Figure 4.5: Distribution of elements across the oxide scales of the ceramics of low substitution level.

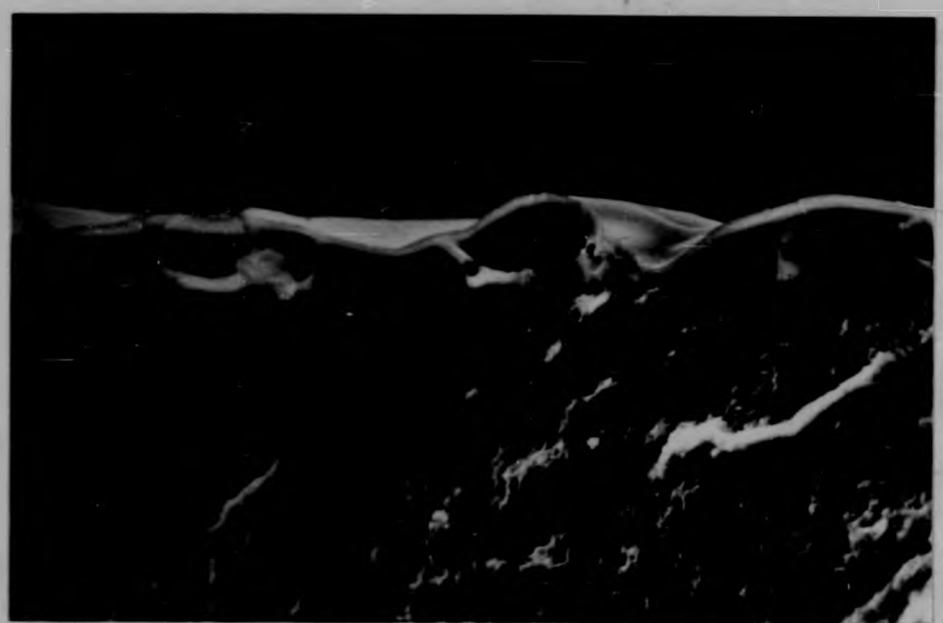

Figure 4.6: Oxide scale distortion due to low scale viscosity (ceramic A2 oxidised at 1350°C for 2 h).

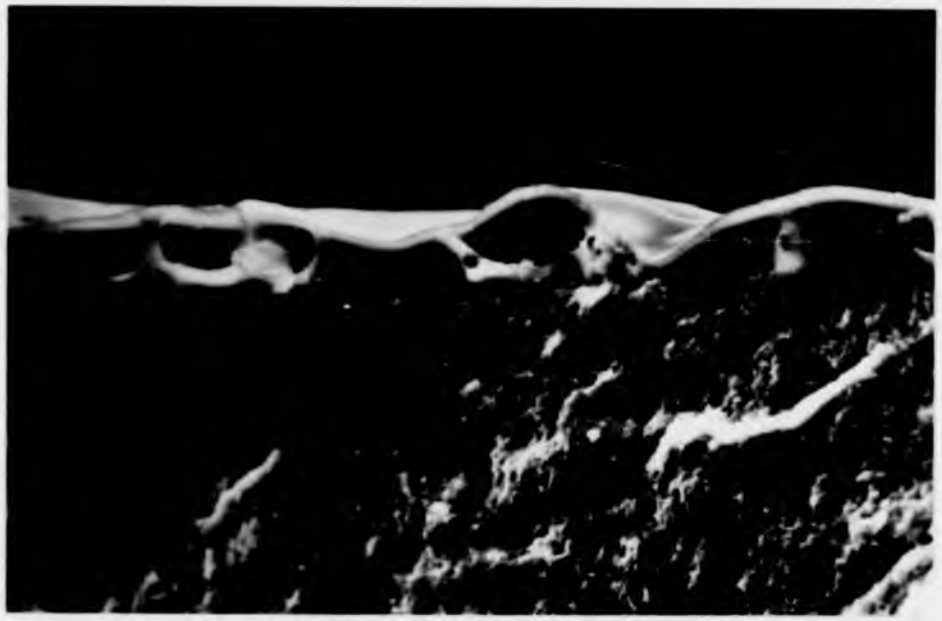

Figure 4.6: Oxide scale distortion due to low scale viscosity (ceramic A2 oxidised at 1350°C for 2 h).

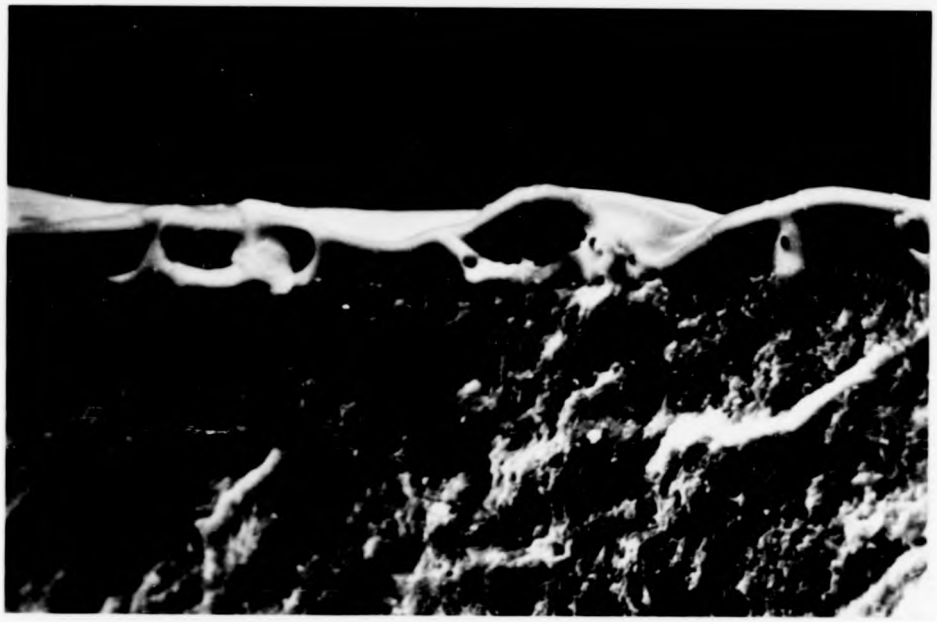

Figure 4.6: Oxide scale distortion due to low scale viscosity (ceramic A2 oxidised at 1350°C for 2 h).

more evenly distributed due to diffusional minimisation of concentration gradients (Figure 4.5).

The quantities of the minor scale constituents in the oxide scales changed little after oxidation of the ceramic for about 20 hours due to their removal from the subscale intergranular regions as depicted in figure 4.7. Despite nearly constant scale thickness with increasing duration of oxidation (Figure 4.19) the quantities do not continuously increase since grain-boundary denudation quickly extends throughout the bulk of the ceramic. Using a simple model of out-diffusion from a block in which the diffusant is initially uniformly distributed the diffusion coefficient of Mg in the bulk of ceramic A1 has been estimated to be similar to that in silicate glasses (Chapter 5, part 1). Using the same model, the intergranular concentration of Mg at the centre of the 0.7 mm oxidation specimens would be expected to be less than half of its original value after oxidation for 20 h at 1350°C.

4.1.2. The oxide scales of ceramics of intermediate substitution level $z \sim 2$ (ceramics B1, B2, C1 and C2)

The oxide scales of the ceramics of substitution level $z \sim 2$ were of similar nature to one another but different to those of ceramics A1 and A2. They were partially crystalline, with the degree of crystallinity being dependent on the quantity of MgO with which the ceramic was hot-pressed.

The visual appearance of the ceramics after oxidation was non-reflective and greyish. X-ray diffractometry confirmed that the scales of the ceramics all contained crystalline phases that were not present prior to oxidation (figures 4.8 - 4.11). However, little evidence for scale crystallinity was apparent from examination of the transverse fracture surfaces in the scanning electron microscope. Large spherical N_2 bubbles give rise to extensive local distortion of the scales of all four ceramics. Escape of the gas through the scale to the atmosphere gave rise to spherical pores at their outer surfaces. Some evidence for scale crystallinity was provided by small, non-spherical pores, most notably in the scales of ceramics C1 and C2. These pores did not exist in large quantitites. In addition the use of a microscope of high resolution (Cambridge 250) revealed that the scale of ceramic B1 was crystalline (Figure 4.8 (d)).

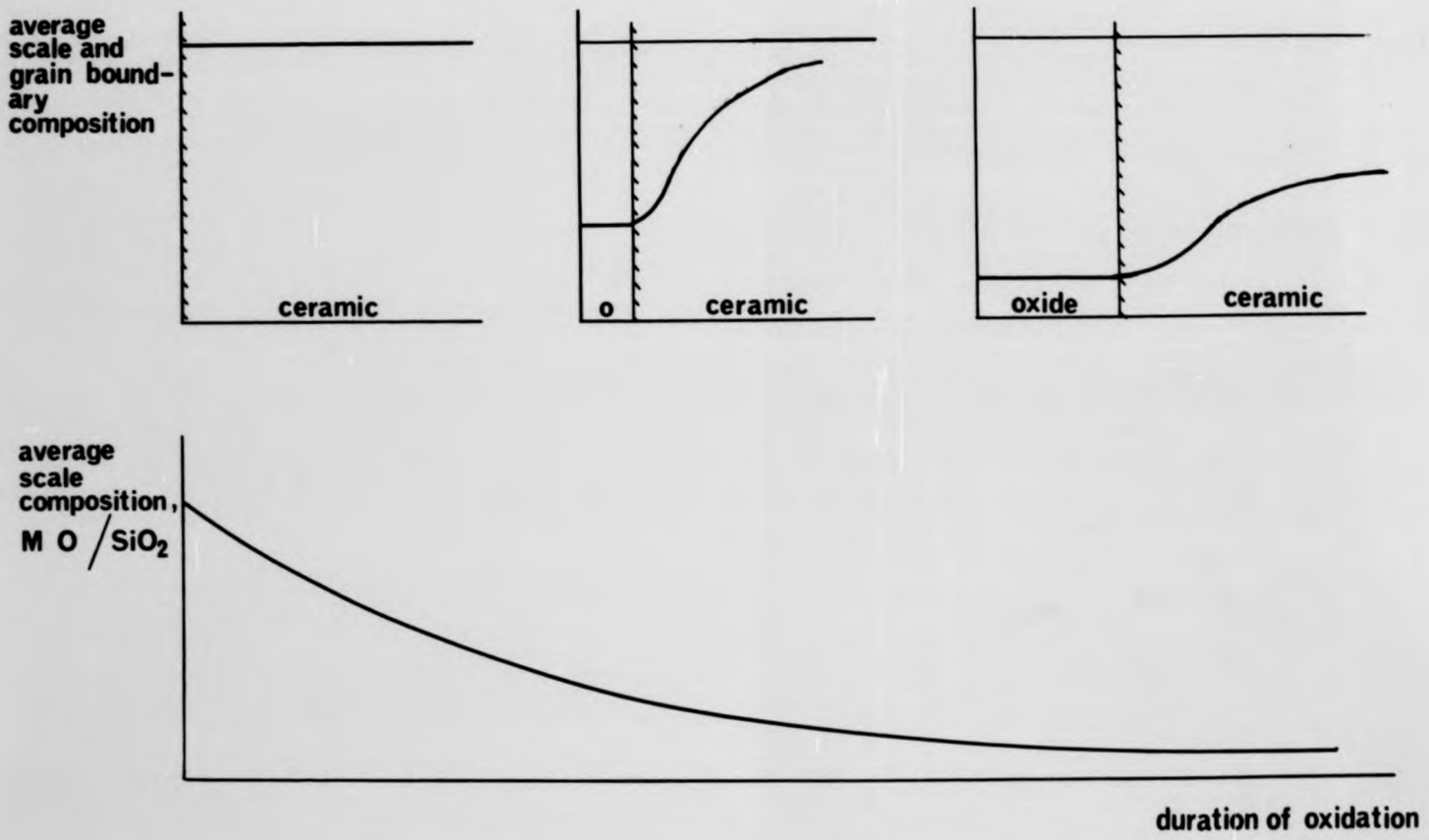

Figure 4.7: Time-dependent oxide scale composition and subscale element denudation.

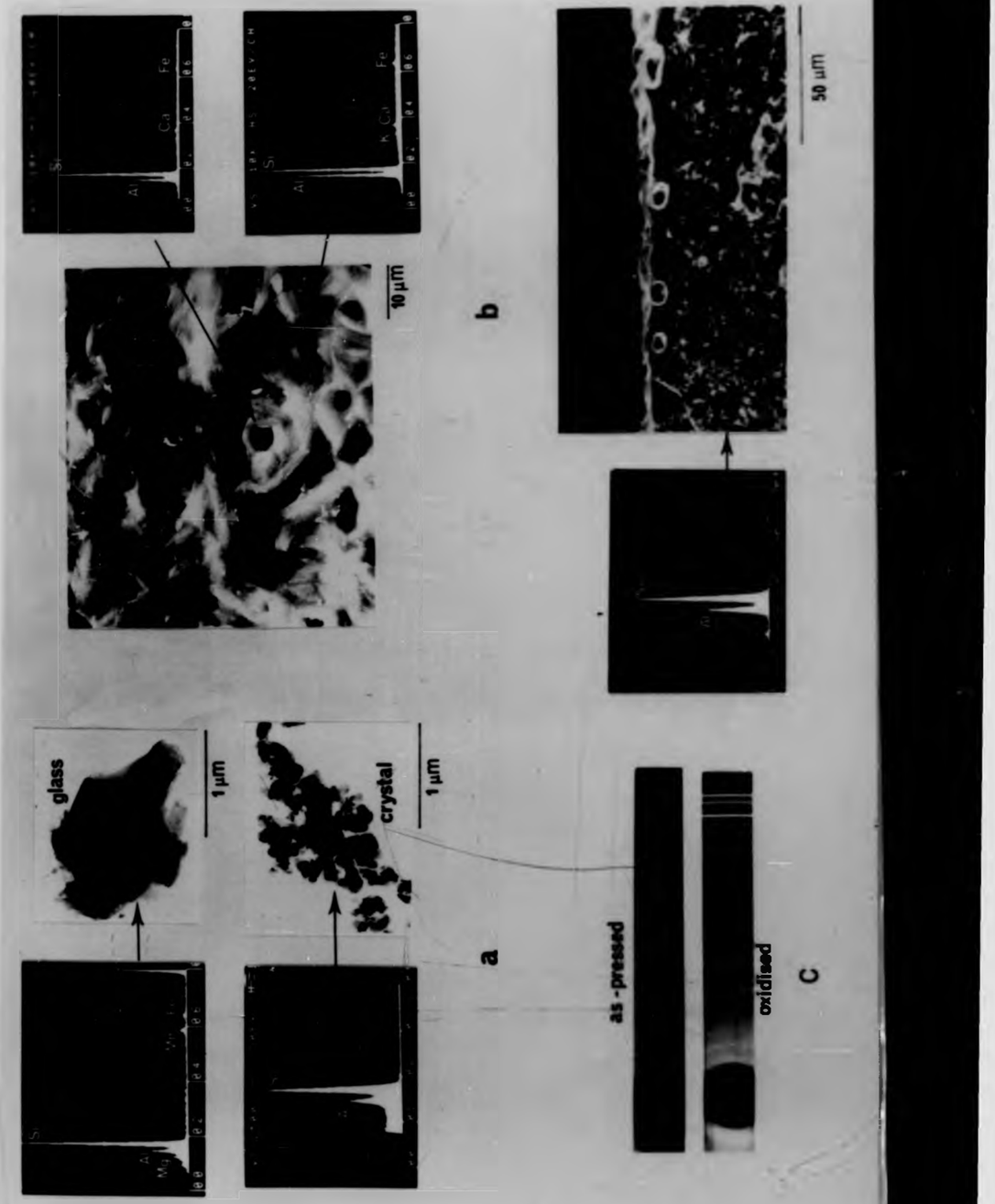

Figure 4.8: Oxide scale of ceramic B1

(a) TEM (b) SEM (c) surface X-ray diffractometry.

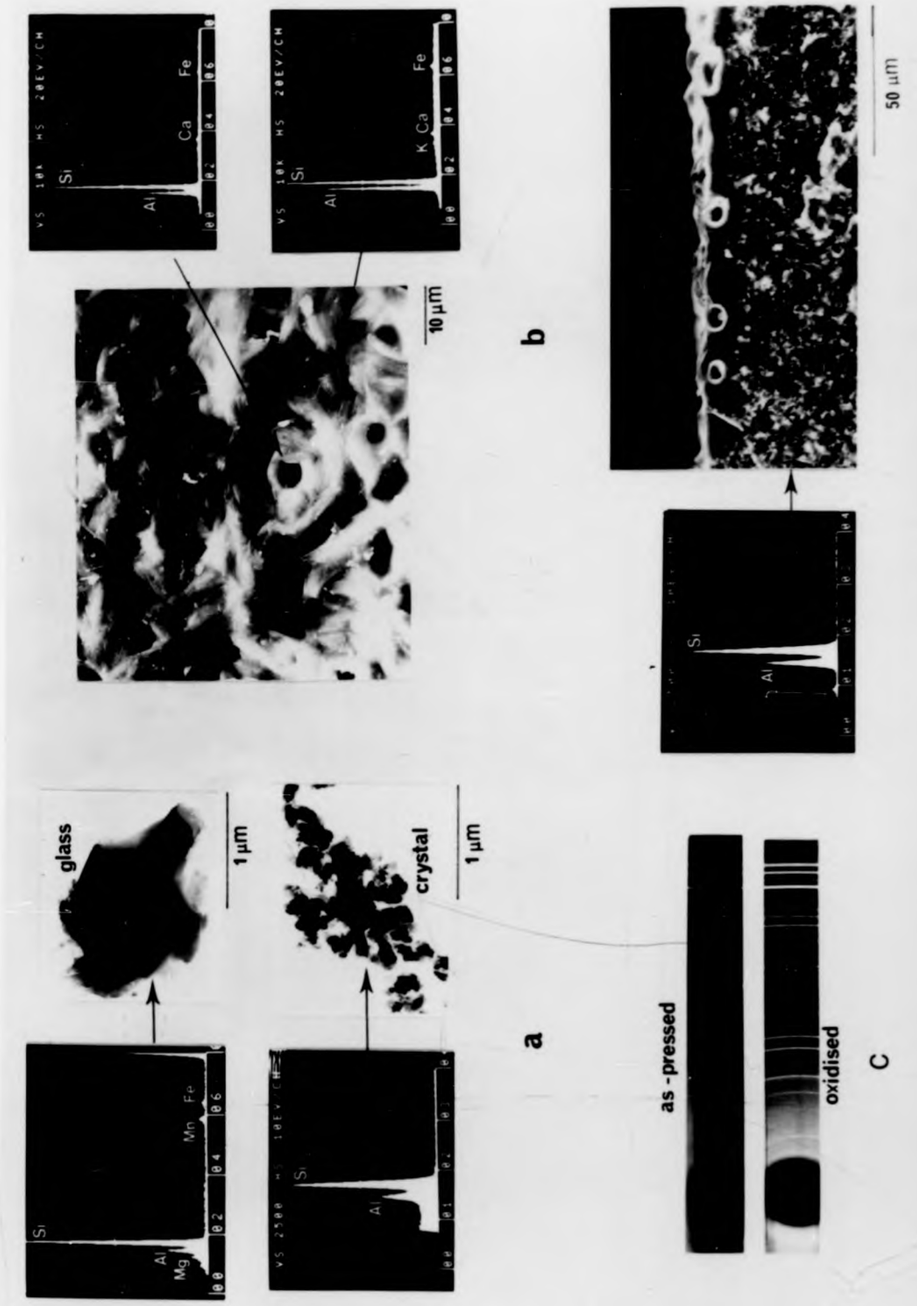

Figure 4.8: Oxide scale of ceramic B1

(a) TEM (b) SEM (c) surface X-ray diffractometry.

Figure 4.8: Oxide scale of ceramic B1

(a) TEM (b) SEM (c) surface X-ray diffractometry.

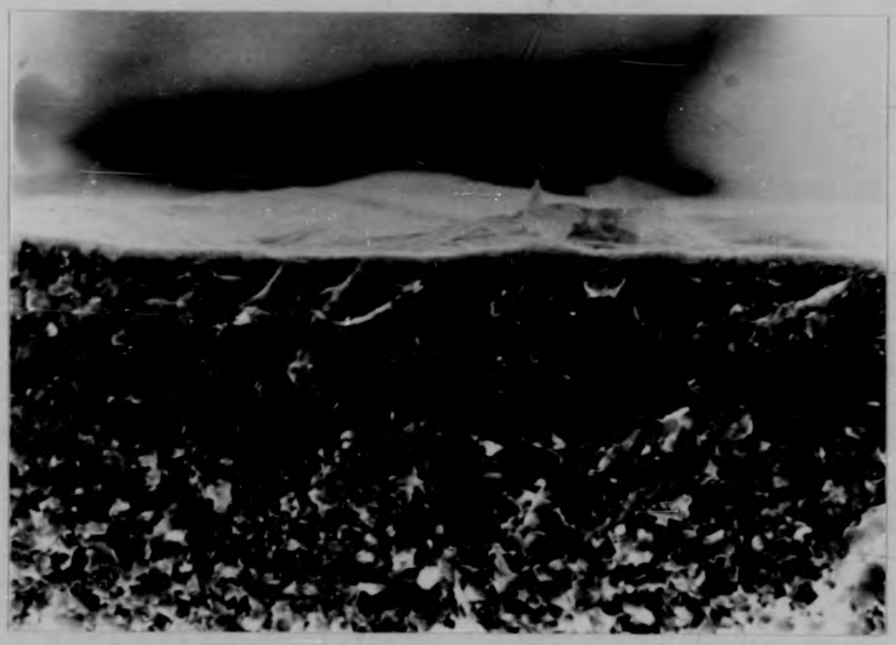

Figure 4.8 (d): Crystalline scale of ceramic B1 oxidised at 1350°C for 120 h.

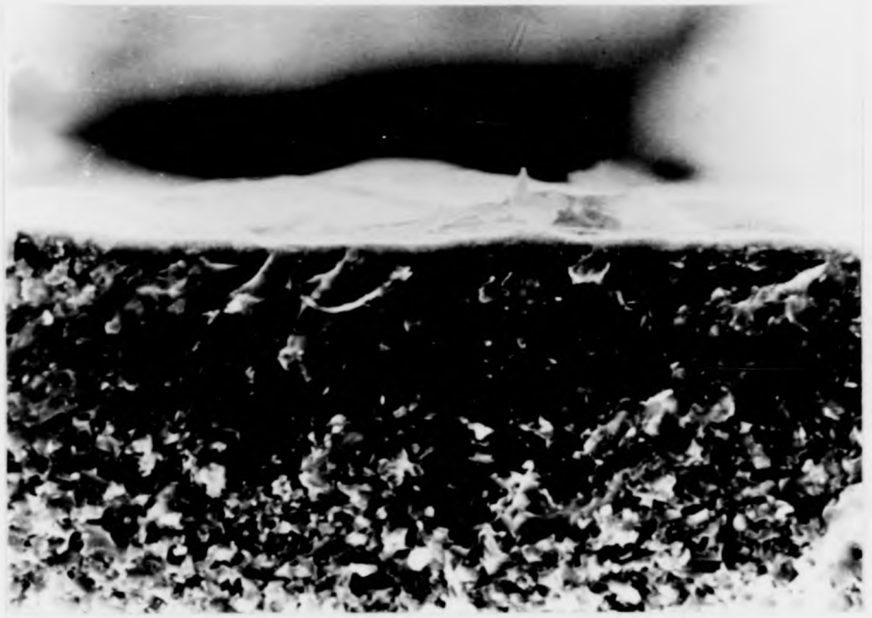

Figure 4.8 (d): Crystalline scale of ceramic B1 oxidised at 1350°C for 120 h.

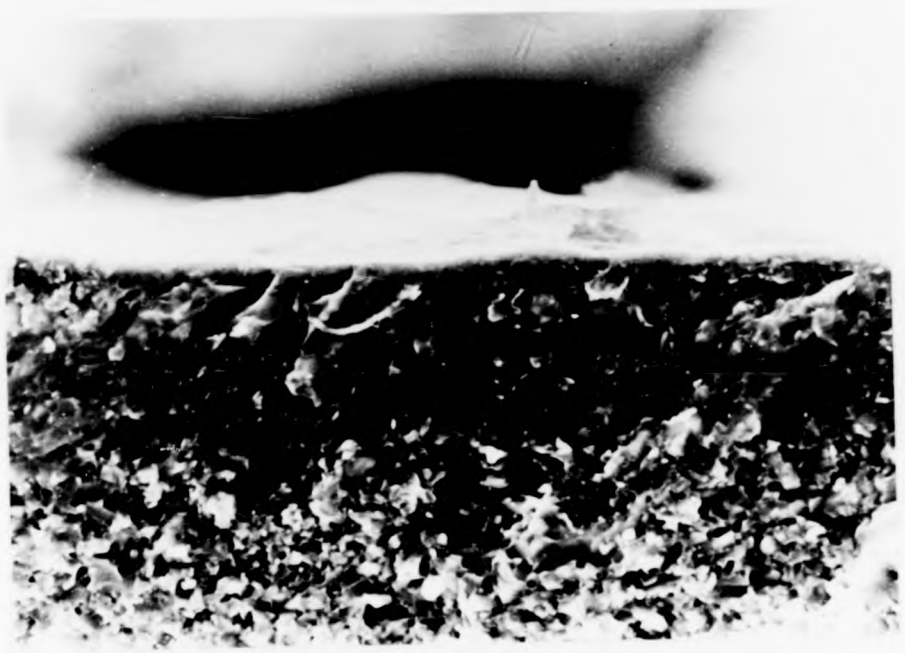

Figure 4.8 (d): Crystalline scale of ceramic B1 oxidised at 1350°C for 120 h.

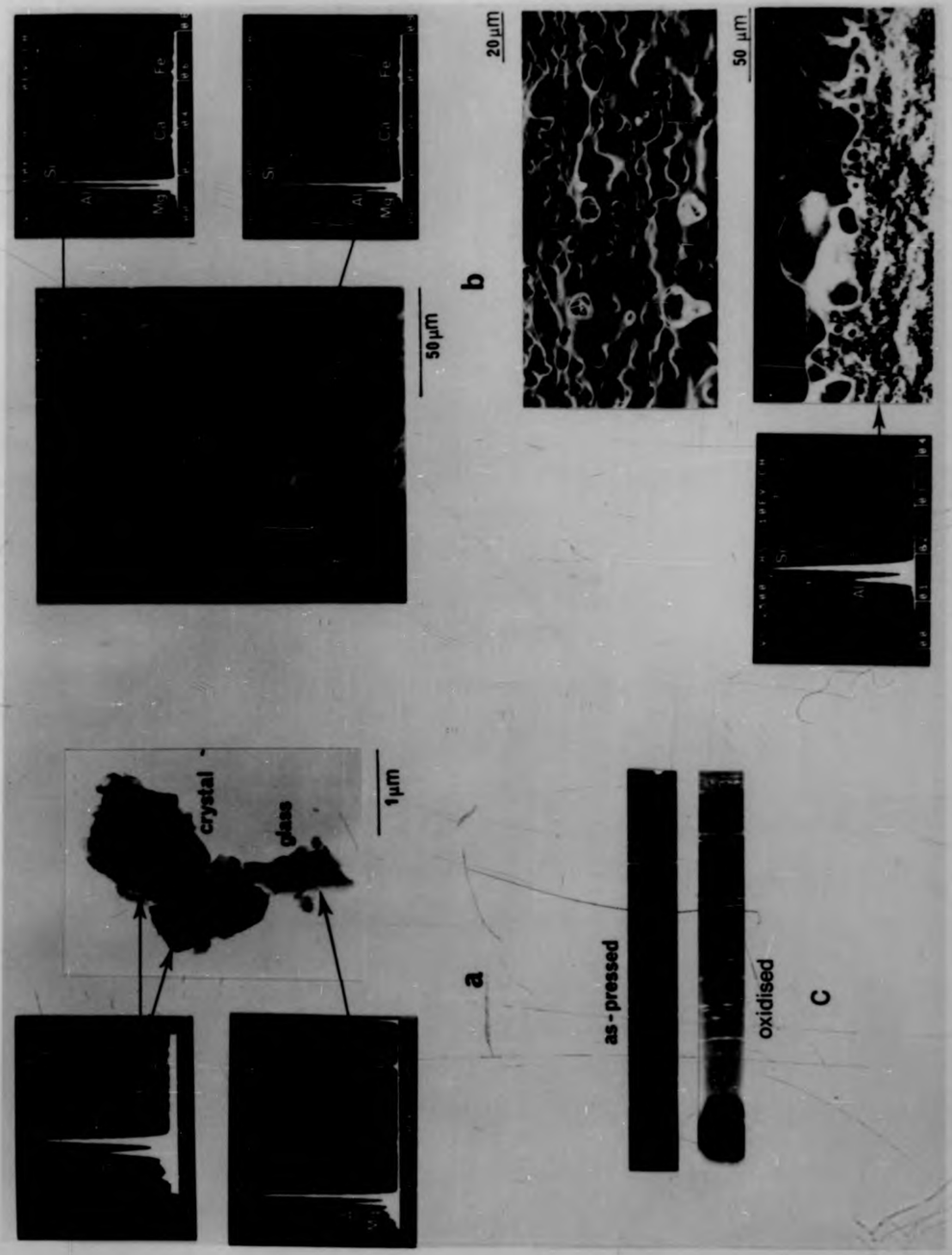

Figure 4.9: Oxide scale of ceramic B2

(a) TEM (b) SEM (c)surface X-ray diffractometry.

Figure 4.9: Oxide scale of ceramic B2

(a) TEM (b) SEM (c) surface X-ray diffractometry.

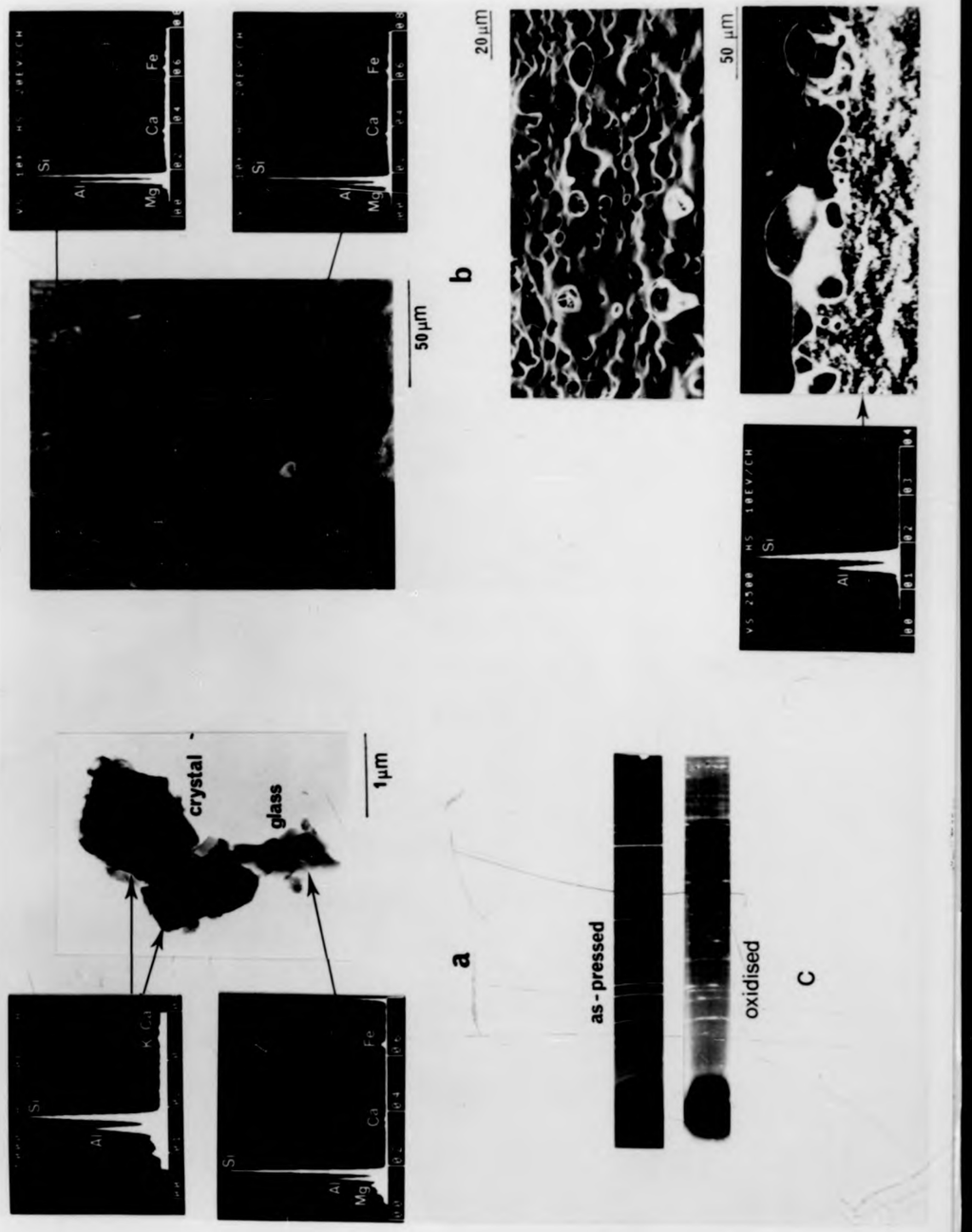

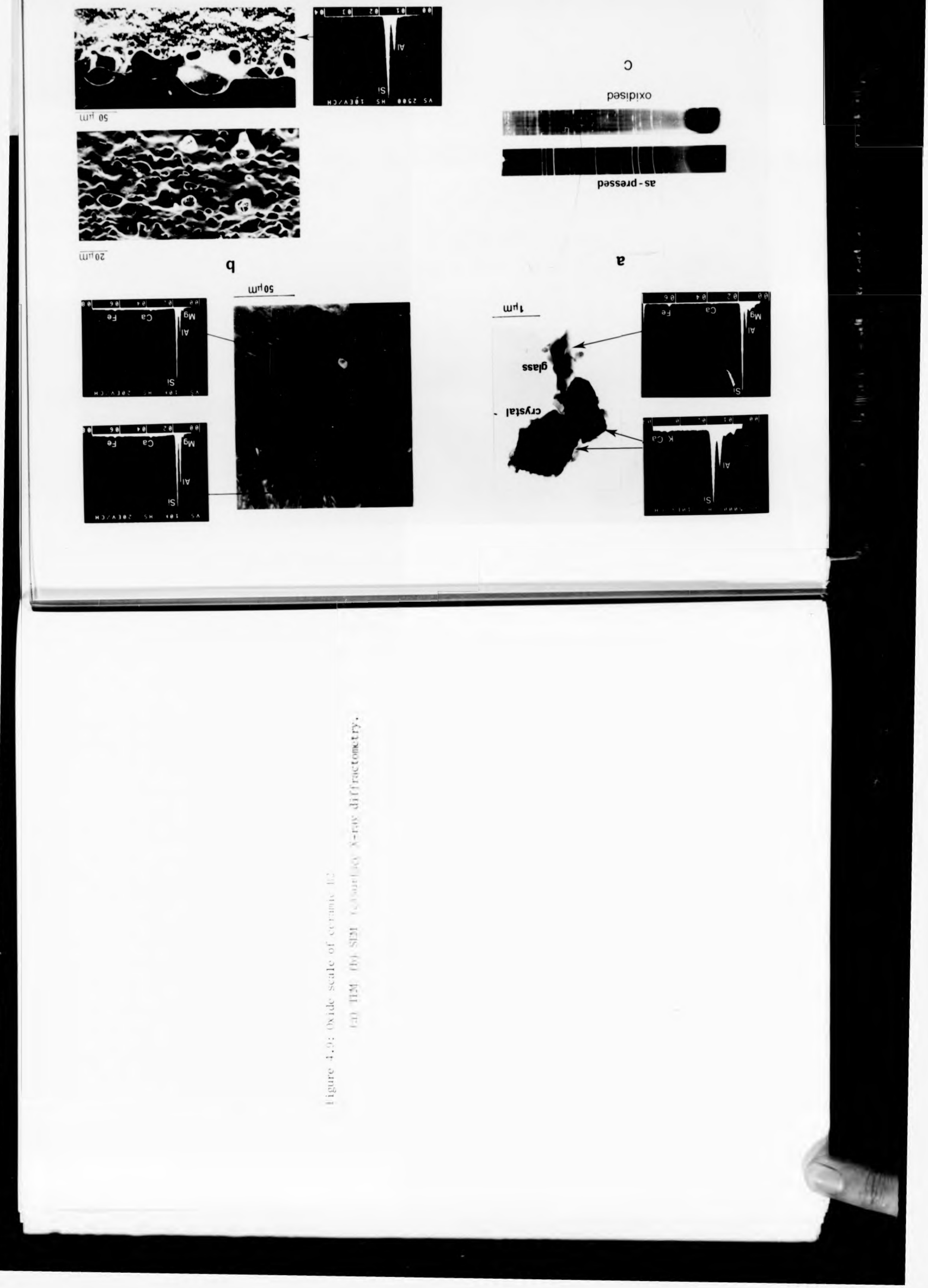

Figure 4.9: Oxide scale of ceramic 12

(a) HM (b) SZI (c) and (d) X-ray diffractometry.

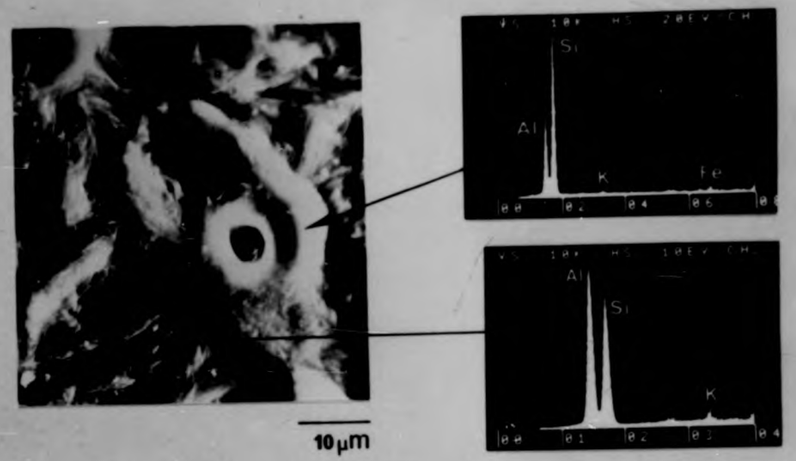

Figure 4.10: Oxide scale of ceramic C1

(a) SEM (b) surface X-ray diffractometry.

Figure 4.10: Oxide scale of ceramic C1

(a) SEM (b) surface X-ray diffractometry.

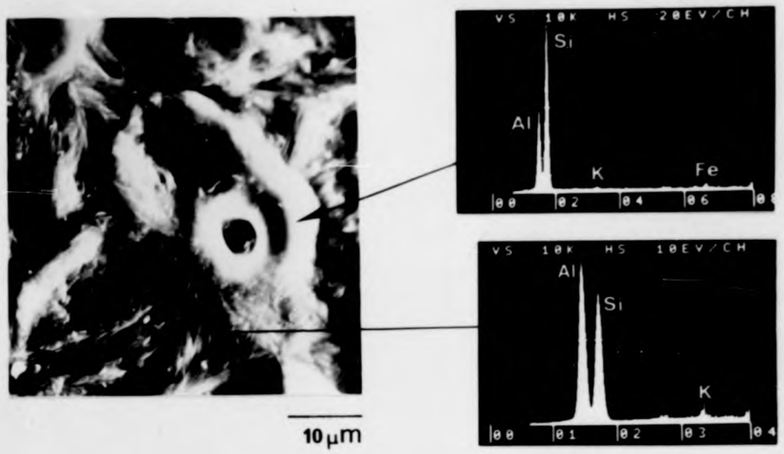

a

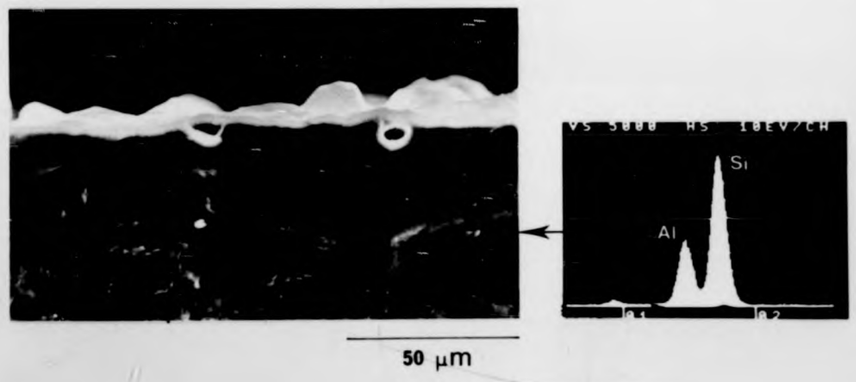

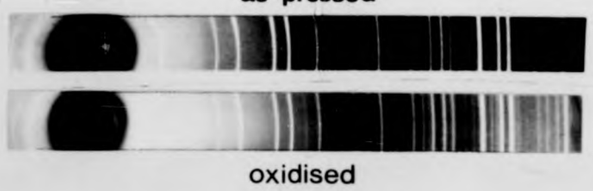

b

Figure 4.10: Oxide scale of ceramic C1

(a) SEM (b) surface X-ray diffractometry.

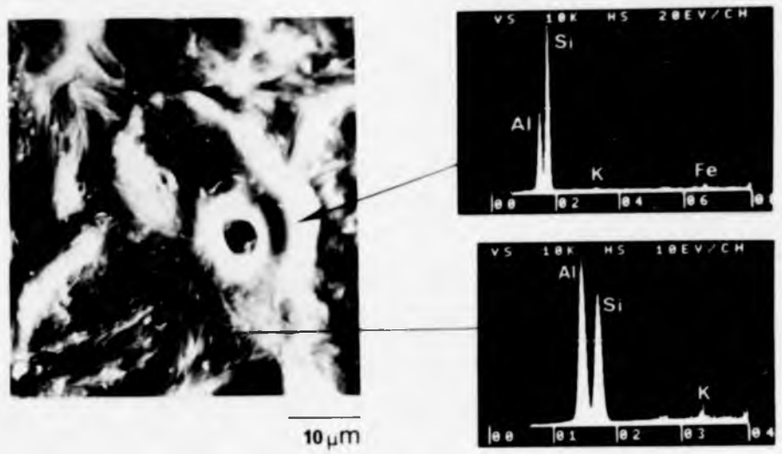

a

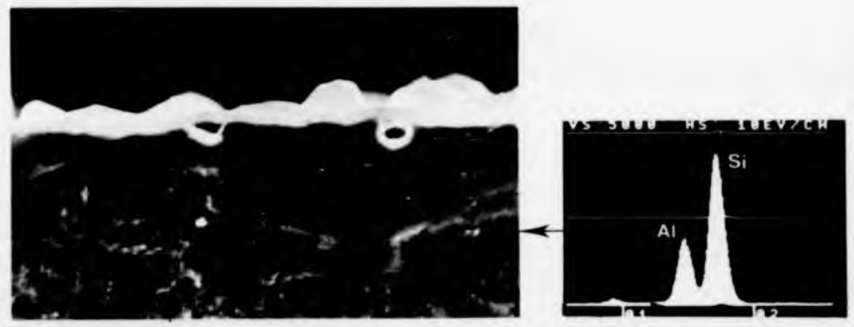

b

Figure 4.11: Oxide scale of ceramic C2

(a) SEM (b) surface X-ray diffractometry.

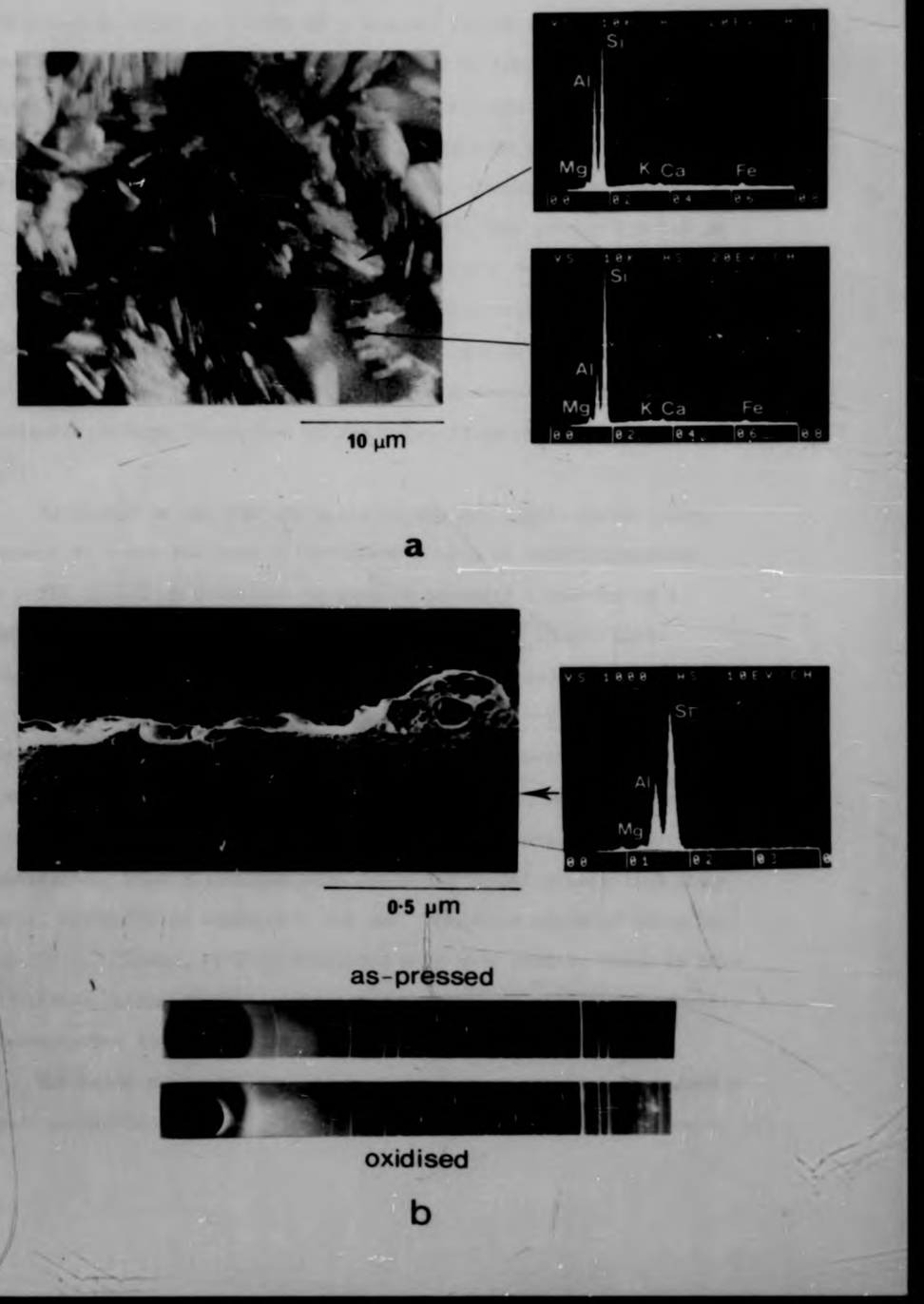

Figure 4.11: Oxide scale of ceramic C2

(a) SEM (b) surface X-ray diffractometry.

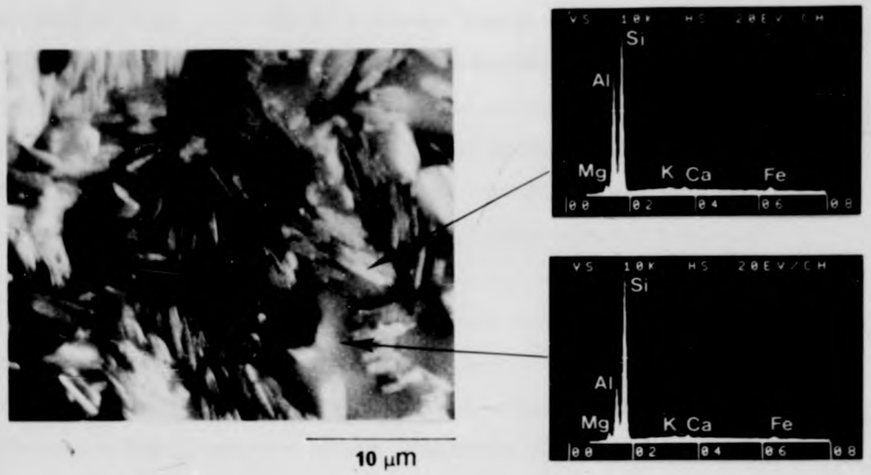

Figure 4.11: Oxide scale of ceramic C2

(a) SEM (b) surface X-ray diffractometry.

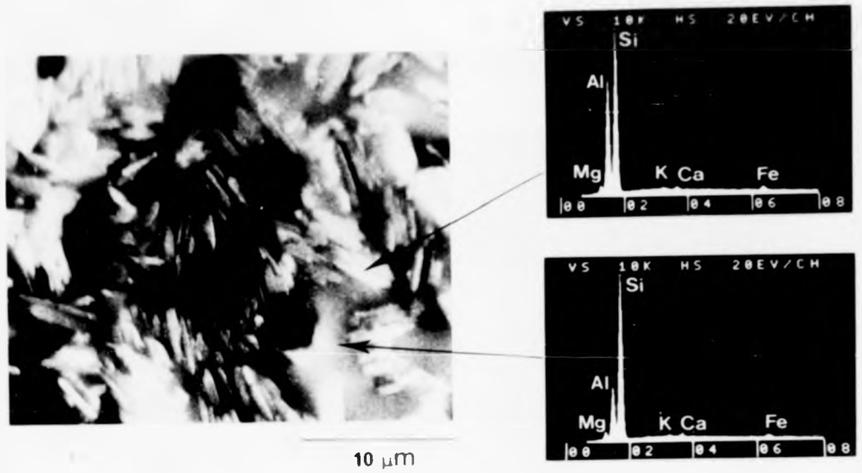

Since the large, spherical pores also present in these scales would not be expected to form in crystalline scales the scale consisted at least partially of a viscous liquid at the oxidation temperature. This conclusion is supported by EDAX microanalysis which showed that the minor elements in the scales of these ceramics were evenly distributed (figure 4.12). Discrete crystals were only observed at the outer surfaces of the scales. On ceramics which had been oxidised for $\sim$ 60 h at 1350°C they were $\sim$ 1 x 0.2 μm and of acicular morphology. They did not cover the whole surface of the scale. Although the crystals were too small for individual EDAX microanalysis the non-crystalline regions of the surfaces of ceramics B2 and C2 were found to be Si-rich compared with regions containing a high proportion of the crystalline phase (Figures 4.8 - 4.11).

As viewed in the TEM the scale of the non additive-containing ceramic B1 which had been oxidised for $\sim$ 60 h at 1350°C consisted of small ($\sim$ 0.1 μm diameter) crystals apparently dispersed in a matrix material (figure 4.8). EDAX microanalysis showed their composition to range between Al/Si ratios of 0.2 and 0.5. This is Si-rich by comparison with the value of 0.5 expected of the β' (z=2) phase. Large, distinct fragments of glass were rarely located. These were Si-rich and contained large quantities of Na, Mg, Fe and Mn. A similar oxide scale was observed for ceramic B2, oxidised under similar conditions. This dispersion also contained larger crystalline fragments, typically of diameter $\sim$ 0.8 μm. The Al/Si ratio of these was $\sim$ 0.2-0.3. Glassy, Si-rich fragments were more readily found in this dispersion, although most contained some small crystalline fragments. They contained large quantities of Mg and Ca (figure 4.9).

The oxide scales of the additive-containing ceramics contained a lower proportion of crystallinity. In addition to the greater degree of

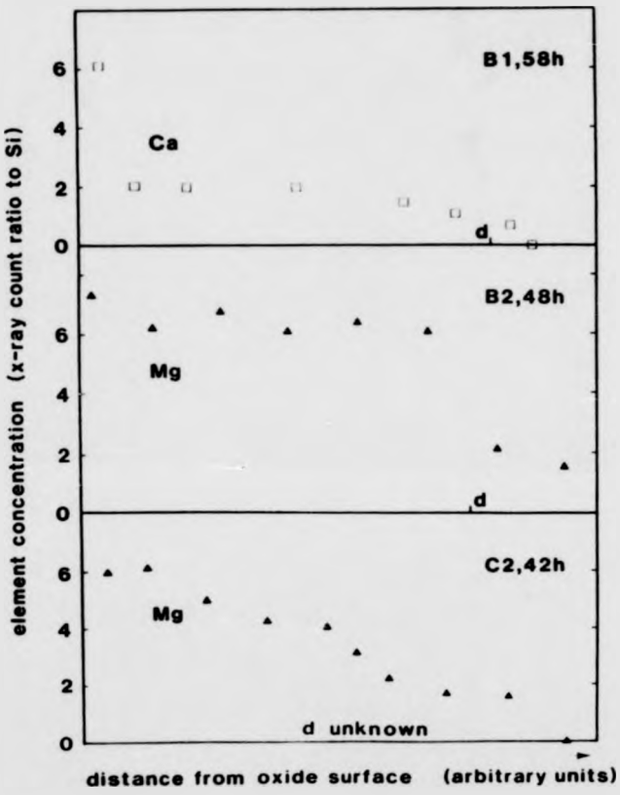

Figure 4.12: Distribution of elements across the oxide scales of the ceramics of intermediate substitution level.

distortion and puncture of their scales by N_2 gas pores, the relative ease with which glass fragments were located in the dispersed scale of ceramic B2, and the lower density of crystals at their scale surfaces, the scale of ceramic B1 was found to be cracked. This was probably due to lack of glass-phase accommodation of differential glass/crystal thermal contraction on cooling.

In summary, the oxide scales of these ceramics are compact and largely pore and bubble-free. They consist of a continuous glassy matrix in which are dispersed very small crystals. Parts of the scale consist of extensive regions of liquid at the oxidation temperatures and large crystals exist only at the outer surface of the scale.

4.1.3. The oxide scales of ceramics of high substitution level, $z \sim 4$ (ceramics D1, D2 and D3)

The oxide scales of the ceramics of high substitution level were of similar character to one another but different to those of the ceramics of low and intermediate substitution levels.

The visual apperance of the scales was non-reflective, whitish and of uneven surface topography. X-ray diffractometry confirmed that the scales contained crystalline phases that were not present in the ceramics prior to oxidation (figures 4.13 - 4.15).

No discrete crystals could be imaged in the transverse surfaces of the oxide scales (figures 4.13 - 15). Large N_2 spherical bubbles in the scales of all three ceramics indicated that they were at least partially liquid at the oxidation temperature. These bubbles were located primarily towards the outer surface of the scale. They caused a slight local distortion of the scales of ceramics D1 and D2 and gave rise to extensive local distortion of the scale of

Figure 4.13: Oxide scale of ceramic D1

(a) SEM (b) surface X-ray diffractometry.

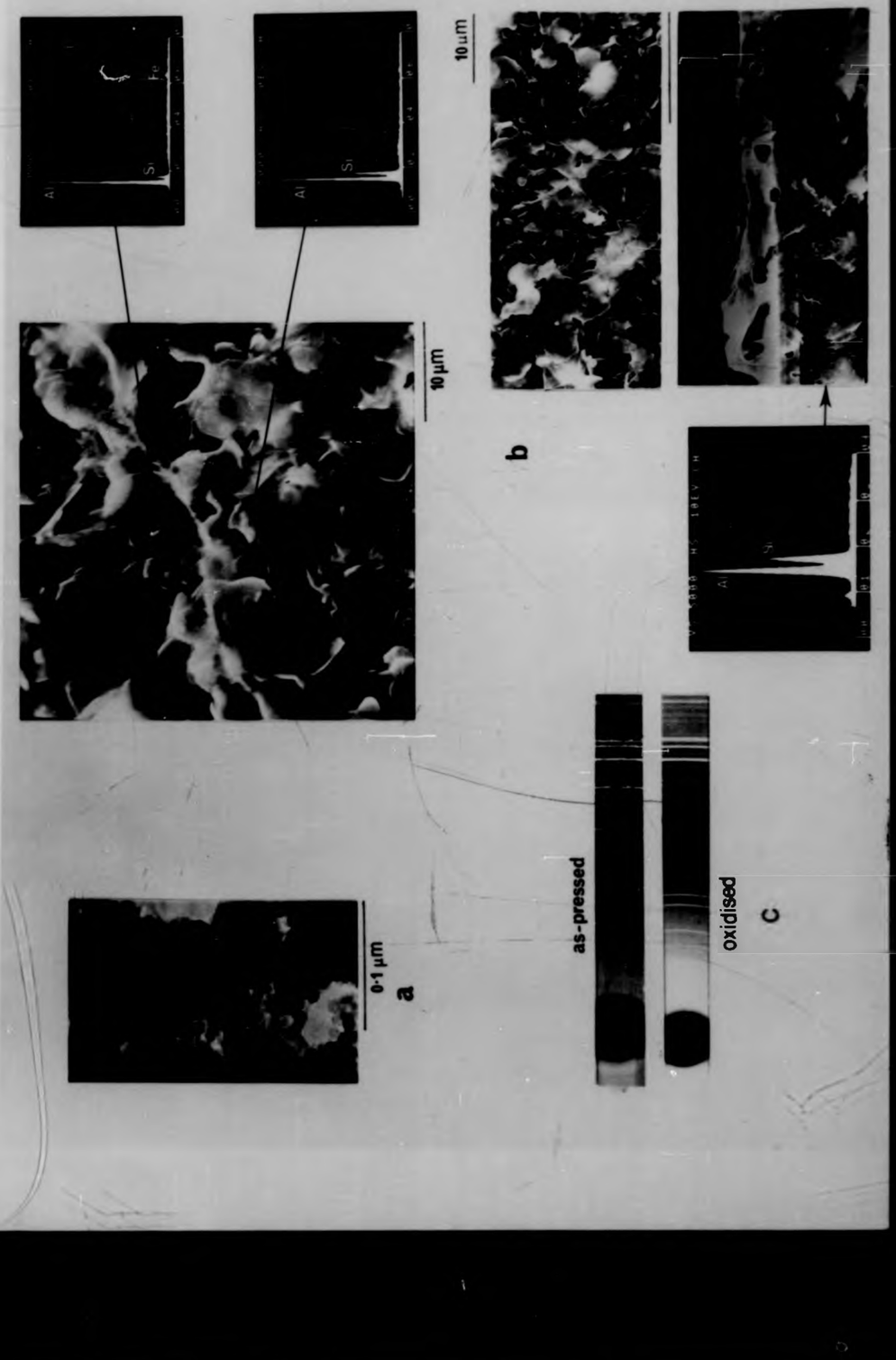

Figure 4.13: Oxide scale of ceramic D1

(a) SEM (b) surface X-ray diffractometry.

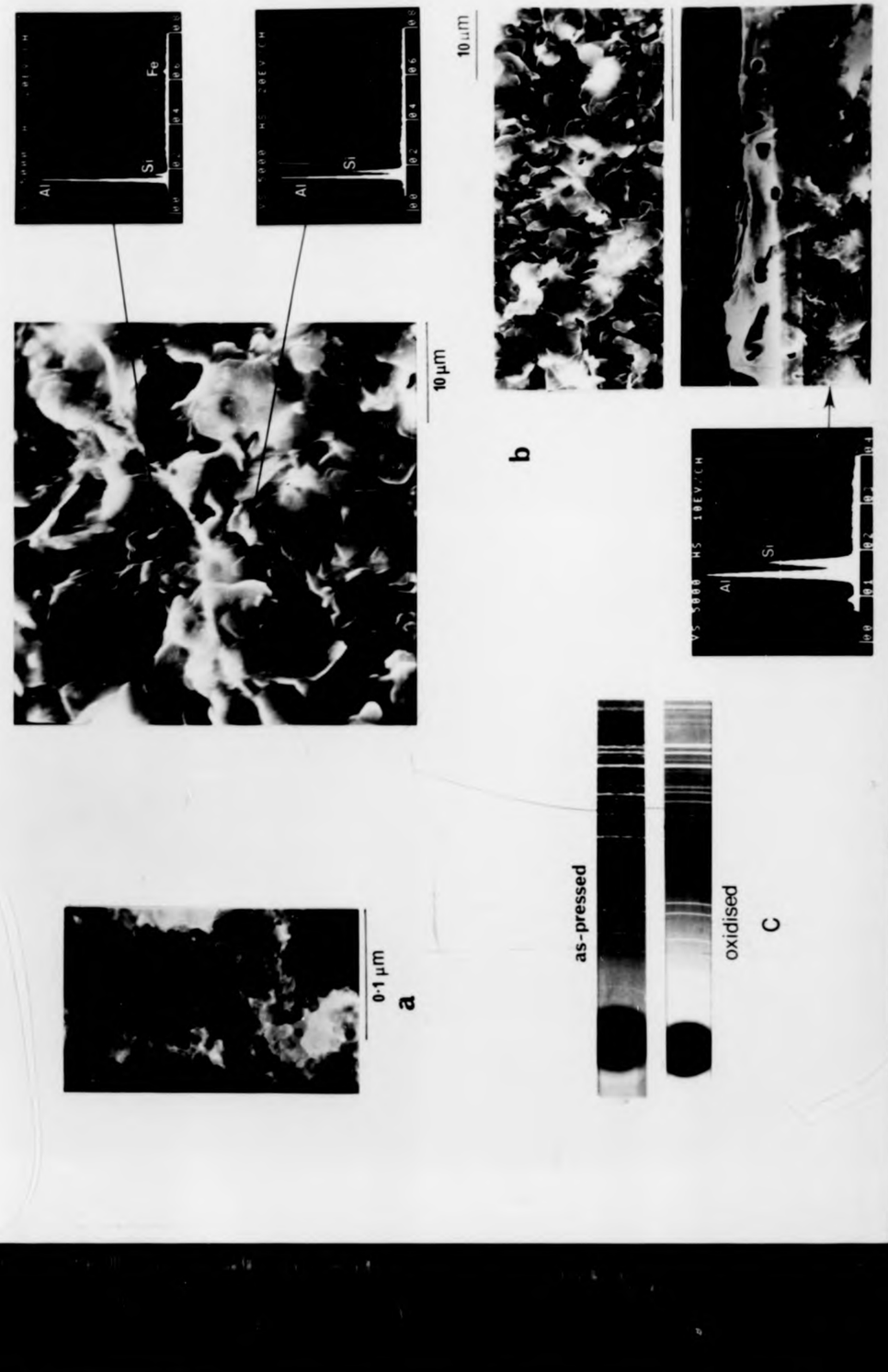

Figure 4.13: Oxide scale of ceramic D1

(a) SEM (b) surface X-ray diffractometry.

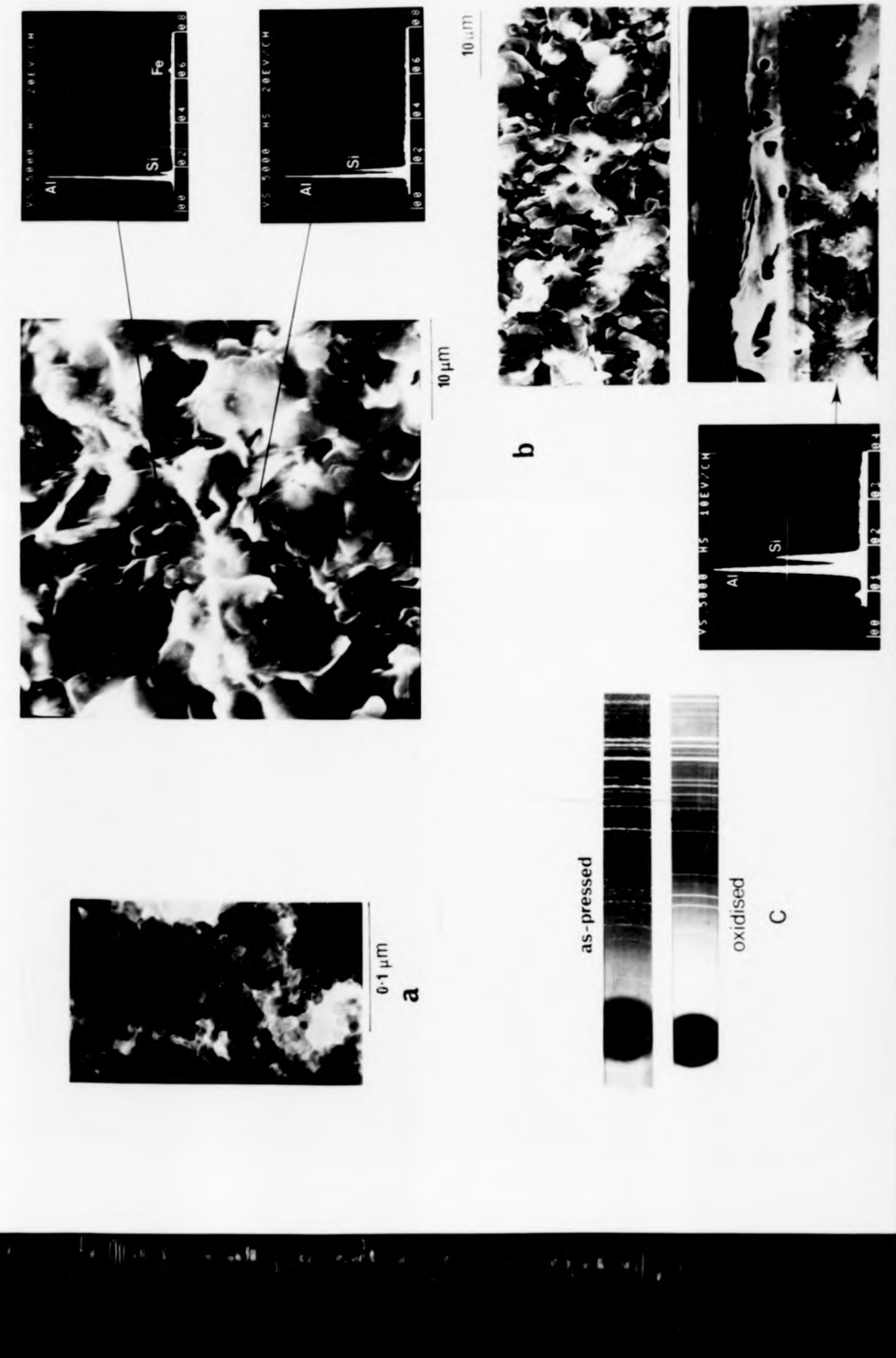

Figure 4.14: Oxide scale of ceramic D2

(a) TEM (b) SEM (a) surface X-ray diffractometry.

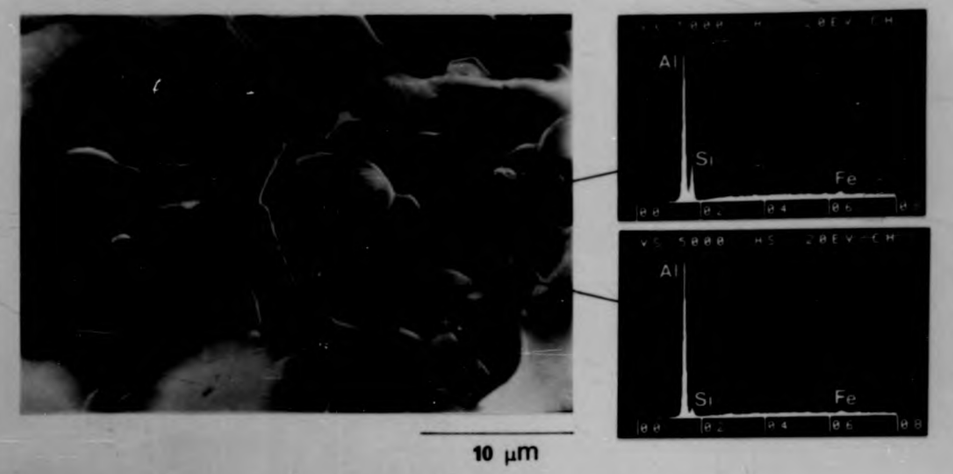

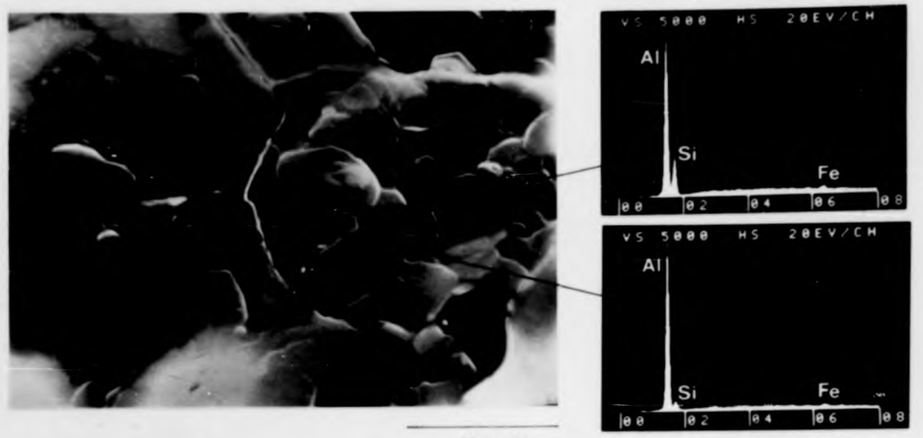

Figure 4.14: Oxide scale of ceramic D2

(a) TEM (b) SEM (a) surface X-ray diffractometry.

Figure 4.14: Oxide scale of ceramic D2

(a) TEM (b) SEM (a) surface X-ray diffractometry.

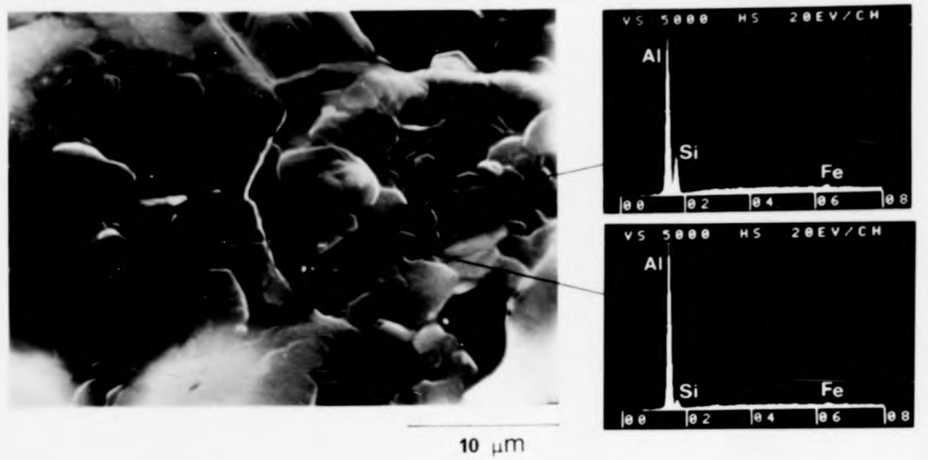

a

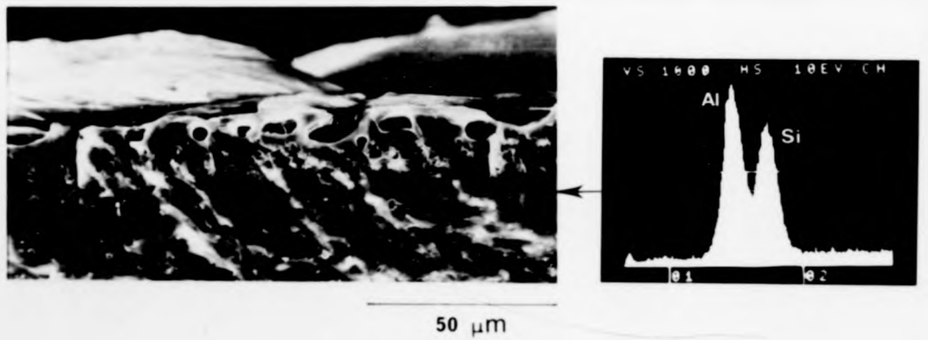

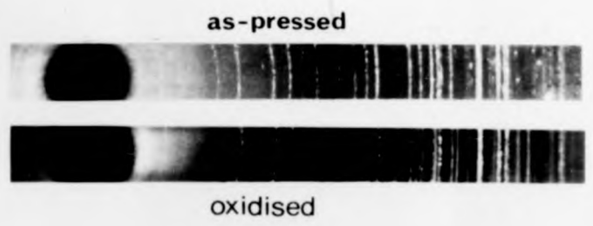

b

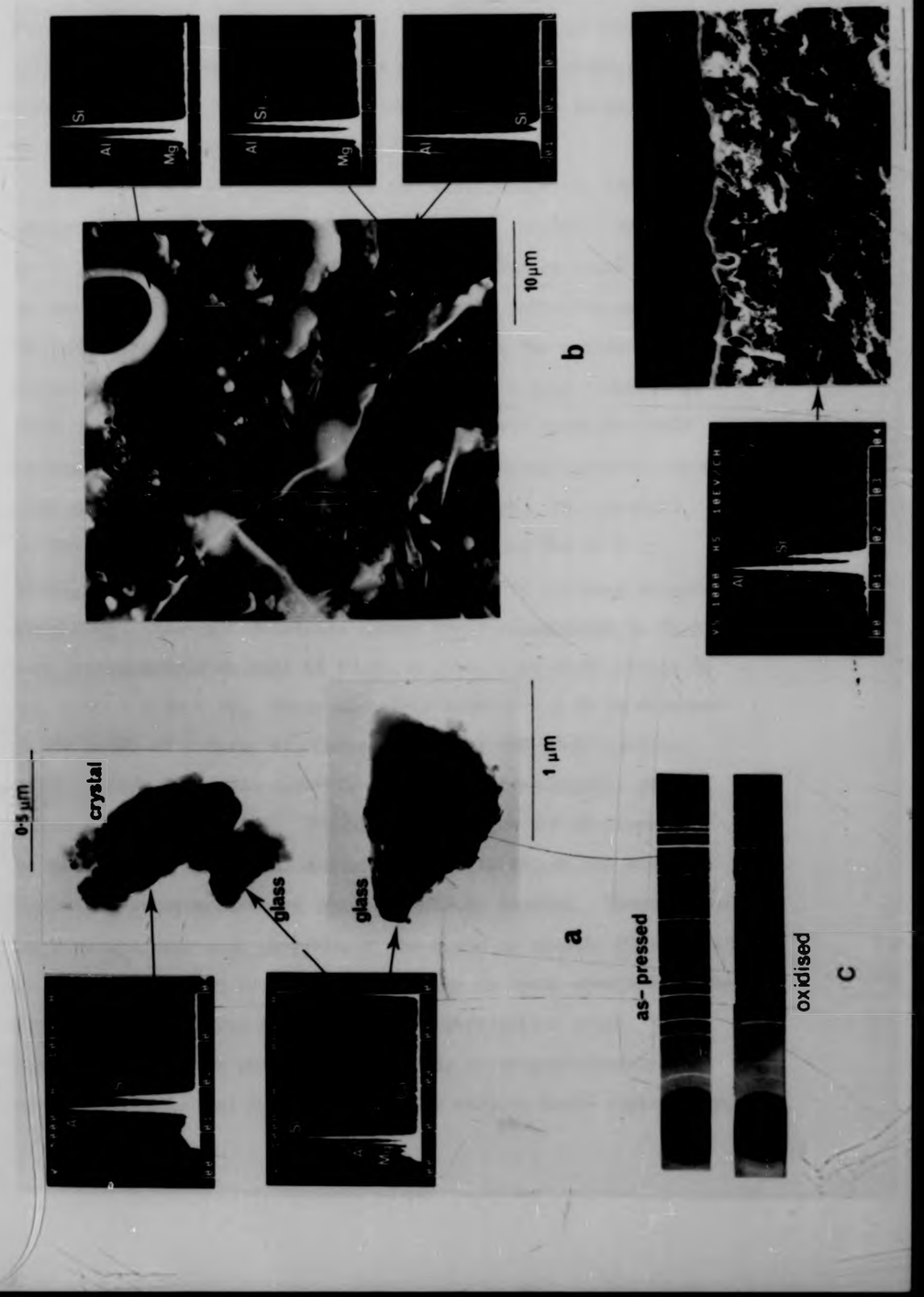

Figure 4.15: Oxide scale of ceramic D3

(a) TEM (b) SEM (c) surface X-ray diffractometry.

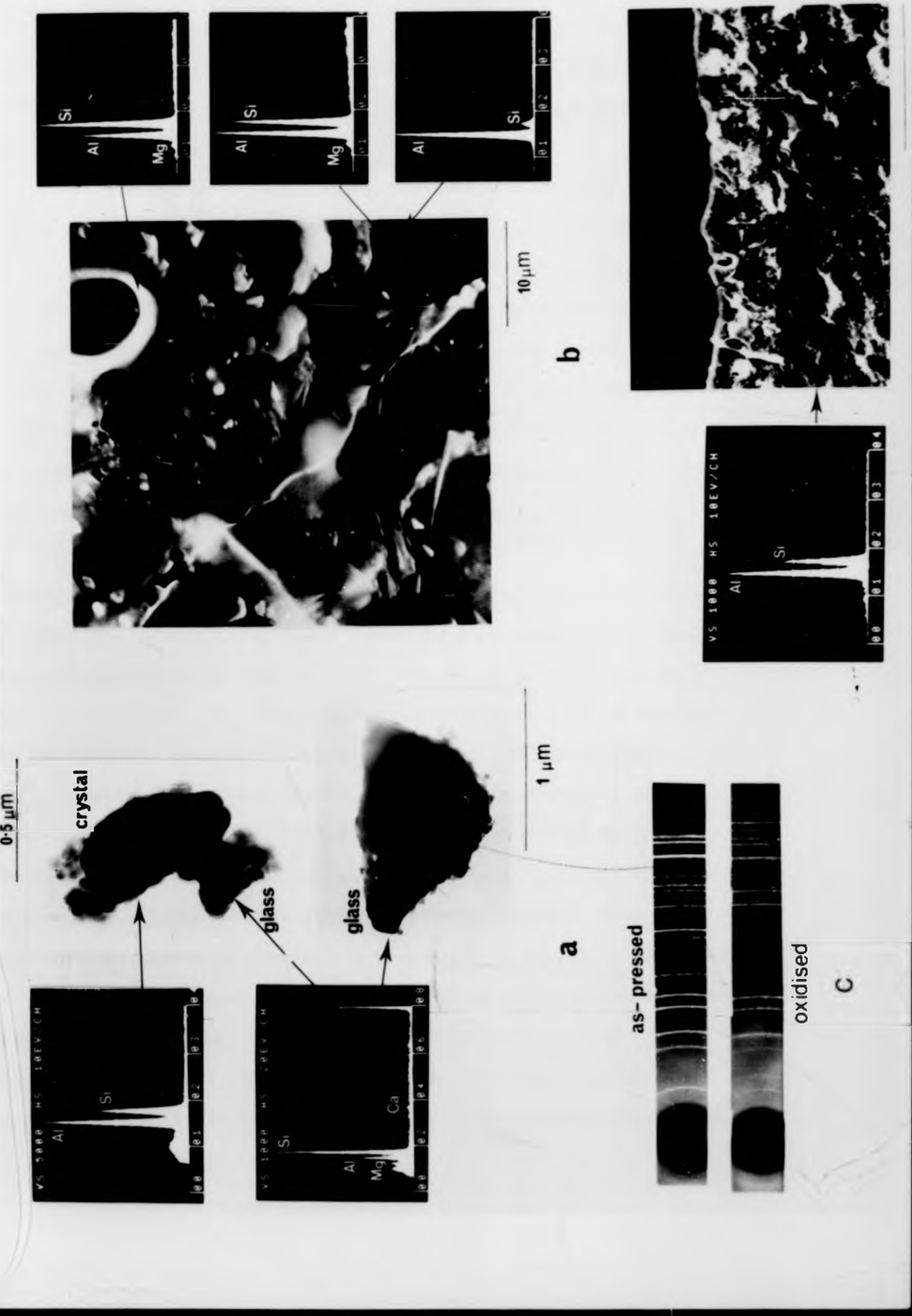

Figure 4.15: Oxide scale of ceramic D3

(a) TEM (b) SEM (c) surface X-ray diffractometry.

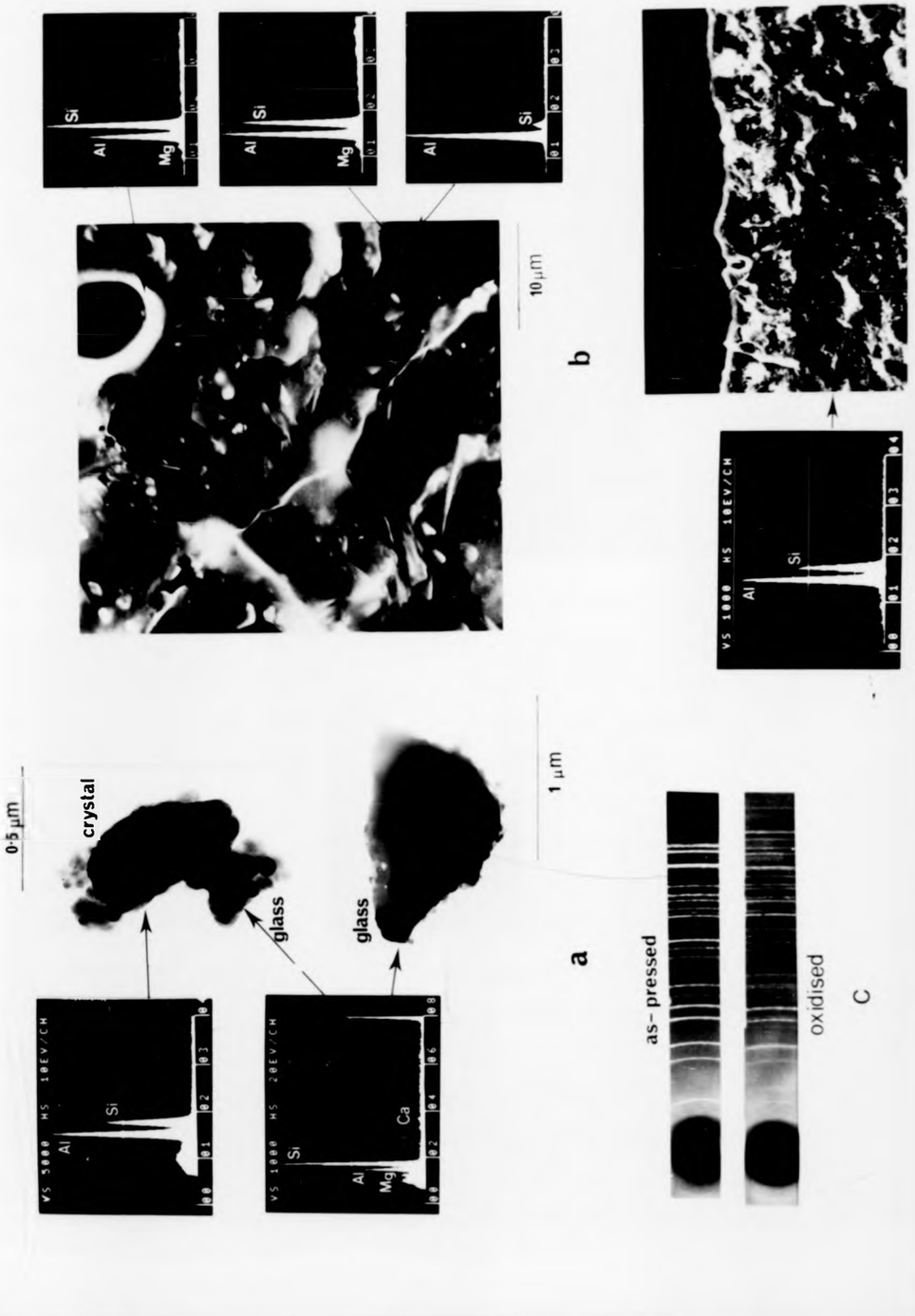

Figure 4.15: Oxide scale of ceramic D5

(a) TEM (b) SEM (c) surface X-ray diffractometry.

the additive-containing ceramic D3. The amorphous nature of the scales was confirmed by the uniform distribution of minor elements across the scales, with the exception of some local inhomogeneity in the scale of ceramic D2 (figure 4.16).

Porosity was also observed in the oxide scales in the region adjacent to the oxidation front. These pores, however, were small (∿ 1 μm diameter) and of angular shape, similar to those located in the scales of the ceramics of intermediate substitution level. The very much higher density of these pores in the scales of the ceramics of high substitution level indicates a higher degree of local scale crystallinity. However, no discrete crystals could be imaged in the vicinity of these pores. Discrete crystals were only imaged at the outer surfaces of the scales. The crystals in the scales of the ceramics D1 and D2 oxidised for 60 h at 1350°C were of platelet form, with approximately equiaxed hexagonal morphology. Edax microanalysis showed their composition to be Al-rich in comparison to that of β´ Si_2 $Al_4O_4N_4$ with Al/Si ratios in the range ∿ 2 to ∿ 10. These platelets were of ∿ 2-10 μm diameter on the scale of ceramic D1, covering much of the scale surface. Angular pores were also observed in structureless regions which appeared to be amorphous. The platelets were ∿ 2-6 μm diameter in the scale of ceramic D2 and covered nearly all of the scale surface. Few structureless regions could be located. These platelet crystals were also observed in the scale of ceramic D3 in addition to acicular crystals of similar morphology to those observed in the scales of the ceramics of intermediate substitution level. Many regions of amorphous phase were observed, often punctured by the bursting of spherical N_2 bubbles. These structureless regions were

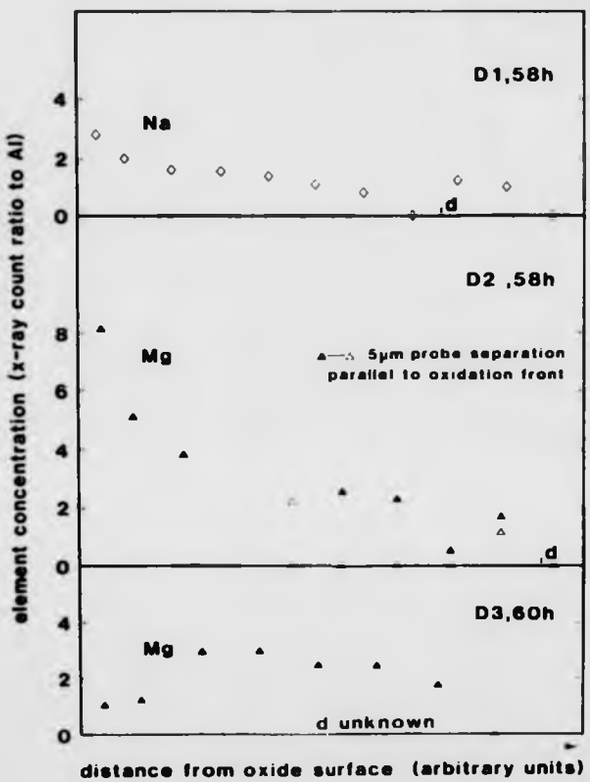

Figure 4.16: Distribution of elements across the oxide scales of the ceramics of high substitution level.

Si-rich in comparison to the platelet crystals or the β′ phase. These glassy regions contained large quantities of Mg and Na.

The observation of these regions in the scale of ceramic D3 and the much higher level of scale distortion caused by the N_2 bubbles is due to its containing a higher proportion of liquid phase than the scales of ceramics D1 and D2. This conclusion is supported by observation of the dispersed scales in the transmission electron microscope. Large glass fragments were found in the scale of ceramic D3 oxidised for ∿ 60 h at 1350°C. These were Si-rich compared with the β′ phase and contained large quantities of Mg, K and Ca. Crystalline fragments of ∿ 0.5 - 2 μm diameter were also located. These crystals were Al-rich compared with the β′ phase. In addition, large areas of the oxide dispersion were observed to consist of what appeared to be small crystals dispersed in a matrix phase, similar to that observed in the dispersed oxide of ceramic B1. The matrix phase was too small for localised microanalysis but areas containing a high proportion of this phase were Si-rich (figure 4.15).

This "agglomerate" type of oxide surrounding crystals of ∿ 0.1 μm diameter was very common in the oxide of the ceramic D2. High-magnification microscopy showed it to be multiphase in character, possibly consisting of ∿ 0.01μm droplets dispersed in a matrix phase (figure 4.14). Very few discrete glass fragments were imaged in this oxide and none in the oxide of ceramic D1, which was found to consist of discrete crystals of ∿ 0.5 μm diameter. These large crystals in the oxides of D1 and D2 were surprisingly Si-rich compared to the β′ (z=4) composition.

In summary, the oxide scales of the ceramics of high substitution level consist of a glass phase containing small, dispersed crystals, similar to that of the ceramics of intermediate substitution

level. Large crystals exist only at the outer surfaces of the scales.

The high degree of surface crystallinity was the cause of the cracking of the scales on cooling, in contrast to the uncracked scales of ceramics A1, A2, B2, C1 and C2. The very much lower distortion of the scales by N_2 gas bubbles and much higher proportion of small angular pores in the scales of the ceramics of high compared with those of intermediate substitution level indicated that their scales are of a more crystalline nature. The proportion of oxide scale crystallinity therefore increased continuously with increased substitution level of the ceramics. The scales of ceramics which had been hot-pressed with MgO additives were less highly crystalline compared with those of nominally pure ceramics of the same substitution level.

4.1.4. The influence of composition on the nature of the oxide scale of β′ Si-Al-O-N ceramics: A discussion

The different natures of the oxide scales of the ceramics was due to their different substitution level and additive and impurity element contents. The scales consist essentially of Al_2O_3-SiO_2 containing additions of $\leq$ 10% concentration of additive and impurity ions such as Mg, Ca and Fe. Some solution of N in the scales may also be expected either in liquid melts (section 4.1.1.) or as oxynitride crystalline phases such as Si_2N_2O. The phase-diagram of the system Al_2O_3-SiO_2 is presented in figure 4.17 together with the expected composition of oxides which would form on pure β′ Si-Al-O-N crystals ("equivalent SiAlON substitution level").

According to this diagram, the formation of non-crystalline phases is not expected at temperatures of $\leq$ 1600°C under equilibrium conditions for any of the oxides corresponding to β′ Si-Al-O-N compositions. However, metastable sub-solidus SiO_2 and Al_2O_3

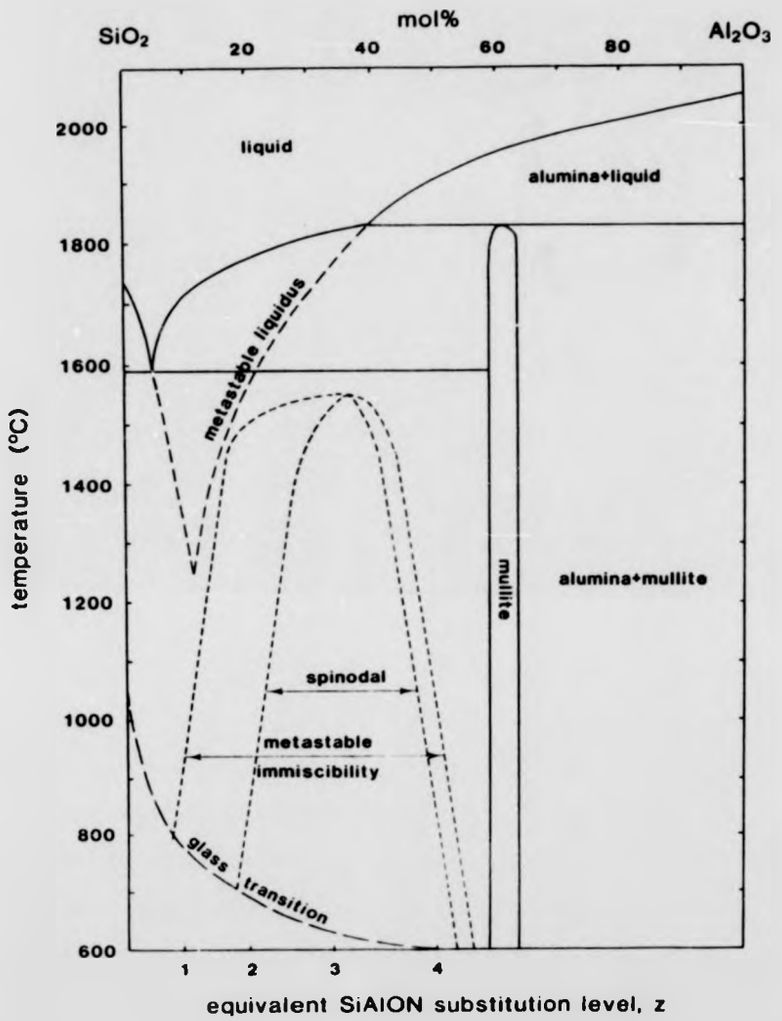

Figure 4.17: Stable and metastable phase equilibria in the system SiO_2-Al_2O_3 [Risbud and Pask 1978].

amorphous phases have been observed on oxidation of Si [Heuer et al 1980], Al [Lawless 1973], SiC [Jorgensen et al 1959] and CVD Si_3N_4 [Hirai et al 1980], in addition to the ceramics of this study.

In ceramics of low substitution level (ceramics A1 and A2) the observed liquid scale may be expected to form metastably if mullite formation is suppressed. A calculation of the metastable liquidus compositions in the system Al_2O_3-SiO_2 in the absence of mullite by Risbud and Pask [1978] showed the liquidii for Si-rich compositions to extend to temperatures as low as $\sim$ 1250°C (figure 4.17). Mullite formation in the oxide scales of ceramics of low substitution level is not favoured kinetically due to their high SiO_2 content. Furthermore, the solution of viscosity-enhancing N^{3-} ions in a Al_2O_3-SiO_2 glass would further reduce any tendency to devitrification.

An alternative explanation for the formation of the scales of ceramics A1 and A2 as glass lies in low liquidus temperatures of silicate melts. The scales would form as a liquid if the oxidation temperature exceeded the liquidus temperature. Additions of any of the observed elements Na, Mg, K, Ca, Mn and Fe reduce liquidus temperatures in M_xO_y-SiO_2-Al_2O_3 ternary systems. Eutectic temperatures in these systems are shown in figure 4.18. Additions of more than one of the elements to a scale would reduce the eutectic temperature still further (figure 4.18). It is possible that the oxidation temperatures were higher than the liquidus temperature of the scale composition.

The development of largely amorphous oxide scales in the ceramics of intermediate substitution level may also be due to their composition lying close to that of a eutectic. With the exception of the monovalent elements K and Na, eutectic temperatures in the

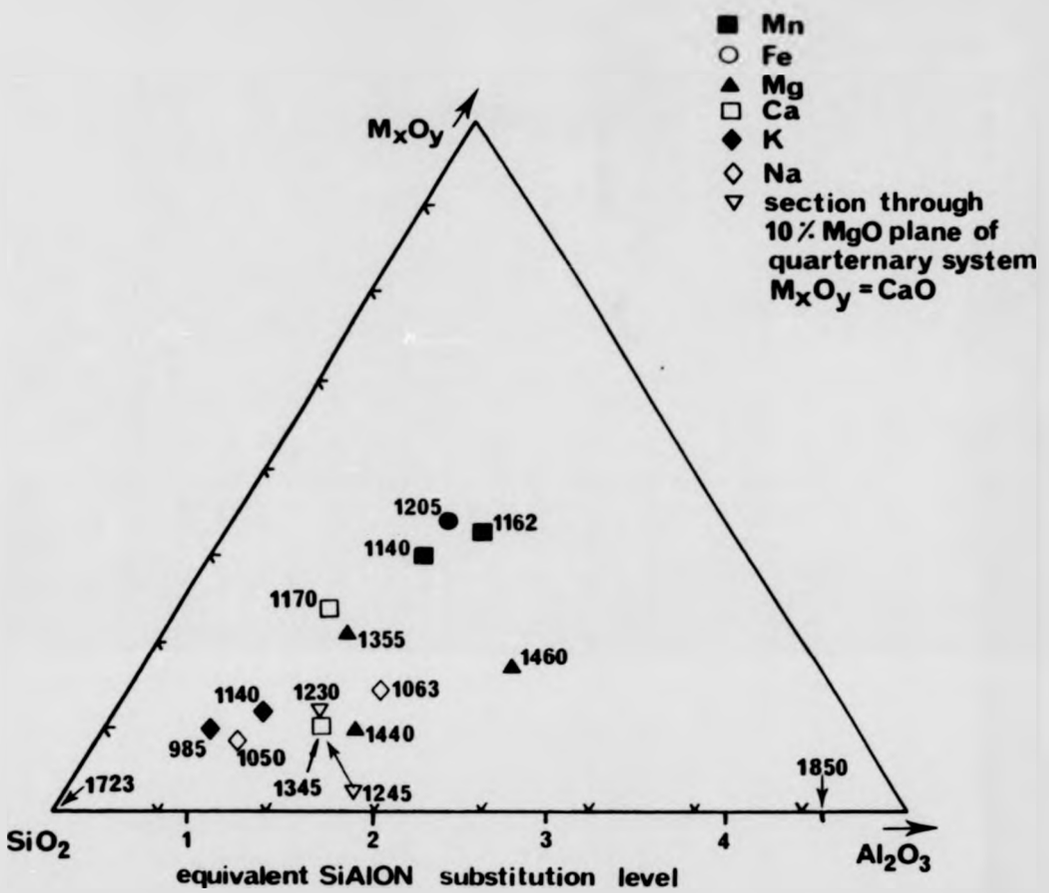

Figure 4.18: Eutectic temperatures in the systems M_xO_y-SiO_2-Al_2O_3.

[Levin et al 1964].

systems M_xO_y-SiO_2-Al_2O_3 are all lower for compositions close to an equivalent Si-Al-O-N substitution level of $z \sim 2$ than of $z \sim 1$ (figure 4.18). The formation of larger quantities of liquid in the oxides of ceramics containing larger quantities of M ions is expected since further additions of such ions reduce liquidus temperatures with increasing additions up to $\sim$ 1 -10%, levels in excess of the proportions found in the scales (figure 4.12).

The partially crystalline oxide scale of these ceramics is expected since their SiO_2-Al_2O_3 composition lies within a region of subsolidus phase separation in this system (figure 4.17). It is not known how this region extends in the ternary systems MO-Al_2O_3-SiO_2. In glasses of compositions lying within the immiscibility dome, glass-in-glass phase separation has been observed to occur prior to crystallisation of mullite [MacDowell and Beall 1968]. The TEM observations of parts of the dispersed oxide fragments of ceramics B1 and B2 as apparently phase-separated structure (section 4.1.2) is consistent with the crystallisation of small Al-rich crystals within a surrounding continuous matrix of Si-rich glass.

The scales of ceramics of high substitution level ($z \sim 4$) were more crystalline than those of ceramics of lower substitution levels for two reasons. First, their composition was more remote from that of ternary eutectic compositions and is close to the immiscibility dome in the system Al_2O_3-SiO_2. Secondly, their average composition was close to that of mullite, $3Al_2O_3.2SiO_2$. Phase separation to mullite plus a Si-rich glass is therefore kinetically more favourable in these scales. The observation of large areas of Si-rich glass in the oxides confirmed that such phase-separation had occurred. Increased proportions of glass in the oxide scale of ceramic D3 were due to its composition being closer to that of a ternary eutectic

than those of the nominally pure ceramics D1 and D2.

4.2. Oxidation kinetics

4.2.1. Oxidation of the "as-pressed" ceramics

The kinetics of oxidation determined by measurement of the thickness of the oxide scales formed on the 3 x 10 mm polished surfaces of the oxidation specimens are presented in figure 4.19. Each data point represents the mean of ∿ 10 measurements across the 3 mm width of the specimen. The thickness of oxide locally distorted by N_2 gas bubbles was omitted from the analysis. It was not possible to determine kinetics of oxidation of ceramics B2 and C2 due to extensive distortion of their oxide scales (figures 4.9 and 4.11).

Initial oxidation was very rapid. Subsequent growth of the scale was very slow, especially in the ceramics of substitution level z ∿ 1. The functional form of the kinetics does not allow an immediate general definition to be made of the oxidation mechanism. The data were fitted by use of a least-squares analysis to an equation of the form

$$d^n = kt$$

where d is the thickness of the oxide scale formed in time t, in order to determine the "oxidation exponent", n. Table 4.1. lists these exponents. Their values lie in the range 0.9 to 8.7, in contrast to the values of 1 or 2 widely and consistently reported for the oxidation of hot-pressed silicon nitride and Si-Al-O-N ceramics (Table 2.1). Linear kinetics of oxidation (n=1) arise when oxidation is rate-controlled by phase-boundary reactions. Parabolic kinetics of oxidation arise when oxidation is rate-controlled by the diffusion of a reacting species through the oxide scale. Such diffusion is described by Fick's "first law" of diffusion which relates the rate of mass transport, dm/dt, to

Figure 4.19(a): Kinetics of oxidation of the ceramics of low substitution level.

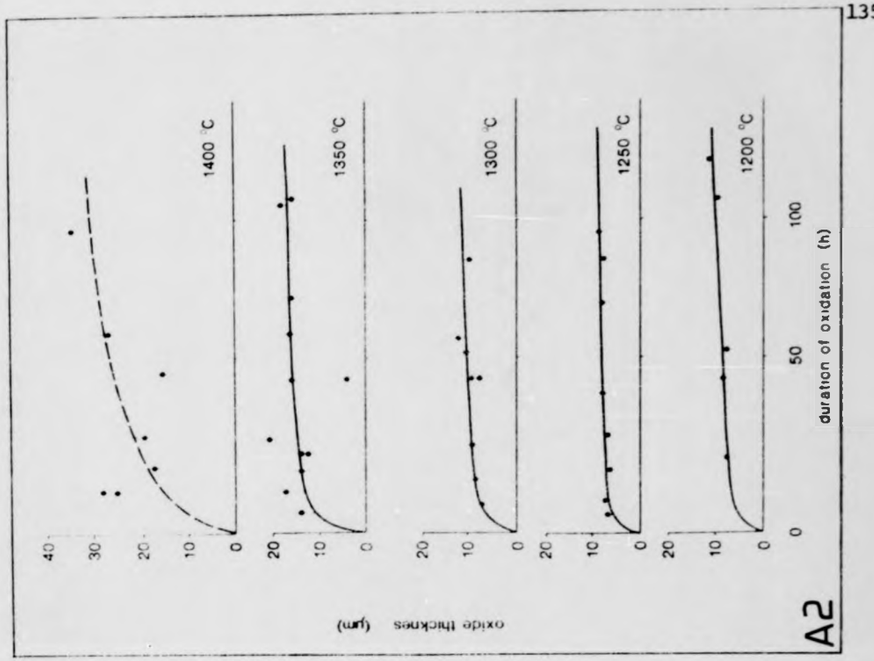

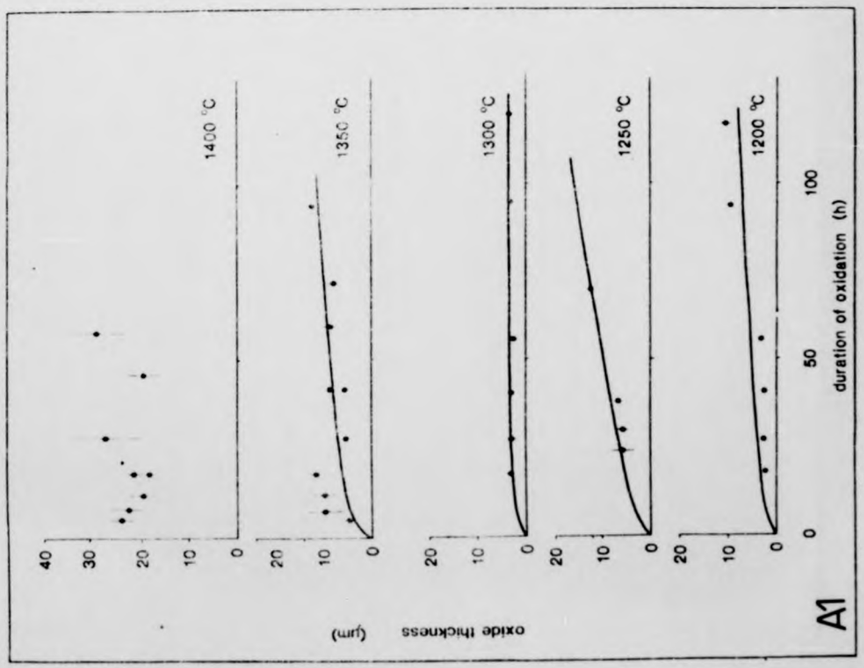

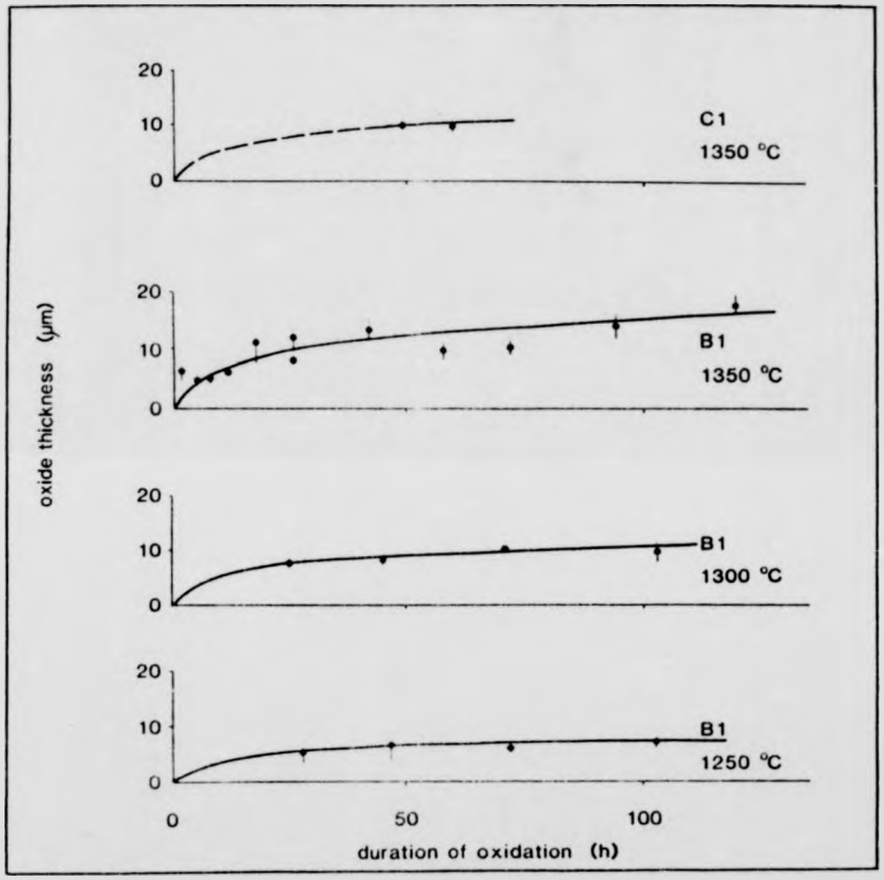

Figure 4.19(b): Kinetics of oxidation of the ceramics of intermediate substitution level.

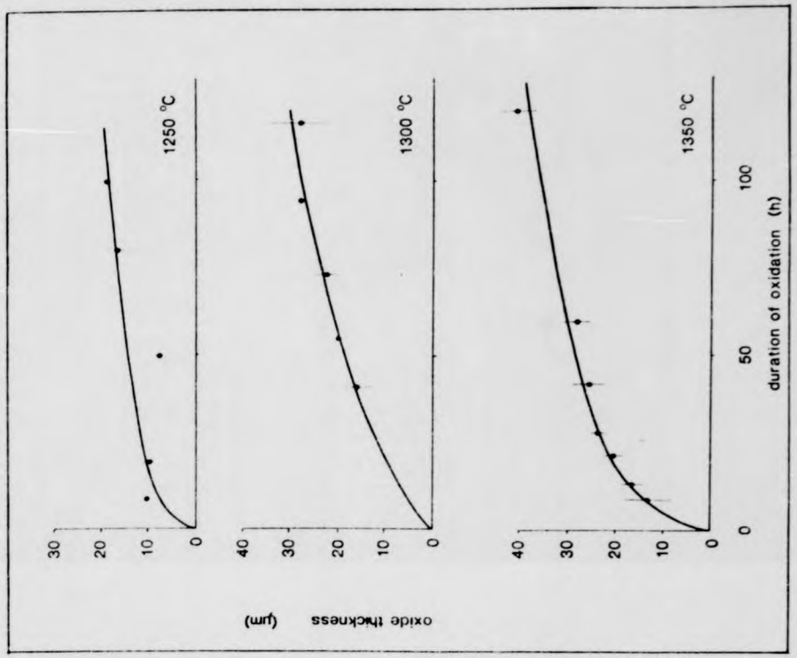

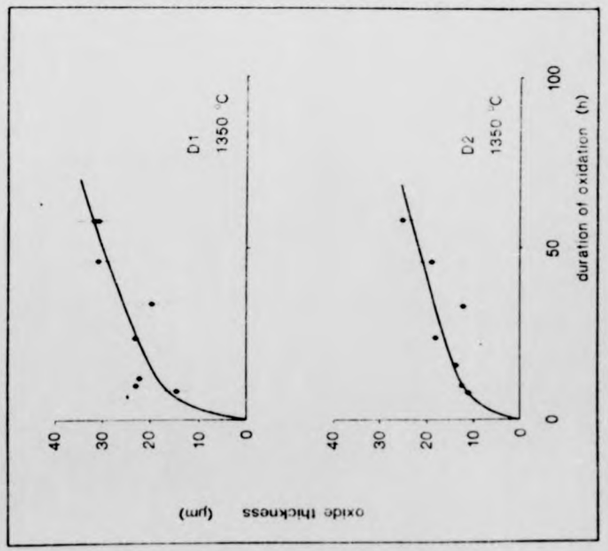

Figure 4.19(c): Kinetics of oxidation of the ceramics of high substitution level.

Table 4.1.

Oxidation Exponents of the β′ Si-Al-O-N Ceramics

Material	Oxidation Temperature	Exponent
A1	1200	1.1
	1250	0.9
	1300	2.3
	1350	1.9
	1400	8.7
A2	1200	2.9
	1250	5.0
	1300	7.1
	1350	7.2
	1400	2.5
B1	1250	5.9
	1300	5.7
	1350	2.9
D1	1350	3.8
D2	1350	3.2
D3	1250	2.3
	1300	1.9
	1350	2.4

the concentration of the diffusing species, C , via its diffusion coefficient, D:

$$\frac{dm}{dt} = - D(c,t) \frac{\partial c}{\partial x} \qquad (4.2)$$

For diffusion of a species with time and concentration-independent diffusion coefficient, in a direction x, along a constant concentration gradient, equation 4.2 integrates to give

$$x^2 = - A\ Dt$$

where A is a constant. Linear or parabolic kinetics of oxidation were observed for only two of the β' ceramics. At 1200 and 1250°C the oxidation exponent of ceramic A1 is n≈1. At 1300 and 1350°C it is n≈2. The very high exponent of 8.7 on oxidation at 1400°C arises from a high scatter in the experimental data occasioned by gross distortion of the low-viscosity liquid scale by evolving N_2 gas bubbles.

Parabolic oxidation kinetics were also observed for ceramic D3. The rate constants of oxidation of this ceramic are presented in figure 4.20. An average scale density of 2.2 g cm^{-3} has been assumed.

Non-parabolic forms of the oxidation kinetics may be caused by

(1) improper determination of the extent of oxidation,
(2) non-parabolic thick-film mechanisms of oxidation, or
(3) time-dependent compositional variations of the oxide scale.

(1) Criticisms of the use of scale thickness determination as a measure of oxidation resistance

There are several situations in which the oxide scale thickness would not be a proper measure of the oxidation resistance of the ceramic. First, time-dependent changes in scale viscosity may cause a changing degree of mechanical scale distortion by N_2 gas bubbles.

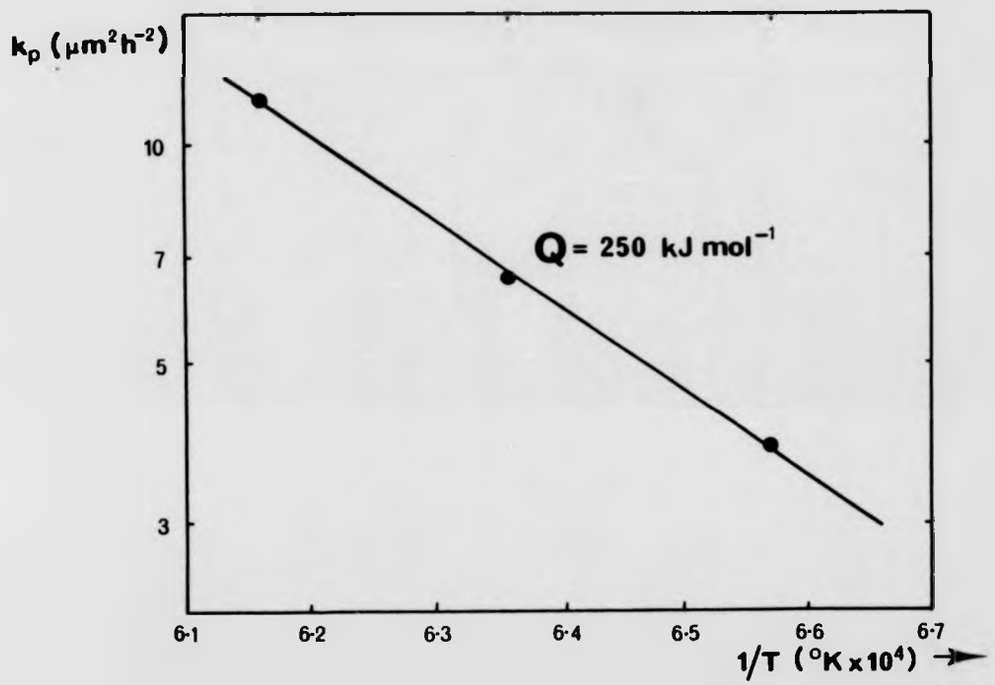

Figure 4.20: Rate constants of oxidation of ceramic D3.

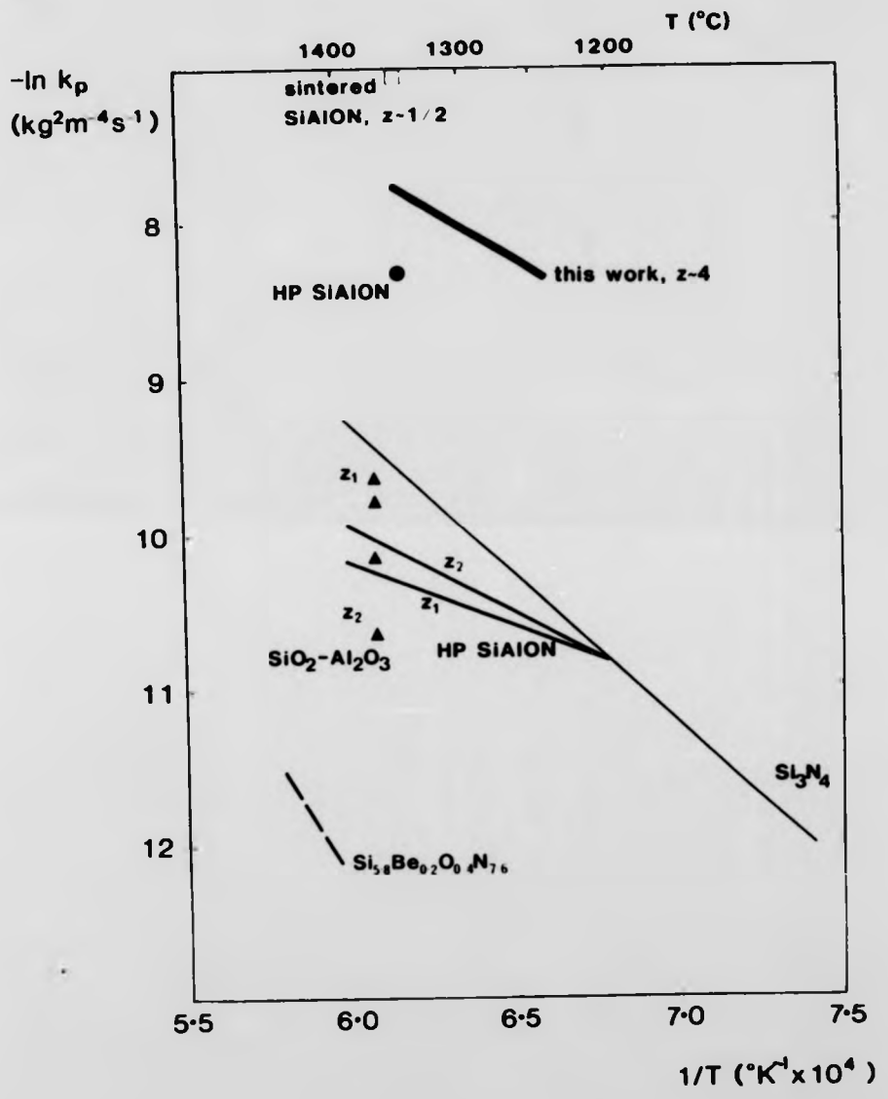

Figure 4.20: Continued

To avoid discrepancies in the determination of the form of the oxidation kinetics the scale thicknesses for low durations of oxidation were omitted. Low scale viscosity in the early stages of oxidation was indicated by the large degree of uncertainty in the measurement of the scale thickness caused by the local distortion of the oxide by the nitrogen gaseous pores (section 4.1.1.). The scale composition is believed to be relatively stable, after as little as 20 h (section 4.1.1.).

Secondly, the collapse of N_2 pores or scale evaporation would cause the oxidation rate measured by the determination of scale thickness to be lower than the actual rate, with consequently larger measured values of the oxidation exponent. An investigation of the oxidation of β´ Si-Al-O-Ns hot-pressed without the use of densifications aids, for example, has shown that the oxide thickness may grow at a lower rate than would be indicated by thermogravimetric measurements [Desmaison and Riley 1981]. There was no evidence, however, for either of these mechanisms in the oxidation of the β´ ceramics which, in all cases, formed a thick, coherent oxide in which, except at low durations of oxidation, the gaseous nitrogen was contained in enclosed pores.

(2) Non-parabolic thick-film mechanisms of oxidation

Thick-film mechanisms of oxidation which give rise to a greater degree of oxidation resistance than that described by parabolic oxidation oxidation kinetics have been proposed. In one model, the paths along which the rate-controlling diffusion occurs are progressively blocked. This may occur, for example, if pores form at the inner scale surface where the oxidation reaction takes place and diffusion of the reacting species is dependent on a solid state mechanism. Such behaviour is described by the equation

$$W = A \ln (B+t)$$

where A and B are constants [Evans 1960]. It is not possible however, to fit the oxidation kinetics of the as-pressed ceramics to an equation of this form.

In an alternative situation where fresh oxide formation blocks the path of the diffusion of the oxidising species, the oxidation kinetics may be described by the assymptotic equation

$$W = a(1-e^{-bt})$$

where a and b are constants [Lawless 1973]. Although the kinetics of oxidation of the materials of low substitution level ($z \sim 1$) appear to take a similar form, it is not believed that this mechanism operates in the oxidation of the hot-pressed β′ Si-Al-O-Ns since rate-controlling diffusion occurs through a continuous glassy scale phase.

(3) Time-dependent oxide scale composition

Oxidation which is rate-controlled by diffusion of a species through a scale of time-dependent composition would be described by non-parabolic ($n \neq 2$) oxidation exponents. In this case the diffusion coefficient of the diffusing species is concentration-or time-dependent and equation 4.2 becomes

$$x^2 = -A\, D(c,t)\, t.$$

Such a time-dependence arises in the case of diffusion through a liquid medium of time-dependent viscosity. The relation between the diffusion coefficient diffusing through a liquid medium of viscosity, η, is described by the Stokes-Einstein relation

$$D = kT/6\pi\eta R$$

where R is the gas constant.

The viscosity of the liquid part of the oxide scales formed on additive-containing β′ ceramics is expected to be time-dependent due to the continuous out-diffusion of such glass-modifying elements as Na, Mg

and Ca on oxidation (section 4.1.1.). In particular, the oxide scale of the ceramics is of initially very low viscosity and thereafter increases continuously due to subscale denudation reducing the quantity of out-diffusing elements relative to the increasing thickness of the oxide scale occasioned by oxidation of the surface of the ceramic.

The addition of glass-modifying elements such as Na, K, Ca, Fe and Mg to SiO_2 melts reduces their viscosity by the breakdown of network-forming Si-O-Si bonds. This viscosity decrease is continuous with increasing additions of the glass-modifying elements. Recent experimental evidence has suggested that a similar simple model does not explain the behaviour of the viscosity of Al_2O_3-SiO_2 melts when additions of glass-modifying elements are made. In particular, the viscosity of Al_2O_3-SiO_2 melts may not continuously decrease with increasing additions of glass-modifying elements. Based on the justification of a mathematical model by the requirement for a single maximum in the viscosity of a ternary alumino-silicate melt in which the molar fraction of silica is held constant whilst the monovalent or divalent oxide to alumina ratio is varied, theoretical viscosity data has been calculated for the system CaO-Al_2O_3-SiO_2 (figure 4.21). Viscosities calculated according to the theoretical model were very close to measured viscosities over a wide range of ternary and binary compositions [Urbain et al 1981].

In glassy Al_2O_3-SiO_2 systems divalent cations have similar effects on melt viscosity with respect to compositional variations (see, for example, Urbain et al 1982). Consideration of the calculated viscosity data for the system CaO-Al_2O_3-SiO_2 demonstrates that the viscosity of Al_2O_3-SiO_2 melts to which increasing quantities of the glass-modifying element has been made does not necessarily decrease continuously. In particular, at high molar fractions of Al_2O_3 (corresponding to Si-Al-O-N substitution levels of $z>2.8$) the melt viscosity initially increases prior to decreasing with further additions of the glass-modifying oxide.

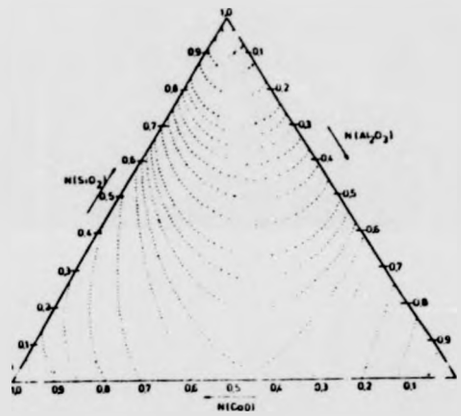

Figure 4.21: Theoretical viscosity data for the system $CaO-Al_2O_3-SiO_2$ [Urbain et al 1981]. (Lines of constant viscosity)

At lower molar fractions of Al_2O_3 (corresponding to Si-Al-O-N substitution levels of <2.8), additions of the glass-modifying oxide are predicted to cause a continuously decreasing melt viscosity, at least up to levels of ~10%, levels inexcess of those found in the oxide scales.

At compositions corresponding to substitution levels of z=4 approximately 10% of CaO would be required before the viscosity of the melt begins to decrease. However, the oxide scale of this ceramic separates to form an aluminium rich phase within a silica rich liquid matrix (section 4.1.3). With respect to additions of glass-modifying elements this liquid phase may be expected to behave similarly to the liquid part of the scale of the ceramics of intermediate substitution level.

The dependence of the viscosity of the scale on minor scale constituent concentration accounts in part for the observed oxidation behaviour of the β' ceramics. In general, the oxidation exponent for the oxidation of the ceramics for periods of up to 20h at 1350^{o}C has been observed to be non-parabolic (n>2), a condition arising from two factors related to the viscosity of the liquid part of the oxide scale.

First, direct oxidation of the ceramic can occur at parts of its surface which have been exposed to the atmosphere by the formation of large fissures by N_2 gas escaping through a scale of low viscosity (figure 4.6). Secondly, the diffusion coefficient of the species diffusing through the liquid phase continuously increases during this period due to the continuously decreasing viscosity of the liquid part of the scale (section 4.1.1).

The approximate compositions of the oxide scales of ceramics A1 and A2 oxidised at 1350^{o}C for periods in excess of 20h have been determined by the measurement of the average quantities of their minor scale constituents (figures 4.3 and 4.4). The experimental technique was too insensitive to

determine whether the scale compositions of the two ceramics changed little on oxidation between 20 and 300h at this temperature or whether slight increases in the quantities of the minor scale constituents occurred, paralleling the slight growth of the oxide scale during this period.

The observed parabolic oxidation exponents for oxidation of ceramic A1 at 1300 and 1350°C may be due to rate-control by the inward diffusion of oxygen through a scale of essentially constant composition. However, according to the data of figure 4.4 the composition of the scale of ceramic A2 oxidised at 1350°C was also largely independent of the duration of oxidation, at least on oxidation for periods in excess of 20h. Parabolic oxidation kinetics may therefore have also been expected in this case. The oxidation exponent of this ceramic was non-parabolic at this temperature, however, being $m \sim 3$. The ambiguity in the interpretation of these results has been removed by an analysis of the results of oxidation experiments using heat-treated ceramic specimens.

4.2.2. Oxidation of heat-treated ceramics

The oxidation resistance of the β′ Si-Al-O-N ceramics was dependent on the oxidation history of the samples. Samples of ceramics A1, A2, B1, and D3 which had been oxidised at 1350°C were reoxidised at the same temperature after removal of the scale which had formed on initial oxidation. The scale was removed by scraping with a piece of unoxidised ceramic followed by light polishing of the ceramic on SiC paper to remove remaining traces of the oxide and to restore the original pre-oxidation surface finish (section 3.1.2.).

The oxide thicknesses which formed on reoxidation are presented in table 4.2. These thicknesses were much lower than those found on oxidation of the as-pressed ceramics, except for the ceramic A1 whose scale thickness was not dependent on the original oxidation history. The oxidation resistance of the heat-treated ceramics was intermediate between that of the as-pressed ceramics and that which would have been expected had oxidation not been interrupted. It

Table 4.2

Thickness of oxide scale on heat-treated ceramics

Ceramic	Duration of original heat-treatment (h)	Duration of second heat-treatment (h)	Thickness of scale (μm)
A1	42	0	5.2/8.2 ± 0.6/0.9
	18	42	5.6/6.9 0.4/1.7
	42	42	4.8/3.2 0.4/0.2
	287	42	8.1 1.2
A2	25	0	13.8/11.1 2.8/1.9
	24	25	4.5 -
	44	25	5.8 0.8
	94	25	7.2/6.2 0.7/0.5
	42	0	15.6/19.6 1.9/3.0
	28	42	11.4 1.3
	58	42	11.5 1.1
	94	42	7.9 0.5
	90	0	15.8 1.9
	90	90	7.9 1.0
	190	90	7.1/5.7 1.5/1.8
	320	90	8.1 1.1
B1	42	0	14.1 2.1
	8	42	7.2 1.2
	28	42	6.1 1.2
	58	42	7.6 1.8
D3	72	0	~ 30 -
	9	72	13.8 5.4
	22	72	10.1 1.1
	120	72	10.8 1.0

was independent of the duration of the original heat-treatment. The rate of oxidation of these ceramics was not therefore controlled by subscale diffusion alone, as proposed for the oxidation of βSi_3N_4 hot pressed with MgO (section 2.2.3).

The oxide scales varied in composition according to their oxidation history. For example, the average quantities of the additive and impurity elements in the scales of the heat-treated ceramics A1 and A2 were lower than those in the scales of the as-pressed ceramics (figures 4.22 and 4.23) due to their extensive subscale denudation on initial oxidation (section 4.1.1).

The rate of oxidation of these ceramics is very sensititive to scale composition. The extent of oxidation of ceramic A1, for example, does not change on reoxidation after heat-treatment, despite a change in the scale composition (figure 4.19 and table 4.2). In contrast, the oxidation resistance of the nominally pure ceramic B1 increases after heat-treatment due to very slight changes in the composition of its oxide scale.

In view of the sensitivity of the rate of oxidation to small changes in scale composition it is believed that the non-parabolic (n>2) rates of oxidation of these ceramics is due to modifications to the oxide scale on heat-treatment caused by the further addition of subscale-derived additive and impurity elements, in Particular compositional changes which lead to a continuously decreasing viscosity of the liquid part of the scale through which the rate-determining diffusion of oxygen takes place.

The changes in the composition of the oxide scale on oxidation and subsequent heat-treatment and hence the enhanced oxidation resistance of heat-treated ceramics was caused by oxidation-induced structural and compositional modifications to the ceramic on heat-treatment. Since no further improvement in oxidation resistance was observed after original heat treatment durations of $\sim$20h ceramics of the size used in the se oxidation experiments appear to reach a "stabilised" form within 20h at 1350^{o}C.

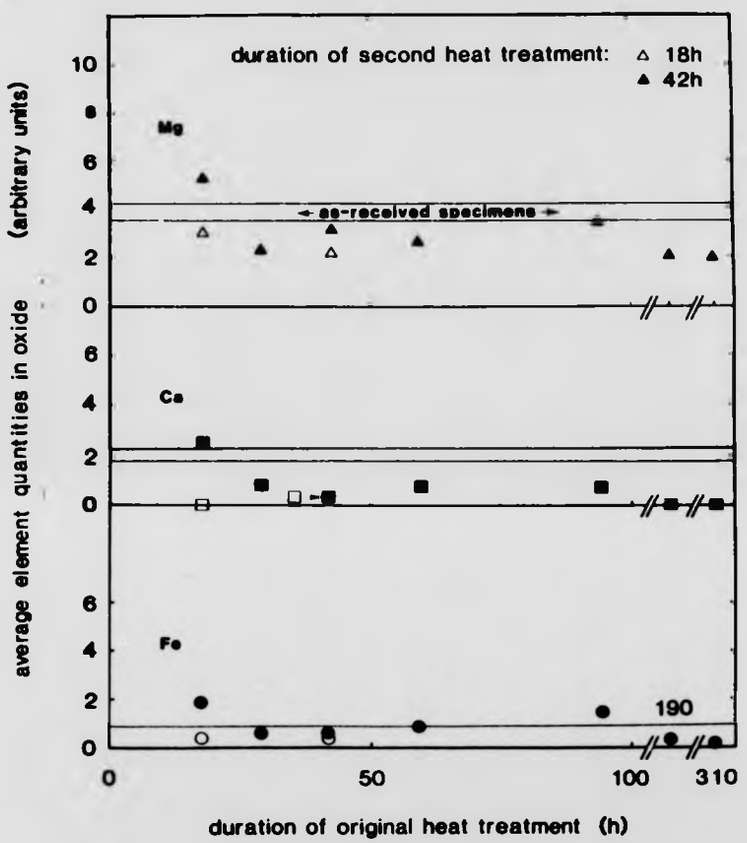

Figure 4.22 : Average quantities of elements in the oxide scales of heat-treated ceramic A1.

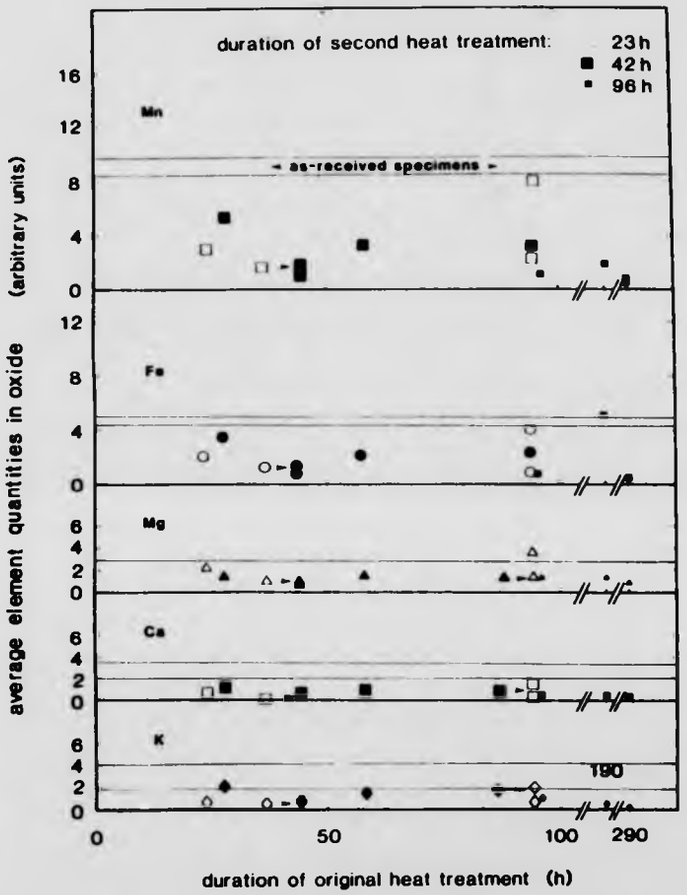

Figure 4.23 : Average quantities of elements in the oxide scales of heat-treated ceramic A2.

The mechanism of this stabilisation was the redistribution of the additive and impurity elements from their intergranular location via migration to the oxide scale or their solution in the β′ Si-Al-O-N crystal phase during oxidation. These subscale mechanisms partly control the oxidation behaviour of small ceramic specimens up to periods of ∿20h at 1350°C and are more fully described and defined in Chapter 5.

The rapid completion of the subscale redistribution processes on oxidation leads to the low oxidation resistance of the heat-treated ceramics. The oxidation behaviour of these ceramics is more representative of β′′′ Si-Al-O-N. Their oxidation resistance increased in the order D3:B1:A2,A1, being a continuously increasing resistance for ceramics of high to low substitution level.

4.3. A model for the oxidation of hot-pressed β′ Si-Al-O-N ceramics

4.3.1. Ceramics of low substitution level, z∿1 (ceramics A1 and A2)

The anomalously high oxidation exponent of ceramic A2 compared with that of n=2 for ceramic A1 and usually produced by diffusion-controlled oxidation is believed to be due to the time-dependent compositional variation of an oxide scale of stable glassy structure.

The high rates of oxidation of both ceramics observed for periods of oxidation up to 20h of the ceramic specimens used here were due to three causes, First, the diffusion coefficient of oxygen in the scale was initially high due to low scale viscosity caused by the initial rapid out-diffusion of grain boundary-segregated cations. This low viscosity has permitted the escape of N_2 gas to the atmosphere (figure 4.6). Secondly, low initial viscosity of the scale allowed the formation of large N_2 gas pores which may be expected to allow direct penetration of gaseous oxygen to the reaction zone. The operation of this "direct" oxidation may be important in the oxidation of ceramic A1 whose oxidation resistance did not improve significantly after heat-treatment despite the large difference in the Mg content of the oxide scales of the as-

pressed and heat-treated specimens. Direct oxidation of this type is not expected to contribute significantly to scale growth after a few hours oxidation at 1350°C due to the development of a thick, coherent scale. Thirdly, the high initial concentration of Mg in the scale may enhance the rate of dissolution of β′ crystals in the scale. A very rapid phase boundary reaction may make a direct contribution to the high initial oxidation rate.

After "healing" of the initially very porous scale to form a coherent protective layer the rate of oxidation was determined by the rate of diffusion of oxygen across the scale to the reaction zone. This rate was solely dependent on the scale composition. The scales of ceramics A1 and A2 were homogeneous, dense and pore-free, except for widely-spaced N_2 bubbles. Enhanced diffusion rates for oxygen via pores or fissures was therefore excluded. The rate of diffusion of oxygen was very sensitive to scale composition. In ceramic A1 the rate of oxidation appeared to be independent of the scale concentration of MgO. In ceramic A2 the rate of diffusion of oxygen decreased with increasing duration of oxidation due probably to the continuously changing scale composition, in particular the decreasing concentration of Mn due to subscale denudation decreasing its continued availibility.

A second oxidation heat treatment after removal of the scale resulted in a scale containing a lower concentration of the glass-modifying elements derived from subscale intergranular regions. Initial oxidation rates of both ceramics on reoxidation were higher than the rate of oxidation prior to scale removal because of some out-diffusion of glass-modifying elements causing low scale viscosity in the initial stages of oxidation.

The rate of oxidation of ceramic A2 was very dependent on the compsition of the oxide scale. The formation of a scale containing relatively fewer additive and impurity elements on heat-treated ceramics led to much lower rates of oxidation. The rate of oxidation of the heat-treated ceramics A1 and A2 is more representative of that of β′ Si_5AlON_7 than the as-pressed ceramics. This was indicated by the similarity in the oxidation resistances of the heat-

treated ceramics (table 4.2). The changes in oxidation rate on heat-treatment was caused by the denudation of grain-boundary segregated additive and impurity elements. These compositional changes are accompanied by structural changes which are described in Chapter 5.

4.3.2. Ceramics of intermediate substitution level, z≈2 (ceramics B1, B2, C1 and C2)

The mechanism of oxidation of ceramics of intermediate substitution level, z≈2, was the same as that of ceramics A1 and A2. The diffusion of oxygen through a scale of stable structure but of time-dependent composition was the rate-controlling step. The scale consisted of a dense, coherent layer in which porosity was generally limited to large, widely-spaced N_2 bubbles. The rate-controlling diffusion took place through the continuous glassy matrix phase between the crystalline phases or through extensive regions of liquid phase.

Rates of oxidation in the first few hours of oxidation at 1350°C were high because of the rapid diffusion of glass-modifying additive and impurity elements into the oxide scale of the ceramic . The increased oxidation resistance of the nominally-pure ceramic B1 after heat-treatment demonstrated the sensitivity of the oxidation resistance to relatively low levels of additive and impurity elements in the scale. The oxidation resistance of this ceramic was improved on heat treatment by removal of much of the additive and impurity elements from the subscale intergranular regions of the ceramic.

The slightly decreased oxidation resistance of the heat-treated ceramic B1 over heat-treated ceramics A1 and A2 was due to its comparatively low scale viscosity and consequent increased diffusion rate for oxygen to the reaction zone. Decreased viscosity was due to the different composition of the scale. Al_2O_3 additions to SiO_2 melts cause reductions in their viscosity ([Rossin et al 1964] and figure 4.17).

4.3.3. Ceramics of high substitution level, z≈4 (ceramics D1, D2 and D3)

The rate of oxidation of the ceramics of high substitution level, z≈4, was controlled by the diffusion of oxygen through the continuous liquid phase of a scale of stable, phase-separated structure. The dependence of the oxidation resistance of the ceramics on the composition of the liquid phase was demonstrated by the increase in oxidation resistance of ceramic D3 after heat treatment.

The dependence of the oxidation resistance on the structure of the scale was demonstrated by the form of the oxidation kinetics. The time-dependence of the oxidation of these ceramics was the most nearly parabolic of the ceramics studied. This was due to the extensive scale porosity which facilitated enhanced oxygen diffusion to the reaction zone. This enhanced-rate oxygen diffusion was the cause of the relatively low oxidation resistance of the ceramics of high substitution level compared with those of low substitution level. The viscosity of the liquid phase of the oxide scale may not be substantially different to that of ceramics of lower substitution level due to possible similarity of composition in view of the phase separation of the scale to Al-rich crystalline phases and a Si-rich glassy matrix.

4.4. The influence of ceramic composition on oxidation behaviour

The oxidation resistance of fully-dense hot-pressed β′Si-Al-O-N ceramics is rate-controlled by the composition and structure of their oxide scales via their permeability for the inward diffusion of atmospheric oxygen to the reaction zone at the ceramic/scale interface. The compositon and structure of the scale is dependent on

(1) the substitution level of the ceramic,

(2) the quantity and type of the grain-boundary segregated hot-pressing additive and accidental impurity elements, and

(3) the previous oxidation history of the material.

The presence of additive and impurity elements such as Mn, Mg and Ca in as-pressed ceramics gives rise to ceramic oxidation resistances which do not follow a regular pattern of behaviour with regard to the ceramic substitution level. The general pattern of behaviour was that of maximum oxidation resistance for ceramics of low substitution level. The oxidation resistance of these ceramics is, however, very dependent on the type of additive element. For example, the oxidation resistance of an Mn-containing Si_5AlON_7 ceramic (ceramic A2) is highly sensitive to the concentration of Mn in its oxide scale whereas that of a Mg-containing ceramic of the same substitution level (ceramic A1), was not dependent on its scale concentration of Mg. The sensitivity of oxidation resistance of the Mn-containing ceramic to Mn concentration was the cause of the oxidation resistance of the as-pressed ceramic being lower than that of a nominally pure ceramic of higher substitution level (ceramic B1, $Si_4Al_2O_2N_6$).

In general the oxidation resistance of these ceramics is substantially modified by the presence of glass-modifying cations which out-diffuse into the oxide scale on heat-treatment. The degree of modification is minimised for elements which do not significantly influence the liquid part of the alumino-silicate oxide scales. However, even small quantities of these elements in the ceramic may give rise to rapid initial oxidation of the ceramic due to their presence in very high concentrations in scales formed at the outset of oxidation.

The prolonged oxidative heat-treatment of the β' ceramics modified their composition via the out-diffusion of the grain boundary segregated additive and impurity elements into the oxide scale. Due to high rates of grain boundary migration in these ceramics (chapter 5, section 1.4), extensive subscale denudation occurs within relatively short periods in small samples of the ceramics (section 4.1.1.).

Substantial through-thickness denudation results in ceramics of "stabilised" and essentially steady-state composition and structure. The oxidation resistance of these stabilised ceramics increased in the order D3: B1: A2,A1 (table 4.2).

The oxidation resistance of pure β' Si-Al-O-N ceramics is therefore expected to decrease with increasing sustitution level, contrary to simple arguments which suggest that the oxidation resistance of Si-Al-O-N should increase as its composition is shifted from Si_3N_4 towards Al_2O_3. Such behaviour would be due to two causes. First, the alumino-silicate scales of ceramics of high substitution level are of lower viscosity, permitting more rapid inward diffusion of oxygen. Secondly, the oxide scales become progressively more crystalline with increasing substitution level, being completely glassy at substitution level z=1. As a consequence they are more porous, facilitating more direct diffusion of oxygen to the reaction zone.

Ceramics of the highest oxidation resistance should therefore be of low substitution level and must contain no elements which affect the integri ty of the oxide scale with respect to its permeability for the diffusion of oxygen.

CHAPTER FIVE

OXIDATION-INDUCED MICROSTRUCTURAL CHANGES AND MECHANICAL PROPERTIES OF β′ Si-Al-O-N CERAMICS

The redistribution on oxidation of grain-boundary-segregated glass-modifying elements such as Mg and Ca gives rise to the development of ceramics of "stabilised" microstructure and increased oxidation resistance (Chapter 4). The subscale mechanisms responsible for this redistribution are the subject of part one of this chapter. Experiments are described which have led to the identification of the mechanisms of redistribution. These mechanisms were also responsible for the relatively low strain at failure of β′ ceramics tested in tension compared with that observed under four-point bend loading conditions. The tensile creep behaviour of the ceramics is described in part two of the chapter. A model of oxidation-assisted growth of surface flaws is proposed for the observed creep rupture behaviour.

Part One: Mechanisms for the redistribution of additive and impurity elements on oxidation

1.1. Indirect evidence for long-range diffusion in hot-pressed β′ Si-Al-O-N ceramics

On heat-treatment, the order of increasing oxidation resistance of the β′ ceramics changed from D3: A2: B1: A1 to D3: B1: A2: A1 (figure 4.19 and table 4.2). Since the duration of heat-treatment at 1350°C was not significant in determining the oxidation resistance of the heat-treated ceramics, the ceramics had become "stabilised" on

oxidation within ∿ 20 h. This rapid evolution of a more stable ceramic on oxidation was especially evident for the ceramics of low substitution level, z ∿ 1 (A1 and A2). After heat-treatment their oxidation resistance was very similar.

A parallel observation has been made in the creep behaviour of these ceramics. In the "as-pressed" condition their creep parameters Q, n, and $\dot{\varepsilon}$ in the creep equation

$$\dot{\varepsilon} = A\sigma^{n}\exp(-Q/RT)$$

were dissimilar. On heat-treatment at 1430°C for 960 h their creep resistance was improved and the creep parameters became similar. Material cut from adjacent to the oxidation surface of 10 x 10 mm blocks of ceramic exhibited a much greater improvement in creep resistance than material which was cut from the centre of the block [Karunaratne 1980]. This was attributed to a modification of the creep-controlling grain-boundary composition and structure. The enhanced creep resistance was caused by the removal of glass-modifying elements such as Mg and Ca into the oxide scale via grain-boundary diffusion. An alternative mechanism of dissolution of the elements in the β′ crystals was not preferred in view of the relatively short migration distances involved [Karunaratne and Lewis 1980b].

The diffusion path of the elements to the oxide scale, driven by composition gradients between the scale and the silicate grain boundary phase, is confined to the intergranular phase. Atomic mobility through this phase is rapid compared to diffusion through the β′ phase. In ceramics A2 and C2, D1 and D3 widespread regions of intergranular phase were located at multiple grain junctions (Chapter 3, part 2). Intergranular channels would exist if this phase extended in three dimensions, along which atomic diffusion would be

relatively rapid. Although most grain junctions in these β´ ceramics did not contain large quantities of second phase, diffusion of elements along these boundaries is relatively rapid due to the local structural inhomogeneity and lower bond strength compared with the highly covalent bonding of the elements in the β´ phase.

1.2. Out-diffusion on oxidation

The out-diffusion of the additive and impurity elements on oxidation is expected to give rise to a concentration profile in the subscale region of oxidised ceramics (figure 4.7). In β Si_3N_4 ceramics which contain a relatively large quantity of intergranular phase such profiles have been determined directly by EDAX microanalysis of cross-sectioned ceramics [Cubicciotti and Lau 1978, Clarke and Lange 1980, Wu et al 1981] (figure 5.1.). It was not possible to detect at a sufficiently high resolution the additive or impurity elements on the fracture surfaces of the ceramics oxidised in this study. The very low levels of additive and impurity elements could not be detected by EDAX microanalysis except in the oxide scale. Auger electron microscopy, which had been used to characterise the average composition of the intergranular regions of ceramics of similar composition to ceramic A1, [Lewis et al 1977], lacked the spatial resolution to determine the diffusion profiles. However, the average concentration of an element in the oxide scale of a ceramic is directly related to the concentration of that element near to the surface of the material prior to oxidation. Ceramics A1 and A2 were chosen for experiments to identify the subscale redistribution processes since their amorphous oxide scales permitted an estimate of these concentrations to be made.

relatively rapid. Although most grain junctions in these β´ ceramics did not contain large quantities of second phase, diffusion of elements along these boundaries is relatively rapid due to the local structural inhomogeneity and lower bond strength compared with the highly covalent bonding of the elements in the β´ phase.

1.2. Out-diffusion on oxidation

The out-diffusion of the additive and impurity elements on oxidation is expected to give rise to a concentration profile in the subscale region of oxidised ceramics (figure 4.7). In β Si_3N_4 ceramics which contain a relatively large quantity of intergranular phase such profiles have been determined directly by EDAX microanalysis of cross-sectioned ceramics [Cubicciotti and Lau 1978, Clarke and Lange 1980, Wu et al 1981] (figure 5.1.). It was not possible to detect at a sufficiently high resolution the additive or impurity elements on the fracture surfaces of the ceramics oxidised in this study. The very low levels of additive and impurity elements could not be detected by EDAX microanalysis except in the oxide scale. Auger electron microscopy, which had been used to characterise the average composition of the intergranular regions of ceramics of similar composition to ceramic A1, [Lewis et al 1977], lacked the spatial resolution to determine the diffusion profiles. However, the average concentration of an element in the oxide scale of a ceramic is directly related to the concentration of that element near to the surface of the material prior to oxidation. Ceramics A1 and A2 were chosen for experiments to identify the subscale redistribution processes since their amorphous oxide scales permitted an estimate of these concentrations to be made.

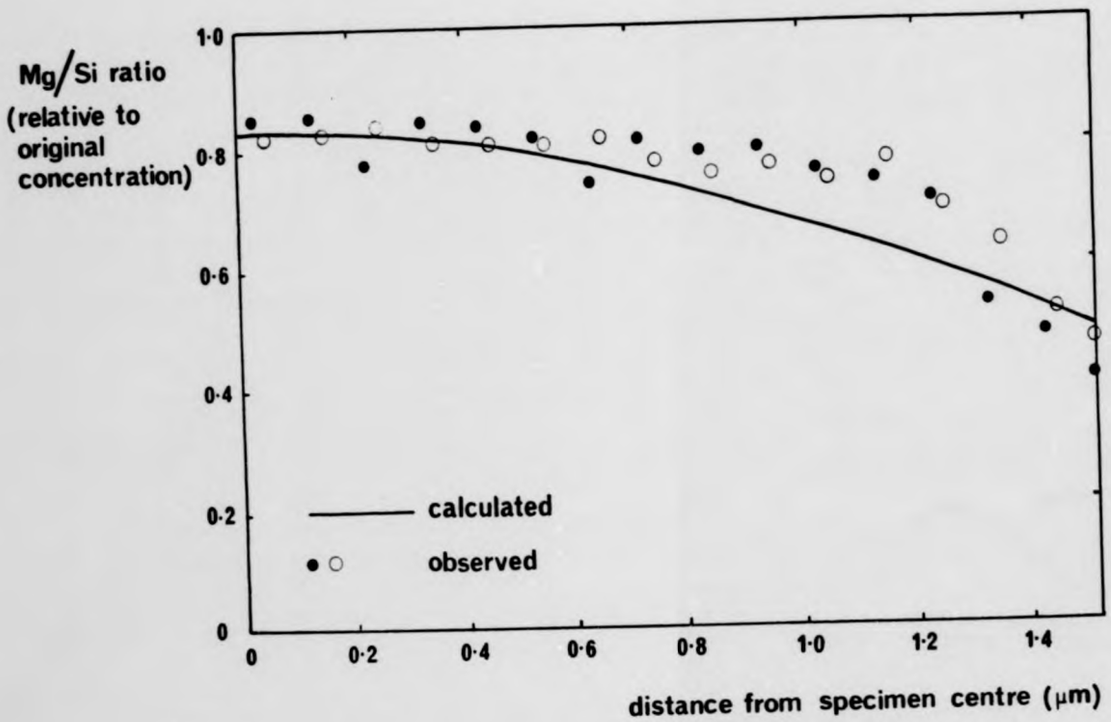

Figure 5.1: Calculated and observed sub-oxide diffusion profiles in Si_3N_4 hot-pressed with MgO [Clarke and Lange 1980].

1.2.1. Ceramic A1

In order to produce subscale diffusion profiles of the out-diffusing elements in ceramic A1 three blocks of ceramic of cross-section 10 x 10 mm were oxidised at 1430°C for 120, 500 and 960 h respectively. (The latter block formed part of the material utilised in the creep study cited above - section 1.1 [Karunaratne 1980]). The oxide scale was removed from the blocks by scraping with a piece of as-pressed ceramic, followed by grinding lightly on water-lubricated SiC paper. The block was cut into sections ∿ 0.7 mm wide, parallel to the original oxidation surface. Material from the centre of these sections was subsequently oxidised at 1350°C for 42 h. Under these conditions a thick glassy scale was produced. Its characteristics were compared with those of the scale formed on oxidation under the same conditions of ∿ 0.7 mm slices of "as-pressed" and heat-treated ceramics.

The thickness of the scale which formed on the reoxidised sections was independent of their origin and was similar to that formed on oxidation of the "as-pressed" ceramic. There were, however, marked differences in the average quantities of the elements Na, Mg, K, Ca and Fe contained in these scales, dependent on both the position of the section in the block and the duration of its oxidation (figure 5.2.).

Na, K, Ca and Fe were not detected in the scales of the sections which had been cut from the region adjacent to the original (block) oxidation surface, indicative of rapid out-diffusion of these elements on heat-treatment of the block. The average quantities of the out-diffusing elements in the scales of the block sections were found to increase with increasing distances from the block oxidation surface, but were always less than corresponding average quantities in the scale

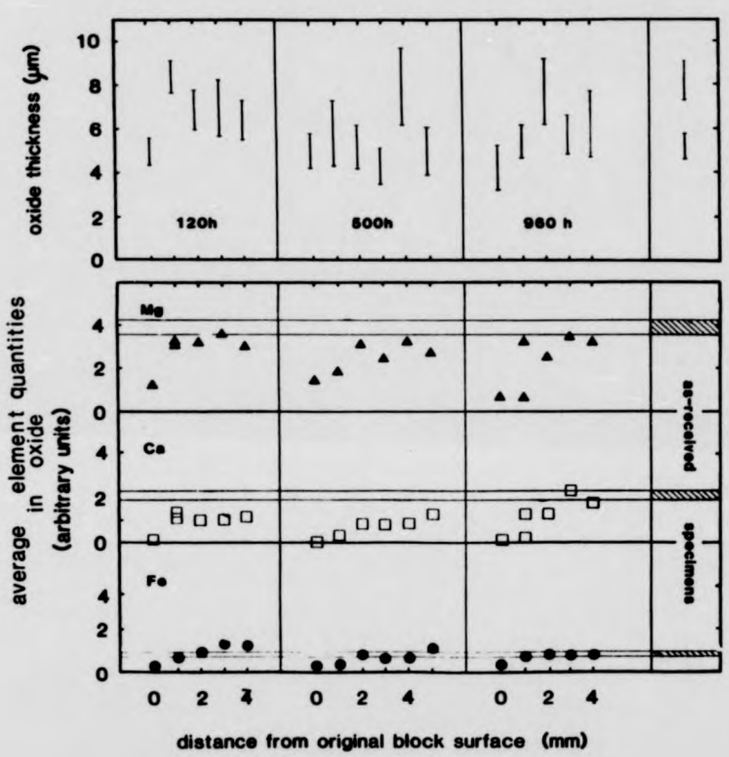

Figure 5.2: Characteristics of the oxide scales of sections cut from heavily oxidised blocks of ceramic A1.

of the "as-pressed" specimen. This effect was most marked for the sections cut from the blocks which had been oxidised for 500 and 960 h.

The maximum average quantity of Mg in the scale of the section cut from the centre of the blocks was less than that in the scale of the "as-pressed" ceramic, being similar to that in the scale of heat-treated ceramics (cf figure 4.4). The average quantities of the other out-diffusing elements in the scales of these sections were also similar to those in the scales of heat-treated ceramics, at least for the blocks heat-treated for 160 and 500 h. The average quantities of these elements in the scale of the section cut from the centre of the block were similar to those in the scale of the "as-pressed" ceramic. Since the blocks were oxidised for much longer lengths of time at higher temperatures than the "as-pressed" or heat-treated "test" ceramic specimens the out-diffusion of additive and impurity elements was not accompanied by their extensive solid solution in the β' crystal phase.

1.2.2. Ceramic A2

The subscale element redistribution processes in ceramic A2 were not identical to that of ceramic A1. A block of ceramic of section 18 x 18 mm heat-treated for 160 h at 1430°C and the 10 x 10 mm block heat-treated for 960 h at 1430°C utilised in the previous creep study [Karunaratne 1980] were sectioned as described for ceramic A1. These sections were heat-treated for 23 h at 1350°C to produce a thick glassy scale whose characteristics were compared with those of "as-pressed" and heat-treated $\sim$ 0.7 mm slices of ceramic heat-treated under similar conditions.

The oxidation resistance of the sections cut from the block heat-treated for 960 h was independent of the origin of the section and was

of similar magnitude in all cases, being similar to that of heat-treated ceramic A2 or of ceramic A1 (figure 5.3). That of the sections cut from the block heat-treated for 160 h was also independent of the position of the section but was of similar magnitude to that of "as-pressed" ceramic A2. This is in contrast to the oxidation resistance of ∿ 0.7 mm slices of "as-pressed" ceramic whose oxidation resistance increased greatly after only ∿ 20 h at 1350°C (table 4.2). The origin of this behaviour lies in the manner of redistribution of Mn on oxidation.

The subscale diffusion profile indicated by the increasing average quantities of elements in scales of the sections cut from progressively deeper regions of the blocks of ceramic A1 was not apparent for Mn in those of ceramic A2. Only at the surface of the blocks did there appear to be any indication of such a profile. The average quantities of Mn in the sections of the blocks cut at subsurface locations were all of similar magnitude. In the sections of the block heat-treated for 160 h these concentrations were similar to those in the scale of the "as-pressed" specimen. They were lower than this in the sections of the block heat-treated for 960 h.

The redistribution of Mn by diffusion occurred only close to the surface of the ceramic. Redistribution by diffusion was very slow in the subscale region of the ceramic. The average quantities of Mn in the oxide scales of heat-treated thin sections of ceramic were therefore very much lower than those in the scales of the sections cut from the subscale regions of the blocks which had undergone more severe heat-treatment.

Mn was contained in the ceramic primarily in the form of Mn-Fe silicide particles (Chapter 3, part two). These particles dissolve only very slowly on oxidation. They were observed in large quantities in the microstructure of the heat-treated sections of ceramic cut from

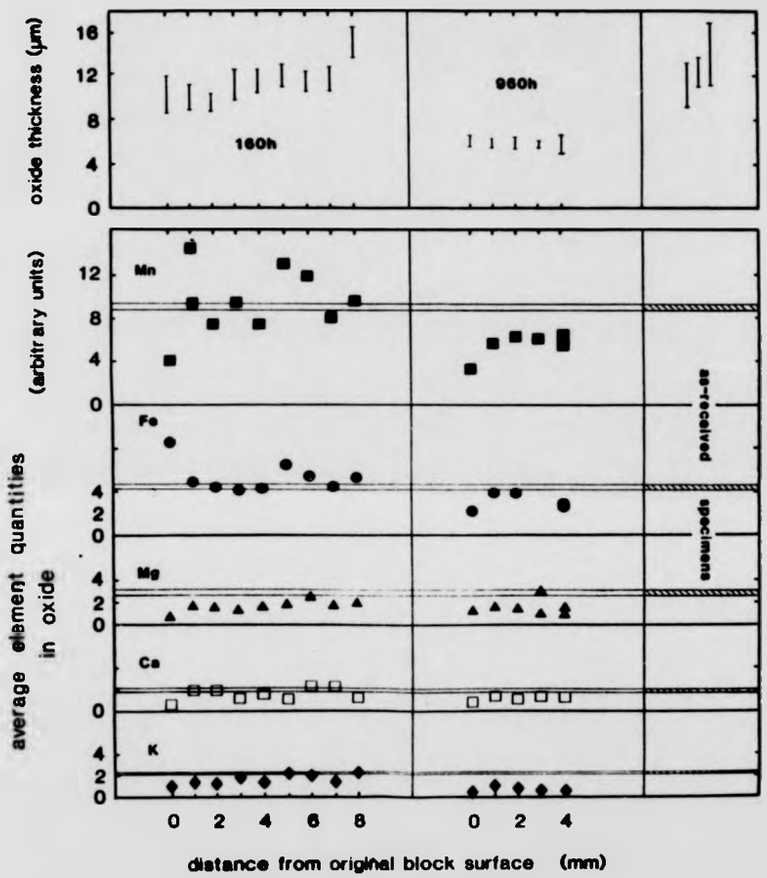

Figure 5.3: Characteristics of the oxide scales of sections cut from heavily-oxidised blocks of ceramic A2.

all parts of the heat-treated blocks.

The average quantities of Mg and the impurity elements K and Ca in the scales of the sections, however, were similar to those in the scales of the heat-treated "as-pressed" ceramic. Although the data do not directly indicate a distinct "profile" these very much lower concentrations are evidence for more rapid, out-diffusive redistribution of these elements on oxidation.

1.3. Microstructural changes

The oxidation resistance of the heat-treated ceramic A2 was similar to that of ceramic A1 after sufficiently severe heat-treatment. This change in oxidation resistance was caused by a compositional change of the intergranular regions due to out-diffusion of metallic cations into the oxide scale. The creep and fracture mechanisms of ceramic A2 had been observed to become similar to that of A1 on heat-treatment due to a structural change via the removal of multiple-grain-junction second phases which had acted as cavity nuclei [Karunaratne and Lewis 1980b].

The pockets of grain boundary phase in ceramic A2 were not observed in any of the heat-treated ceramics, even on oxidation for only 2 h at 1350°C. The two possible mechanisms responsible for the removal of the second phase pockets are illustrated in figure 5.4. First, removal of the additive and impurity cations into the oxide scale may have facilitated the local growth of β′ crystals, incorporating excess boundary Si, Al, O and N ions. Secondly, the phases may internally crystallise to such phases as Si_2N_2O, by reactions similar to those proposed to account for the oxidation behaviour of hot-pressed β Si_3N_4 (figure 2.10).

Of the ceramics studied here, ceramic C2 contained the largest quantity of intergranular phase (chapter 3, part 2). The microstructure

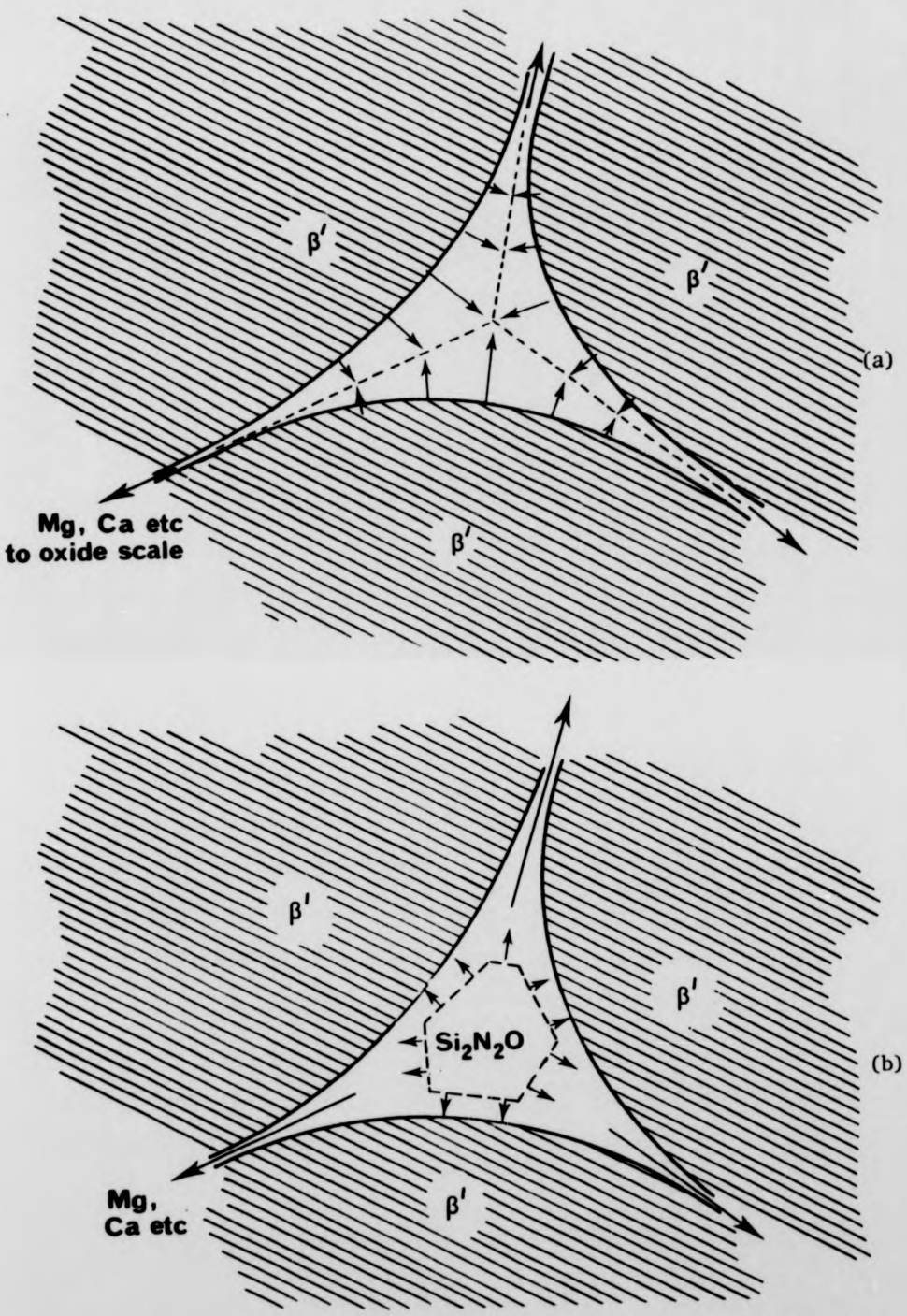

Figure 5.4: Mechanisms of removal of intergranular phase pockets on oxidation (a) β′ grain growth (b) crystallisation.

of a sample of this ceramic which had been heat-treated for 60 h at 1350°C contained no intergranular phase. The microstructure consisted entirely of non-faceting β′ grains (figure 5.5). The removal of the intergranular phase had occurred by the dual processes of long-range diffusion and local β′ grain growth.

No microstructural or chemical changes could be resolved in the bi-grain junctions of any of the ceramics due to their very limited width. The increased creep resistance of the ceramics A1 and A2 after heat-treatment was caused by increased intergranular cohesion [Karunaratne and Lewis 1980b]. This cohesion was produced by the out-diffusion of the additive and impurity elements into the oxide scale, increasing the number of primary β′ bonds across the narrow grain boundary.

1.4. Diffusion coefficients

The restriction of the diffusion of the additive and impurity cations to grain boundary regions due to their very low solubility in the β′ phase (Chapter 2, part 1), allows an estimate to be made of grain boundary diffusion coefficients. As a first approximation the out-diffusion of the additive and impurity elements may be compared with that of elements of an initially uniform concentration diffusing from a slab into a sink (figure 5.6). The solution of the diffusion equation for this system for the concentration, N, of the diffusing element is

$$N(x,t) = \frac{N_o}{2}\left\{\operatorname{erf}\left(\frac{h+x}{2\sqrt{Dt}}\right) + \operatorname{erf}\left(\frac{h-x}{2\sqrt{Dt}}\right)\right\} \qquad (5.1)$$

where N_o is the initial concentration

D is the diffusion coefficient

x is the distance from the centre of the slab

Figure 5.5: Microstructure of ceramic C2 oxidised at 1350°C.

Figure 5.5: Microstructure of ceramic C2 oxidised at 1350°C.

Figure 5.5: Microstructure of ceramic C2 oxidised at 1350°C.

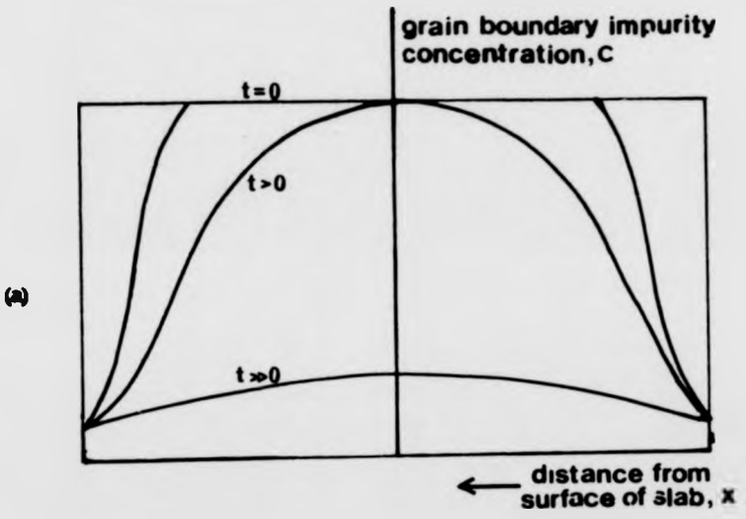

Figure 5.6: Concentration profiles generated by uniform out-diffusion into an infinite sink.

h is the slab half-thickness

and erf is the error function,

$$\text{erf } y = \frac{2}{\sqrt{\pi}} \int_0^y e^{-z^2} \, dz$$

[Jost 1960].

Assuming that the diffusion coefficient is concentration-independent the flux diffusing from the slab is given by

$$J = \frac{C_o \sqrt{D}}{2\sqrt{\pi t}}$$

where C_o is the initial concentration. The theoretical distribution of Mg in the subscale region of hot pressed β Si_3N_4 as determined using equation 5.1 has been superimposed on the data of figure 5.1, assuming the concentration of Mg at the centre of the slab to be invariant.

In view of the finite thickness of the intergranular phase a more precise model of the out-diffusion process may be that of diffusion along a pipe of time-dependent (decreasing) radius. In this case the out-diffusive flux is given by

$$J = a_o \, C_o \, \sqrt{D}/\sqrt{\pi t} \quad ,$$

where a_o is the initial cross-sectional area of the diffusion channel (Appendix). This is of the same form as the case of the uniform distribution of the diffusing element.

Substitution of appropriate values of N/N_o, n, x and t in equation 5.1 allows an estimation to be made of the diffusion coefficient of Mg in ceramic A1. The grain-boundary concentration of Mg at the centre of the blocks was ∿ 80% of the original concentration. Assuming the solubility of Mg in β′ to be negligible, the diffusion coefficient, D_b is ∿ 10^{-12} m^2 s^{-1} at 1430°C. This value is similar to that of divalent cations in

silicate materials (table 5.1). It is some six orders of magnitude higher than that predicted for grain boundary diffusion in ceramic A1 from an analysis of creep and microstructural data [Karunaratne 1980]. However, accommodation of grain shape changes in boundary diffusion-controlled creep requires the diffusion of Si and N and Al and O. The boundary diffusion rates of these elements is unknown and their slow diffusion may occur as groups such as SiN_4 tetrahedra.

Under conditions where the diffusion of creep-controlling complex groups does not cause the crack blunting otherwise observed [Karunaratne 1980], the rapid boundary diffusion of Mg and Ca leads to the instability of surface flaws. The effect of this behaviour of the creep rupture of the ceramics is discussed below (part two).

Part Two: Creep rupture of hot-pressed β′ Si-Al-O-N ceramics

Ceramics A1 and A2 have been deformed in tension to characterise their creep rupture behaviour. These ceramics were chosen because their creep behaviour under bending and compressive conditions have been well-characterised in a previous study [Karunaratne 1980]. Improvements in their creep resistance on heat-treatment were attributed to the oxidation-related changes in the composition and structure of the grain boundary regions which have been discussed in part one.

2.1. Tensile creep of ceramics A1 and A2

Incremental stress tests were performed on samples of ceramic A1 at temperatures of 1300°C and 1325°C at stresses in the range 5-45 MN m^{-2}. These stress levels were lower than those used in the previous bending and compression tests. Low stress levels were chosen to ensure that creep rates were not excessively high. The

Table 5.1.

Diffusion coefficients of ions in silicate and silicon nitride ceramics at ~ 1430 C

Diffusant	Host	Diffusion coefficient, D ($m^2 s^{-1}$)	Activation energy, Q (kJ mol^{-1})	Notes	Reference
Glasses and melts					
Ca	$CaO-Al_2O_3-SiO_2$	~ 10^{-10}	249	-	Terai & Hayami 1975
Al	0.44 CaO. 0.12 Al_2O_3 0.44 SiO_2	~ 10^{-11}	251	-	Henderson 1961
M cation	70 MnO. 30 SiO_2	~ 10^{-10}	226	from electrical conductivity	Bockris et al 1948
M cation	0.55 CaO. 0.45 SiO	~ 10^{-10}	147	from electrical conductivity	Bockris et al 1948
Polycrystals					
Mg	$MgAl_2O_4$	1.8×10^{-13}	360.5	extrapolated from 1400	Freer 1980
Ca	Ca_2SiO_4	1.7×10^{-14}	271.7	sintered pellet	Freer 1981
Ca	SiO_2	3.3×10^{-14}	460	extrapolated from 1370 C	
				sintered pellet extrapolated from 1393 C	Brown 1982
Ca	Al_2O_3	2.0×10^{-13}	371	sintered pellet	Mackenzie 1981
Single Crystal					
N	β-Si_3N_4	8.1×10^{-22}	776	extrapolated from 1410 C	Kijima 1976

tensile creep rates of HPSN hot-pressed with MgO are ∿ 10 times greater than compressive creep rates [Kossowsky 1973] due to the lower tensile stresses generated under compressive conditions [Birch et al 1976]. Creep rates were measured from steady-state portions of the strain-time curves. Steady-state conditions were observed for periods of 3-12 h duration throughout the test runs.

Two samples of ceramic A1 were tested. Their creep histories are summarised in table 5.2 and illustrated in figure 5.7. The transient nature of the creep of this ceramic is illustrated in figure 5.8 which depicts the creep rates observed under a stress of 30 MN m^{-2} at 1325°C. The source of the wide scatter in the data is unknown. Examination of the creep traces showed that diurnal temperature fluctuations were not responsible.

The high-stress level creep rates were similar to those obtained under bend and compression conditions (figure 5.7). The mechanism of tensile creep was therefore that of diffusion-controlled creep previously determined from the bend and compression studies [Karunaratne 1980] which showed a linear stress dependence of the strain rate.

Constant-temperature incremental stress tests were performed on samples of ceramic A2 at 1275°C, 1300°C and 1325°C at stresses in the range 5-40 MN m^{-2}. Creep was observed to be steady state for periods between 1 and 10 h throughout the tests. The creep histories are summarised in table 5.3 and illustrated in figure 5.9.

The scatter in the data does not allow a direct and unambiguous interpretation of the mechanism of creep to be made. In particular, the creep rates of the two specimens deformed at 1300°C differ by approximately one order of magnitude. The lower values of creep rate lie close to those observed for the ceramic deformed under compressive

tensile creep rates of HPSN hot-pressed with MgO are ~ 10 times greater than compressive creep rates [Kossowsky 1973] due to the lower tensile stresses generated under compressive conditions [Birch et al 1976]. Creep rates were measured from steady-state portions of the strain-time curves. Steady-state conditions were observed for periods of 3-12 h duration throughout the test runs.

Two samples of ceramic A1 were tested. Their creep histories are summarised in table 5.2 and illustrated in figure 5.7. The transient nature of the creep of this ceramic is illustrated in figure 5.8 which depicts the creep rates observed under a stress of 30 MN m^{-2} at 1325°C. The source of the wide scatter in the data is unknown. Examination of the creep traces showed that diurnal temperature fluctuations were not responsible.

The high-stress level creep rates were similar to those obtained under bend and compression conditions (figure 5.7). The mechanism of tensile creep was therefore that of diffusion-controlled creep previously determined from the bend and compression studies [Karunaratne 1980] which showed a linear stress dependence of the strain rate.

Constant-temperature incremental stress tests were performed on samples of ceramic A2 at 1275°C, 1300°C and 1325°C at stresses in the range 5-40 MN m^{-2}. Creep was observed to be steady state for periods between 1 and 10 h throughout the tests. The creep histories are summarised in table 5.3 and illustrated in figure 5.9.

The scatter in the data does not allow a direct and unambiguous interpretation of the mechanism of creep to be made. In particular, the creep rates of the two specimens deformed at 1300°C differ by approximately one order of magnitude. The lower values of creep rate lie close to those observed for the ceramic deformed under compressive

Table 5.2

Tensile creep history of ceramic A1

Temperature (°C)	1325		1300		1300	
	Stress ($MN\ m^{-2}$)	Strain Rate ($s^{-1} \times 10^{9}$)	Time (h)	Strain Rate ($s^{-1} \times 10^{9}$)	Time (h)	Strain Rate ($s^{-1} \times 10^{9}$)	Time (h)
	10	2.1	0-3			0.71	0-19
	15	2.0	6-11	12	167-172		
	20			3.3	180-177	0.40	20-31
	25		12-16	7.3	192-205		
	30	[illegible]	12-16	9.5	218-222		
		19	16-22				
		11	20-26				
		12	28-38				
		79	52-63				
		55	70-87				
	40			4.1	226-235	6.3	43-55
				3.3	245-246		
	45	12	145-158	4.5	246-249		
		31	157-162				
	50			7.1	250-253		
	40			11	254-264		
Failure Strain (%)		see →		0.90		0.28	
'Run Up' Time (h)		17		← see		≤ 10	

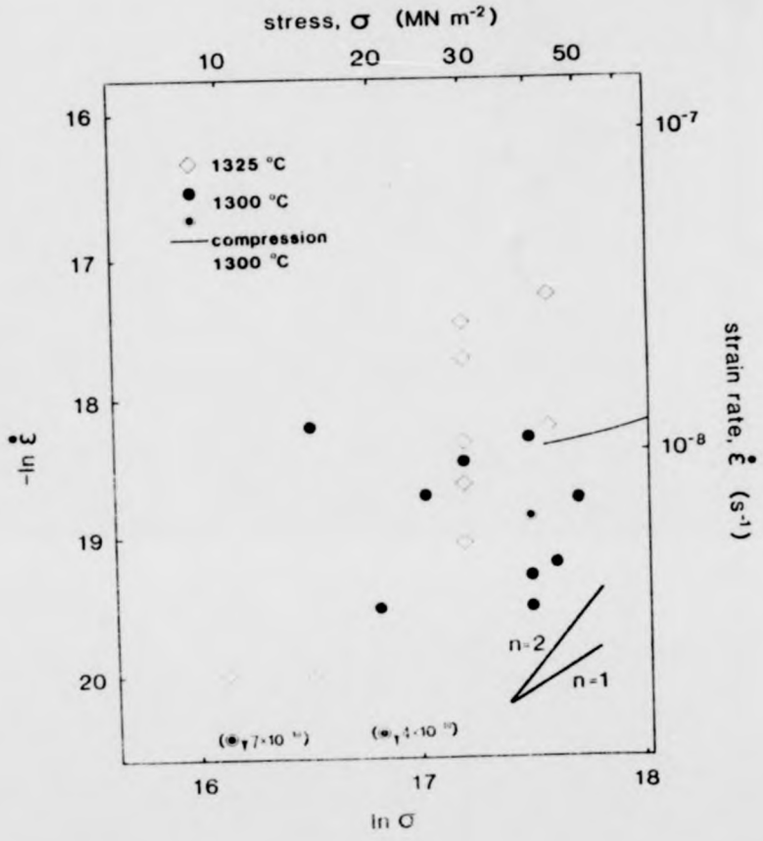

Figure 5.7: Characteristics of tensile creep of ceramic A1.

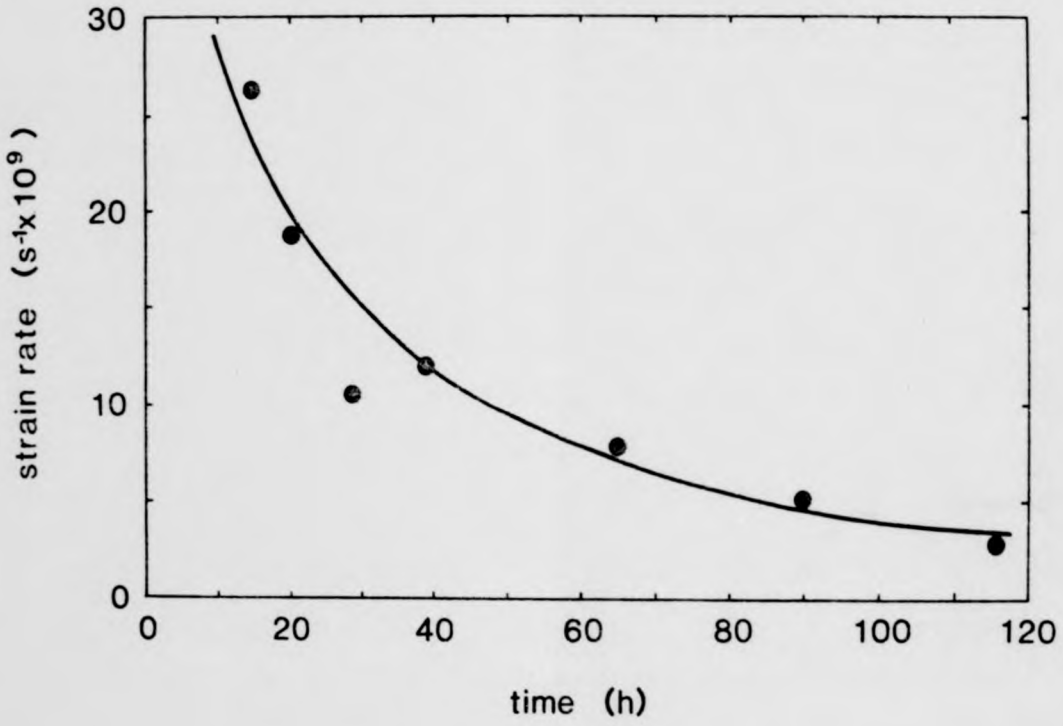

Figure 5.8: Transient creep of ceramic A1.

Table 5.3

Tensile creep history of ceramic A2

Temperature (°C)	1325		1300		1300		1275	
Stress σ_2 (MN m^{-2})	Strain Rate (s^{-1} x10^9)	Time (h)	Strain Rate (s^{-1} x 10^9)	Time (h)	Strain Rate (s^{-1} x 10^9)	Time (h)	Strain Rate (s^{-1} x 10^9)	Time (h)
5			4.1	0-3				
10			1.7	12-22	29	0-5		
15			5.8	55-65				
			3.9	70-78				
20	112	0-4			46	22-26		
	87	4-11						
23							17	0-9
25			12.3	133-142				
26							7.7	23-38
29							8.1	57-65
30	47	11-12	9.1	156-166			11	66-79
	35	12-12½			36	31-39		
	19	12½-14						
	54	14-15						
35			1.2	180-190			9.6	85-96
							10	105-112
							12	127-134
39							45	139-141
40					106	45-47		
Failure Strain (%)	2.34		0.63		0.95		0.57	
'Run up' Time (h)	48		unknown		< 15		~ 40	

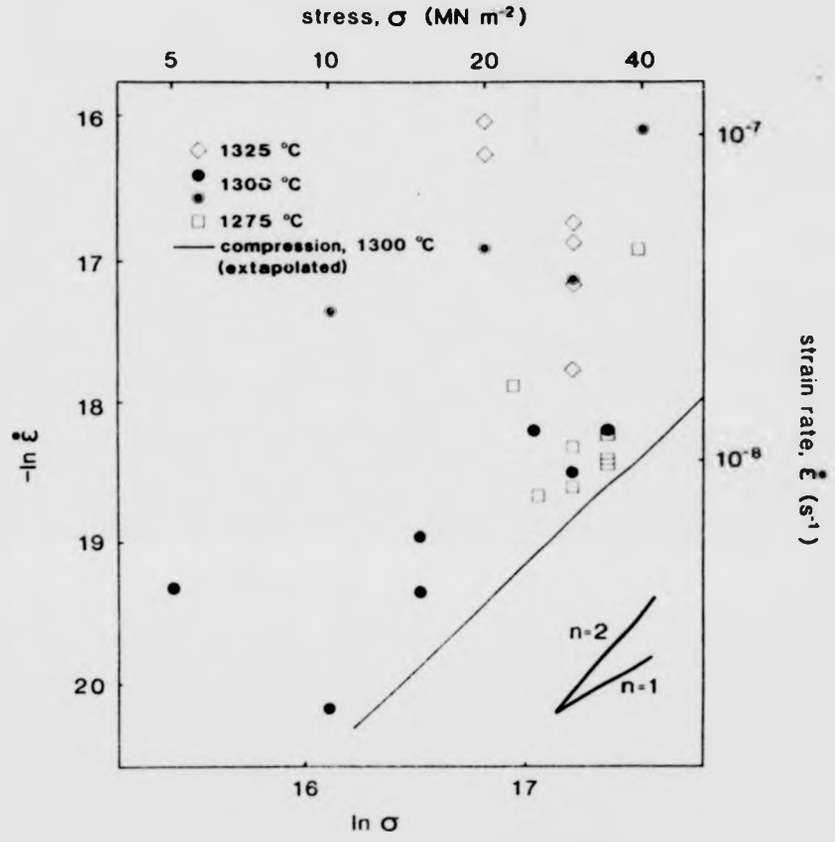

Figure 5.9: Characteristics of tensile creep of ceramic A2.

or bending loading conditions [Karunaratne 1980]. The specimen yielding these lower creep rates in tension had been creep tested for a relatively long period, the test at 1300°C being a continuation of an earlier test (table 5.3). Grain boundary denudation of glass-modifying elements is therefore likely to be more extensive in this material, giving rise to increased intergranular cohesion and lower creep rates.

Based on this assumption the observed tensile creep behaviour of ceramic A2 may be explained as follows. On initial high-temperature deformation creep is rate-controlled by crack growth or formation of cavities sensitive to tensile stresses. This is the behaviour demonstrated for HPSN hot-pressed with magnesia whose creep rate under tension is some 7-10 times that observed under compressive deformation stress conditions [Kossowsky et al 1975]. The creep rate of the ceramic is therefore an order of magnitude greater than that observed under compressive stress conditions. On heat-treatment the multiple grain junction cavities are removed by growth of the β' grains accompanying out-diffusion of segregated elements. Thereafter the creep rates of the ceramic are similar under both compressive and tensile stress conditions due to rate-control by the accommodation of grain boundary sliding by atomic diffusion.

2.2. Fast fracture mechanisms of creep rupture

The creep samples did not fail due to the fast fracture of pre-existing flaws. The surface of the gauge length of the samples were grooved perpendicular to the direction of the applied stress. Such grooves enhance the local stress to a value σ given by

$$\sigma = AK/\sqrt{\pi a} \qquad (5.1)$$

where a is the depth of the groove, K is the stress intensity factor of the ceramic, and A is a constant dependent on a/w where w is the

width of the ceramic perpendicular to the direction of the groove. Values of A have been tabulated for pin-loaded tension by Kendall [1983]. For typical grooves depths of $\sim$ 2 μm, a/w $\sim 10^{-3}$ and A $\sim$ 0.89. For a stress levels of 5-60 MN m^{-2} the stress intensity factors for the ceramics loaded in tension, from equation 5.1, is $\sim$ 0.01 - $\sim$ 0.2 MPa $m^{\frac{1}{2}}$. This is much lower than the critical stress intensity factors of ceramics A1 and A2. These have been determined from notched beam tests to be $\sim$ 6 and 10 MPa $m^{\frac{1}{2}}$ respectively at the test temperatures [Karunaratne 1980].

2.3. Slow fracture creep rupture mechanisms

The mechanism of slow crack growth from the most severe machining flaws assised by oxidation was responsible for the creep rupture of the ceramics. Both samples of ceramic A1 failed on loading at 60 MN m^{-2}. One failed at the upper sample bearing, the other across its gauge length. The greatest strain at failure, $\sim$ 0.9%, was much lower than the maximum strain produced by bend tests, $\sim$ 4% [Karunaratne 1980]. All samples of ceramic A2 failed across the gauge length after prolonged testing at strain levels $\leq$ 1% (The sample which failed at > 2% strain had failed via stress concentration at a square gauge length corner).

The fracture surfaces of the tensile samples of ceramic A2 displayed a wide region of rough topographic contrast parallel to one side of the gauge length which contained the worst machining flaws (figure 5.10). The remaining area was topographically smooth. This was the nature of the fracture surface of double-torsion and notched-beam specimens of this ceramic [Karunaratne 1980]. The rough topography extended from the root of notches and resulted from the interlinkage of stress-induced creep cavities. The spatially inhomogeneous nucleation of these cavities caused the formation of a crack whose path

Figure 5.10: Fracture surface of tensile creep specimen of ceramic A2.

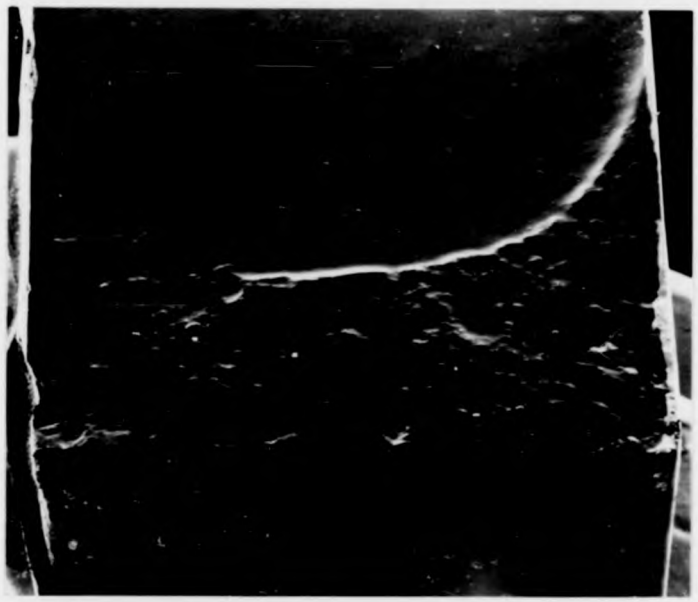

Figure 5.10: Fracture surface of tensile creep specimen of ceramic A2.

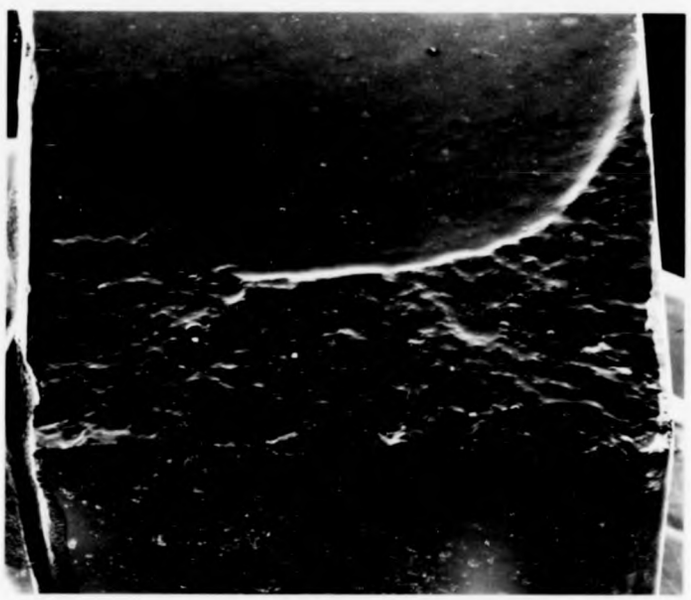

Figure 5.10: Fracture surface of tensile creep specimen of ceramic A2.

deviated by several grain diameters from a direct cleavage plane.

The slow growth of such a crack caused the failure of the tensile specimens. The rough, subcritical region extended across $\sim \frac{1}{2}$ of the cross-section of the fracture surfaces. Substitution of appropriate values of A, σ and σ in equation 5.1 yields a value of 6.8 MPa $m^{\frac{1}{2}}$ for the critical stress intensity factor, similar to that of $\sim$ 8 MPa $m^{\frac{1}{2}}$ determined by notched-beam tests [Karunaratne 1980].

The fracture surface of the tensile sample of ceramic A1 was topographically smooth (figure 5.11). Subcritical crack growth in this material occurs via the propagation of a single crack whose path does not deviate more than a few grain diameters from a cleaveage plane. However, subcritical crack growth is not expected in this ceramic at stress intensity factors $\leq$ 10 MPa $m^{\frac{1}{2}}$ at $\sim$ 1300°C [Karunaratne 1980]. A crack of $\sim$ 100 μm would be required for the initiation of slow crack growth in this ceramic under a stress of 50 MN m^{-2} in vacuum conditions. Fast fracture under a stress of 60 MN m^{-2} would require a crack depth of $\sim$ 250 μm.

2.4. Oxidative corrosion of surface flaws

The room-temperature flexural strength of β' Si_3N_4 hot-pressed with MgO is decreased by oxidative heat treatment due to formation of stress-raising pits in the specimen surface. These pits were associated with the presence of MgO in the ceramic since none were formed in CVD ceramics [Wu et al 1981]. Large pits have also been observed in ceramics which contained relatively large quantities of Al_2O_3 or CaO at grain boundaries [Wiederhorn and Tighe 1978].

Oxidation pits were formed at the surface of ceramic A2 which had been oxidised at 1430°C for 960 h (figure 5.12(a)). Non-planarity of the oxidation front was also apparent in specimens of ceramic A2

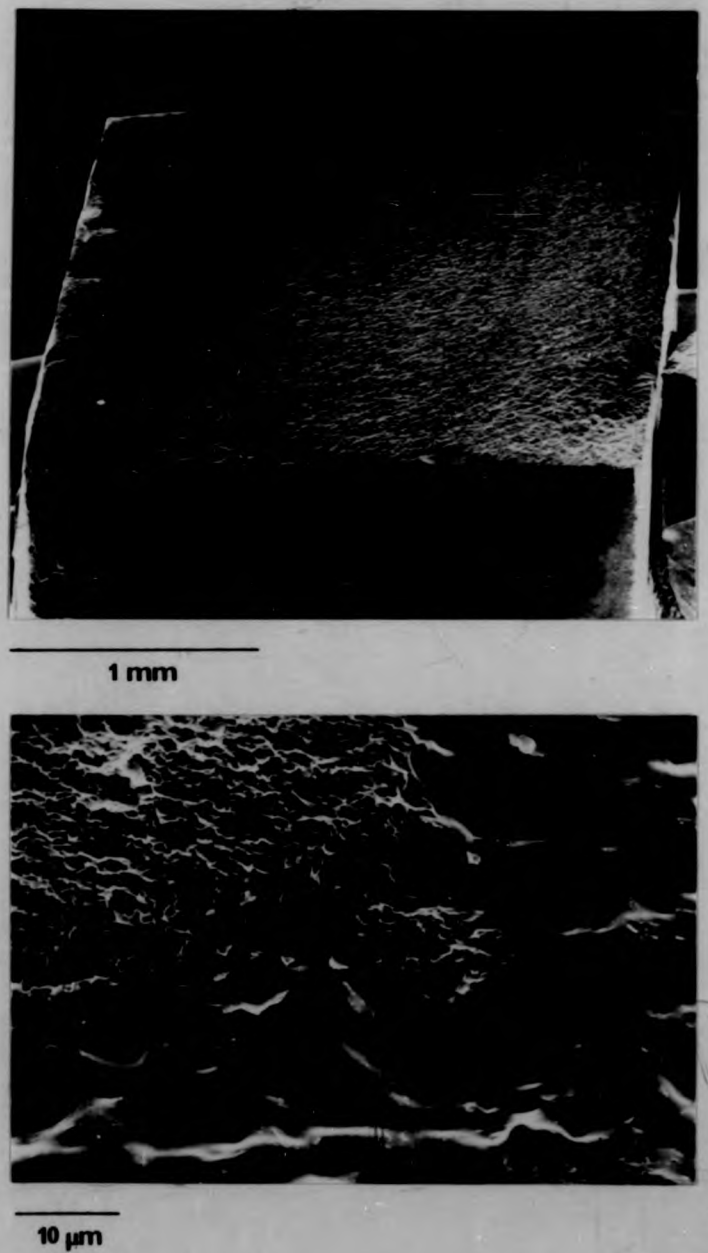

Figure 5.11: Fracture surface of tensile creep specimen of ceramic A1.

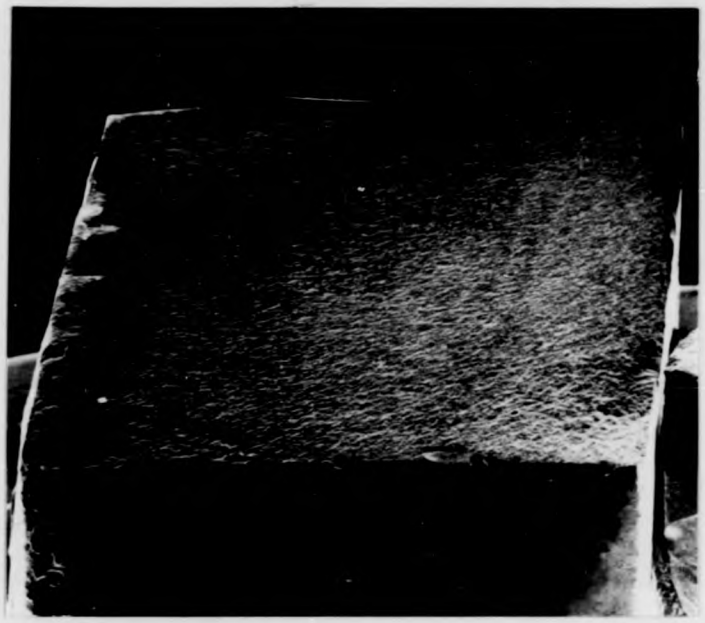

1 mm

10 µm

Figure 5.11: Fracture surface of tensile creep specimen of ceramic A1.

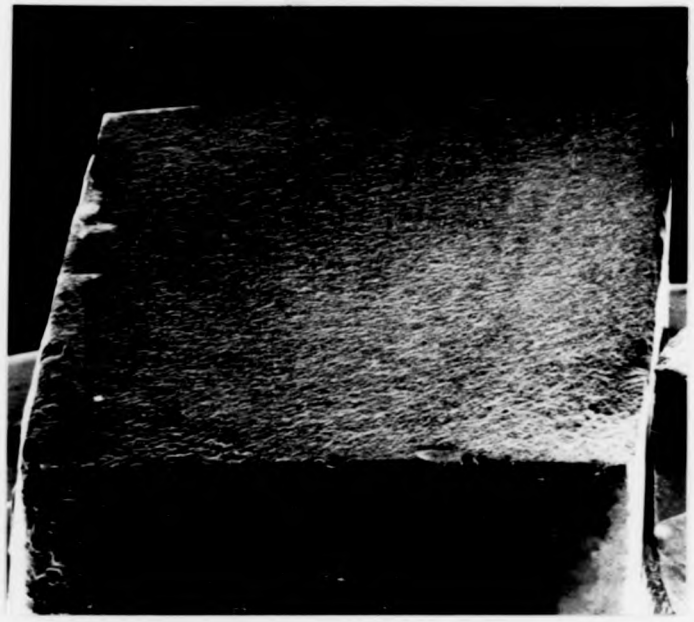

1 mm

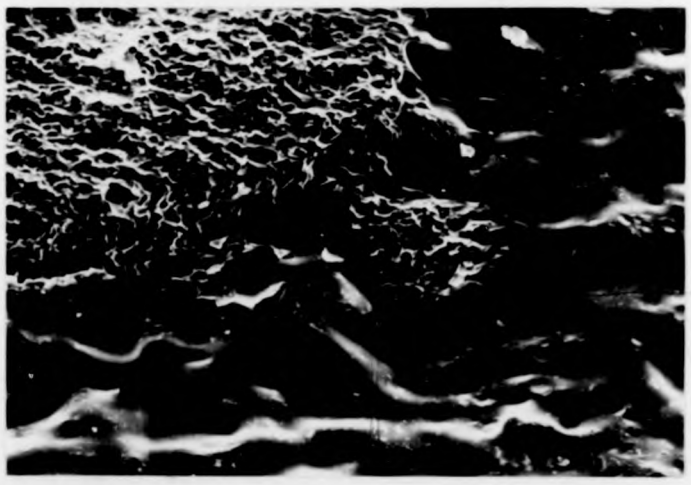

10 µm

Figure 5.11: Fracture surface of tensile creep specimen of ceramic A1.

(a)

(b)

Figure 5.12: Oxidation pits in the surfaces of ceramic A2
(a) oxidised at ∿ 1430°C for 960 h.
(b) oxidised at 1350°C for 96 h.

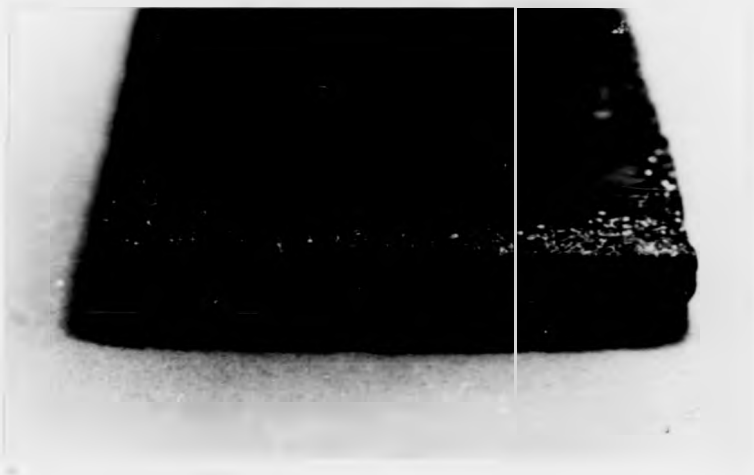

(a)

(b)

Figure 5.12: Oxidation pits in the surfaces of ceramic A2
(a) oxidised at ∿ 1430°C for 960 h.
(b) oxidised at 1350°C for 96 h.

(a)

1 cm

(b)

50 µm

Figure 5.12: Oxidation pits in the surfaces of ceramic A2
(a) oxidised at ∿ 1430°C for 960 h.
(b) oxidised at 1350°C for 96 h.

which had undergone far less severe oxidation; figure 5.12b illustrates the appearance of a ground surface of a specimen oxidised at 1350°C for 96 h. The non-planarity was caused by relatively rapid oxidation at regions of locally high concentrations of Mg Ca, and Fe.

Enhanced solution of β Si_3N_4 at crack tips has been proposed to account for the growth of fatigue cracks [Kossowsky 1973]. Such solution causes the formation of oxidation pits and forms the basis for the growth of surface flaws in the β′ ceramics to a size where they cause brittle failure.

The rate of oxidation of the ceramics A1 and A2 was dependent on the concentration of Mg, Ca and Mn at the oxidation front. Deep cracks or pits are unstable in these ceramics due to the relatively high density of grain-boundaries which intersect the local oxidation front (figure 5.13). These boundaries provide channels for the migration of the oxidation enhancing Mg, Ca and Fe elements, raising their relative local concentration near the crack tip. Local oxidation is therefore enchanced via the mechanisms discussed in Chapter 4 (section 4.3.1) deepening the groove relative to the less heavily oxidised surrounding surfaces as illustrated in figure 5.13. The rate of oxidation at the tip of the crack is enhanced by the rapid diffusion of the oxide-modifying ions caused by the locally steep concentration gradient (figure 5.13) leading to growth of the crack independently of applied mechanical stress.

CONCLUSION: The optimisation of mechanical properties by heat-treatment and surface finishing

Cavity-free β′ Si-Al-O-N ceramics (ceramic A1 and oxidised ceramic A2) have been shown to be capable of withstanding very high creep strains to failure under conditions of good surface finish and four-point bend loading. Creep rates and strain to failure were found to decrease and increase repectively on oxidation due to increased intergranular

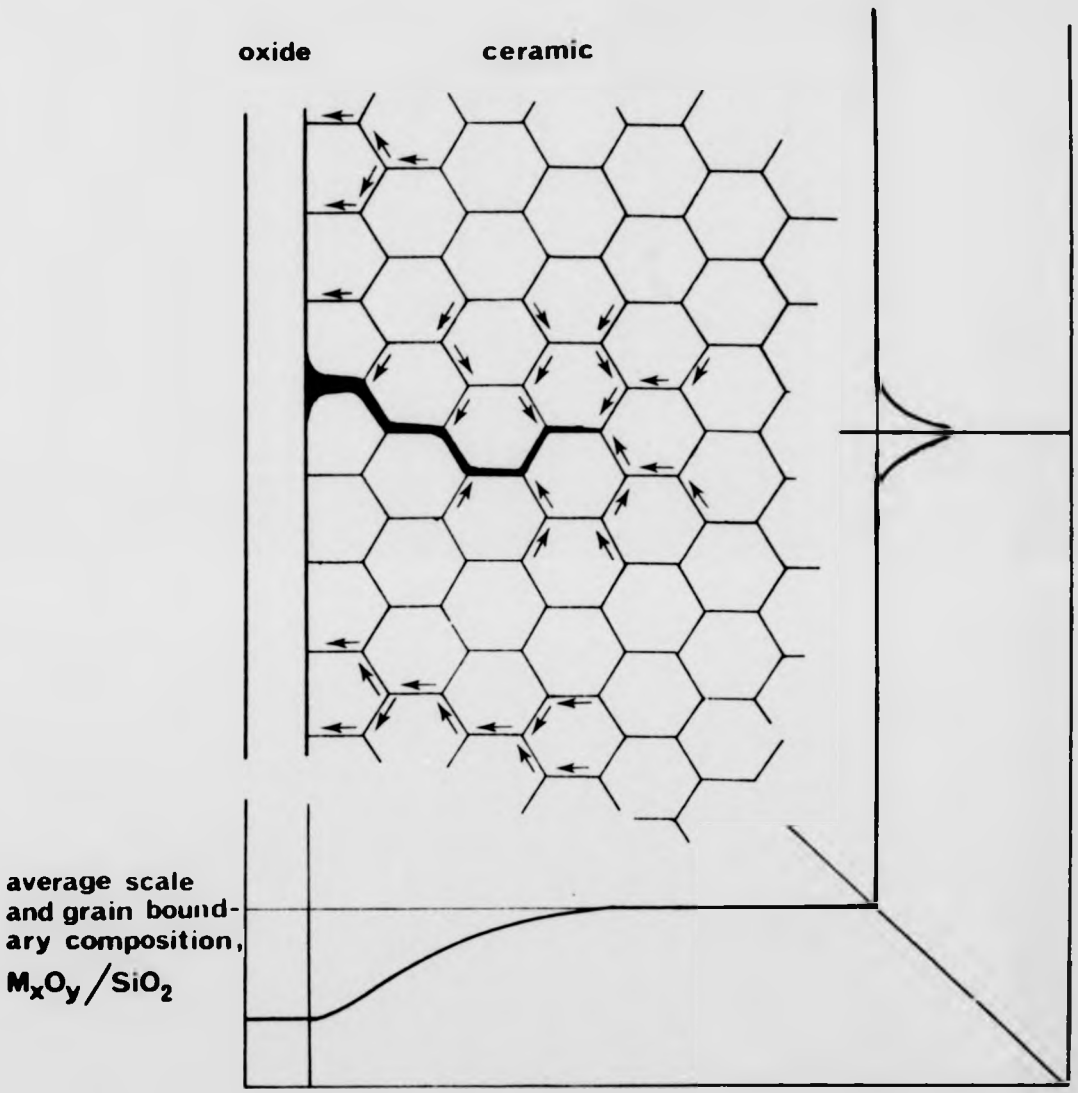

Figure 5.13: Formation of unstable oxidation pits in Si-Al-O-N ceramics.

cohesion occasioned by the out-

diffusion of glass-modifying elements such as Mg and Ca into the oxide scale [Karunaratne 1980]. This work has confirmed that oxidative out-diffusion of these elements is not accompanied by their significant dissolution in the β′ grains (section 1.2.1), and has permitted an estimation of the rate of intergranular diffusion of these elements via the determination of the diffusion coefficient of the migrating species (section 1.4).

This work has also demonstrated, however, that the oxidation of ceramics containing glass-modifying elements has a detrimental effect on their mechanical properties by reducing the strain to failure and initiating crack growth at stress levels otherwise too low to initiate crack growth, even at subcritical stress levels. The proposed model for this behaviour is relatively high localised oxidation of the ceramic at the tips of deep surface flaws (section 2.4). This crack growth occurs independently of the application of mechanical stresses.

A suitable processing route for the production of components of the highest strength would therefore be as follows. A highly oxidising heat treatment would remove large quantities of glass-modifying elements from intergranular regions in the bulk of the ceramic into the oxide scale. The inherent strength of the ceramic would thereby be increased via an increase in intergranular bond strength, and the rate of subsequent ceramic oxidation would be reduced. Since the oxidation of the creep resistant ceramics A1 and A2 is highly protective (figure 4.19) this stage need not involve the wastage of large volumes of material. The final stage of the component production would necessarily be the removal of sufficient material to produce a planar surface. Since the rate of intergranular diffusion of the glass-modifying elements in as-pressed ceramics is much greater than that of the species controlling the mechanism of crack blunting during creep (section 2.4), this process route should be applied to all components which are required to operate under highly oxidising conditions, over and above the classical

necessity of the removal of sharp surface flaws in the ceramic.

CHAPTER SIX

THE OXIDATION AND MECHANICAL PROPERTIES OF HOT-PRESSED β′ SI-AL-O-N CERAMICS: CONCLUSIONS AND SUGGESTIONS FOR FUTURE WORK

The work presented here has demonstrated the sensitivity of the oxidation and deformation behaviour of hot-pressed Si-Al-O-N ceramics to small changes in ceramic composition due to diffusional processes occurring on heat treatment. A full description of the behaviour of these ceramics therefore requires a precise description of their composition and microstructure and their variation on heat treatment.

The ceramics studied here were microstructurally characterised as consisting of nominally single phase, β′Si-Al-O-N, construction with a narrow β′ composition distribution with respect to the substitution level of the ceramic,z. When detectable in the transmission electron microscope additive and impurity elements, notably Mg, Ca, and Fe, were located at intergranular regions, either in glassy pockets located at multiple grain junctions or in the form of silicide particles. All the ceramics were found to be locally fully dense.

6.1. Oxidation behaviour

As opposed to published descriptions of the oxidation behaviour of ceramics of a single composition or of a limited compositional range this work describes the oxidation behaviour of a closely-related set of microstructurally well-characterised β′ Si-Al-O-N ceramics of a wide range of substitution levels and additive and impurity types and quantities. It has permitted a definition to be made of the general oxidation behaviour of these materials.

On heat treatment in air at temperatures in the range 1200-1400^{o}C the additive and impurity cations collected in large quantities in the oxide scale of the ceramics due to the formation of a diffusion couple between the alumino-silicate oxide and the silicate intergranular phase.

The scales of the ceramics were completely amorphous at low substitution level ($z \sim 1$) becoming increasingly more crystalline with increasing substitution level.

Subscale intergranular diffusion of these elements is very rapid. An estimate of the diffusion coefficient of Mg, based on the quantity of the element in the oxide scales of ceramic pieces cut from large oxidised blocks, was similar to that of Mg in silicate glasses, being $\sim 10^{-12}$ $m^2 s^{-1}$. The same experiments indicated that the dissolution of the additive and impurity elements in the β' phase was negligible by comparison. This out-diffusion has a profound effect on the relative oxidation resistances of the ceramics.

Ceramics from which much of these elements have been removed by a previous oxidative heat treatment were generally of a relatively high oxidation resistance compared to the as-pressed materials. The proposed model for the oxidation behaviour of the ceramics is therefore that of rate-control by the inward diffusion of oxygen through a non-porous liquid scale phase to the reaction zone at the ceramic/scale interface. Such a model accounts for the main experimental observations of the oxidation behaviour.

(1) The form of the oxidation kinetics of as-pressed ceramics was generally non-parabolic. ($n > 2$).
This is due to the formation of a scale in the early stages of oxidation which contains a high concentration of glass-modifying additive and impurity elements. Initial rapid rates of oxidation were caused by a low viscosity scale permitting relatively more rapid diffusion of oxygen to the reaction zone, both via the liquid phase and via gaseous pores and fissures which form more readily in a scale of low viscosity. In addition the rate of dissolution of β' into the scale may be more rapid when it is relatively more rich in these elements.

(2) The oxidation resistance of the as-pressed ceramics is highly dependent on both the substitution level of the ceramic and the type and quantity of the additive and impurity elements. The

oxidation resistance of small samples of ceramic which had undergone extensive oxidative heat treatment decreased continuously with increasing substitution level. This was due to the continuously decreasing scale viscosity with increasing substitution level permitting more rapid diffusion of oxygen and possibly also due to the increasing scale crystallinity permitting more direct diffusion.

The presence of large quantities of subscale-derived glass-modifying elements in the liquid part of the oxide scales of the ceramics decreases their oxidation resistance via a reduction in scale viscosity and hence an increased diffusion coefficient for oxygen. Thus a Mn-containing ceramic of composition Si_5AlON_7 had a lower oxidation resistance than a nominally- pure ceramic of composition $Si_4Al_2O_2N_6$. The <u>type</u> of additive element is important in that no change in oxidation resistance is expected for ceramics whose out-diffusing elements have no physical effect on the nature of the oxide scale. This behaviour was demonstrated by the Mg containing ceramic of composition Si_5AlON_7 whose oxidation resistance did not decrease on heat treatment depite large differences in the concentrations of Mg in the oxide scales of the as-pressed and heat-treated ceramics. The apparently similar physical nature of the scales of the two ceramics was probably due to the configurational nature of Mg in silicate melts, it being capable of acting as both an intermediate and modifying cation.

The work described here needs to be clarified by more fundamental studies and by further oxidation experiments. Fundamentally, characterisation of the composition of the intergranular regions is required in order to gain a more precise estimate of subscale diffusion rates, either by direct measurement on sample specimens or by recourse to the literature. It should be noted that these estimated rates may be overestimates due to the constricting effect on diffusion caused by locally high inter-

granular bond strengths in narrow intergranular diffusion channels.

The suggestion that extensive subscale denudation leads to ceramics of a more stabilised structure (and hence of higher oxidation resistance) and that subscale denudation alone rate-controls the oxidation of these ceramics in its initial stages needs to be tested by oxidation experiments similar to those described here. These experiments need to be performed either on ceramic pieces of much larger dimensions or on slices of ceramic cut from a large block which has been oxidised to form a shallow subscale composition gradient for the additive and impurity elements. The more precise estimates of the subscale diffusion coeffients gained from the the experiments outlined above would allow a prediction to be made of appropriate oxidation conditions. Experiments on a ceramic of single substitution level but a wide range (say 1 - 10%) MgO would complement this study.

The kinetics of oxidation should preferably be determined using the technique of continuous thermogravimetry on a single ceramic specimen taking simultaneous account of the gaseous evolution of N_2 to the atmosphere during heat treatment. A more precise technique is required for the estimation of the composition of the oxide scales. For glassy scales this may be gained by repeated cross-scale probing in the scanning electron microscope as employed here. A lower electron beam energy should be employed to increase spatial and compositional definition. Clean, polished surfaces would be preferred to fracture surfaces for the same reasons. A preferred technique for the estimation of average scale composition would be the chemical analysis of removed scales. For crystalline scales quantitative X-ray analysis should permit a definition to be made of the quantity and type of the crystalline phases present.

It is believed that the use of these techniques would demonstrate that the oxidation of single-phase hot-pressed Si-Al-O-N ceramics containing small quantities of additive and impurity elements is increasingly protective with time in the initial stages of oxidation due to

scale modification by the out-diffusing additive and impurity cations. Ceramics of stabilised microstructure should display parabolic oxidation rates, as commonly described in the literature for Si_3N_4 and Si-Al-O-N materials. These rates would be much lower than those of the as-pressed ceramics, as observed for hot-pressed Si_3N_4 (figure 2.4).The oxidation rates of ceramics of high substitution level, however, may be linear or paralinear in view of the extensively crystalline nature of their oxide scales. This behaviour is similar to that described by Desmaison et al [1983] for the β′ Si-Al-O-N of substitution level z=0.75 and to the linear oxidation kinetics observed by Hirai et al [1980]for a β Si_3N_4 ceramic with a porous oxide scale,.

It is believed that on very extensive oxidation the ceramics studied by Cubicciotti and Lau [1978,1979] and Clarke and Lange [1980]would demonstrate similar behaviour, as indicated by the work of Palm and Greskovich [1980] and Lange [1978b] on similar materials (section 2.2.3(d)).

Finally, it is suggested that some work is carried out in parallel on a hot-pressed β Si_3N_4 ceramic with similar additive type and quantities since this ceramic would represent the end member of the series of ceramics whose behaviour has been described here, and which would allow a direct comparison to be made between the oxidation rates of β Si_3N_4 and β′ Si-Al-O-N throughout the entire range of substitution levels.

6.2. Microstructural characteristics

The microstucture of the β′ Si-Al-O-Ns has been defined in chapter three. The mechanism of redistribution on oxidation of the grain-boundary segregated additive and impurity elements which are detrimental to both the creep and oxidation properties of these ceramics has been defined in the literature to be primarily that of their out-diffusion into the oxide scale [Karunaratne and Lewis 1980b, Clarke and Lange 1980, Cubicciotti and Lau 1978, Wu et al 1981]. This redistribution leads to ceramics of stabilised microstructure and enhanced creep and oxidation

resistance.

The mechanism of redistribution in the ceramics studied here has been defined to be also that of out-diffusion via microscopical studies and analysis of the compositions of the glassy oxide scales of Si_5AlON_7 ceramic slices cut from the bulk of large blocks of heat-treated ceramic.

The results of these experiments indicate that elements which are distributed as free cations in the intergranular regions of the ceramic (Mg, K, Ca, and Na) redistribute by diffusion into the oxide scale, leading to the formation of subscale diffusion profiles. Such profiles have been directly experimentally determined for ceramics containing a relatively high additive content ([Clarke and Lange 1980], figure 5.1). Rapid intergranular diffusion in these ceramics is facilitated by the presence of wide intergranular silicate channels. Cations such as Mn and Fe which are located in the bulk of the ceramic mainly in the form of silicide particles appear only to diffuse into the scale from regions of high concentration gradient close to the oxidation reaction zone. The rapidity of these processes leads to rapid compositional and structural stabilisation which makes simple ceramic components amenable to simple processing for property enhancement prior to service after relative ease of fabrication.

The same oxidation experiments have indicated that solution of the additive and impurity cations in the β' ceramic phase is negligible in comparison to their out-diffusion, due to limited solubility of these ions in the β' phase as suggested by independent solubility studies published in the literature (chapter 2, section 1.3).

Limited microstructural evidence has been presented here which suggests that the out-diffusion of the additive and impurity elements is accompanied by the closure of intergranular glassy regions by the local growth of the β' phase , as defined for the Mn-containing ceramic Si_5AlON_7 by Karunaratne and Lewis [1980b].

Further microstructural characterisation is required to permit a more precise definition to be made of the extent and relative importance

of the mechanisms of additive and impurity element redistribution on oxidation. As indicated above (section 6.1) the technique of compositional determination of glassy oxide scales employed in this work lacks the experimental precision to allow more than a qualitative assessment of out-diffusive behaviour to be made. Due to the low concentrations of the additive and impurity elements in the hot-pressed Si-Al-O-N ceramics direct analysis of their structure and composition will necessarily involve the use of such techniques as "lattice" imaging in the transmission electron microscope and high-resolution auger electron spectroscopy. In particular it is necessary

(1) to study a large number of grain boundaries and intergranular regions of the as-pressed and oxidised ceramics in the transmission electron microscope in order to define changes in their width and size distribution respectively on oxidation,

(2) to analyse the composition of subscale sections of oxidised ceramic using X-ray diffraction techniques (after Mc Donough et al 1981) in order to define the growth and distribution of intergranular phases during oxidation,

(3) to define the size, composition and distribution of impurity-containing silicide particles and their rate of dissolution during oxidation,and

(4) to determine the composition of the intergranular phase by high-resolution auger electron spectroscopy of intergranular fracture surfaces of as-pressed and oxidised ceramics, as performed by Lewis et al [1977] for β' Si-Al-O-N. By suitable in-situ etching of these surfaces the extent of additive and impurity solution into the β' phase on oxidation may be determined.

Completion of this work will allow a precise definition to be made of the subscale redistribution processes occurring on oxidation. It is believed that the work described here is sufficient to define the major

redistribution process to be that of out-diffusion into the oxide scale accompanied by the closure of intergranular channels by the local growth of β′ grains.

6.3. Mechanical properties

This work has extended the understanding of the creep behaviour of two highly creep-resistant Si_5AlON_7 ceramics whose behaviour under four-point bend and compression loading conditions has been reported by the Warwick Si-Al-O-N research group [Karunaratne and Lewis 1980] . A Mg hot-pressed ceramic containing minimal quantities of intergranular phase was characterised as undergoing creep by a non-cavitating , diff-usional mechanism and was capable of withstanding tensile strains of up to 4% prior to failure. This is the highest reported strain to failure for ceramics of the Si-Al-O-N group.

This work has demonstrated that this behaviour is dependent on a sufficiently fine surface finish. In addition to classical mechanical failure due to subcritical crack growth failure of the ceramic under tensile stress conditions has occurred due to oxidation-assisted crack growth. This has been demonstrated by the failure of the ceramic at stresses below which subcritical crack growth is expected. Preferential oxidation is believed to occur at surface crack tips due to the locally high compositional gradients of the out-diffusing glass-modifying elements. These enhance oxidation rates when present in large quantities in the oxide scale.

Prior to failure, however, the Mg-containing ceramic displayed the transient creep behaviour previously attributed to time-dependent strengthening of the intergranular bond due to the out-diffusion of glass-modifying elements into the oxide scale [Karunaratne 1980] .

This behaviour has also been observed in β Si_3N_4 ceramics which contain additive elements and hence a viscous intergranular phase (section 3.3.1).

Creep rates of this ceramic tested in tension were similar to those reported for testing in compression (figure5.7), indicating that rate-control of creep was due to the grain-boundary diffusional mechanism previously defined for this ceramic [Karunaratne 1980]. The creep rates of an Mn-containing Si_5AlON_7 ceramic, however, were an order of magnitude higher on initial testing under tensile conditions than that reported under compressive stress conditions (figure 5.9).On extended testing creep rates under tensile loading were similar to those observed under compressive loading. Although the scatter in creep data was high these results are compatible with a model of creep which defines creep as being dominated by cavitational processes in the initial stages. After extensive oxidation and removal of intergranular cavitation by the out-diffusion of additive and impurity cations, creep is controlled by the diffusional mechanisms defined for the non-cavitating Mg-containing ceramic by Karunaratne [1980].

The change in creep rates for the cavitating ceramic when tested under tensile as opposed to compressive stress conditions is expected in view of the analysis which proposes that the tensile stresses generated in ceramics under compressive stress conditions is some 7-10 times less than that generated under tensile stress conditions [Birch et al 1976], cavitational creep being controlled by tensile forces.

Further work in this area falls into two categories:

(1) Oxidative corrosion of surface flaws

It is necessary to define critical flaw sizes for these ceramics above which they will fail under tensile stresses under oxidising conditions at stresses below those expected to give rise to sub-critical crack growth. Ceramics with well-characterised surface flaws must be creep tested under tensile loading conditions to evaluate the critical flaw sizes under given stress, temperature and atmospheric conditions. Tests under oxidising and non-oxidising atmospheres will confirm the essentially oxidational nature of this

phenomenon. In addition, long-term oxidation prior to testing in order to produce ceramics of a stabilised structure of minimal additive and impurity content will also confirm the essentially out-diffusive nature of the phenomenon.

(2) Tensile creep behaviour

It is necessary to define more precisely the creep behaviour of these ceramics under tensile loading conditions via further experimentation on both as-pressed and oxidised specimens. Multiple-specimen testing is required to eliminate the statistical scatter in the results presented here and to provide data for the evaluation of the creep exponent,n, and activation energy,Q, for comparison with the data gained from the results of the creep experiments performed under compressive and bend conditions. Creep testing of oxidised samples of the Mn-containing ceramic is necessary to confirm the model of creep behaviour outlined above.

Creep specimens should contain no surface flaws which would lead to their premature failure via their oxidative corrosion as described above. Alternatively, the creep experiments could be performed in vacuum. Redesign of the creep testing rig should include more precise temperature monitoring close to the ceramic specimen and a greater temperature uniformity along its gauge length.

The tensile creep testing of thoroughly oxised ceramics of composition extending from βSi_3N_4 to $\beta' Si_2Al_2O_2N_4$ as proposed for the study of oxidation behaviour should permit a general definition to be made of the mechanical behaviour of the most highly creep-resistant materials in the system Si-Al-O-N.

It is believed that the results of these experiments and the results reported here will confirm the work of Karunaratne [1980] in proposing that Si-Al-O-N ceramics of minimal intergranular phase content (or stabilised microstructure) are very highly creep-resistant and are capable

of very high (superplastic) strains to failure, as has already been indicated by preliminary reports in the literature (section 3.3.3.).

APPENDIX

Solution of the diffusion equation for atomic diffusion along a pipe of time-dependent radius

Let c = concentration of diffusing atoms in pipe

c_o = concentration at t=0

D = diffusion coefficient of diffusing atoms

r = pipe radius

z = direction of diffusion along pipe

The diffusion equation is

$$\frac{\partial c}{\partial t} = D \left\{ \frac{1}{r} \frac{\partial}{\partial r} \left(r \frac{\partial c}{\partial r} \right) + \frac{\partial^2 c}{\partial z^2} \right\}$$

subject to the boundary conditions

$$c = 0 \text{ at } z = 0$$

and

$$D \frac{\partial c}{\partial r} = - c \frac{dR(t)}{dt}$$

where R(t) is the time-dependent pipe radius.

Let $x = r/R(t)$

and $c = c_\infty(z,t)\psi(x,t)$

where $$\frac{\partial c_\infty}{\partial t} = \frac{\partial^2 c_\infty}{\partial z^2}$$

$$c_\infty (z = 0) = 0$$

$$c_\infty (t = 0) = c_o$$

$$t = Dt$$

and

$$\frac{\partial \psi}{\partial t} = \frac{1}{R^2}\left\{\frac{1}{x}\frac{\partial}{\partial x}\left(x\,\frac{\partial \psi}{\partial x}\right) + \alpha(t)\; x\,\frac{\partial \psi}{\partial x}\right\}$$

where $\alpha = \frac{R}{D}\frac{dR}{dt}$

and $\frac{\partial \psi}{\partial x} = -\alpha\psi$ at $x = 1$.

Now, $\frac{\partial}{\partial t}\int_0^1 x\psi(x)dx = \frac{1}{R^2}\left\{-\alpha\psi(x=1,t) + \alpha\int_0^1 x^2\,\frac{\partial \psi}{\partial x}\,dx\right\}$

$$= \frac{1}{R^2}\left\{-\alpha\psi(x=1,t) + \alpha\psi(x=1,t) - 2\alpha\int_0^1 x\,\psi\,dx\right\}$$

Thus $\frac{\partial}{\partial \tau}\int_0^1 x\psi(x)dx = -\frac{2\alpha}{R^2}\int_0^1 x\psi dx$

$$\int_0^1 x\,\psi(x)dx = \frac{A}{R^2(t)} \quad \text{where A is a constant.}$$

At $t = 0$, $\psi = 1$ so $\frac{A}{R^2} = \frac{1}{2}$.

Whence $\int_0^1 x\,\psi(x,t)dx = \frac{1}{2}\frac{R_o^2}{R(t)^2}$

The flux, J, at the end of the pipe ($z = 0$) is

$$J = -D\,\frac{\partial c}{\partial z}\bigg|_{z=0} = -D\psi\,\frac{\partial c_\infty}{\partial z}\bigg|_{z=0} \quad .$$

Now, $c_\infty = c_o \text{ erf } \frac{z}{2\sqrt{\tau}}$

where erf $a = \frac{2}{\sqrt{\pi}} \int_o^a e^{-b^2} db$.

Thus $J = \frac{- D\psi(x,t)C_o}{2\sqrt{\tau}} \frac{2}{\sqrt{\pi}}$

$$= - \frac{Dc_o}{\sqrt{\pi\tau}} \psi(x,\tau)$$

The average flux is

$$J_A = 2\pi \int_o^{R(t)} Jr \, dr$$

$$= 2\pi R^2(t) \int_0^1 Jx \, dr$$

$$= - \frac{Dc_o}{\sqrt{\pi\tau}} 2\pi R^2(t) \int_0^1 x \psi \, dx$$

$$= - \frac{A_o c_o \sqrt{D}}{\sqrt{\pi t}}$$

where A_o is the initial cross-sectional area of the pipe.

REFERENCES

Ando, K., Oishi, Y., 1974, J. Chem. Phys. 61, 625.

Arias, A., 1979, J. Mater. Sci., 14, 1353.

Arons, R. M., Tien, J. K., 1980, J. Mater. Sci. 15, 2046.

Ashcroft, W., 1975, p.245 in Special Ceramics 6, Ed. Popper, P., Brit. Ceram. Res. Assoc. Stoke-on-Trent.

Bakini, G. N., Bellosi, A., Vincenzini, P., 1981, J. Amer. Ceram. Soc., 64, 578.

Babini, G. N., Bellosi, A., Vinenzini, P., 1983, J. Mater. Sci. 18, 231.

Barlier, P., Torre, J. P., 1979, J. Mater. Sci., 14, 235.

Benn, M., Riley, F. L., 1980, J. Mater. Sci. 15, 529.

Bennett, M. J., Houlton, M. R., 1979, J. Mater. Sci. 14, 184.

Billy, M., 1983, p.403 in Progress in Nitrogen Ceramics, Ed. Riley, F.L., Martinus, Nijhoff The Hague.

Birch, J. M., Wilshire, B., Owen, D. J. R., Shantaram, D., 1976, J. Mater. Sci., 11, 1817.

Birch, J. M., Wilshire, B., 1978, J. Mater. Sci., 13, 2627.

Bockris, J. O'M., Kitchener, J. A., Ignatowiz, S. Tomlinson, J. W., 1948, Disc. Far. Soc., 4, 265.

Bowen, L. J., Weston, R. J., Carruthers, T. G., Brook, R. J., 1978, J. Mater. Sci., 13, 341.

Brossard, M., Bracket, D. Goursat, P., Billy, M., 1979, Ann. Chim. Fr., 4, 7.

Brown, I. W. M., Mackenzie, K. J. D., 1982, J. Mater. Sci., 17, 2663.

Cannon, W. R., Langdon, T. G., 1983, J. Mater. Sci., 18, 1.

Clarke, D. R., Lange, F. F., 1980, J. Amer. Ceram. Soc. 63, 586.

Clarke, D. R., Lange, F. F., Schmittgrund, E. P., 1982, J. Amer. Ceram. Soc., 65, C-51.

Coppola, J. A., Bradt. R. C., Richerson, D. W., Alliegro, R. A., 1972, Amer. Ceram. Soc. Bull. 51, 847.

Cubiciotti, D., Lau, K. H., Jones, R. L., 1977, J. Electrochem Soc. 124, 1955.

Cubiciotti, D., Lau, K. H., 1978, J. Amerc. Ceram. Soc. 61, 512.

Cubiciotti, D., Lau, K. H., 1979, J. Electrochem. Soc. 126, 1723.

Dancy, E. A., Jansen, D., 1976, Can Metall Quarts, 15, 103.

Das, G., Mendiratta, M. G., Cornish, G. R., 1982, J. Mater. Sci. 17, 2486.

Davidge, R. W., Evans, A. G., 1970, Mater. Sci. Eng. 6, 280.

Davidge, R. W., Evans, A. G., Gilling, D., Wilyman, P. R., 1972, p.329, in Special Ceramics 5, Ed. Popper P. Brit. Ceram. Res. Assoc. Stoke-on-Trent.

Desmaison, J. G., Riley, F. L., 1981, J. Mater. Sci., 16, 2625.

Desmaison, J. G., Brossard, M., Desmaison-Brut, M., Goursat, P. 1983, p.439 in Progress in Nitrogen Ceramics, Ed. Riley, F. L., Martinus Nijhoff, The Hague.

Din, U. S., Nicholson, P. S., 1975, J. Mater. Sci., 10, 1375.

Dixon-Stubbs, P. J., Wilshire, B., 1979, J. Mater. Sci, 14, 2773.

Drew, P., Lewis, M. H., 1974, J. Mater. Sci., 9, 261.

Dutta, S., 1982, J. Amer. Ceram. Soc. 65, C-2.

Evans, A. G., Davidge, R. W., 1970, J. Mater. Sci., 5, 314.

Evans, A. G., Rice, J. R., Hirth, J. P., 1980, J. Amer. Ceram. Soc., 63, 368.

Evans, A. G., Sharp, J. V., 1971, J. Mater. Sci., 6, 1292.

Evans, U. R., 1960, The Corrosion and Oxidation of Metals, Edwin Arnold, London.

Fisher, D. J., 1977, p.1 in High Temperature Chemistry of Inorganic and Ceramic Materials, Chem. Soc. London.

Freer, R., 1980, J. Mater. Sci., 15, 803.

Freer, R., 1981, Contrib. Mineral Petrol, 76, 440.

Gauckler, L. J., Weiss, J., Tien, T. Y., Petzow, G., 1978, J. Amerc. Ceram. Soc., 61, 397.

Gillot, L., Cowlan, N., Bacon, G. E., 1981, J. Mater. Sci., 16, 2263.

Giachello,A., Martinengo, P.C., Tommasini, G.,1980, Amer. Ceram. Soc. Bull.,59, 1212.

Glasson, D.R., Jayaweera,S.A.A.,1968,J. App. Chem. 18, 65.
Godfrey, D. J., 1968, Metals Mat., 2, 305.

Greil, P., Weiss, J., 1982, J. Mater. Sci., 17, 1571.

Griffith, A. A., 1920, Phil. Trans. Roy. Soc., (London), A221, 163.

Hallwig, D., Schactner, R., Sockel, H. G., 1981, in Proc. 9th Int. Symp. Reactivity of Solids, Elsevier (quoted by Freer 1981).

Hartley, J., 1982, Engineer, 254, 6579, 38.

Hendry, A., Pererra, D. S., Thompson, D. P., Jack, K. H., 1975, p.321 in Special Ceramics, 6, Ed. Popper, P., Brit. Ceram. Res. Assoc. Stoke-on-Trent.

Henshall, J. L., Rowcliffe, D. J., Edington, J. W., 1975, p.185 in Special Ceramics, 6, Ed. Popper, P., Brit. Ceram. Res. Assoc. Stoke-on-Trent.

Heuer, A. H., Ogbuji, L. U., Mitchell, T. E., 1980, J. Amer. Ceram. Soc., 63, 354.

Hirai, T., Niihara, K., Goto, T., 1980, J. Amer. Ceram. Soc., 63, 419.

Horton, R. M., 1979, J. Amer. Ceram. Soc., 52, 121.

Jack, K. H., 1976, J. Mater. Sci. 11, 1135.

Jorgenson, P. J., Wadsworth, M. E., Cutler, I. B., 1959, J. Amer. Ceram. Soc., 42, 613.

Jost, W., 1960, Diffusion in Solids, Liquids, Gases, Academic Press, New York.

Karunaratne, B. S. B., 1980, Ph.D. Thesis, University of Warwick.

Karunaratne, B. S. B., Lewis, M. H., 1980a, J. Mater. Sci., 15, 449.

Karunaratne, B. S. B., Lewis, M. H., 1980b, J. Mater. Sci., 15, 1781.

Katz, B. N., 1983, Progress in Nitrogen Ceramics, Ed. Riely, F. L., Martinus Nijhoff, The Hague.

Kendall, K., 1983, J. Mater. Sci. Lett, 2, 115.

Kiehle, A. J., Heung, L. K., Gielisse, P. J., Rockett, T. J., 1975, J. Amer. Ceram. Soc., 58, 17.

Komeya, K., Inoue, H., 1975, J. Mater. Sci., 10, 1243.

Kossowsky, R., 1973, J. Mater. Sci., 8, 1603.

Kossowsky, R., Miller, D. G., Diaz, E. S., 1975, J. Mater. Sci., 10, 983.

Krivanek, O. L., Shaw, T. M., Thomas, G., 1979, J. App. Phys., 50, 4223.

Kuwabara, M., Benn, M., Riley, F. L., 1980, J. Mater. Sci., 15, 1407.

Lange, F. F., 1978a, J. Amer. Ceram. Soc., 61, 53.

Lange, F. F., 1978b, J. Amer. Ceram. Soc., 61, 270.

Lange, F. F., Diaz, E. S., Anderson, C. A., 1979, Amer. Ceram. Soc. Bull. 58, 845.

Lange, F. F., Davis, B. I., Clarke, D. R., 1980, J. Mater. Sci., 15, 601.

Lange, F. F., Davis, B. I., 1982, J. Mater. Sci., 17, 3637.

Lawless, K. R., 1973, Rep. Prog. Phys., 37, 231.

Lewis, M. H., Powell, B. P., Drew, P., Lumby, R. J., North, B., Taylor, A. J., 1977, J. Mater. Sci., 12, 61.

Lewis, M. H., Bhatti, A. R., Lumby, R. J., North, B., 1980, J. Mater. Sci. 15, 438.

Lewis, M. H., Barnard, P., 1980, J. Mater. Sci., 15, 443.

Levin, E. M., Robbins, C. R., McMurdie, H. F., 1964, Phase Diagrams for Ceramists, Amer. Ceram. Soc., Columbus, Ohio.

Linder, R., Parfitt, G. D., 1957, J. Chem. Phys., 26, 182.

Loehman, R. E., 1980, J. Non. Cryst. Sols., 42, 433.

Lowell, R. F., 1983, Amer. Ceram. Soc., Bull. 62, 349.

MacDowell, J. F., Beall, G. H., 1969, J. Amer. Ceram. Soc., 52, 17.

McLean, A. F., 1982, Amer. Ceram. Soc. Bull., 61, 861.

McDonough, W. J., Wu, C. C. M., Morgan, P. E. D., 1981, J. AMer. Ceram. Soc., 64, C-45.

Mackenzie, K. J. D., Ryan, M. J., 1981, J. Mater. Sci. 16, 579.

Mayer, M. I., Riley, F. L., 1978, J. Mater. Sci., 13, 1319.

Mehan, R. L., Jackson, M. R., McConnell, M. D., Lewis, N., 1983, J. Mater. Sci., 18, 508.

Messier, D. R., Schioler, L. J., Quinn, G. D., 1981, Amer. Ceram. Soc. Bull., 60, 812.

Mitomo, M., Kuramoto, N., Inomata, Y., 1979, J. Mater. Sci., 14, 2309.

Morrell, R., Ashby, K. H. G., 1973, J. Mater. Sci., B, 1253.

Mosher, D. R., Raj, R., Kossowsky, R., 1976, J. Mater. Sci., 11, 49.

Moulson, A. J., 1979, J. Mater. Sci., 14, 1017.

Niihara, K., Hirai, T., 1976, J. Mater. Sci., 11, 593.

North, B., Baker, R. D., 1983, Engineers' Digest Conference, Monte Carlo.

Nuttall, K., Thompson, D. P., 1974, J. Mater. Sci., 9, 850.

Oishi, Y., Nanba, M. Pask, J. A., 1982, J. Amer. Ceram. Soc. 65, 247.

Palm, J. A., Greskovich, C. D., 1980, Amer. Ceram. Soc. Bull., 59, 447.

Parr, N. L., 1960, Research 13, 261.

Phelps, F. E., Weyland, D., 1983, Amer. Ceram. Soc. Bull., 62, 434.

Procazka, S., Greskovich, C., 1978, Amer. Ceram. Soc. Bull, 57, 579.

Proust, H. B., 1980, Amer. Ceram. Soc. Bull. 59, 206.

Quackenbush, C. L., Smith, J. T., 1980, Amer. Ceram. Soc. Bull., 59, 533.

Rahaman, M. N., Riley, F. L., Brook, R. J., 1980, J. Amer. Ceram. Soc., 63, 648.

Rahaman, M. N., Riley, F. L., Brook, R. J., 1981, J. Mater. Sci. 16, 660.

Raj, R., Morgan, P. E. D., 1981, J. Amer. Ceram. Soc., 64, C-143.

Reddy, K. P. R., Cooper, A. R., 1981, J. Amer. Ceram. SOc., 64, 369.

Richerson, D. W., 1973, Amer. Ceram. Soc. Bull., 52, 560.

Risbud, S. H., Pask, J. A., 1978, J. Mater. Sci., 13, 2449.

Roebuck, R., 1979, J. Mater. Sci., 14, 2837.

Rossin, R., Bersan, J., Urbain, G., 1964, C. R. Acad. Sci. Paris, 258, 562.

Russ, J. C., 1972, Thin-section Microanalysis, Ed. Russ, J. C., Panessa, B. T., EDAX Labs, Rayleigh, NC.

Sanders, W. A., 1978, J. Amer. Ceram. Soc., 61, 278.

Schaeffer, H. A., 1980, J. Non Cryst. Sol., 38 & 39, 545.

Schlicting, J., Gauckler, L. J., 1977, Powder Metall Int., 9, 36.

Seltzer, M. S., 1977, Amer. Ceram. Soc. Bull., 56, 418.

Sheehan, J. E., 1982, J. Amer. Ceram. Soc., 65, C-111.

Singhal, S. C., 1976a, J. Mater. Sci. 11, 500.

Singhal, S. C., 1976b, pp697-712 in Properties of High Temperature Alloys Ed. Foroulis, Z. A. and Pettit, F. S., Electrochem, Soc. Princeton, N.J.

Singhal, S. C., 1976c, J. Amer. Ceram. Soc., 59, 81.

Singhal, S. C., Lange, F. F., 1977, J. Amer. Ceram. Soc., 60, 190.

Smith, J. T., 1977, Amer. Ceram. Soc. Bull., 56, 734.

Sucov, E. W., 1963, J. Amer. Ceram. Soc., 46, 14.

Talty, P. K., Dirks, R. A., 1978, J. Mater. Sci., 13, 580.

Terai, R., Hayami, R., 1975, J. Non Cryst. Sol., 18, 217.

Terwilliger, G. R., Lange, F. F., 1975, J. Mater. Sci., 10, 1169.

Tighe, N. J., 1978, J. Mater. Sci., 13, 1455.

Towers, H., Paris, M., Chipman, J., 1953, Trans. Metall. Soc., AIME, 197, 1455 (quoted by Terai and Hayami 1975).

Tressler, R. E., Meiser, M. D., Yonushonis, T., 1976, J. Amer. Ceram. Soc., 59, 278.

Tripp, W. C., Graham, H. C., 1976, J. Amer. Ceram. Soc., 59, 399.

Tsai, R. L., Raj, R., 1980, J. Amer. Ceram. Soc., 63, 513.

Ueda, H., Oishi, Y., 1970, Proc. Ashai Glass Assoc. Promotion Indust. Eng., 16, 201 (Quoted by Terai and Hayami 1975).

Urbain, G., Cambier, F, Deletter, M., Anseau, M. R., 1981, Trans. J. Brit. Ceram. Soc., 80, 139.

Urbain, G., Bottinga, Y., Richet, P., 1982, Geochimica et Cosmochimica Acta, 46, 1061.

Wagner, C., 1933, Z. Phys. Chem. 21B, 25.

Wagner, C, 1958, J. App. Phys., 29, 1295.

Warburton, J. B., Antill, J. E., Hawes, R. W. M., 1978, J. Amer. Ceram. Soc., 61, 67.

Weeks, R. A., Sander, E., 1980, J. Amer. Ceram. Soc., 63, 92.

Widerhorn, S. M., Tighe, N. J., 1978, J. Mater. Sci., 13, 1781.

Wild, S., Leng-Ward, G., Lewis, M. H., 1981, J. Mater. Sci., 16, 1815.

Williams, E. L., 1965, J. Amer. Ceram. Soc., 48, 190.

Williams, R. O., Tennery, V. J., 1979, J. Mater. Sci., 14, 1567.

Wu, C. C. M, McKinney, K. R., Rice, R. W., McDonough, W. J., Freiman, S. W., 1981, J. Mater. Sci., 16, 3099.

Yamada, T., Shimada, M., Koizumi, M., 1981a, Amer. Ceram. Soc. Bull., 60, 1281.

Yamada, T., Shimada, M., Koizumi, M., 1981b, Amer. Ceram. Soc. Bull., 60, 1225.

Yeh, H. C., Sikora, P. F., 1979, Amer. Ceram. Soc. Bull., 58, 444.

Zucrow, M. J., 1976, p52 in Gas Dynamics, Wiley.

Widerhorn, S. M., Tighe, N. J., 1978, J. Mater. Sci., 13, 1781.

Wild, S., Leng-Ward, G., Lewis, M. H., 1981, J. Mater. Sci., 16, 1815.

Williams, E. L., 1965, J. Amer. Ceram. Soc., 48, 190.

Williams, R. O., Tennery, V. J., 1979, J. Mater. Sci., 14, 1567.

Wu, C. C. M, McKinney, K. R., Rice, R. W., McDonough, W. J., Freiman, S. W., 1981, J. Mater. Sci., 16, 3099.

Yamada, T., Shimada, M., Koizumi, M., 1981a, Amer. Ceram. Soc. Bull., 60, 1281.

Yamada, T., Shimada, M., Koizumi, M., 1981b, Amer. Ceram. Soc. Bull., 60, 1225.

Yeh, H. C., Sikora, P. F., 1979, Amer. Ceram. Soc. Bull., 58, 444.

Zucrow, M. J., 1976, p52 in Gas Dynamics, Wiley.

2